The GDH sum rule and extension to photoproduction off neutron targets in the Jülich-Bonn model

Dissertation

zur
Erlangung des Doktorgrades (Dr. rer. nat.)
der
Mathematisch-Naturwissenschaftlichen Fakultät
der
Rheinischen Friedrich-Wilhelms-Universität Bonn

vorgelegt von
Carolin Schneider
aus
Bonn

Bonn, 2026

Angefertigt mit Genehmigung der Mathematisch-Naturwissenschaftlichen Fakultät
der Rheinischen Friedrich-Wilhelms-Universität Bonn

Gutachter/Betreuer:	apl. Prof. Dr. Christoph Hanhart
Gutachter:	Prof. Dr. Dr. h.c. Ulf-G. Meißner

Tag der Promotion:	24.07.2026
Erscheinungsjahr:	2026

Summary

In this thesis, the light baryon spectrum of nucleon and delta resonances is studied up to center-of-mass energies of 2.5 GeV. In this energy region, the strong interaction is non-perturbative and other methods are required. For this purpose, the Jülich-Bonn dynamical coupled-channel framework is employed. The model uses hadrons as the relevant degrees of freedom and the interaction is constructed from an effective Lagrangian. Furthermore, s-channel diagrams are included as genuine resonance states. The Lippmann-Schwinger scattering equation preserves analyticity, which is essential for a reliable extraction of resonance properties.

The Jülich-Bonn model was originally developed for pion-induced reactions such as $\pi N \to \pi N$, ηN, $K\Lambda$ and $K\Sigma$. It was later extended in a phenomenological way to include the photoproduction processes $\gamma p \to \pi^0 p$, $\pi^+ n$, $K^0\Lambda^+$, $K^0\Sigma^+$ and $K^+\Sigma^0$.

In this thesis, we present an updated fit result with new photoproduction data for the processes $\gamma p \to \pi^0 p$, $\pi^+ n$ and ηp. So far, only photoproduction reactions with proton targets were analysed with this framework. One of the main achievements of this thesis is the extension of the framework to photoproduction off neutron targets, allowing for a simultaneous description of $\gamma n \to \pi^0 n$ and $\pi^- p$, in addition to the reactions listed above.

Another important aspect of this thesis is the Gerasimov-Drell-Hearn (GDH) sum rule, which follows from fundamental principles of quantum field theory and provides access to the spin structure of the nucleon. Using the Jülich-Bonn framework, the contributions of individual reaction channels to the GDH sum rule are determined. These contributions are calculated for photoproduction processes on both proton and neutron targets, providing new insights into the spin-dependent structure of the nucleon.

This thesis is structured as follows: Chapter 1 gives a short introduction to the Standard Model, the strong interaction, and light baryon spectroscopy. Chapter 2 presents the theoretical foundations relevant to this work. In Chapter 3, the Jülich-Bonn dynamical coupled channel framework is described. In Chapter 4, the fit results of the analysis recently published in Ref. [1] is presented. The extension of the Jülich-Bonn model to photoproduction with neutron targets and the fit to the data base for the final-states $\pi^0 n$ and $\pi^- p$ is presented in Chapter 5. Finally, Chapter 6 presents and discusses the contributions of the individual channels to the GDH sum rule, based on the fits performed in Chapters 4 and 5.

Contents

1. Introduction

This chapter serves as a brief introduction to the field of light baryon spectroscopy. It first outlines the essential concepts of the Standard Model and the strong interaction, and the basic properties of hadrons are introduced. Based on these foundations, the chapter then introduces the light baryon spectrum and further lists some important experimental efforts as well as the main analysis approaches in the field.

1.1. Standard Model

As a starting point, we briefly review the Standard Model of particle physics. The Standard Model is the quantum field theory that unifies the electromagnetic, weak and strong forces of nature, but so far the gravitational force could not be included.

The fermionic particle content of the Standard Model can be grouped into leptons and quarks which each can be categorized into three generations. The leptons consist of the electrically charged leptons: (electron e, muon μ and tau τ), and their corresponding lepton-neutrinos: $(\nu_e, \nu_\mu, \nu_\tau)$, which do not carry electric charge. The first generation of quarks consist of the up- (u) and down-quark (d), the second of the charm- (c) and strange-quark (s), and the third of the top- (t) and bottom-quark (b). Each fermion also has an antiparticle. All fermionic particles can interact under the weak interaction and the electrically charged ones (all except for the lepton-neutrinos) interact via the electromagnetic force. However, only the quarks additionally participate in the strong interaction because they carry the color charge. The bosonic particles in the Standard Model are given by the massless gluons and photon, as well as the massive $W^{\pm}$ and Z and the Higgs particle. This particle content is illustrated in Fig. 1.

The Standard Model is an $SU(3)_C \times SU(2)_L \times U(1)_Y$ gauge theory that is spontaneously broken by the Higgs potential. Here, $SU(3)_C$ is the color group of the strong interaction and implies 8 massless, color-carrying gauge bosons called gluons. The gluons are the mediators of the strong force. The combination $SU(2)_L \times U(1)_Y$ corresponds to the electroweak interaction. The mediators of the weak force are the massive $W^{\pm}$- and the Z-boson, while the electromagnetic force is mediated by the massless photon γ. Furthermore, the Standard Model includes the Higgs boson as a scalar field. The Higgs potential has a degenerate minimum with a non-zero vacuum expectation value, such that symmetry gets spontaneously broken. This generates effective masses for the $W^{\pm}$- and Z-boson as well as for the quarks and leptons. Initially, the neutrinos were considered massless in the Standard Model, but observed phenomenona like the neutrino oscillations lead to the conclusion of a non-zero mass for the neutrinos [2].

The Standard Model includes up to 28 parameters [3]:

- six lepton masses and six quark masses,
- three gauge coupling constants,
- three quark-mixing angles and one complex phase,

- three neutrino-mixing angles and as many as three complex phases[1],
- one Higgs mass and one quartic coupling constant,
- one QCD vacuum angle.

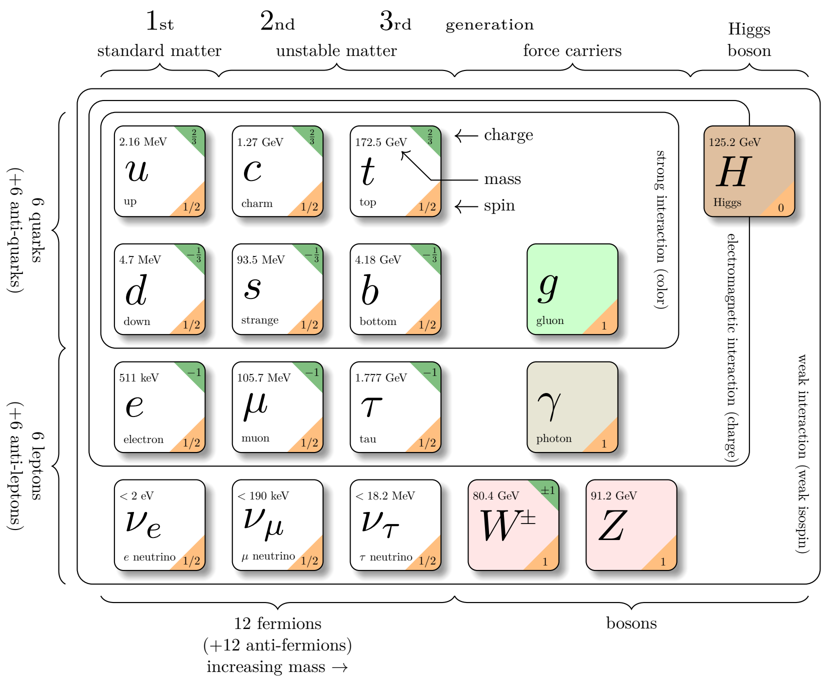

Figure 1: Graphical representation of the Standard Model of Particle Physics. The mass values of the particles are taken from the PDG particle listings [5].

1.2. Strong Interaction and Hadrons

The electromagnetic interaction can be described by quantum electrodynamics (QED), which is a quantum field theory in which scattering amplitudes can be calculated using perturbative methods due to the small coupling constant. It provides very precise predictions of fundamental observables and the perturbative approach can be applied at all energies probed until today[2]. In contrast to this, the strong interaction cannot be treated perturbatively at all energies. This is due to the fact, that the gluon carries color itself, which leads to the effect of the ”running coupling”. This means that the strong coupling constant is low only in the high energy regime (”asymptotic freedom”) and becomes large

[1]If the neutrinos are Majorana fermions there are as many as three CP-violating complex phases. In the case of a Dirac neutrinos there is only one complex phase [4].

[2]The binding of atoms and molecules is clearly a non-perturbative phenomenon, but here perturbation theory can be employed to control the binding potential.

for low energies. The gauge theory of the strong interaction is called quantum chromodynamics (QCD) (see Sec. 2.2) and it can only be treated perturbatively for higher energies. A further consequence of the nature of the strong interaction leads to the phenomenon of "confinement": Quarks cannot be observed as free particles and are confined within color-neutral objects, called hadrons. The most simple hadronic states are built of a quark-antiquark pair (meson) and 3 quark states (baryon). Hadrons with a more complex quark content are called "exotics". These exotic states are structures like "glueballs", multiquark states, hadronic molecules or hybrid states [6–9].

In the original quark model developed by Gell-Mann, Niemann and Zweig in the 1960s, it was found that the mesons and baryons could be grouped into multiplets. By considering $SU(3)$ symmetry for the light quark flavors (u, d, s), they found that mesons and baryons form multiplets with respect to the isospin I_3 and the strangeness S. The pseudoscalar (spin 0) and vector (spin 1) mesons constitute an octet and a singlet each. These are shown in Fig. 2. Similarly for the baryons one found a spin 1/2 octet and a spin 3/2 decuplet as shown in Fig. 3. This was also known as the "eight-fold way" and Gell-Mann predicted the existence and the mass of the Ω^- baryon, which was observed experimentally shortly after very close to the predicted value [10].

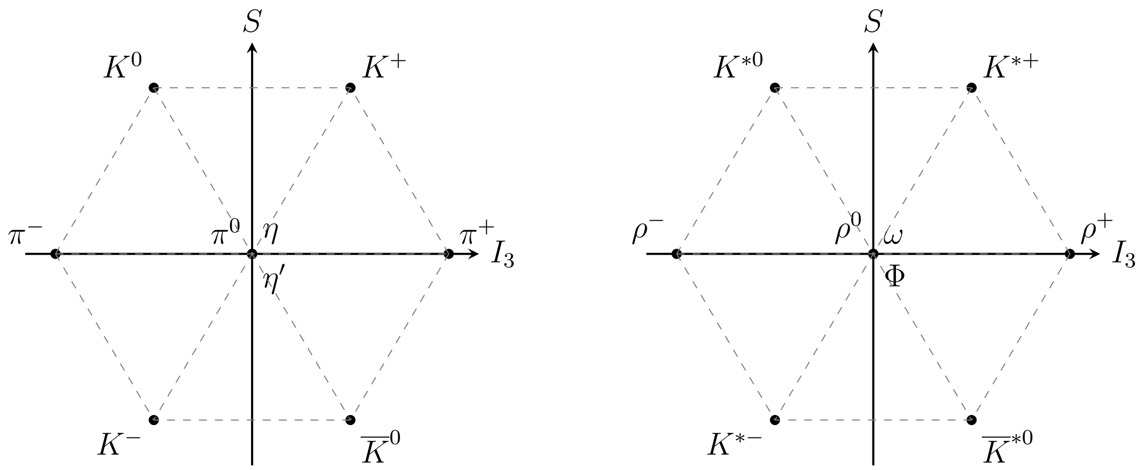

Figure 2: Left: Pseudoscalar meson multiplet. Right: Vector meson multiplet.

Since then, further hadrons were discovered at higher energies and the quark picture was extended to three heavy quark flavors: c (charm), b (bottom) and t (top). However, there are no hadrons with top-quarks, since its lifetime is shorter than the timescale of non-perturbative strong interactions, which prevents a hadronization process [5]. Even though the picture of hadrons being formed by valence quarks ($q\bar{q}$ and qqq) can predict the quantum numbers of many hadrons (except for exotics), it cannot explain their masses. This is due to the fact that the main part of the hadron masses originates from the gluon-field instead of the masses of the quarks.

Almost all hadrons are resonances (see Sec. 2.1) and therefore unstable states. Up to now we only discussed ground states for hadrons, but there are many more excited

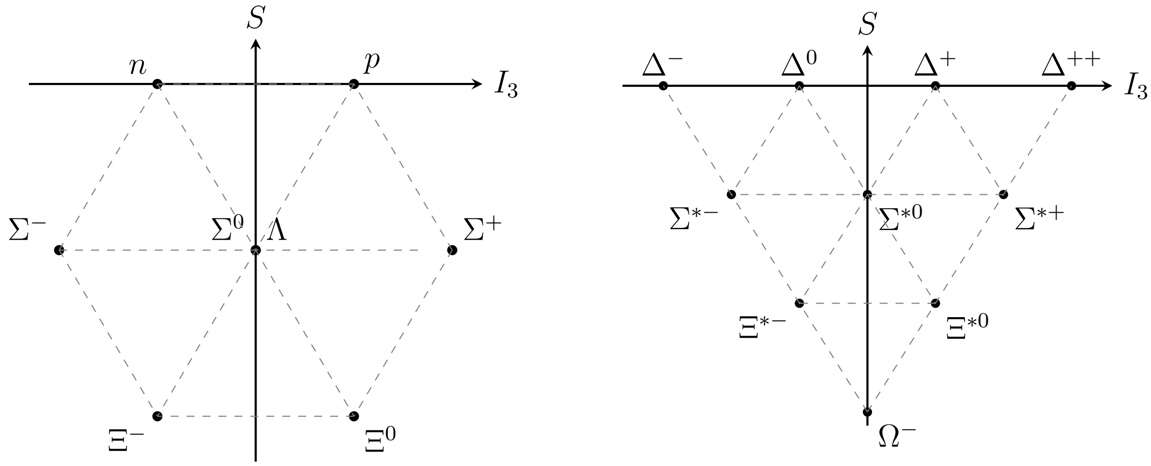

Figure 3: Left: Baryon octet. Right: Baryon decuplet.

states which also appear as resonances in scattering processes and decay back into ground states. These resonances may appear as structures (e.g. peaks) in the experimental data. However, identifying resonances in a region with multiple, overlapping resonances is not straightforward. This is the case for energies, in which nucleon N^* and Delta Δ^* resonances exist.

1.3. Light baryon spectroscopy

In light baryon spectroscopy one studies the excited nucleon N^* and Delta Δ^* spectra. Some recent reviews on the topic of Light Baryon Spectroscopy are given in Refs. [11–14].

Quark Models and Lattice QCD predictions for the N^* and Δ^* spectrum

One of the major challenges to this day in hadron physics is to fully understand the excitation spectrum of the nucleons and Deltas. There exist different approaches to predict these spectra. The two most prominent ones are from quark models and lattice QCD. There are also other approaches that we will not cover further here (see Refs. [15–21]).

After the initial quark model by Gell-Mann, Niemann and Zweig, the ideas were developed further to also describe the sprectrum of excited hadrons. Constituent quark models assume that hadrons are bound states of so called "constituent quarks". These kind of models were initally proposed by Isgur and Karl [22, 23] and several groups further developed them to advanced quark models [24–26] or to include relativistic effects [27–31]. These constituent quarks are the fundamental "current" quarks from the QCD Lagrangian with modified properties to allow for a surrounding cloud of gluons and quarks. Interactions for these phenomena cannot be derived from QCD itself and thus needs to be modeled as effective potentials. Generally a linearly rising confinement-potential is assumed for the long-range interaction and the approaches differ in the parametrization of the short-range potential of QCD. After the potential is fixed, one uses either a differential (Dirac-/Schrödinger-) or an integral (Lippmann-Schwinger-/Bethe-Salpeter-) equation that needs to be solved to find the spectrum. Predictions of quark models for low-lying resonances are in good agreement with analyses using experimental data. However, many predicted states at higher energies could not be observed in data. This was often referred to as the "missing resonance problem" [32]. One special low lying state is the so called Roper resonance, $N(1440)1/2^+$, which is the first nucleon excitation with positive parity. Quark models usually predicted the mass of this state to be larger than the first negative-parity state, $N(1535)1/2^-$. However, it was found by studies that the mass of the Roper resonance actually lies below the $N(1535)1/2^-$. This led to the interpretation of some analysis groups that the Roper resonance is dynamically generated from meson-baryon interactions, but the nature of the $N(1535)1/2^-$ is still not fully understood and remains an active subject of ongoing research [11–13, 33–35]. Also note that there are hardly any reliable predictions for decay widths of hadronic resonances from quark model studies. Today, fundamental approaches like effective field theories (see Sec. 2.3) play a more central role than quark models.

Lattice QCD, originally formulated by Wilson [36], provides a non-perturbative, first-principles framework to study the spectrum of hadrons directly from the underlying quark-gluon dynamics. Reviews relevant for hadron spectroscopy can be found in Refs. [37–39]. Euclidean-time correlation functions from suitably interpolating operators are evaluated numerically on a discretized four-dimensional spacetime with finite lattice spacing a and volume V. The resulting finite-volume energy levels give information on the QCD spectrum. For the case of stable states these energy levels can be directly related to hadron masses.

The study of resonances is essential for light baryon spectroscopy, but it is more complicated in lattice QCD. Since lattice QCD is formulated in Euclidean spacetime and yields a discrete finite-volume spectrum, it does not provide direct access to real-time scattering observables or resonance properties such as decay widths. Consequently, resonance information has to be obtained indirectly by using finite-volume formalisms, such as the prominent "Lüscher's method" [40–42], which relates the discrete energy levels to infinite-volume scattering phase shifts. Applications of these techniques to the light baryon sector can be found in Refs. [43–53], with more recent studies focusing in particular on the $\Delta(1232)$ resonance [54–56].

To get reliable predictions for the light baryon spectrum one requires extrapolations to the continuum limit ($a \to 0$) and infinite volume ($V \to \infty$), as well as a careful treatment of multi-hadron states and scattering effects. Additionally, simulations are often performed at heavier than physical quark masses, leading to unphysically large pion masses, which further complicates the extraction of resonance properties. To get the connection to the physical spectrum, one requires chiral extrapolations [57].

Experiments

There are many experimental efforts to study the light baryons. The beginning for the excited nucleon spectrum was given by experiments studying pion nucleon scattering. A large amount of data originated from the LAMPF experiment in Los Alamos, USA, the TRIUMF experiment in Vancouver, Canada, and experiments from the Paul-Scherrer-Institute (PSI) in Villigen, Switzerland [11]. Already in the early days of pion-nucleon scattering, researchers found a lack of resonances compared to quark models (*missing resonance problem*).

More recent experiments contributing to the pion-nucleon world data base are given by the Crystal Ball experiment at Brookhaven National Lab [58, 59], experiments from the PSI [60, 61] and the ITEP-PNPI [62].

Another contribution to the pion-nucleon scattering data base was produced by the HADES experiment at GSI [63, 64].

In recent years the experiments in the field mainly focused on photoproduction data. Among those facilities are:

- The Electron Stretcher Accelerator (ELSA) is located at the University of Bonn [65]. The different experiments at this facility were the SAPHIR [66], the CB-ELSA, the CB-TAPS and the CBELSA/TAPS experiments. The CB-TAPS experiment was moved and used for the new BGOOD experiment [67].

- The Mainz Microtron (MAMI) accelerator facility located at the University of Mainz [68]. Different experiments were performed at the facility such as the TAPS experiment [69], the GDH experiment in collaboration with the group at ELSA to study the Gerasimov-Drell-Hearn sum rule [70], and Crystal Ball/TAPS.

- The CLAS experiment (CEBAF large acceptance spectrometer) is located in Hall B at the CEBAF accelerator at the Thomas Jefferson national Accelerator Facility in Newport News, Virginia, USA [71].

- The GRenoble Anneau Accélérateir Laser (GRAAL) experiment is located at the European Synchrotron Radiation Facility (ESRF) at Grenoble, France [72, 73].

- The Super Photon ring 8-GeV (SPRING-8) facility is located at the Harima Science Park City, Japan. Experiments performed here are the LEPS experiment [74], the BGOegg experiment [75], and the LEPS2 experiment [76].

These photoproduction experiments allow the production of high precision polarization data. The main source of data is given by the photoproduction of pseudoscalar mesons (π, η, K). In such processes up to 16 polarization observables can be measured. The question of how many observables one needs to measure to fully determine the photoproduction amplitude is addressed in different studies and lead to the search of the so called "complete experiments" [77, 78], which received more attention again in the recent years [11, 79–82]. It was found that certain sets of eight selected observables could resolve all discrete ambiguities up to an overall phase. However, each set of observables requires the polarization of the incident photon beam and the target and the measurement of the recoil particle, which is a considerable challenge for experiments. In case of pion and eta photoproduction experiments one requires the measurement of the polarization of recoil nucleon, which needs further experimental setups. Strangeness photoproduction reactions have the advantage that the hyperon polarization can be determined from the parity violating weak decays by measuring the angular distribution of the products from $\Sigma^0 \to \Lambda\gamma$ and $\Lambda \to \pi^- p$ [83]. We also have to keep in mind that the assumption of eight observables being sufficient only holds if measurements are free of uncertainties. The number of observables required to remove all ambiguities is in fact larger as mentioned in Refs. [79, 81, 84, 85].

Another way to study the light baryon sector is through electroproduction experiments, which allows to access virtual photons with $Q^2 \neq 0$. Electroproduction processes give further insights on the internal structure of resonance states [45, 86, 87]. In contrast to photoproduction, there are six helicity amplitudes in electroproduction of pseudo-scalar mesons. Thus, more measurements are required for a "complete experiment" [88]. Advances in the field of electroproduction experiments in the last decades have been made by several groups, including JLAB [89–92] and MAMI [93–95].

The recent years brought major advancements in the field of light baryon spectroscopy. Many experimental facilities provide high-precision measurements with polarized photon beams and/or polarized targets which give analysis groups the ability to more reliably extract the resonance spectrum. There are also new experiments being built or planned for the future. Among those is the PANDA experiment at the FAIR facility at GSI in Darmstadt, Germany, to study $p\bar{p}$ collisions [96–98]. There is also the future INSIGHT experiment, which is an important upgrade for the BGOOD and CBELSA/TAPS experiments at ELSA, and it focuses on the excited hyperon spectrum [99, 100]. There are also plans at JLab to built the KLF facility in Hall D using a K_L beam to scatter on nucleon targets [101, 102].

Analysis groups in the Light Baryon Spectroscopy

There are different analysis groups and approaches to study the N^*- and Δ^*-spectra. In order to determine resonance parameters from the experimental data, one parameterizes the amplitude as a function of energy and perform an energy dependent fit to the data (or perform single energy fits). Then the amplitude needs to be analytically continued into the complex energy plane to extract the pole parameters of resonances. These pole parameters from an analytic function characterize the resonances. A further challenge in light baryon spectroscopy is given by the large number of thresholds within the respective energy region and resonances couple to these different channels. Thus, analysis groups perform a so-called "coupled channel" approach, where partial-wave analyses to study the resonances in the individual partial waves are performed. In the following, we outline some of these different approaches.

The **Jülich-Bonn** group uses a **dynamical coupled channel** (DCC) approach to study pion- and photon-induced processes [1, 33, 103–118]. It was further developed by the **Jülich-Bonn-Washington** group to study electroproduction reactions [119–122]. We will describe the Jülich Bonn model in more detail in Chapter 3. Another DCC approach was developed by the **ANL-Osaka** group [123, 124].

Dynamical coupled channel models use an amplitude parametrization with mesons and baryons as their respective degrees of freedom. A recent review on this topic can be found in Ref. [125]. In DCC approaches the scattering equations are solved iteratively with off-shell integrations such as the Lippmann-Schwinger equation. They respect S-matrix principles such as unitarity and preserve analyticity (see Sec. 2.1). With this, one can determine resonance parameters in the complex energy plane reliably. The scattering potential is based on effective Lagrangians, that preserve the symmetries of QCD. The background is provided by t- and u-channel diagrams from meson- and baryon-exchange potentials. Genuine resonances are included as s-channel diagrams, but due to the nature of the scattering equation a dynamical generation of resonances is also possible. In contrast to K-matrix approximations the real dispersive parts of the intermediate propagator are kept in the scattering equation. However, DCC approaches require substantial computational and formal efforts when keeping the field theoretical approach as well as the coupled channel aspect.

The **SAID**-analysis is one of the earliest energy dependent studies in the field to study pion- and photon-induced reactions. It is developed by the George-Washington University (GWU) [126–132]. They use a K-matrix type approach with a Chew-Mandelstam function and the real part of this function is retained to keep analyticity. For the photoproduction part a so called "P-vector" (production-vector) formalism is used [133]. Within this SAID-approach the energy dependence is given by phenomenological polynomials and the only genuine resonance used as input is the $\Delta(1232)$. Thus, all other poles of the T-matrix are generated dynamically.

Note, the SAID analysis for the elastic pion-nucleon process serves as input for other partial-wave analysis groups. Thus, the SAID analysis is an important study for the field. Furthermore the SAID group maintains a large database collecting pion- and photon-induced data sets [126].

Another partial-wave analysis using a coupled-channel formalism is the **Bonn-Gatchina** (BnGa) model [131, 134–136]. The BnGa group uses a K-matrix approach and for photon-induced reactions they introduce a P-vector. They recently extended the model by a N/D-inspired technique and for reactions with weakly coupled decays (e.g. 3-body final-states) they use a D-vector approach [131]. If both the production and decay couple weakly, they use a PD-vector technique. Furthermore, the BnGa group is using so-called "reggeized" amplitudes for forward-peaks at high energies originating from t-channel exchanges. No low-energy constraints from chiral perturbation theory or Watson theorem are included, but the analysis satisfies the Watson theorem to some degree. Resonances are included as input to the K-matrix and t- and u-channel diagrams parametrize the main part of the background. The BnGa model is optimized to allow many fits within short runtimes.

The **MAID** analysis is used to study photo- and electroproduction reactions [137–139]. The MAID group uses a unitary isobar model with a background and resonant T-matrix. For the resonant parts they use multi-channel Breit-Wigner amplitudes. The background part is defined by Born-terms together with an amplitude modeling pion-nucleon rescattering. In recent studies the MAID group introduced Regge-amplitudes for selected reactions. Within the model, the phases of the total amplitude are adjusted to fulfill Watson's theorem below the 2π-threshold.

This list is not to be taken as complete. There are further approaches, e.g. Kent State University model [140–143] and Gießen model [144, 145], or older πN-scattering studies, e.g. by Cutkosky [146], Höhler [147, 148] or Arndt [149].

The different analysis groups also differ in the number of resonances found within their studies. Some studies allow for dynamical generation of resonances and thus do not need to include each resonance as input for the model. For example the SAID-analysis only uses the $\Delta(1232)$ as input. The different approaches lead to a difference in importance of some resonances (or some are not even found). From this arises the discussion of which resonances are actually needed to build a "minimal model" that can describe the experimental data. This topic is further explored in the review on "N and Δ Resonances" of the Particle Data Group (PDG) [5]. The PDG introduced a "star-rating" for these excited states (as can be seen in Tabs. 10, 11, 24 and 25). For a listing of the resonances with their star rating and the resonances that each analysis groups finds in their studies, we refer to Sec. 7.2 in Ref. [11].

2. Theoretical Background

In this chapter we provide some theoretical background relevant to this work. We start with elements of scattering theory and introduce the S-matrix. After that we explain briefly the fundamentals of Quantum Chromodynamics (QCD) and introduce the concept of Effective Field Theory (EFT) and Chiral Perturbation Theory (ChPT). At last we introduce the Gerasimov-Drell-Hearn (GDH) sum rule and outline its derivation.

2.1. Properties of the S-matrix and elements of scattering theory

The S-matrix is the operator that connects asymptotic in and out states. We can separate the interacting part of the S-matrix and define the T-matrix (sometimes called transfer or transition matrix) in operator form by [150, 151]

$$S = \mathbb{1} + 2iT \; . \tag{2.1}$$

Note that the prefactor $2i$ is conventional. Scattering processes are characterised by the Mandelstam variables. For $2 \to 2$ processes with incoming momenta (p_1, p_2) and outgoing momenta (p_1', p_2') the Mandelstam variables are defined by:

$$\begin{aligned} s &= (p_1 + p_2)^2 = (p_1' + p_2')^2 & (2.2) \\ t &= (p_1 - p_1')^2 = (p_2 - p_2')^2 & (2.3) \\ u &= (p_1 - p_2')^2 = (p_2 - p_1')^2 \; . & (2.4) \end{aligned}$$

These three variables are not independent and are related by the sum of the squared masses of the involved particles:

$$s + t + u = m_1^2 + m_2^2 + m_1'^2 + m_2'^2 \; . \tag{2.5}$$

The Mandelstam variable s is related to the center-of-mass energy $E_{cm} = \sqrt{s}$. The variable t defines the momentum transfer from the particle 1 (2) to the particle $1'$ $(2')$. Consequently, the S-matrix and the amplitudes are in general functions of Lorentz-invariants of the process. In the case of a $2 \to 2$ process, one uses the Mandelstam variables s and t. For a general $2 \to n$ reaction with $n \geq 2$ the amplitudes depend on a set of $3(2 + n) - 10$ invariants.

Consider the scattering process $1+2 \to 1'+2'$ via a s-channel diagram as shown in Fig. 4. One may instead view the process as scattering between the incoming particle 1 and the antiparticle of $1'$, denoted by $\bar{1}'$, with momenta p_1 and $-p_1'$, and the outgoing antiparticle $\bar{2}$ and particle $2'$, with momenta $-p_2$ and p_2'. Under this transformation, the Mandelstam variable t plays the role that s had in the original process. Thus, the amplitudes in the s- and t-channels are related by the so-called "crossing symmetry". An analogous argument can be made to the u-channel and this context the t- and u-channel are also referred to as "crossed channels".

The S-matrix is a unitary operator $S^\dagger S = \mathbb{1}$. This property is linked to the conservation of probabilities in Quantum Mechanics. Imposing unitarity on the S-matrix leads to the

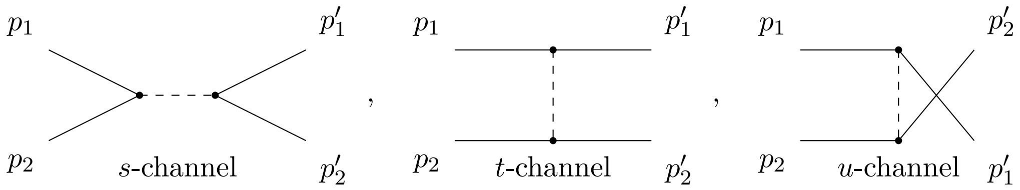

Figure 4: Sketch of s-, t- and u-channel diagrams for the scattering process $1+2 \to 1'+2'$. Time flows from left to right.

optical theorem, which puts constraints on the T-matrix:

$$\frac{1}{2i}\left(T - T^{\dagger}\right) = T^{\dagger}\, T \ . \tag{2.6}$$

Considering asymptotic states $|\mu\rangle$ and $|\nu\rangle$ for a process $\mu \to \nu$ and the corresponding matrix elements as $\langle\mu|\, T\, |\nu\rangle \equiv T_{\mu\nu}$, one can write this relation as:

$$\frac{1}{2i}(T_{\mu\nu} - T^{\dagger}_{\mu\nu}) = \sum_{\kappa} T_{\mu\kappa} T^{\dagger}_{\kappa\nu} \ . \tag{2.7}$$

Here the sum over intermediate states $\mathbb{1} = \sum_{\kappa} |\kappa\rangle\, \langle\kappa|$ should be understood as an integration and a summation over all discrete and continuous quantum numbers. The T-matrix as defined in Eq. (2.1) is not Lorentz invariant. One can define a Lorentz invariant amplitude τ by introducing phase space factors ρ_{μ} as

$$T_{\mu\nu} = \sqrt{\rho_{\mu}}\tau_{\mu\nu}\sqrt{\rho_{\nu}} \ . \tag{2.8}$$

With this one would also introduce an integration over the phase space of the intermediate state κ in Eq. (2.7).

Considering asymptotic and intermediate two-body particle states, one talks about "two-body unitarity", if the optical theorem is fulfilled by the amplitudes. Unitarity for more than two-body states is generally harder to implement. Especially the three-body unitarity is a current research topic [152–155].

Every parametrization for amplitudes should maintain the unitarity of the S-matrix. The Breit-Wigner parametrization is commonly used for isolated resonances, but does not maintain unitarity in case of multiple overlapping resonances. Another widely used parametrization for coupled-channel frameworks is the "K-matrix" approach [133, 156, 157]. The operator relation of the T-matrix in Eq. (2.7) can be rewritten to:

$$\left(T^{-1} + i\mathbb{1}\right)^{\dagger} = T^{-1} + i\mathbb{1} \ . \tag{2.9}$$

This leads to the definition of K-matrix given by:

$$K^{\dagger} \equiv T^{-1} + i\mathbb{1} \ . \tag{2.10}$$

The T-matrix in terms of K can be written as:

$$T = K\left(\mathbb{1} - iK\right)^{-1} = \left(\mathbb{1} - iK\right)^{-1} K \ . \tag{2.11}$$

To obtain a unitary S-matrix, one has to parameterize K in a way that it is real and symmetric. Apart from that, there is a lot of freedom in choosing a form of K. Some studies use a K-matrix approximation, in which the real dispersive parts of intermediate states are neglected, which breaks analyticity of the amplitude [158].

For the case of $2 \to 2$ scattering, the amplitudes are functions of the Mandelstam variables. In fact, these amplitudes are analytic (complex differentiable) functions of these external invariants up to poles, branch points and branch cuts. Branch points occur whenever a new channel becomes available: $s_{thr} = (m_{1,a} + m_{2,a})^2$, where $m_{i,a}$ denote the masses of the two particles in channel a. These channels introduce a square-root singularity. There exist two solutions to the equation $x = y^2$: $\sqrt{x}$ and $-\sqrt{x}$, which are represented as two "Riemann sheets" in the complex plane. Thus, each square-root from a channel opening doubles the number of Riemann sheets. Each branch point has an associated branch cut. The usual convention is that those cuts run from the corresponding threshold to infinity and are called "right-hand cuts". Note, that there is a freedom of choosing the direction of the cuts. In the Jülich-Bonn framework, these right hand cuts are rotated towards the negative imaginary axis [111, 113]. One can make an analytic continuation by continuing the Mandelstam variable s into the complex plane. The Riemann sheet related to the positive imaginary part is called the "physical sheet". The other sheets are called "unphysical sheets".

The physical sheet is free of singularities apart from the cut on the real axis (except for bound states). Note, that there can also be left-hand cuts originating from thresholds in the crossed channels. This originates from the principle of analyticity of the S-matrix and is inherently linked to causality. Causality ensures that effects follow their causes in chronological order.

On the unphysical sheets one can find poles and branch points. The poles of the amplitude can be characterised as:

- Bound states: Poles on the real axis below threshold on the physical sheet,
- Virtual states: Poles on the real axis below threshold on the unphysical sheet,
- Resonances: Poles inside the complex plane on the unphysical sheet.

Furthermore, analyticity leads to each pole in the complex plane at s_P having a second pole at its complex conjugate s_P^*. This originates from the "Schwarz reflection principle":

$$T(s)^* = T(s^*)\,. \tag{2.12}$$

These singularities, poles and branch points determine the visible structures in physical observables, of which one can only measure the values on the real axis. However, not every bump or peak in the observables relates to a resonance. Note also, that not all resonances lead to visible structures in observables. For example, the Roper resonance in the baryon sector $N(1440)1/2^+$ did not occur in the πN-observables or phase shift, however detailed analyses still found this pole in the complex plane [159].

2.2. Quantum Chromodynamics

Quantum Chromodynamics (QCD) is the nonabelian gauge theory of the color $SU(3)_C$ [3, 151]. In the Standard Model the quarks are the only fermions that carry color charge and they exist in 6 flavors (u, d, s, c, b, t). Furthermore, the gauge bosons for the strong interaction are the 8 gluons and these carry color charge themselves. The Lagrangian of QCD is given by:

$$\mathcal{L}_{QCD} = -\frac{1}{4}F^{a,\mu\nu}F^{a}_{\mu\nu} + \sum_{\alpha} \bar{\psi}^{\alpha}_{j}(i\not{D}_{jk} - m^{\alpha}\delta_{jk})\psi^{\alpha}_{k} + \dots \ , \tag{2.13}$$

where ψ^{α}_{k} defines the quark field of the flavor α and color k. The omitted terms, indicated by "…", include the gauge-fixing and ghost-field contributions that arise in the quantization of the non-abelian gauge theory [151]. The covariant derivative is defined by:

$$D^{ab}_{\mu} = \partial_{\mu}\delta^{ab} + igT^{ab}_{c}A^{c}_{\mu} \ , \tag{2.14}$$

where T^{ab}_{c} are the $SU(3)$ generators in the adjoint representation. The gluon field strength tensor is given by:

$$F^{a}_{\mu\nu} = \partial_{\mu}A^{a}_{\nu} - \partial_{\nu}A^{a}_{\mu} - gf^{abc}A^{b}_{\mu}A^{c}_{\nu} \tag{2.15}$$

with the gluon fields A^{a}_{μ} $(a = 1, \dots, 8)$ and f^{abc} being the totally antisymmetric structure constants of $SU(3)$ defined by $\left[T^{a}, T^{b}\right] = if^{abc}T_{c}$. The quarks and antiquarks transform under the fundamental and anti-fundamental representation in this gauge theory. Note, in QED one deals with the abelian gauge group $U(1)$ for the gauge field of the photon and the last term of the field strength tensor is absent $F^{\mathrm{QED}}_{\mu\nu} = \partial_{\mu}A_{\nu} - \partial_{\nu}A_{\mu}$.

There is another additional gauge invariant term of mass dimension 4 called the QCD-θ term given by [3]:

$$\mathcal{L}^{\theta}_{QCD} = \frac{g^{2}\theta}{32\pi^{2}}\epsilon^{\mu\nu\alpha\beta}F^{a}_{\mu\nu}F^{a}_{\alpha\beta} \ . \tag{2.16}$$

This term transforms odd under parity and even under charge conjugation. Thus, it is a CP-violating term, but has yet not been observed by experiments, i.e. strong interaction seems to preserve CP-symmetry. An upper bound was derived from the existing upper bound of the neutron electric dipole moment as $\theta \leq 2.5 \times 10^{-10}$ [160]. Up to now there is no explanation, why this term is so small.

Compared to Quantum Electrodynamics (QED) there is a significant difference when it comes to QCD, which is the renormalization of the coupling constants:

$$\beta(g_{r}) = -\left(11 - \frac{2n_{f}}{3}\right)\frac{g^{3}}{16\pi^{2}} + \mathcal{O}\left(g^{5}\right) \ , \tag{2.17}$$

where n_{f} is the number of flavors. At one loop order one finds the solution:

$$\alpha_{s}(Q^{2}) = \frac{g_{r}(Q^{2})^{2}}{4\pi} = \frac{2\pi}{\left(11 - \frac{2n_{f}}{3}\right)}\frac{1}{\log\left(\frac{Q^{2}}{\Lambda_{QCD}}\right)} \ . \tag{2.18}$$

This leads to the phenomenon of "running coupling", where α_s decreases for larger Q^2, but increases for small Q^2. This is different to QED, where the coupling is small for low momentum transfers $\alpha_{em}(Q^2 = 0) \approx 1/137$ and rises for increasing Q^2. We further have introduced an energy scale $\Lambda_{QCD} \approx 200\,\text{MeV}$ which is a fundamental parameter of QCD. QCD perturbation theory is usually applicable, if mass scales large compared to this scale are probed $(\Lambda_{QCD}/M)^2 \ll 1$. In the low energy region one has to use other methods such as the concept of effective field theories.

2.3. Effective Field Theory and Chiral Perturbation Theory

In physics there are many different areas studying phenomena at different scales (e.g. length, time, energy or mass). In particle physics the range of observed particle masses is large. Neglecting neutrino masses, the masses of the fermions in the Standard Model ranges from the electron mass $m_e \approx 0.5$ MeV up to the top quark of $m_t \approx 170$ GeV. However, one can calculate the spectrum of e.g. the hydrogen atom with high accuracy without considering the top-quark at all. Thus, one can neglect effects of much heavier particles in such a theory. When studying a certain energy range of particles, one needs to identify the relevant degrees of freedom of this energy regime. Weinberg stated, that one only needs to write out the most general Lagrangian including all terms consistent with all relevant symmetries [161]. One further needs to establish a power counting to then get proper amplitudes up to a given order in the expansion.

A nice example for this is light-by-light scattering at energies much lower than the electron mass $E \ll m_e$ in QED. One can then write down an effective Lagrangian only considering photons as the respective degrees of freedom: $\mathcal{L}_{\text{QED}}[\psi, \bar{\psi}, A_\mu] \to \mathcal{L}_{\text{eff}}[A_\mu]$. However, the electrons of the underlying full theory also contribute to the photon-photon scattering (e.g. via box diagrams). These diagrams of the underlying theory then determine the coupling constants in the effective theory of the invariant terms of the Lagrangian (in this case orders of $(F_{\mu\nu}F^{\mu\nu})^2$ and $(F_{\mu\nu}\tilde{F}^{\mu\nu})^2$). This effective theory for light-by-light scattering is known as the Euler-Heisenberg effective Lagrangian [162].

Now let us consider the strong interaction, where the underlying theory is QCD. Many hadron states exist above the mass scale of $\Lambda_{\text{had}} \approx 1$ GeV for mesons and baryons. There are only a few hadrons lighter than this. QCD is formulated in terms of gluons and quarks, while the relevant degrees of freedom at low energies are the hadrons. Let us investigate the theory of the three light quark flavors (u, d, s), which are relevant in light baryon spectroscopy. The QCD Lagrangian is given by

$$\mathcal{L}_{QCD} = -\frac{1}{4} F^{a,\mu\nu} F^a_{\mu\nu} + \bar{q}(i\not{D} - M)q \ , \tag{2.19}$$

where q are the light quark fields $q^T = (u, d, s)$ and M is the quark mass matrix $M = \text{diag}(m_u, m_d, m_s)$. We can decompose the quark fields into their chiral components by:

$$q = \frac{1}{2}(1 - \gamma_5)q + \frac{1}{2}(1 + \gamma_5)q = P_L q + P_R q = q_L + q_R \ , \tag{2.20}$$

where we introduced the left-handed q_L and right-handed q_R quark fields. Using the properties of the Dirac-matrices γ_i, one can rewrite the Lagrangian to:

$$\mathcal{L}_{QCD} = \bar{q}_L i \not{D} q_L + \bar{q}_R i \not{D} q_R - \bar{q}_L M q_R - \bar{q}_R M^\dagger q_L - \frac{1}{4} F^{a,\mu\nu} F^a_{\mu\nu} \ . \tag{2.21}$$

This Lagrangian obeys symmetries like Lorentz-invariance, $SU(3)_C$ gauge invariance as well as P, C and T. Note that the masses of the three lightest quarks are much smaller than Λ_{QCD}. This motivates the study of an effective field theory in the case $M = 0$. In such a limit, the Lagrangian has a global symmetry

$$U(3)_L \times U(3)_R = SU(3)_L \times SU(3)_R \times U(1)_V \times U(1)_A \ , \tag{2.22}$$

where we introduced the vector $V = L + R$ and the axial vector $A = L - R$ transformations, which transform left- and right-handed fields, accordingly. This symmetry is called the "chiral symmetry" and the limit of vanishing light quark masses is called the "chiral limit". Each of these symmetry groups exhibit an associated Noether current. The $U(1)_V$ symmetry is connected to the conservation of baryon number, which is fulfilled in the Standard Model. The associated current for the $U(1)_A$-symmetry is not conserved, since the symmetry is broken by the $U(1)_A$-anomaly. The currents connected to $SU(3)_L \times SU(3)_R$ are explicitly broken by the quark masses. In nature the chiral symmetry is realized in the Nambu-Goldstone mode [163, 164]. The Vafa-Witten theorem states that the vector subgroup remains unbroken [165]. However, the axial charges do not leave the ground state invariant. Goldstone's theorem states that such a spontaneously symmetry breaking leads to the appearance of massless spin-0 particles, which are called "Goldstone bosons" [163, 164]. The spontaneous breaking of the chiral symmetry leads to the existence of 8 Goldstone bosons, which are identified with the 8 lightest pseudoscalar mesons $(\pi^\pm, \pi^0, K^\pm, K^0, \bar{K}^0, \eta)$. These are massless in the chiral limit.

The effective field theory describing low-energy strong interactions is the so called "chiral perturbation theory" (ChPT). Here, we give an outline on how to construct an effective theory for the Goldstone bosons.

One can build a unitary matrix U containing the Goldstone boson fields [166]:

$$U = \exp\left(\frac{i\sqrt{2}\Phi}{F_\pi}\right), \quad \Phi = \begin{pmatrix} \frac{\pi^0}{\sqrt{2}} + \frac{\eta}{\sqrt{6}} & \pi^+ & K^+ \\ \pi^- & -\frac{\pi^0}{\sqrt{2}} + \frac{\eta}{\sqrt{6}} & K^0 \\ K^- & \bar{K}^0 & -\frac{2\eta}{\sqrt{6}} \end{pmatrix}, \tag{2.23}$$

where F_π is the pion decay constant in the chiral limit. Under the chiral group with transformations $(R, L) \in SU(3)_L \times SU(3)_R$ the Goldstone boson fields U transform as

$$U \to L U R^\dagger \ . \tag{2.24}$$

In this effective theory the momenta of the Goldstone bosons p_{GB} are small compared to the typical hadronic scale $\Lambda_{\mathrm{had}} \approx 1$ GeV. Thus, one can expand the terms of the Lagrangian in orders of $p_{\mathrm{GB}}/\Lambda_{\mathrm{had}}$ and introduce a power counting. Lorentz invariance demands that the Lagrangian terms only come in even powers of derivatives (and thus momenta):

$$\mathcal{L} = \sum_n \mathcal{L}^{(2n)}, \quad \mathcal{L}^{(2n)} = \mathcal{O}\left(\left(\frac{p_{\mathrm{GB}}}{\Lambda_{\mathrm{had}}}\right)^{2n}\right) . \tag{2.25}$$

The term $\mathcal{L}^{(0)}$ can only be a constant and from Goldstone's theorem one finds that the leading term is given by $\mathcal{L}^{(2)}$:

$$\mathcal{L}^{(2)} = \frac{F^2}{4}\langle \partial_\mu U \partial^\mu U^\dagger \rangle . \tag{2.26}$$

where $\langle \dots \rangle$ defines the trace in flavor space. A general formalism to build an effective Lagrangian with a spontaneously broken symmetry and taking into account anomalies, that we neglected here, is presented in Refs [167, 168].

Furthermore, there are electromagnetic effects that one needs to take into account in ChPT. At higher orders, one also needs to include loop diagrams. A power counting scheme to determine which terms are needed at each order was established by Weinberg [161]. The coupling constants in ChPT are called low-energy constants (LEC) and they include effects of heavy degrees of freedom. These LECs cannot be determined by the underlying theory of QCD, but will be extracted from fits to experimental data or lattice QCD.

We are interested in the field of baryon spectroscopy. Baryon masses are much larger than Goldstone bosons. Nevertheless, the lightest ground state baryons can be included in the ChPT formalism as matter fields and one can build a chiral Lagrangian including both Goldstone bosons and those matter fields. To construct a meson-baryon Lagrangian, one needs to choose a suitable representation and tranformation law for the baryons. It is convenient to introduce the new field u for the Goldstone boson fields, which is related to U by $u^2 = U$. The transformation property is given as

$$u \to \sqrt{LUR^\dagger} = LuK^\dagger(L,R,U) = K(L,R,U)uR^\dagger , \tag{2.27}$$

where we introduced the so called "compensator field" $K(L,R,U)$, that depends on L, R and U in the following way [169]

$$K(L,R,U) = \sqrt{LU^\dagger R^\dagger}R\sqrt{U} . \tag{2.28}$$

The representation for the baryons is given by

$$B = \begin{pmatrix} \frac{\Sigma^0}{\sqrt{2}} + \frac{\Lambda}{\sqrt{6}} & \Sigma^+ & p \\ \Sigma^- & -\frac{\Sigma^0}{\sqrt{2}} + \frac{\Lambda}{\sqrt{6}} & n \\ \Xi^- & \Xi^0 & -\frac{2\Lambda}{\sqrt{6}} \end{pmatrix} . \tag{2.29}$$

The baryon fields transform as $B \to KBK^\dagger$. In contrast to the case of only mesons before, the meson-baryon Lagrangian now allows for odd powers of momenta due to the presence of spin (Dirac structures). The leading order term is given by

$$\mathcal{L}^{(1)}_{\phi B} = \langle \bar{B}(i\not{D} - mB\rangle + \frac{D}{2}\langle \bar{B}\gamma_\mu\gamma^5 \left[\Delta^\mu, B\right]_+\rangle + \frac{F}{2}\langle \bar{B}\gamma_\mu\gamma^5 \left[\Delta^\mu, B\right]_-\rangle , \tag{2.30}$$

where we introduced the covariant derivative D^μ and the chiral vielbein Δ^μ, which transform as $D^\mu B \to K D^\mu B K^\dagger$ and $\Delta^\mu \to K \Delta^\mu K^\dagger$ [169, 170]. The new parameters D and F are the two axial vector couplings in $SU(3)$, which can be determined from semileptonic hyperon decays and have to fulfill the $SU(2)$ constraint $D+F = g_A$. The axial vector coupling g_A is known from neutron beta decays as $g_A = 1.26$. For the case of only considering chiral $SU(2)$ to study pions and nucleons, the leading order is given by

$$\mathcal{L}_{\pi N}^{(1)} = \bar{\Psi} \left(i\not{D} - m + \frac{g_A}{2} \gamma_\mu \gamma^5 \Delta^\mu \right) \Psi \ , \tag{2.31}$$

where Ψ is the nucleon field

$$\Psi = \begin{pmatrix} p \\ n \end{pmatrix} \ , \tag{2.32}$$

which transforms as $\Psi \to K\Psi$.

The new mass scale of the baryons breaks the power counting scheme used for the Goldstone bosons [171]. Further methods like heavy-baryon chiral perturbation theory [172–174], infrared regularizations [175] or extended on-mass shell schemes [176, 177] need to be employed to resolve this problem.

There are different approaches developed from ChPT to study the low-energy regime of the strong interaction. One example is the unitarized perturbation theory, in which a scattering kernel is derived from a chiral Lagrangian and iterated in a Bethe-Salpeter equation. This allows one to study some baryon resonances in a few partial waves. There are also coupled-channel calculations where resonances can be dynamically generated [178–183]. Furthermore, the πN-scattering in the low energy regime is completely understood in ChPT [184, 185]. But for the complete resonance spectrum at medium energies one needs further model assumptions for a proper description. Further details on ChPT developments can be found Refs. [169, 186–190].

Although the present work does not employ chiral perturbation theory in the strict perturbative sense, the interaction kernel in the Jülich-Bonn framework is based on the Wess-Zumino Lagrangian [191], which provides an effective chiral description of the relevant meson-baryon dynamics.

2.4. Gerasimov-Drell-Hearn sum rule

The Gerasimov-Drell-Hearn (GDH) sum rule [192, 193] is derived from fundamental principles of Quantum Field Theory. It allows one to study the spin structure of the nucleon experimentally [194–198]. Even though the value of the nucleon spin is known, one challenge that remains is to quantify individual contributions from different reaction channels. The GDH sum rule is a relation that connects the anomalous magnetic moment κ_N of the nucleon to the integrated difference of the total helicity-dependent photoproduction cross-sections $\Delta\sigma = \sigma_{3/2} - \sigma_{1/2}$, which involves all possible photon-induced final-states:

$$I_{\mathrm{GDH}} = \int_{E_\gamma^0}^{\infty} \mathrm{d}E_\gamma \, \frac{\Delta\sigma(E_\gamma)}{E_\gamma} = \frac{4\pi^2 S \alpha \kappa^2}{M^2} \, , \tag{2.33}$$

where M is the mass of the target particle, S is its spin, E_γ^0 the pion-photoproduction threshold and $\alpha = e^2/4\pi$ is the fine-structure constant in terms of the electromagnetic coupling constant e. For the case of a nucleon target we have:

$$I_{\mathrm{GDH}} = \int_{E_\gamma^0}^{\infty} \mathrm{d}E_\gamma \, \frac{\Delta\sigma(E_\gamma)}{E_\gamma} = \frac{2\pi^2\alpha\kappa_N^2}{M_N^2} \, . \tag{2.34}$$

There is more than one method to derive the GDH-sum rule. A dispersion theoretical approach was used by Gerasimov, Drell and Hearn [192, 193]. There is also a derivation using the current algebra as done by Hosoda and Yamamoto [199] and another way using current algebra on the light cone as it was done by Dicus and Palmer [200]. We will outline the dispersion theoretical derivation in the following, since it is illustrative to understand the different fundamental principles entering. For a more detailed derivation we refer to Refs. [197, 201].

Derivation of the GDH sum rule

The dispersion theoretical derivation need the following assumptions: Lorentz invariance, gauge invariance, unitarity, causality, crossing symmetry and rotational invariance. These are all fundamental principles that are used in modern relativistic quantum field theories and makes the confirmation of the GDH sum rule an important check of modern physics.

The derivation starts with the Compton scattering off spin-1/2 particles. If one considers virtual or real photons, one would have in general 16 helicity amplitudes that depend on the Mandelstam variables s and t [202]. From parity invariance the number already decreases to 8 amplitudes and time reversal invariance further reduces them to 6 [203]. We restrict our derivation to real photons and adopt the Coulomb gauge $\epsilon^0 = 0$. We define the incoming (outgoing) photon polarization by $\vec{\epsilon}_1$ ($\vec{\epsilon}_2$) and their momenta by $\vec{k}_1$ ($\vec{k}_2$). From crossing symmetry we find that the Compton scattering amplitude is symmetric under the exchange of the incoming and outgoing photons ($\vec{k}_1 \leftrightarrow -\vec{k}_2$ and $\vec{\epsilon}_1 \leftrightarrow \vec{\epsilon}_2^{\,*}$). Thus, the Compton amplitude has the property:

$$F(\vec{k}_1, \vec{k}_2, \vec{\epsilon}_1, \vec{\epsilon}_2) = F(-\vec{k}_2, -\vec{k}_1, \vec{\epsilon}_2^{\,*}, \vec{\epsilon}_1^{\,*}) \, . \tag{2.35}$$

We now restrict this derivation to forward scattering where $\vec{k} = \vec{k}_1 = \vec{k}_2$ and switch into the nucleon rest frame. Then the amplitude F can be written as a linear combination of scalar functions f_i:

$$\begin{aligned} F = \Big\langle \chi_2^\dagger \Big| \, & f_1(\vec{\epsilon}_2^{\,*} \cdot \vec{\epsilon}_1) + f_2 i\vec{\sigma}(\vec{\epsilon}_2^{\,*} \times \vec{\epsilon}_1) + f_3(\vec{\epsilon}_2^{\,*} \cdot \vec{k})(\vec{\epsilon}_1 \cdot \vec{k}) + f_4 i\vec{\sigma}\Big(\vec{\epsilon}_2^{\,*}(\vec{\epsilon}_1 \cdot \vec{k}) - \vec{\epsilon}_1(\vec{\epsilon}_2^{\,*} \cdot \vec{k})\Big) \\ & + f_5 i\vec{\sigma}\Big((\vec{\epsilon}_2^{\,*} \times \vec{k})(\vec{\epsilon}_1 \cdot \vec{k}) - (\vec{\epsilon}_1 \times \vec{k})(\vec{\epsilon}_2^{\,*} \cdot \vec{k})\Big) \, |\chi_1\rangle \ , \end{aligned} \tag{2.36}$$

where $\vec{\sigma}$ is the vector of Pauli spin matrices and $\chi_{1,2}$ define the incoming and outgoing nucleon spinors. We can further reduce the number of relevant terms by considering

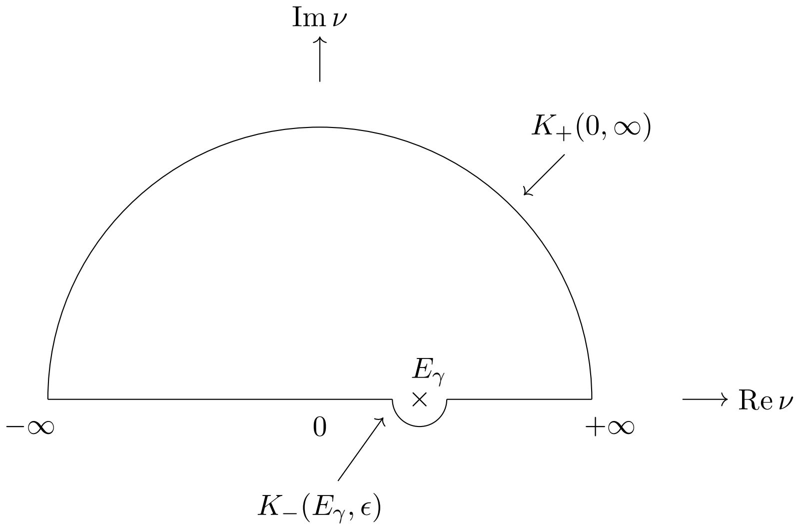

Figure 5: Sketch of the integration path $\mathcal{C}$ of Eq. (2.39).

the transversality condition for real photons $\vec{\epsilon}\cdot\vec{k} = 0$. This leaves us with two terms contributing to the forward scattering amplitude:

$$F(\theta = 0, E_\gamma) = \left\langle \chi_2^\dagger \right| f_1(E_\gamma)(\vec{\epsilon}_2^{\,*}\cdot\vec{\epsilon}_1) + f_2(E_\gamma) i\vec{\sigma}(\vec{\epsilon}_2^{\,*}\times\vec{\epsilon}_1) \left|\chi_1\right\rangle \ . \tag{2.37}$$

We now consider our z-axis along the photon momentum. Note, that we only need to distinguish two orientations of nucleon and photon spins, which are parallel (3/2) and anti-parallel (1/2). We can then write the Compton amplitude for these spin configurations as:

$$f_{3/2}(E_\gamma) = f_1(E_\gamma) - f_2(E_\gamma), \quad f_{1/2}(E_\gamma) = f_1(E_\gamma) + f_2(E_\gamma) \ . \tag{2.38}$$

Causality lets us analytically continue the forward scattering amplitude to complex values of photon energies E_γ. This lets us apply Cauchy's integral formula:

$$f(E_\gamma) = \frac{1}{2\pi i}\oint_{\mathcal{C}} \mathrm{d}\nu\, \frac{f(\nu)}{\nu - E_\gamma} \ . \tag{2.39}$$

The integration path $\mathcal{C}$ (sketched in Fig. 5) is chosen as a half-circle in the upper half plane with a smaller half circle in the lower half plane with its center at the pole position $\nu = E_\gamma$. Labeling the upper half circle at infinity $K_+(0,\infty)$ and the smaller one $K_-(E_\gamma,\epsilon)$, we can write

$$\begin{aligned} f(E_\gamma) =& \frac{1}{2\pi i}\mathcal{P}\int_{-\infty}^{\infty} \mathrm{d}\nu\, \frac{f(\nu)}{\nu - E_\gamma} + \frac{1}{2\pi i}\int_{K_+(0,\infty)} \mathrm{d}\nu\, \frac{f(\nu)}{\nu - E_\gamma} \\ &+ \lim_{\epsilon\to 0}\frac{1}{2\pi i}\int_{K_-(E_\gamma,\epsilon)} \mathrm{d}\nu\, \frac{f(\nu)}{\nu - E_\gamma} \ . \end{aligned} \tag{2.40}$$

with the Cauchy principle value

$$\mathcal{P}\int_{-\infty}^{\infty} = \lim_{\epsilon\to 0}\left[\int_{-\infty}^{\nu-\epsilon} + \int_{\nu+\epsilon}^{\infty}\right] \ . \tag{2.41}$$

The integral over $K_-(E_\gamma, \epsilon)$ is equal to half the residue of a full circle $f(E_\gamma)/2$. We assume that the integral over $K_+(0,\infty)$ vanishes, which is called the "No-subtraction hypthesis" and we refer to Refs. [197, 204] for remarks on its validity. We are then left with:

$$f(E_\gamma) = \frac{1}{\pi i}\mathcal{P}\int_{-\infty}^{\infty} \mathrm{d}\nu\, \frac{f(\nu)}{\nu - E_\gamma} \ . \tag{2.42}$$

We can now use the crossimg property of the Compton scattering amplitude $F(\theta = 0, -E_\gamma) = F^*(\theta = 0, E_\gamma)$ to find:

$$f_1(-E_\gamma) \ = \ f_1^*(E_\gamma) \tag{2.43}$$

$$f_2(-E_\gamma) \ = \ -f_2^*(E_\gamma) \tag{2.44}$$

$$\frac{f_2(-E_\gamma)}{-E_\gamma} \ = \ \frac{f_2^*(E_\gamma)}{E_\gamma} \ . \tag{2.45}$$

Note, because of the properties found here we can go on with the crossing relation to find the Kramer-Kronig dispersion relations for f_1 and f_2/E_γ but not f_2. Eq. (2.42) can then be rewritten to:

$$f(E_\gamma) = \frac{1}{\pi i}\mathcal{P}\int_0^{\infty} \mathrm{d}\nu \left(\frac{f(\nu)}{\nu - E_\gamma} + \frac{f^*(\nu)}{-\nu - E_\gamma}\right) \tag{2.46}$$

$$= \frac{1}{\pi i}\mathcal{P}\int_0^{\infty} \mathrm{d}\nu\, \frac{2i\nu\,\mathrm{Im}\, f(\nu) + 2E_\gamma\,\mathrm{Re}\, f(\nu)}{\nu^2 - E_\gamma^2} \ . \tag{2.47}$$

Now we can only consider the real part and simplify this to the Kramer-Kronig dispersion relations for f_1 and f_2/E_γ:

$$\mathrm{Re}\, f_1(E_\gamma) \ = \ \frac{2}{\pi}\mathcal{P}\int_0^{\infty} \mathrm{d}\nu\, \nu \frac{\mathrm{Im}\, f_1(\nu)}{\nu^2 - E_\gamma^2} \ , \tag{2.48}$$

$$\mathrm{Re}\, \frac{f_2(E_\gamma)}{E_\gamma} \ = \ \frac{2}{\pi}\mathcal{P}\int_0^{\infty} \mathrm{d}\nu\, \nu \frac{\mathrm{Im}\, f_2(\nu)/\nu}{\nu^2 - E_\gamma^2} \ . \tag{2.49}$$

Another important relation is the "optical theorem". It is derived from the unitarity of the S-matrix and it relates the elastic forward scattering amplitude to the total cross section:

$$\mathrm{Im}\, F(E_\gamma) = \frac{E_\gamma}{4\pi}\sigma \ . \tag{2.50}$$

Using the found relations for the amplitudes f_1 and f_2 one obtains:

$$\mathrm{Im}\, f_1(E_\gamma) \ = \ \frac{E_\gamma}{4\pi}(\sigma_{1/2}(E_\gamma) + \sigma_{3/2}(E_\gamma)) \ , \tag{2.51}$$

$$\mathrm{Im}\, \frac{f_2(E_\gamma)}{E_\gamma} \ = \ \frac{1}{4\pi}(\sigma_{1/2}(E_\gamma) - \sigma_{3/2}(E_\gamma)) \ . \tag{2.52}$$

Note that the cross section here included elastic and inelastic contributions (photoabsorption and Compton scattering). However, if one considers Compton forward scattering up to the lowest non-trivial order in the electromagnetic coupling with intermediate hadronic states

$$\mathcal{F} = i\frac{e^2}{16\pi M}\epsilon^*_\mu\epsilon_\nu \int \mathrm{d}^4x\, e^{ikx} \sum_{X_{had}} \langle p', s'|\, J^\mu(x)\, |X_{had}\rangle \langle X_{had}|\, J^\nu(0)\, |p, s\rangle \ . \tag{2.53}$$

one then finds the optical theorem to instead only include the photoabsorption cross section σ_{abs} [197]

$$\mathrm{Im}\, \mathcal{F}(E_\gamma) = \frac{E_\gamma}{4\pi}\sigma_{abs} \ . \tag{2.54}$$

Even though only the first non-vanishing order was used here, only further radiative corrections need to be included at higher orders.

Now that we have found the imaginary parts, we are left with determining the real parts for f_1 and f_2/E_γ. For this we explore the low-energy theorems obtained by Low [205] and Gell-Mann and Goldberger [206]. The proof is based on crossing symmetry, Lorentz invariance and gauge invariance. It is based on the principle of minimal coupling including the anomalous magnetic moment κ [207]. The Dirac equation for the nucleon is modified to:

$$\left(i\partial\!\!\!/ - eA\!\!\!/ - \frac{\kappa\mu_N}{2}\sigma_{\mu\nu}F^{\mu\nu} - M_N\right)\psi = 0 \ , \tag{2.55}$$

with $\mu_N = e/(2M_N)$. Considering forward scattering and expressions up to linear order in the photon momentum k, one finds the following expression after simplifying:

$$f(E_\gamma) = -\frac{\alpha}{M_N}\vec{\epsilon}^{\,*}_2 \cdot \vec{\epsilon}_1 - \frac{\alpha}{2M_N^2}\kappa^2 E_\gamma i\vec{\sigma} \cdot (\vec{\epsilon}^{\,*}_2 \times \vec{\epsilon}_1) \ . \tag{2.56}$$

This expression is the lowest order result. If one would expand one order further and identify the terms with f_1 and f_2 respectively, one arrives at:

$$f_1(E_\gamma) \quad = \quad -\frac{\alpha}{M_N} + (\alpha_E + \beta_M)E_\gamma^2 + \mathcal{O}(E_\gamma^4) \ , \tag{2.57}$$

$$\frac{f_2(E_\gamma)}{E_\gamma} \quad = \quad -\frac{\alpha}{2M_N^2}\kappa^2 + \gamma_0 E_\gamma^2 + \mathcal{O}(E_\gamma^4) \ . \tag{2.58}$$

Note that f_1 is an even and f_2 is an odd function of E_γ, as we found with their properties from crossing symmetry. The leading term $f_1(0)$ is called the Thomson term and the terms at order E_γ^2 describes the Rayleigh scattering with the electric α_E and magnetic β_M dipole polarizabilities, which are describe the internal nucleon structure. For the terms in f_2/E_γ, we identify the leading term with the anomalous magnetic moment and the quadratic term with the forward spin polarizability γ_0, which is connected to the spin structure of the nucleon.

Finally, we can connect all relations found up to now. At first we insert the optical theorem relations (2.51) and (2.52) into the right hand side of the Kramer-Kronig dispersion relations:

$$\mathrm{Re}\, f_1(E_\gamma) = \frac{1}{4\pi^2}\mathcal{P}\int_0^\infty \mathrm{d}\nu\, \nu^2 \frac{\sigma_{1/2}(\nu)+\sigma_{3/2}(\nu)}{\nu^2 - E_\gamma^2}\,, \tag{2.59}$$

$$\mathrm{Re}\, \frac{f_2(E_\gamma)}{E_\gamma} = \frac{1}{4\pi^2}\mathcal{P}\int_0^\infty \mathrm{d}\nu\, \nu \frac{\sigma_{1/2}(\nu)-\sigma_{3/2}(\nu)}{\nu^2 - E_\gamma^2}\,. \tag{2.60}$$

We now want to compare these to the results found in the low-energy expansion. In the limit $E_\gamma \to 0$, one finds for f_2/E_γ:

$$\lim_{E_\gamma\to 0} \mathrm{Re}\, \frac{f_2(E_\gamma)}{E_\gamma} = \frac{1}{4\pi^2}\int_0^\infty \mathrm{d}\nu\, \frac{\sigma_{1/2}(\nu)-\sigma_{3/2}(\nu)}{\nu}\,. \tag{2.61}$$

Now we can insert the leading term of Eq. (2.58) into the left hand side of the relation to arrive at the GDH sum rule [192, 193]:

$$\frac{\alpha\kappa^2}{2M_N^2} = \frac{1}{4\pi^2}\int_0^\infty \mathrm{d}\nu\, \frac{\sigma_{3/2}(\nu)-\sigma_{1/2}(\nu)}{\nu}\,. \tag{2.62}$$

Using current values from the PDG [5] for the anomalous magnetic moment κ and the nucleon masses M_N of the target particle one can calculate the right hand side of Eq. (2.34) for proton and neutron targets:

$$I^p_{\mathrm{GDH}} \equiv \int_{E_\gamma^0}^\infty \mathrm{d}E_\gamma\, \frac{\Delta\sigma^p(E_\gamma)}{E_\gamma} = \frac{2\pi^2\alpha\kappa_p^2}{M_p^2} \approx 204.784\,482(35)\,\mu\mathrm{b}\,, \tag{2.63}$$

$$I^n_{\mathrm{GDH}} \equiv \int_{E_\gamma^0}^\infty \mathrm{d}E_\gamma\, \frac{\Delta\sigma^n(E_\gamma)}{E_\gamma} = \frac{2\pi^2\alpha\kappa_p^2}{M_n^2} \approx 232.251\,59(13)\,\mu\mathrm{b}\,. \tag{2.64}$$

Note, that we replaced the lower limit of the integral by E_γ^0, which is the pion-photoproduction threshold. It is the lowest possible threshold in a photoproduction process. In Chapter 6 we will investigate whether our model satisfies the GDH sum rule. Furthermore, our coupled-channel approach allows us to calculate the individual channel contributions, which we will also discuss.

3. Jülich-Bonn dynamical coupled-channel model

In this section, we introduce the Jülich-Bonn dynamical coupled-channel (DCC) approach [1, 33, 103–118]. First we start by deriving the scattering equation of the JüBo model for pion-induced reactions. We also give an overview on the channel space and the effective three body channel $\pi\pi N$. We further explain how the potential in our framework is constructed and how the nucleon pole is treated. At last we present the extension to photoproduction processes and the determination of resonance parameters.

3.1. Scattering Equation

The Jülich-Bonn model is a dynamical coupled-channel approach, which was originally used to describe elastic pion-nucleon scattering close to threshold [103]. The formalism for πN scattering is based on a coupled-channel meson exchange model [208].

The scattering of two relativistic particles is described by the covariant Bethe-Salpeter equation [209], which is given in operator form as

$$T = K + KGT \; , \tag{3.1}$$

where T is the T-matrix, G is the relativistic two-particle propagator and K is the scattering kernel. The scattering kernel K includes all irreducible diagrams. Consequently, K includes an infinite series of diagrams. To perform proper calculations one has to truncate K and this approximated scattering kernel is called the pseudopotential V. The scattering equation in momentum space is then given by:

$$T(p,p',W) = V(p,p',W) - \frac{i}{(2\pi)^4}\int \mathrm{d}^4q\, V(p,q,W)\, G(q,W)\, T(q,p',W) \; , \tag{3.2}$$

where W denotes the center-of-mass energy and q (p', p) are the intermediate (incoming, outgoing) momenta.

In this framework the formalism of time-ordered (*old-fashioned*) perturbation theory (TOPT) [151, 210, 211] and the Haftel-Tabakin scheme [212] are used to solve this four-dimensional scattering equation. The advantage of the non-covariant TOPT approach is that it gives us a specific prescription for the construction of the off-shell potentials. Moreover, all integrals, that need to be determined, are three dimensional. However, one needs to explicitly consider each time ordering, which increases the number of diagrams to be calculated (see Fig. 7).

TOPT is based on the Hamiltonian formulation. Starting from the Lagrangian density, the Hamiltonian density is obtained through the Legendre transformation

$$\mathcal{H} = \sum_j \frac{\delta\mathcal{L}}{\delta\dot{\phi}_j}\dot{\phi}_j - \mathcal{L} \tag{3.3}$$

where the ϕ_j denotes the fields appearing in the Lagrangian. The Hamiltonian density can be written as

$$\mathcal{H} = \mathcal{H}_0 - \mathcal{L}_{\text{int}} + \mathcal{H}_{\text{ct}} \tag{3.4}$$

where $\mathcal{H}_0$ is the free Hamiltonian density, $\mathcal{L}_{\text{int}}$ is the interaction Lagrangian and $\mathcal{H}_{\text{ct}}$ contains non-covariant TOPT contact terms. Such contact terms arise when interaction terms depend on time derivatives of the fields or when non-dynamical field components are present, for example the zeroth component of a vector field [213]. One obtains the Hamiltonian via spatial integration of the density

$$H = \int \mathrm{d}^3x\, \mathcal{H}(x) = H_0 + H_I \ . \tag{3.5}$$

The S-matrix is defined by

$$S = \lim_{t\to\infty, t'\to-\infty} \hat{U}(t,t') \ , \tag{3.6}$$

where the evolution operator is given in the interaction picture as

$$\hat{U}(t,t') = e^{iH_0 t} e^{-iH(t-t')} e^{-iH_0 t'} \ . \tag{3.7}$$

For a transition from an initial state i to a final-state f, the T-matrix is introduced through

$$S_{fi} = \delta_{fi} - i2\pi\delta(E_f - E_i) T_{fi} \ . \tag{3.8}$$

Here E_i and E_f denote the initial and final energies and δ_{fi} is the unit matrix. At this point the T-matrix is defined as on-shell.

To formulate the problem as a two-body scattering equation, the transition operator is written as

$$T = H_I + H_I \frac{1}{W - H + i\epsilon} H_I = H_I + H_I \frac{1}{W - H_0 - H_I + i\epsilon} H_I \ . \tag{3.9}$$

This expression can be expanded perturbatively in H_I to obtain the series

$$T = H_I \frac{1}{1 - \mathcal{G} H_I} = H_I + H_I \mathcal{G} H_I + H_I \mathcal{G} H_I \mathcal{G} H_I + \dots \ , \tag{3.10}$$

where the Green's function $\mathcal{G}$ is given as

$$\mathcal{G} = \frac{1}{W - H_0 + i\epsilon} = \sum_n \frac{|n\rangle\langle n|}{W - E_n + i\epsilon} \ . \tag{3.11}$$

Here the sum extends over all possible multi-particle intermediate states and is meant as integration over the continuum and summation over discrete variables.

Since we are interested in two-body initial and final-states, the Green's function is split into a part containing all intermediate states except two-body ones $\tilde{\mathcal{G}}$ and a part containing only two-body states $\mathcal{G}^{(2)}$

$$\mathcal{G} = \tilde{\mathcal{G}} + \mathcal{G}^{(2)} \tag{3.12}$$

with

$$\tilde{\mathcal{G}} = \sum_{\tilde{n}} \frac{|\tilde{n}\rangle\langle\tilde{n}|}{W - E_{\tilde{n}} + i\epsilon}, \quad \mathcal{G}^{(2)} = \sum_{n^{(2)}} \frac{\left|n^{(2)}\right\rangle\left\langle n^{(2)}\right|}{W - E_{n^{(2)}} + i\epsilon} \ , \tag{3.13}$$

where $\left|n^{(2)}\right\rangle$ are the two-body states and $|\tilde{n}\rangle$ are all intermediate states except two-body ones. This separation leads to an effective two-body equation of the following form

$$T = V + V\mathcal{G}^{(2)}T \ , \tag{3.14}$$

where the effective potential is defined by

$$V = H_I \frac{1}{1-\tilde{\mathcal{G}}H_I} = H_I \sum_{k=0}^{\infty} \left(\sum_{\tilde{n}} \frac{|\tilde{n}\rangle \langle \tilde{n}| H_I}{W - E_{\tilde{n}} + i\epsilon} \right)^k \ . \tag{3.15}$$

This sum corresponds to the set of all two-body irreducible diagrams with an arbitrary number of particles in the intermediate state. These equations can be generalized for the off-shell case ($E \neq E_i \neq E_f$). One arrives at the T-matrix in matrix form:

$$T_{fi} = V_{fi} + \sum_j \frac{V_{fj}T_{ji}}{W - E_j + i\epsilon} \ . \tag{3.16}$$

Here the states i, f and j denote two-body ones and the sum stands for integration over 3-momenta of the particles and summation over the types of particles and spin variables.

In a next step, the system of reference is chosen to be the center of mass frame of the two particles. One further chooses a basis where the states are characterized by their helicities λ and isospins I. The scattering equation is then written as

$$\begin{aligned} T^I_{\mu\nu}(\vec{p},\lambda,\vec{p}',\lambda',W) &= V^I_{\mu\nu}(\vec{p},\lambda,\vec{p}',\lambda',W) \\ &+ \sum_{\kappa,\lambda_\kappa} \int \mathrm{d}^3q \, V^I_{\mu\kappa}(\vec{p},\lambda,\vec{q},\lambda_\kappa,W)\, G_\kappa(q,W)\, T^I_{\kappa\nu}(\vec{q},\lambda_\kappa,\vec{p}',\lambda',W) \ , \end{aligned} \tag{3.17}$$

where W denotes the center-of-mass energy, q (p', p) are the intermediate (incoming, outgoing) momenta, G_κ the two-body propagator and the incoming (outgoing) two body channels are given by μ (ν).

Even though the scattering equation is reduced to a three dimensional integral, solving this integral numerically is still very costly and one needs further simplifications. To reduce the dimension of the integral to one, one can make use of the rotational invariance of the strong interaction, where the scattering equation decouples into partial waves with fixed total angular momentum J. It is convenient to perform a partial wave decomposition in Eq. (3.18) and transform from the helicity- to the JLS-basis. Here J is the total angular momentum, L is the sum of orbital angular momenta and S denotes the total spin. This transformation is carried out using angular momentum algebra and Clebsch-Gordan coefficients as well as appropriate rotation matrices that connect helicity states to partial-wave states [151, 214, 215]. Note, that we use the convention of Brink and Satchler for the small d-functions [216]. The resulting scattering equation in the JLS-basis is then written as:

$$\begin{aligned} \langle LSp| T^{IJ}_{\mu\nu} |L'S'p'\rangle &= \langle LSp| V^{IJ}_{\mu\nu} |L'S'p'\rangle \\ &+ \sum_{\kappa,L_\kappa,S_\kappa} \int \mathrm{d}q\, q^2 \, \langle LSp| V^{IJ}_{\mu\kappa} |L_\kappa S_\kappa q\rangle \; G_\kappa(q) \; \langle L_\kappa S_\kappa q| T^{IJ}_{\kappa\nu} |L'S'p'\rangle \ . \end{aligned} \tag{3.18}$$

Until now, partial-waves up to $J = 9/2$ are considered in the JüBo framework.

The two-body propagator G_κ for the stable channels has the form

$$G_\kappa(p, W) = \frac{1}{W - E(p) - \omega(p) + i\epsilon} \tag{3.19}$$

with the energies $\omega = \sqrt{m_m^2 + p^2}$ and $E = \sqrt{m_b^2 + p^2}$ of the intermediate meson m and baryon b in the meson-baryon channel κ.

Decomposition of the T-matrix

The hadronic meson-baryon scattering equation can be written in a shortened notation as

$$T_{\mu\nu}(p, p', W) = V_{\mu\nu}(p, p', W) + \sum_\kappa \int_0^\infty dq\, q^2\, V_{\mu\kappa}(p, q, W) G_\kappa(q, W)\, T_{\kappa\nu}(q, p', W) \ , \tag{3.20}$$

a Lippmann-Schwinger like equation, which is consistent with two-body unitarity. In this approach the three-body unitarity is approximately fulfilled (see Ref. [152]). It is convenient to use a two-potential formalism [113, 123, 125, 217], where the potential is split into a pole and non pole part

$$V_{\mu\nu} = V_{\mu\nu}^{\mathrm{NP}} + V_{\mu\nu}^{\mathrm{P}} \tag{3.21}$$

This also decomposes the T-matrix into a pole and non-pole part

$$T = T^{\mathrm{P}} + T^{\mathrm{NP}} \ . \tag{3.22}$$

The non-pole part T^{NP} is constructed from the potentials for the t- and u-channel exchanges

$$\begin{aligned} T_{\mu\nu}^{\mathrm{NP}}(p, p', W) &= V_{\mu\nu}^{\mathrm{NP}}(p, p', W) \\ &+ \sum_\kappa \int_0^\infty dq\, q^2\, V_{\mu\kappa}^{\mathrm{NP}}(p, q, W) G_\kappa(q, W)\, T_{\kappa\nu}^{\mathrm{NP}}(q, p', W) \ , \end{aligned} \tag{3.23}$$

where V^{NP} contains the t- and u-channel exchange diagrams.

This separation into a pole and non-pole part is only for technical reasons. For the non-pole part the numerical evaluation is more time consuming than for the pole part. This way one can employ a nested fitting procedure, where for every step in the determination of fit parameters of T^{NP}, all T^{P} parameters are fully optimized.

Another advantage of our model, is that the scattering equation Eq. (3.23) for the non-pole part can dynamically generate poles. These dynamical poles are not included as genuine poles via s-channel terms. The pole part T^{P} includes the genuine s-channel pole terms and is also evaluated from the non-pole parts T^{NP} by

$$T_{\mu\nu}^{\mathrm{P}}(p, p', W) = \sum_{i,j} \Gamma_{\mu,i}^a(p)\, (D^{-1})_{ij}(W)\, \Gamma_{\nu,j}^c(p') \ , \tag{3.24}$$

where $\Gamma^a_{\mu,i}$ is the dressed vertex function which describes the annihilation of the i-th resonance in a given partial wave into channel μ, and $\Gamma^c_{\nu,j}$ is the dressed vertex function for the creation of the j-th resonance from the channel ν. The dressed resonance vertex functions are constructed using $T^{\rm NP}$ as shown in Eq. (3.25) below,

$$
\begin{aligned}
\Gamma^a_{\mu,i}(p) &= \gamma^a_{\mu,i}(p) + \sum_\kappa \int_0^\infty \mathrm{d}q\, q^2\, T^{\rm NP}_{\mu\nu}(p,q,W)\, G_\kappa(q,W)\, \gamma^a_{\kappa,i}(q) \\
\Gamma^c_{\nu,j}(p') &= \gamma^c_{\nu,j}(p') + \sum_\kappa \int_0^\infty \mathrm{d}q\, q^2\, \gamma^c_{\kappa,j}(q)\, G_\kappa(q,W)\, T^{\rm NP}_{\mu\nu}(q,p',W) \\
D_{ij}(W) &= \delta_{ij}(W - m^b_i) - \Sigma_{ij}(W) \\
\Sigma_{ij}(W) &= \sum_\kappa \int_0^\infty \mathrm{d}q\, q^2\, \gamma^c_{\kappa,j}(q)\, G_\kappa(q,W)\, \Gamma^a_{\mu,i}(q)\ ,
\end{aligned}
\tag{3.25}
$$

where the propagator D^{-1} for s-channel resonances contain the self-energies Σ_{ij} as listed in Eq. (3.25). The bare vertex functions are given by the γ's and their explicit forms can be found in the appendix in Sec. B and the m^b_i are the bare mass parameters of the i-th resonance. The bare masses m^b_i and the bare couplings inside the γ's are free parameters of the model. The indices $i, j = 1, 2, 3$ characterize the s-channel state $(i, j = 1, 2)$ or phenomenological contact term $(i, j = 3)$ in a given partial wave. We have one or two bare s-channel states per partial wave and this is chosen as demanded by the fit. The phenomenological contact terms cannot induce a genuine s-channel pole in the amplitude, but they can play an important role for dynamically generated poles. Note, one cannot unambiguously relate a pole to a given s-channel term. This is due to the highly nonlinear nature of this approach. A classification of "s-channel poles" as genuine three-quark states and associating a purely molecular nature to dynamically generated poles is too simplistic. Instead one has to employ compositeness or elementariness criteria as it was done in Refs. [218, 219] in the JüBo framework.

From the T-matrix one can determine observables and then fit these to experimental data. For this, one defines the normalised, dimensionless partial-wave amplitude τ by

$$
\tau_{\mu\nu} = -\pi\sqrt{\rho_\mu \rho_\nu}\, T_{\mu\nu}\ , \tag{3.26}
$$

where ρ is the kinematical phase factor

$$
\rho_\kappa = \frac{p_\kappa}{W} E^{\rm on}_\kappa \omega^{\rm on}_\kappa\ ,
$$

with

$$
E^{\rm on}_\kappa = \sqrt{\vec{p}^{\,2}_\kappa + m^2_\kappa}, \quad \omega^{\rm on}_\kappa = \sqrt{\vec{p}^{\,2}_\kappa + m^2_\kappa}
$$

being the on-shell energies of the baryon and meson in channel κ respectively. This can be related to observables as shown in Sec. B.4.

3.2. Channel space of the Jülich-Bonn model

We present the different channels used in the JüBo framework in Fig. 6. In the JüBo model the channels πN, ηN, $K\Lambda$ and $K\Sigma$ are considered as stable. Thus, the relation given in Eq. (3.19) holds for these channels. Recently the process $\pi N \to \omega N$ was included in an analysis restricted to pion-induced reactions [118], but was not yet included in the analysis of this thesis. Furthermore, the unstable channels $\pi\Delta$, ρN and σN are included to

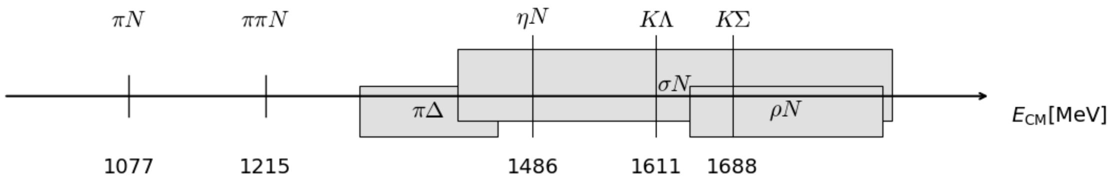

Figure 6: Channel space in the JüBo model. The unstable channels $\pi\Delta$, σN and ρN are sketched as grey bars to represent their decay width.

effectively represent the three body channel $\pi\pi N$. Each of these consist of a stable (π,N) and an unstable (Δ,ρ,σ) particle. To consider the decays of the σ and ρ into $\pi\pi$ and of the Δ into πN systems the following procedure is used. Here, the two-body propagator are modified by introducing the self-energy Σ for the effective three-body channels [33, 106, 108, 111]

$$G_{\pi\Delta}(p,E) = \frac{1}{E - \sqrt{m_\pi^2 + p^2} - \sqrt{(m_\Delta^0)^2 + p^2} - \Sigma_\Delta(E_\Delta)} \,, \tag{3.27}$$

$$G_{\sigma N}(p,E) = \frac{1}{E - \sqrt{m_N^2 + p^2} - \sqrt{(m_\sigma^0)^2 + p^2} - \Sigma_\sigma(E_\sigma)} \,, \tag{3.28}$$

$$G_{\rho N}(p,E) = \frac{1}{E - \sqrt{m_N^2 + p^2} - \sqrt{(m_\rho^0)^2 + p^2} - \Sigma_\rho(E_\rho)} \,. \tag{3.29}$$

where the arguments of the self-energies take into account the movement of the unstable particle and subtracts the energies of the spectators

$$E_\sigma = E - \omega_\pi(p) - (\sqrt{(m_\sigma^0)^2 + p^2} - m_\sigma^0) \,, \tag{3.30}$$

$$E_\rho = E - \omega_\pi(p) - (\sqrt{(m_\rho^0)^2 + p^2} - m_\rho^0) \,, \tag{3.31}$$

$$E_\Delta = E - E_N(p) - (\sqrt{(m_\Delta^0)^2 + p^2} - m_\Delta^0) \,. \tag{3.32}$$

For the self-energies a simple model with interaction vertices for the corresponding decays is considered [33, 106]. The effective Lagrangians are given by

$$\mathcal{L}_{\pi\pi\sigma} = g_{\pi\pi\sigma} m_\pi \vec{\phi}_\pi \vec{\phi}_\pi \phi_\sigma \ , \tag{3.33}$$

$$\mathcal{L}_{\pi\pi\rho} = -g_{\pi\pi\rho} (\vec{\pi} \times \partial^\mu \vec{\pi}) \vec{\rho}^{\,\mu} \ , \tag{3.34}$$

$$\mathcal{L}_{\pi N\Delta} = \frac{f_{\pi N\Delta}}{m_\pi} \bar{\Delta}^\mu \vec{T}^\dagger \partial_\mu \vec{\pi} \Psi_N \ . \tag{3.35}$$

In this kind of model the T-matrix for each channel only has the pole part of the form

$$T = \frac{v v^\dagger}{W - m_0 - \Sigma} \ , \tag{3.36}$$

where the self-energy Σ is calculated via the vertex functions as given in Eq. (3.25) and v labels the vertex functions in this simplified model. These vertex functions can be equipped with the corresponding form factors taken from Refs. [33, 106] to get the following form

$$v^{\pi\pi\sigma}(p) = \frac{\sqrt{3} g_{\pi\pi\sigma} m_\pi}{2\pi \omega_\pi(p) \sqrt{\omega_\sigma^0(p)}} \frac{\Lambda_{\pi\pi\sigma}^2}{\Lambda_{\pi\pi\sigma}^2 + p^2} \tag{3.37}$$

$$v^{\pi\pi\rho}(p) = \frac{g_{\pi\pi\rho}}{2\pi\sqrt{3}} \frac{p}{\omega_\pi(p)\sqrt{\omega_\rho^0(p)}} \frac{\Lambda_{\pi\pi\rho}^2 + m_\rho^2}{\Lambda_{\pi\pi\rho}^2 + 4\omega_\pi(p)^2} \ , \tag{3.38}$$

$$v^{\pi N\Delta}(p) = -\frac{f_{\pi N\Delta}}{\sqrt{24}\pi m_\pi} \frac{p\sqrt{E_N + m_N}}{\sqrt{\omega_\pi E_N}} \frac{\Lambda_{\pi N\Delta}^4 + m_\Delta^4}{\Lambda_{\pi N\Delta}^4 + (E_N(p) + \omega_\pi(p))^4} \ , \tag{3.39}$$

with the meson energies $\omega_\sigma^0(p) = \sqrt{(m_\sigma^0)^2 + p^2}$ and $\omega_\rho^0(p) = \sqrt{(m_\rho^0)^2 + p^2}$ and the bare masses m_σ^0 and m_ρ^0. The vertex function for the $\pi N\Delta$ has the same form as for the Δ pole diagram in the πN channel listed in appendix B.2. The different parameters are then fitted to match the $\pi\pi$- and the πN-phase shift data [33, 106].

3.3. Construction of the potential

For the energies we are probing, a perturbative treatment in the framework of ChPT is not possible since the perturbation series does not converge and a QCD description in terms of quarks and gluons fails. One has to employ effective field theory methods that respect the symmetries of QCD, but uses the relevant hadronic degrees of freedom, namely mesons and baryons. The potential in the Jülich-Bonn framework is constructed from the Wess-Zumino Lagrangian [191], from which the interactions involving nucleons, pions, ρ and the a_1 meson are taken. The Lagrangian was extended to include the $\pi\rho\omega$ vertex as done in Ref. [220] and studies for a general form of effective Lagrangians with vector mesons consistent with chiral symmetry can be found in Refs. [173, 221]. The ωNN vertex is constructed analogously to the ρNN vertex except for the isospin structure. Furthermore, the Δ and the σ meson are incorporated as done in Ref. [222]. Note that the σ is not included as a genuine meson in the πN channel but instead is a parametrization of the correlated $\pi\pi$ interaction in the partial wave $(I, J) = (0, 0)$.

The construction of the Wess-Zumino Lagrangian [191] starts from the nonlinear σ-model with pion fields π and nucleon fields Ψ. One then introduces auxiliary fields for the pion ξ and nucleon N by

$$\xi = \frac{\vec{\pi} \cdot \vec{\tau}}{F_\pi} , \tag{3.40}$$

$$N = \left(\frac{1 - i\gamma_5 \xi}{1 + i\gamma_5 \xi}\right)^{\frac{1}{2}} \Psi = \frac{1 - i\gamma_5 \xi}{(1 + \xi^2)^{1/2}} \Psi , \tag{3.41}$$

where F_π is the pion decay constant. These fields transform under chiral symmetry as

$$\begin{aligned} \xi &\rightarrow e^{i\beta} \xi & (3.42) \\ \Psi &\rightarrow e^{i\alpha\gamma^5} \Psi & (3.43) \\ \frac{1 - i\gamma_5 \xi}{1 + i\gamma_5 \xi} &\rightarrow e^{-i\alpha\gamma_5} \frac{1 - i\gamma_5 \xi}{1 + i\gamma_5 \xi} e^{-i\alpha\gamma^5} , & \\ N &\rightarrow e^{i\beta} N , & (3.44) \end{aligned}$$

with the group parameters of the axial $\alpha = \vec{\alpha}\vec{\tau}$ and the vector $\beta = \vec{\beta}\vec{\tau}$ $SU(2)$ group. One now performs a gauge transformation and allow the parameters α and β to be coordinate dependent. To restore the invariance of the Lagrangian, one introduces two additional gauge fields, namely the vector gauge field $\rho_\mu = \vec{\rho}_\mu \vec{\tau}$ and the axial gauge field $a_\mu = \vec{a}_\mu \vec{\tau}$. These are associated with the ρ- and the a_1-meson, respectively. The infinitesimal vector gauge transformation is written as

$$\delta\rho_\mu = i[\beta, \rho_\mu] + \frac{2}{g}\partial_\mu \beta, \quad \delta a_\mu = i[\beta, a_\mu] , \tag{3.45}$$

and the infinitesimal axial gauge transformation is given by

$$\delta\rho_\mu = i[\alpha, a_\mu], \quad \delta a_\mu = i[\alpha, \rho_\mu] + \frac{2}{g}\partial_\mu \alpha , \tag{3.46}$$

where g is a coupling constant. This coupling constant $g \equiv g_\rho \equiv g_{\pi\pi\rho} = 2g_{\rho NN}$ is related to the pion decay constant $F_\pi = \sqrt{2} m_\rho / g$ through the KSFR relation [223, 224].

For the fields ξ, N, ρ_μ and a_μ the Lagrangian can be constructed with three parts. One part $\mathcal{L}_1$ is invariant under gauge transformations. The next part $\mathcal{L}_2$ containing the mass terms of vector mesons has only global $SU(2) \times SU(2)$ invariance and breaks gauge invariance. The last part $\mathcal{L}_3$ containing the pion mass term is only invariant under isospin transformations. The complete Wess-Zumino Lagrangian is quite lengthy and the terms relevant for our approach are taken.

As mentioned before, TOPT is used to construct the effective potential in the Jülich-Bonn approach. By considering the time ordering, one exchange diagram in covariant perturbation theory corresponds to a pair of diagrams in TOPT and one contact term if applicable. These diagrams are called first and second time ordering and correspond to an exchange of a particle or anti-particle (see Fig. 7). The scattering potential V as defined

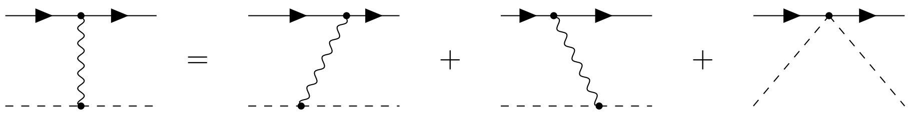

Figure 7: Difference of diagrams in covariant perturbation theory (left) and TOPT (right)

in Eq. (3.15) is in general build by the set of all two-particle irreducible diagrams with an arbitrary number of virtual particles in the intermediate states. This infinite series is truncated and all diagrams with three or less intermediate particles are kept.

The following types of diagrams contribute to the potential

- Diagrams containing three particles in the intermediate state, which correspond to t- and u-channel exchanges. The intermediate σ and ρ are treated in the $\pi N \to \pi N$ potential as correlated $\pi\pi$ pairs [103, 109].
- There are three sources for contact terms. The first kind originates from the Wess-Zumino Lagrangian for vector mesons and the second kind is from the TOPT prescription (see Fig. 7). The last type are phenomenological contact terms that are included in the pole part of the amplitude as shown in Eq. (3.25).
- The last type of diagrams are the genuine s-channel pole graphs, which contribute to the pole part of the potential V^{P}. The only exception is the nucleon pole, which has a special treatment to determine the bare parameters and ensures the correct values of the physical mass and coupling. This procedure is presented in Sec. 3.4.

For a full list of the exchange diagrams and explicit expressions for the non-pole potentials, we refer to Appendix B.3. Details on the pole part of the diagram can be found in Appendix B.2.

Correlated two-pion exchange for the σ and ρ in elastic πN scattering

For elastic πN scattering in the Jülich-Bonn model the σ and ρ mesons are treated as correlated $\pi\pi$-exchanges [103, 109]. This is done by using "quasi-empirical" $N\bar{N} \to \pi\pi$ amplitudes, obtained by analytic continuation of $\pi\pi$ and πN data [225, 226]. These amplitudes are then related to $\pi N \to \pi N$ by using dispersion relations.

In the scalar channel (σ) one finds a large attractive contribution, but low energy theorems for πN scattering put constraints on the forward scattering amplitude at the Cheng-Dashen point [227]. Consequently, a subtraction at the Cheng-Dashen point is included to get a correct low-energy behaviour.

The construction of the corresponding off-shell potentials for πN scattering starts with a stable meson exchange with TOPT propagators. The invariant amplitudes of the σ and ρ mesons are weighted with spectral functions, which contain the information on the dispersion relations for the correlated pion pair. The resulting potential is defined in such a way, that it can be extended to the off-shell region. Furthermore, the high momentum behaviour is regularized by introducing suitable form factors as done for other potentials [103, 109].

3.4. Nucleon Pole

Within the Jülich-Bonn model the nucleon is treated as a genuine s-channel state in the pole part of the amplitude with dressed quantities as described in Eq. (3.25). The only difference for the nucleon pole compared to other genuine s-channel states is that one does not consider the bare parameters as free, since the πNN coupling constant $f_{\pi NN} = 0.989$ [228] and the nucleon mass $m_N = 939$ MeV are known physical quantities. To acquire the correct values for the nucleon pole, one introduces a renormalization procedure in the P_{11} partial wave as described in Refs. [229, 230].

For this one starts from the pole part T^{P} in the one-resonance case and in the πN channel with only the nucleon as a s-channel state

$$T^{\mathrm{P}} = \frac{\Gamma_1^a \Gamma_1^c}{W - m_N^b - \Sigma_{11}} \ , \tag{3.47}$$

where m_N^b is the bare mass of the nucleon. One demands that T^{P} has a pole at the physical nucleon mass m_N

$$W_0 = m_N^b + \Sigma_{11}(W_0) \overset{!}{=} m_N \ . \tag{3.48}$$

Now the self energy is expanded around this point $W = W_0$

$$\Sigma_{11}(W) = \Sigma_{11}(W_0) + (W - W_0) \frac{\partial \Sigma_{11}(W)}{\partial W}\bigg|_{W=W_0} + \mathcal{O}\left((W - W_0)^2\right) \ . \tag{3.49}$$

The bare πNN coupling constant is defined as $f_N^b = x f_{\pi NN}$ with $x \in \mathbb{R}$ and from this the reduced quantities $\hat{\Sigma}_{11}$ and $\hat{\Gamma}_1^{a,c}$ are given by factorizing off the bare coupling

$$\Sigma_{11} = x^2 \hat{\Sigma}_{11}, \quad \Gamma_1^{a,c} = x \hat{\Gamma}_1^{a,c} \ . \tag{3.50}$$

The two introduced quantities $\hat{\Sigma}_{11}$ and $\hat{\Gamma}_1^{a,c}$ are the nucleon self-energy and the dressed nucleon vertex function determined with the physical nucleon coupling constant $f_{\pi NN}$ instead of the bare parameter. The pole part of the amplitude can now be written as

$$T^{\mathrm{P}} = \frac{1}{W - W_0} \left(\frac{x^2 \hat{\Gamma}_1^a \hat{\Gamma}_1^c}{1 - x^2 \partial_W \hat{\Sigma}_{11}(W)} \right)\bigg|_{W=W_0} + \mathcal{O}\left((W - W_0)^0\right) \ . \tag{3.51}$$

Now, one needs to find the bare coupling f_N^b which is used as an input for the model. This is done by calculating x and using the known value for $f_{\pi NN}$. The physical residue of the nucleon pole is given by

$$a_{-1} = \hat{\gamma}_1^a \hat{\gamma}_1^c \ , \tag{3.52}$$

with the bare nucleon vertices $\hat{\gamma}_1^{a,c}$ at $W = W_0$ with the physical nucleon coupling $f_{\pi NN}$. Their expressions are given by

$$\hat{\gamma}_1^a = i f_{\pi NN} \frac{\sqrt{3}}{\sqrt{8}\pi} \frac{k}{m_\pi} \frac{\omega_\pi + E_N + m_N}{\sqrt{\omega_\pi E_N (E_N + m_N)}} \ , \tag{3.53}$$

with the center of mass momentum k. Comparing the physical residue of Eq. (3.52) with the one of T^{P}, one finds the relation

$$\frac{1}{x^2} = \left(\partial_W \hat{\Sigma}_{11}(W) + \frac{\hat{\Gamma}_1^a \hat{\Gamma}_1^c}{\hat{\gamma}_1^a \hat{\gamma}_1^c}\right)\Big|_{W=W_0} . \tag{3.54}$$

This can now be used to calculate the bare quantities m_N^b and f_N^b by

$$m_N^b = m_N - x^2 \hat{\Sigma}_{11}(W_0) \ , \quad f_N^b = x f_{\pi NN} \ . \tag{3.55}$$

Note, that this is valid for a s-channel state coupling to only one channel. In our model the nucleon only couples to the πN channel, since the nucleon pole lies at $W_0 = 939$ MeV and we see no need to let it couple to higher lying channels. The impact of neglecting the coupling to other channels at the nucleon pole is absorbed into the value of x.

There is another s-channel state within the JüBo model in the P_{11} partial wave, which can couple to multiple channels. Furthermore, there is an additional contact term in the P_{11} partial wave. This means that this procedure has to be modified. The nucleon pole is now given as a zero of the determinant of D^{-1} defined in Eq. (3.25)

$$\det D^{-1}\big|_{W=W_0} = \det \begin{pmatrix} W - m_1^b - \Sigma_{11} & -\Sigma_{12} & -\Sigma_{13} \\ -\Sigma_{21} & W - m_2^b - \Sigma_{22} & -\Sigma_{23} \\ -\Sigma_{31} & -\Sigma_{32} & m_N - \Sigma_{33} \end{pmatrix}^{-1} \Bigg|_{W=W_0} = 0 \ . \tag{3.56}$$

where $W_0 = m_N$ and we label the nucleon with the index 1 as before. The bare mass of the second genuine resonance m_2^b and the bare coupling is a free parameter in the JüBo model. The reduced quantities of the self-energies are given by

$$\begin{aligned} \Sigma_{11} &= x^2 \hat{\Sigma}_{11} \ , \\ \Sigma_{12} &= x \hat{\Sigma}_{12} \ , \\ \Sigma_{13} &= x \hat{\Sigma}_{13} \ , \\ \Sigma_{21} &= x \hat{\Sigma}_{21} \ , \\ \Sigma_{31} &= x \hat{\Sigma}_{31} \ . \end{aligned} \tag{3.57}$$

This leads to the following relation for the bare nucleon mass $m_1^b = m_N^b$

$$m_N^b = m_N + x^2 \frac{G_3^{-1} \hat{\Sigma}_{12}^2 + \hat{\Sigma}_{13} \left(G_2^{-1} \hat{\Sigma}_{13} + 2\hat{\Sigma}_{12} \Sigma_{23}\right)}{\Sigma_{23}^2 - G_2^{-1} G_3^{-1}} \Bigg|_{W=m_N} - x^2 \hat{\Sigma}_{11} \Big|_{W=m_N} \ , \tag{3.58}$$

where a short-hand notation was introduced by

$$G_2^{-1} = \left(W - m_2^b - \Sigma_{22}(W)\right)|_{W=m_N} \tag{3.59}$$

$$G_3^{-1} = (m_N - \Sigma_{33}(W))|_{W=m_N} \tag{3.60}$$

To find an expression for x, one compares the physical residue a_{-1} in the πN channel with the residue of $T^{\rm P}$

$$\begin{aligned} a_{-1} &= \hat\gamma_1^a \hat\gamma_1^c\big|_{W=m_N} = (\text{Res } T^{\rm P})\big|_{W=m_N} \\ &= \frac{\det D^{-1}}{\partial_W \det D^{-1}} (x\hat\Gamma_1^a, \Gamma_2^a, \Gamma_3^a) \\ &\times \begin{pmatrix} W - m_N^b - x^2\hat\Sigma_{11} & -x\hat\Sigma_{12} & -x\hat\Sigma_{13} \\ -x\hat\Sigma_{21} & W - m_2^b - \Sigma_{22} & -x\hat\Sigma_{23} \\ -x\hat\Sigma_{31} & -x\hat\Sigma_{32} & m_N - \Sigma_{33} \end{pmatrix}^{-1} \begin{pmatrix} x\hat\Gamma_1^c \\ \Gamma_2^c \\ \Gamma_3^c \end{pmatrix}\Bigg|_{W=m_N} . \end{aligned} \tag{3.61}$$

This relation allows one to calculate x, which only depends on the fitted quantities and from this the bare mass and coupling of the nucleon can be determined. The calculation is performed in each step of the fitting procedure. We ensure the correct values for the physical quantities of the nucleon pole with this procedure in the presence of a second genuine s-channel state and a contact term. In principal one could extend this procedure to other boundary conditions on the nucleon in higher lying channels. However, the effects are rather small since the channels are several hundred MeV higher than the nucleon pole.

3.5. Photoproduction processes

In recent years the data base for photoproduction processes was growing much larger than the pion-induced ones. Different experimental studies as mentioned in Sec. 1.3 contributed high precision photoproduction data [11, 14]. Therefore, a combined analysis of photoproduction and πN data may help to clarify the nature of controversial resonance states or even reveal new ones [86, 231].

The first study to connect the hadronic Jülich-Bonn model with pion photoproduction was done by Huang et. al. in Ref. [232]. This approach used a field-theoretical framework from generalized off-shell Ward-Takahashi identities [233–235] and the hadronic final-state interaction was described by the JüBo model for πN scattering. Implementing photoproduction in a fully field-theoretical manner, as done in Ref. [232], is a highly (especially numerically) demanding and technically complicated task. Consequently, the Jülich-Bonn DCC approach was extended to photoproduction reactions in a semi-phenomenological way in Ref. [114], which we will describe in the following.

The photoproduction amplitude J of a pseudoscalar meson can be constructed in terms of four amplitudes J_i, as shown in Ref. [236]

$$J = iJ_1\vec\sigma\cdot\vec\epsilon + J_2\vec\sigma\cdot\hat q\,\vec\sigma\cdot(\vec k\times\vec\epsilon) + iJ_3\vec\sigma\cdot\hat k\,\hat q\cdot\vec\epsilon + iJ_4\vec\sigma\cdot\hat q\,\hat q\cdot\vec\epsilon\,, \tag{3.62}$$

with the meson momentum $\vec q$, the photon momentum $\vec k$ and the photon polarization vector $\vec\epsilon$. In this notation $\hat a$ denotes the unit vector of a vector $\vec a$. The amplitudes J_i are complex functions depending on the scattering angle θ, defined by $\cos\theta = \hat q\cdot\hat k$, and the total energy W. Furthermore, one rewrites Eq. (3.62) as done in Ref. [237] to get the photoproduction amplitudes:

$$\hat{\mathcal{M}} = -iJ = F_1\vec\sigma\cdot\vec\epsilon + iF_2(\hat k\times\hat q)\cdot\vec\epsilon + F_3\vec\sigma\cdot\hat k\,\hat q\cdot\vec\epsilon + F_4\vec\sigma\cdot\hat q\,\hat q\cdot\vec\epsilon\,, \tag{3.63}$$

where the amplitudes F_i are related to J_i by:

$$
\begin{aligned}
F_1 &\equiv J_1 - \cos\theta\, J_2 \ , \\
F_2 &\equiv J_2 \ , \\
F_3 &\equiv J_2 + J_3 \ , \\
F_4 &\equiv J_4 \ .
\end{aligned} \tag{3.64}
$$

The forms of the amplitudes J and $\hat{\mathcal{M}}$ are coordinate independent. The multipole decomposition for the amplitudes J_i is given by [236]:

$$
\begin{pmatrix} J_1 \\ J_2 \\ J_3 \\ J_4 \end{pmatrix} = \frac{4\pi}{m_N} \sum_{L=0}^{\infty} \tilde{D}_L(\cos\theta) \begin{pmatrix} E_{L+} \\ E_{L-} \\ M_{L+} \\ M_{L-} \end{pmatrix} \ . \tag{3.65}
$$

Here, L is the orbital angular momentum of the final meson-baryon state. The matrix $\tilde{D}_L(\cos\theta)$ is given by:

$$
\tilde{D}_L = \begin{pmatrix} P'_{L+1} & P'_{L-1} & LP'_{L+1} & (L+1)P'_{L-1} \\ 0 & 0 & (L+1)P'_L & LP'_L \\ P''_{L+1} & P''_{L-1} & -P''_{L+1} & P''_{L-1} \\ -P''_L & -P''_L & P''_L & -P''_L \end{pmatrix} \ , \tag{3.66}
$$

with

$$
P'_L \equiv \frac{\mathrm{d}P_L(\cos\theta)}{\mathrm{d}\cos\theta} \quad \text{and} \quad P''_L \equiv \frac{\mathrm{d}^2 P_L(\cos\theta)}{\mathrm{d}\cos\theta^2}
$$

denoting the derivatives of the Legendre polynomials of the first kind. The full expressions for the amplitudes F_i depending on the electric and magnetic multipoles $(E_{L\pm}, M_{L\pm})$ as well as the definitions of observables are given in Ref. [114] and presented in App. B.4.2. The electric and magnetic multipoles are defined by the photoproduction multipole amplitudes M

$$
M_{\mu\gamma}(p,W) = V_{\mu\gamma}(p,W) + \sum_{\kappa} \int_0^{\infty} dq\, q^2\, T_{\mu\kappa}(p,q,W) G_\kappa(q,W) V_{\kappa\gamma}(q,W) \ . \tag{3.67}
$$

The channel index γ defines the initial photo-channel of γN with a real photon ($Q^2 = 0$), while μ and κ are the final and intermediate meson-baryon channels. Note, the T-matrix $T_{\mu\kappa}$ used in Eq. (3.67) is the same T-matrix that was introduced in Eq. (3.20) with the off-shell momentum q and the on-shell momentum p. The hadronic two-body propagator G_κ is also the same as the one in Eq. (3.20). The meson-baryon channels included within the photoproduction part are $\kappa = (\pi N, \eta N, K\Lambda, K\Sigma, \pi\Delta)$. Further extensions to this channel space to two pion or vector meson photoproduction are planned in the future. The Jülich-Bonn-Washington (JBW) group applied a similar parameterization for electroproduction reactions [119–122], in which the Jülich-Bonn amplitude was included as input at the photon point at $Q^2 = 0$.

The photoproduction potential $V_{\mu\gamma}$ is given by

$$V_{\mu\gamma}(p, W) = \alpha^{\rm NP}_{\mu\gamma}(p, W) + \sum_i \frac{\gamma^a_{\mu,i}(p)\gamma_{\gamma,i}(W)}{W - m^b_i} \,. \tag{3.68}$$

The $\gamma^a_{\mu,i}$ is the same vertex function as introduced in Sec. 3.1 and $\gamma_{\gamma,i}$ denotes the photon-to-resonance vertex function. The photon-vertex function $\gamma_{\gamma,i}$ is parameterized by a polynomial function in the energy W and includes free parameters for each genuine s-channel state as shown in Eq. (3.69) and (3.70)

$$\gamma_{\gamma,i}(W) = \sqrt{m_N} P^{\rm P}_i(W) \,, \tag{3.69}$$

$$P^{\rm P}_i(W) = \sum_{j=1}^{l_i} g^{\rm P}_{i,j} \left(\frac{W - W_s}{m_N}\right)^j e^{-\lambda^{\rm P}_i (W-W_s)} \,, \tag{3.70}$$

where g and $\lambda > 0$ are free parameters which are fitted to data and the expansion point W_s is chosen close to πN threshold $W_s = 1077\,\text{MeV}$. Here we have n polynomials per multipole, where n denotes the number of resonances. Furthermore, the sum starts with $j = 1$ to fulfill the decoupling theorem. This means a parametrically suppression of the resonance contributions at threshold.

For the non-pole part in Eq. (3.67) we also use a polynomial parametrization for $\alpha^{\rm NP}_{\mu\gamma}$ as shown in Eqs. (3.71) and (3.72)

$$\alpha^{\rm NP}_{\mu\gamma}(p, W) = \frac{\tilde{\gamma}^a_\mu(p)}{\sqrt{m_N}} P^{\rm NP}_i(W) \,, \tag{3.71}$$

$$P^{\rm NP}_\mu(W) = \sum_{j=0}^{l_\mu} g^{\rm NP}_{\mu,j} \left(\frac{W - W_s}{m_N}\right)^j e^{-\lambda^{\rm NP}_\mu (W-W_s)} \,, \tag{3.72}$$

and introduce additional fit parameters $g^{\rm NP}_{\mu,j}$ and $\lambda^{\rm NP}_\mu$ depending on the partial wave and the final hadronic state. The vertex function $\tilde{\gamma}^a_\mu(p)$ is equal to $\gamma^a_{\mu,i}$ but without the dependence on the resonance number i. The nucleon mass m_N is used to ensure that the parameters g are dimensionless. The upper limits of the sum l_i and l_μ are chosen as demanded by the data but we restrict to a maximum polynomial degree of 3. We list further details on this in Sec. 4.2. This kind of polynomial parameterization is numerically advantageous to a field-theoretical description such as used in Ref. [232].

3.6. Determination of resonance parameters

In hadron spectroscopy, the reliable characterization of resonances is given by pole positions and residues in the complex energy plane on the unphysical Riemann sheet. The description in terms of poles is largely model independent and well suited to compare results from different analyses. One defines the resonance mass by the real part of the pole position, $M = \operatorname{Re} W_0$, and the width is related to the imaginary part through $\Gamma = -2 \operatorname{Im} W_0$.

The extraction of pole positions requires an analytic continuation of the scattering amplitude onto the relevant unphysical Riemann sheets. This requires a careful treatment of the singularity structure of the S-matrix, since each open channel introduces branch points and corresponding cuts. In the Jülich-Bonn model, the stable channels πN, ηN, $K\Lambda$ and $K\Sigma$ generate branch points on the physical axis, while channels with unstable particles (ρN, σN and $\pi\Delta$) lead to branch points in the complex plane. To account properly for unstable intermediate states, the integration contour is deformed into the complex momentum plane so that the analytic continuation avoids the branch cuts associated with the unstable propagators [111].

To access the second sheet, we follow the analytic continuation procedure described in Ref. [111]. The amplitude on the second sheet $T^{(2)}$ for stable intermediate states is given by

$$T^{(2)}_{\mu\nu}(p,p',W) - V_{\mu\nu}(p,p',W) = \delta G(p,p',W) + \int \mathrm{d}q\; p^2 \frac{V_{\mu\kappa}(p,q,W)T^{(2)}_{\kappa\nu}(q,p',W)}{W - E(q) - \omega(q) + i\epsilon} \; , \tag{3.73}$$

where we introduced δG which is given by

$$\delta G(p,p',W) = \frac{2\pi i p^{>}_{\mathrm{on}} E^{\mathrm{on}} \omega^{\mathrm{on}}}{W} V_{\mu\kappa}(p,p_{\mathrm{on}},W)T^{(2)}_{\kappa\nu}(p_{\mathrm{on}},p',W) \; , \tag{3.74}$$

where E^{on} and ω^{on} defines the on-shell energies of the meson and baryon respectively and the on-shell momentum in the center of mass frame is given by:

$$p_{\mathrm{on}} = \frac{1}{W}\sqrt{(W^2 - (m_m - m_b)^2)(W^2 - (m_m + m_b)^2)} \; , \tag{3.75}$$

where the index m (b) denotes the meson (baryon). The on-shell momentum is double valued to explicitly distinguish the two Riemann sheets:

$$p^{>}_{\mathrm{on}} = \begin{cases} -p_{\mathrm{on}} & \text{if } \mathrm{Im}\; p_{\mathrm{on}} < 0 \\ p_{\mathrm{on}} & \text{else} \end{cases} \; . \tag{3.76}$$

This kind of construction is required to properly locate resonance poles in the complex plane. For channels including unstable particles in the intermediate state this procedure becomes more involved, since the unstable propagator contains additional branch points. As a consequence, more than two sheets may need to be considered. One needs to access the correct sheets by employing an appropriate contour deformation. Since poles may occur on any of these sheets, specific criteria must be used to decide on which sheets the pole search is performed [111].

In addition to the pole position, one also needs the residue $|r|$ and its phase θ to properly characterize the resonance pole. Expanding the amplitude $T^{(2)}$ around the pole position W_0 gives a Laurent series of the form

$$T^{(2)}_{\mu\nu} = \frac{a_{-1,\mu\nu}}{W - W_0} + a_{0,\mu\nu} + \mathcal{O}(W - W_0) \; , \tag{3.77}$$

where a_{-1} is the pole residue. It can be calculated with a closed contour integration along a path $\Gamma(W_0)$ around the pole W_0:

$$a_{-1,\mu\nu} = \frac{1}{2\pi i}\oint_{\Gamma(W_0)} T^{(2)}_{\mu\nu}(W)\mathrm{d}W \; . \tag{3.78}$$

An alternative way is a determination given by an iterative procedure [112]:

$$\frac{\partial}{\partial W}\bigg|_{W=W_0} \frac{1}{T^{(2)}_{\mu\nu}(W)} = \frac{1}{a_{-1,\mu\nu}} \,, \tag{3.79}$$

$$\frac{\partial^2}{\partial W^2}\bigg|_{W=W_0} \frac{1}{T^{(2)}_{\mu\nu}(W)} = -\frac{2a_{0,\mu\nu}}{a^2_{-1,\mu\nu}} \,, \tag{3.80}$$

$$\frac{\partial^3}{\partial W^3}\bigg|_{W=W_0} \frac{1}{T^{(2)}_{\mu\nu}(W)} = \frac{6(a^2_{0,\mu\nu} - a_{-1,\mu\nu}a_{1,\mu\nu})}{a^3_{-1,\mu\nu}} \,. \tag{3.81}$$

This procedure is numerically fast, since it does not require an integration. The residue $a_{-1,\mu\nu}$ and the constant term $a_{0,\mu\nu}$ can also be expressed in terms of the dressed quantities introduced in Eq. (3.25). For the case of one resonance i it is given by [112, 238]

$$a_{-1,\mu\nu} = \frac{\Gamma^a_{\mu,i}\Gamma^c_{\nu,i}}{1-\partial_W\Sigma_{ii}} \,, \tag{3.82}$$

$$a_{0,\mu\nu} = \frac{a_{-1,\mu\nu}}{\Gamma^a_{\mu,i}\Gamma^c_{\nu,i}}\left(\frac{\partial}{\partial W}\Gamma^a_{\mu,i}\Gamma^c_{\nu,i} + \frac{a_{-1,\mu\nu}}{2}\frac{\partial^2}{\partial W^2}\Sigma_{ii}\right)\bigg|_{W=W_0} + T^{(2),\mathrm{NP}}_{\mu\nu}(W_0) \,. \tag{3.83}$$

These relations show that there is a contribution to the constant term of T^{NP} and one from the pole term. This is one of the reasons which shows that identifying the non pole part T^{NP} as "background" is to simplistic [238]. In the case of two resonances the expression for the residue is given by

$$a_{-1,\mu\nu} = \left[\frac{\det\Big(D^{(2)}(W)\Big)}{\partial_W \det(D^{(2)}(W))} T^{(2),\mathrm{P}}_{\mu\nu}\right]_{W\to W_0} \,. \tag{3.84}$$

The residue $a_{-1,\mu\nu}$ is directly related to the pole residue $r = |r|^{i\theta}$ according to the PDG convention [5] by

$$|r| = |a_{-1}\rho_\mu| \,, \tag{3.85}$$

$$\theta = -\pi + \arctan\left[\frac{\mathrm{Im}(a_{-1}\rho_\mu)}{\mathrm{Re}(a_{-1}\rho_\mu)}\right] \,. \tag{3.86}$$

where

$$\rho_\mu = \frac{p^{\mathrm{on}}_\mu E^{\mathrm{on}}_\mu \omega^{\mathrm{on}}_\mu}{E} \,. \tag{3.87}$$

Here p^{on}_μ is the on-shell three momentum and E^{on}_μ (ω^{on}_μ) is the baryon (meson) energy in channel μ. In addition to the pole position, we also determine normalized residues. These normalized residues (NR) are defined by

$$NR_{\pi N\to\mu\nu} = \frac{\pi\sqrt{\rho_{\pi N}\rho_\mu}\, g_{\pi N} g_\mu}{\Gamma_{\mathrm{tot}}/2} \tag{3.88}$$

where the parameters g_μ are defined from $a_{-1,\pi N\mu} = g_{\pi N} g_\mu$ and the resonance width is given by $\Gamma_{\rm tot} = -2\,{\rm Im}\,W_0$. The transition branching ratios are given by the modulus of these normalized residues:

$$\frac{\Gamma_{\pi N}^{1/2}\Gamma_\mu^{1/2}}{\Gamma_{\rm tot}} = |NR_{\pi N\to\mu\nu}| \; . \tag{3.89}$$

In Ref. [239] a novel approach is presented to relate the complex residues to the more intuitive branching fractions. The authors present a formalism to derive line shapes of resonances from its pole parameters and from this allow for an unambiguous definition of branching ratios by properly integrating over the line shapes. They apply this to the $\rho(770)$ and the $f_0(500)$ resonances, since their pole parameters are determined from dispersive studies on $\pi\pi$ scattering to high precision.

For photoproduction processes the photocouplings can be determined to characterize the coupling of a resonance to a specific photo-channel. These are defined from the residue of the helicity multipoles $A^h_{L\pm}$ at the pole position by:

$$\tilde{A}^h_{\rm pole} = N {\rm Res} A^h_{L\pm} \; , \tag{3.90}$$

with $h = 1/2$ or $3/2$ and the factor N is given by:

$$N = I_F \sqrt{\frac{q_p}{k_p}\frac{2\pi(2J+1)M}{m_N r_{\pi N}}} \; . \tag{3.91}$$

The isospin factor I_F has the values $I_{1/2} = -\sqrt{3}$ and $I_{3/2} = \sqrt{2/3}$. The meson (photon) momentum in the c.m. frame at the pole is given by q_p (k_p). J is the total angular momentum, L is the πN orbital angular momentum and m_N is the nucleon mass. M and $r_{\pi N}$ are the pole position and the elastic πN residue of the resonance. Note that ${\rm Res}A^h_{L\pm}$ and $r_{\pi N}$ are here defined with a minus sign in contrast to the mathematical residues and the elastic πN amplitude, respectively.

These helicity multipoles can be written in terms of electric and magnetic multipoles by

$$\begin{aligned} A^{1/2}_{L+} &= -\frac{1}{2}\left[(L+2)E_{L+} + LM_{L+}\right] \; , \\ A^{3/2}_{L+} &= \frac{1}{2}\sqrt{L(L+2)}\left[E_{L+} - M_{L+}\right] \; , \end{aligned} \tag{3.92}$$

for total angular momentum $J = L + 1/2$. For $J = L - 1/2$ we have:

$$\begin{aligned} A^{1/2}_{L-} &= -\frac{1}{2}\left[(L-1)E_{L-} - (L+1)M_{L-}\right] \; , \\ A^{3/2}_{L-} &= -\frac{1}{2}\sqrt{(L-1)(L+1)}\left[E_{L-} + M_{L-}\right] \; . \end{aligned} \tag{3.93}$$

4. Recent results for photoproduction processes with proton targets

In this chapter, we present recent fit result from the Jülich-Bonn model published in Ref. [1]. We included new data sets for $\gamma p \to \pi^0 p$, $\pi^+ n$ & ηp in the analysis of Ref. [1] and discuss their impact on the resonance spectrum. Furthermore, we describe the numerical details of the analysis for photoproduction processes off proton targets.

4.1. Database

We begin by giving an overview of the data included within this study. The references for the data sets newly included in the present study are listed in Tab. 4.1. The references for the photon induced data can be found in Tabs. 7, 8 and 9. These photoproduction data sets are mainly obtained from the GWU/SAID [126] and BnGa webpages [240]. The references for the pion induced data sets are given by the Refs. [58, 128, 241–289]. Note that we do not fit directly to data for the elastic πN channel and instead use the partial-wave amplitudes of the GWU/SAID WI08 analysis [290] similar to other analysis groups in the field. Here we use their energy-dependent solution in steps of 5 MeV from the πN threshold up to $W = 2400$ MeV. This results in the number of points for the elastic πN channel as quoted in Tab. 4.1.

We include recent data for the double polarization observable E for the process $\gamma p \to \pi^0 p$. These were published by CLAS in Ref. [291]. The observable E is related to the difference of helicity cross sections by

$$\frac{\mathrm{d}\Delta\sigma}{\mathrm{d}\Omega} = \frac{\mathrm{d}\sigma_{3/2}}{\mathrm{d}\Omega} - \frac{\mathrm{d}\sigma_{1/2}}{\mathrm{d}\Omega} = -2\frac{\mathrm{d}\sigma_0}{\mathrm{d}\Omega} E \,. \tag{4.1}$$

Therefore, the inclusion of the polarization observable E is particularly important for the determination of the GDH sum rule which contains the quantity $\Delta\sigma$ (see Eq. (2.63)). The data sets on E or $\Delta\sigma$ in $\gamma p \to \pi^0 p$, $\pi^+ n$, ηp from MAMI [70, 292–294], CBELSA [295–297], and CLAS [298, 299] were also included in the fit. New data on $d\Delta\sigma/d\Omega$ were also recently published by the A2 Collaboration at MAMI [300]. We present the data together with the solution of this study in the Appendix in Sec. D.1 in Figs. 24 and 25. Although we did not include this dataset in the current fit, because it was published shortly after the major part of the simulations was completed, we achieve a good data description.

In this study we further include new data on the double polarization observable G for the finals states $\pi^0 p$ and $\pi^+ n$ by the CLAS Collaboration [301]. Note, that this data increases the data base for this observable considerably. It is especially noteworthy for the $\pi^+ n$ channel, in which only 86 data points existed before and this measurement added 217 new ones, more than tripling the data base in this observable and channel.

In addition to that, we included recent η-photoproduction data from Ref. [302] of the LEPS2/BGOegg collaboration. The differential cross section $d\sigma/d\Omega$ and the photon beam asymmetry Σ [302] were measured over a large polar angle region $-1 < \cos\theta_{\mathrm{c.m.}} < 0.6$. Note that the beam asymmetry data for center of mass energies above 2.1 GeV was covered for the first time in that work.

In addition, we also include the recent polarization data for $\gamma p \to K^0\Sigma^+$ by CLAS [303] which were already presented by an earlier JüBo fit in Ref. [303].

Reaction	Observables (# data points)	# data p./channel
$\pi N \to \pi N$	PWA GW-SAID WI08 (ED solution)	8,396
$\pi^- p \to \eta n$	$d\sigma/d\Omega$ (676), P (79)	755
$\pi^- p \to K^0\Lambda$	$d\sigma/d\Omega$ (814), P (472), β (72)	1,358
$\pi^- p \to K^0\Sigma^0$	$d\sigma/d\Omega$ (470), P (120)	590
$\pi^- p \to K^+\Sigma^-$	$d\sigma/d\Omega$ (150)	150
$\pi^+ p \to K^+\Sigma^+$	$d\sigma/d\Omega$ (1124), P (551) , β (7)	1,682
$\gamma p \to \pi^0 p$	$d\sigma/d\Omega$ (18721), Σ (3287), P (768), T (1404), $\Delta\sigma_{31}$ (140), G (393+198) [301], H (225), E (1227+495) [291], F (397), $C_{x'_\mathrm{L}}$ (74), $C_{z'_\mathrm{L}}$ (26)	27,355
$\gamma p \to \pi^+ n$	$d\sigma/d\Omega$ (5670), Σ (1456), P (265), T (718), $\Delta\sigma_{31}$ (231), G (86+217) [301], H (128), E (903)	9,674
$\gamma p \to \eta p$	$d\sigma/d\Omega$ (9112+320) [302], Σ (535+80) [302], P (63), T (291), F (144), E (306), G (47), H (56)	10,954
$\gamma p \to K^+\Lambda$	$d\sigma/d\Omega$ (2563), P (1663), Σ (459), T (383), $C_{x'}$ (121), $C_{z'}$ (123), $O_{x'}$ (66), $O_{z'}$ (66), O_x (314), O_z (314)	6,072
$\gamma p \to K^+\Sigma^0$	$d\sigma/d\Omega$ (4381), P (402), Σ (280) T (127), $C_{x'}$ (94), $C_{z'}$ (94), O_x (127), O_z (127)	5,632
$\gamma p \to K^0\Sigma^+$	$d\sigma/d\Omega$ (281), P (188) , Σ (21), T (21), O_x (21), O_z (21)	553
	in total	73,171

Table 1: Data included in the fit with new data sets highlighted in red.

4.2. Numerical details

To fit our free model parameters to the experimental data, we perform a χ^2 minimization by using MINUIT [304] on the JURECA-DC supercomputer at the Jülich Supercomputing Center [305]. The set of free parameters used in the fit are the same as in our previous analysis JüBo2022 [117] with a few exceptions. The only difference is that we neglected 3 parameters of the phenomenological contact terms, since they were assigned very small values by the fit process leading.

In Tab. 2 we list which genuine s-channel states couple to which channel. Each state has a bare mass parameter and each checkmark (✓) corresponds to a coupling parameter. We have one bare mass and six couplings for each of the 12 nucleon resonance states aside from the nucleon ground state $N(938)$, which only contributes one bare mass and one coupling to πN. The bare mass and coupling of the nucleon ground state are not fit parameters, but are renormalized to the physical values as discussed in Sec. 3.4. Each of the 10 Δ states amount for four coupling parameters (since they can not couple to the ηN and $K\Lambda$

channels due to isospin conservation) and one bare mass. Thus, we have 86 nucleon and 50 Δ parameters resulting in a total of 136 parameters from s-channel diagrams.

We list all the parameters from the phenomenological contact terms in Tab. 3. We noticed that the fit procedure tuned the coupling parameters to the πN channel for the partial waves F_{15}, P_{31} and D_{35} to very small values, resulting in numerical instabilities. Thus, we decided to set these parameters to 0 and remove them from the list of free parameters. This is the only difference compared to the list of free parameters from the previous analysis JüBo2022 [117]. In total we have 58 free parameters from the phenomenological contact terms.

In Tab. 4 one finds the degree of the polynomial parametrization for the pole part of the photoproduction potential (see. Eq. 3.70). In addition to the numbers shown each term is accompanied by another parameter λ_i^{P} from the exponential. There is no constant term in the polynomial parametrization in the pole part. The pole part contributes 155 parameters. The degrees of the polynomials for the non-pole part of the photoproduction potential (see. Eq. 3.72) are listed in Tab. 5. Each term also contains a constant term in the polynomial parametrization as well as the parameter of the exponential $\lambda_\mu^{\mathrm{NP}}$. This amounts to 608 parameters from the non-pole part of the photoproduction potential. Consequently, we have 763 free parameters from the photoproduction parametrization in the Jülich-Bonn model.

We further have 68 parameters from t-, u-channel and "background" diagrams which are from the non-pole part of the amplitude (see Appendix B.3). Fitting these non-pole parameters increases the amount of computation time significantly compared to the pole parameters mentioned above. After testing, we found that including these as free parameters did not change the χ^2 significantly enough. To reduce computation time, we decided to keep these non-pole parameters fixed at the values found in past JüBo studies [33, 110, 112, 113].

Note that even though we always use the full data base to determine the parameter values, it is not possible to fit all parameters simultaneously due to the complexity of the model and numerical limitations. It should further be noted, that a majority of the parameters comes from the polynomial parameterization of the photoproduction amplitude. These can not induce resonance poles in the scattering matrix $T_{\mu\nu}$. The number of these parameters is not predetermined by the model and likely not all of them are indispensable. However, this flexibility can be regarded advantageous since it prevents the inclusion of superfluous genuine s-channel states into the model. One could use model selection tools such as the LASSO method [306–308] as a systematic way to reduce the number of parameters.

Experimental systematic errors are usually only available for more recent data sets. They are included as angle-independent normalization factors, as done in the GWU/SAID analysis [309]. We consider an additional 5% uncertainty for older data sets on top of the statistical one to compensate for potential missing systematic errors.

The varying number of data points for different channels and observables is noteworthy (see Tab. 4.1). Unfortunately, this leads to small data sets being mostly ignored in a χ^2 minimization. To increase the impact of smaller data sets, we introduce weights in the χ^2

	πN	ρN	ηN	$\pi\Delta$	$K\Lambda$	$K\Sigma$
$N(1535)\ 1/2^-$	✓	✓	✓	✓	✓	✓
$N(1650)\ 1/2^-$	✓	✓	✓	✓	✓	✓
$N(939)\ 1/2^+$	✓					
$N(1710)\ 1/2^+$	✓	✓	✓	✓	✓	✓
$N(1720)\ 3/2^+$	✓	✓	✓	✓	✓	✓
$N(1900)\ 3/2^+$	✓	✓	✓	✓	✓	✓
$N(1520)\ 3/2^-$	✓	✓	✓	✓	✓	✓
$N(1675)\ 5/2^-$	✓	✓	✓	✓	✓	✓
$N(1680)\ 5/2^+$	✓	✓	✓	✓	✓	✓
$N(1990)\ 7/2^+$	✓	✓	✓	✓	✓	✓
$N(2190)\ 7/2^-$	✓	✓	✓	✓	✓	✓
$N(2250)\ 9/2^-$	✓	✓	✓	✓	✓	✓
$N(2220)\ 9/2^+$	✓	✓	✓	✓	✓	✓
$\Delta(1620)\ 1/2^-$	✓	✓		✓		✓
$\Delta(1910)\ 1/2^+$	✓	✓		✓		✓
$\Delta(1232)\ 3/2^+$	✓	✓		✓		✓
$\Delta(1920)\ 3/2^+$	✓	✓		✓		✓
$\Delta(1700)\ 3/2^-$	✓	✓		✓		✓
$\Delta(1930)\ 5/2^-$	✓	✓		✓		✓
$\Delta(1905)\ 5/2^+$	✓	✓		✓		✓
$\Delta(1950)\ 7/2^+$	✓	✓		✓		✓
$\Delta(2200)\ 7/2^-$	✓	✓		✓		✓
$\Delta(2400)\ 9/2^-$	✓	✓		✓		✓

Table 2: List of the parameters for each genuine s-channel state in the Jülich-Bonn model

	πN	ηN	$\pi\Delta$	$K\Lambda$	$K\Sigma$
S_{11}	✓	✓		✓	✓
P_{11}	✓	✓		✓	✓
P_{13}	✓	✓	✓	✓	✓
D_{13}	✓	✓		✓	✓
D_{15}	✓	✓		✓	✓
F_{15}		✓		✓	✓
F_{17}		✓		✓	✓
G_{17}	✓	✓		✓	✓
G_{19}	✓	✓		✓	✓
H_{19}	✓	✓		✓	✓

	πN	$\pi\Delta$	$K\Sigma$
S_{31}	✓		✓
P_{31}			✓
P_{33}	✓		✓
D_{33}	✓		✓
D_{35}			✓
F_{35}	✓		✓
F_{37}	✓		✓
G_{37}	✓		✓
G_{39}	✓		✓
H_{39}	✓		✓

Table 3: List of the parameters from phenomenological contact terms. Here we use the partial wave notation $L_{2I,2J}$ with respect to the πN channel.

	$N(1535)\ 1/2^-$	$N(1650)\ 1/2^-$	$N(939)\ 1/2^+$	$N(1710)\ 1/2^+$	$N(1720)\ 3/2^+$
l_i^E	3	3	-	-	3
l_i^M	-	-	2	3	3

	$N(1900)\ 3/2^+$	$N(1520)\ 3/2^-$	$N(1675)\ 5/2^-$	$N(1680)\ 5/2^+$	$N(1990)\ 7/2^+$
l_i^E	3	3	3	3	3
l_i^M	3	3	3	3	3

	$N(2190)\ 7/2^-$	$N(2250)\ 9/2^-$	$N(2220)\ 9/2^+$		
l_i^E	3	3	2		
l_i^M	3	3	2		

	$\Delta(1620)\ 1/2^-$	$\Delta(1910)\ 1/2^+$	$\Delta(1232)\ 3/2^+$	$\Delta(1920)\ 3/2^+$	$\Delta(1700)\ 3/2^-$
l_i^E	3	3	2	3	3
l_i^M	-	-	2	3	3

	$\Delta(1930)\ 5/2^-$	$\Delta(1905)\ 5/2^+$	$\Delta(1950)\ 7/2^+$	$\Delta(2200)\ 7/2^-$	$\Delta(2400)\ 9/2^-$
l_i^E	3	3	3	3	3
l_i^M	3	3	3	3	3

Table 4: List of the chosen degrees l_i for the pole part of the polynomial parametrization P_i^{P}. The superscript of the l_i denotes the respective multipole.

	S_{11}	P_{11}	P_{13}	D_{13}	D_{15}	F_{15}	F_{17}	G_{17}	G_{19}	H_{19}
$l_{\pi N}^E$	3	-	3	3	3	3	3	2	2	1
$l_{\eta N}^E$	3	-	3	3	3	3	3	2	2	2
$l_{\pi\Delta}^E$	3	-	1	3	3	1	1	1	1	1
$l_{K\Lambda}^E$	3	-	3	3	3	3	3	3	1	1
$l_{K\Sigma}^E$	3	-	3	3	3	3^*	3	2	1	1
$l_{\pi N}^M$	-	3	3	3	3	3^*	3	3	1	1
$l_{\eta N}^M$	-	3	3	3	3	3	3^*	3	2	2
$l_{\pi\Delta}^M$	-	3	2	2	1	0	1	1	1	1
$l_{K\Lambda}^M$	-	3	3	3	2	3	3	3	1	1
$l_{K\Sigma}^M$	-	3	3	3	3	2	2	2	1	1

	S_{31}	P_{31}	P_{33}	D_{33}	D_{35}	F_{35}	F_{37}	G_{37}	G_{39}	H_{39}
$l_{\pi N}^E$	3	-	3	3	3	3	2	2	2	2
$l_{\pi\Delta}^E$	3	-	2	2	2	0	1	1	1	1
$l_{K\Sigma}^E$	3	-	3	3	3	3	2	2	2	2
$l_{\pi N}^M$	-	$3^\dagger$	2	3^*	3	3^*	2	2	2	2
$l_{\pi\Delta}^M$	-	1	2	3	1	1	2	1	1	1
$l_{K\Sigma}^M$	-	3	3	3	3	3	2	2	2	2

Table 5: List of the chosen degrees l_μ for the non pole part of the polynomial parametrization P_μ^{NP}. The superscript of the l_μ denotes the respective multipole. The superscript * denotes that the 0-th order term is 0 and the superscript † means that the 2nd-order term is 0.

for each data set. Such a procedure is widely used for these kind of analyses in the field [5, 134, 149, 310].

Uncertainty estimation

Another challenge is the estimation of uncertainties on the parameters resulting from the fit procedure. Due to numerical limitations, we cannot perform the χ^2 minimization with MINUIT by varying all parameters simultaneously. Instead, we must minimize the χ^2 using subsets of parameters. As a result, the uncertainties provided by MINUIT cannot be used as reliable full-parameter uncertainties. Furthermore, performing a proper statistical error analysis requires one to study the propagation of systematic and statistical uncertainties from the experimental data to the extracted resonance parameters. This includes incorporating the covariance matrices of the data sets or employing methods such as bootstrap resampling and pseudo-data generation to estimate the uncertainties on the fitted parameters. All of this leads to a considerable numerical challenge which is beyond the scope of the current study. Note, that until now such a thorough error analysis has not been carried out in a rigorous way by any coupled-channel analysis group in the field.

Here, we follow a different procedure for this analysis, which was already used in the previous study [117]. We modify the parametrization of our model by including additional s-channel states and perform re-fits. We add one genuine s-channel state in each of the 16 partial waves with zero or one s-channel resonance in the original fit and perform extensive new fits, in which all ”pole” and ”photo” parameters, as well as the ones from contact terms are optimized. We then use the maximal deviation of the re-fits from the original fit value on each resonance parameter as our estimated uncertainties. We show an example for the spread of the pole position of the Roper resonance $N(1440)1/2^+$ in Fig. 8.

Since the re-fits did not significantly improve the data description, we conclude that none of the additional s-channel states should be included in the original parametrization of our model. This procedure leads to a qualitative estimation of uncertainties on the resonance parameter. This is considered a compromise since a rigorous error analysis is not yet possible in the present analysis.

4.3. Fit results for new data sets

The current fit result (labeled as ”JüBo2025”) is presented in Figs. 9 to 13 for the newly included data sets. We added the previous solution ”JüBo2022” from Ref. [117] in the plots for comparison. A complete presentation of the fit result can be found in the supplementary material of this thesis. We further list the χ^2-values of the new data sets in Tab. 6. The full list of χ^2 as well as the references for photoproduction final-states and observables are shown in Tabs. 7, 8 and 9.

As one can see in Fig. 9, the inclusion of the data set from Ref. [291] in the fit leads to improvements on the double polarization observable E for the process $\gamma p \to \pi^0 p$.

For the double polarization observable G, we achieved a large improvement for the process $\gamma p \to \pi^+ n$, c.f Fig. 11. This is due to the significant increase in number of data

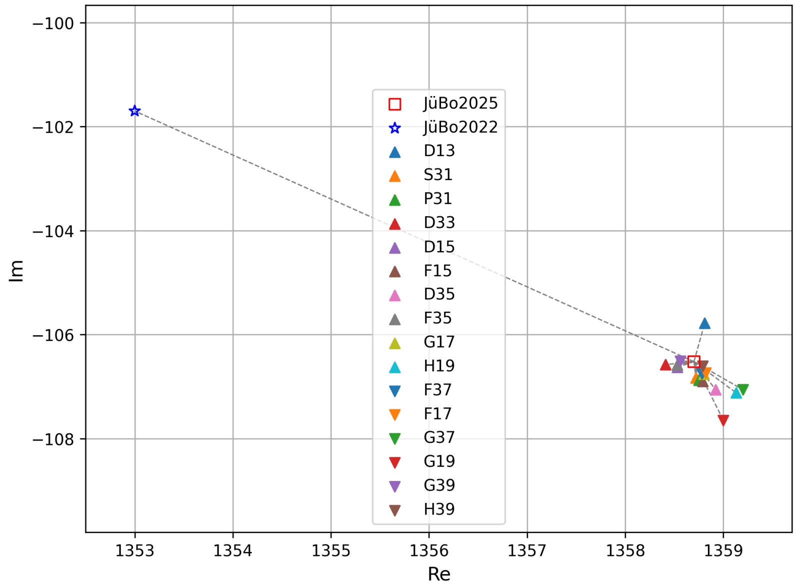

Figure 8: Shown is the spread of the pole position for the Roper resonance $N(1440)1/2^+$ in the re-fits together with the values of the current solution ”JüBo2025” and the 2022 solution ”JüBo2022”.

Table 6: χ^2-values per number of data points (#) and weights used in the weighted fit for the newly included datasets presented in Figs. 9 to 13.

Reaction	Observable (#)	$\chi^2/\#$	weight
$\gamma p \to \pi^0 p$	E (495) [291]	1.62	60
	G (198) [301]	1.57	100
$\gamma p \to \pi^+ n$	G (217) [301]	3.02	130
$\gamma p \to \eta N$	$d\sigma/d\Omega$ (320) [302]	0.85	60
	Σ (80) [302]	0.63	90

Reaction	Observable (# data points)	$\chi^2/\#$
$\gamma p \to \pi^0 p$	$d\sigma/d\Omega$ (18,721) [70, 72, 292, 311–370]	1.6
	Σ (3287) [72, 331, 348, 359, 361, 363, 367, 371–395]	1.4
	P (768) [332, 376, 380, 381, 386, 396–430]	2.7
	T (1404) [348, 368, 370, 376, 380, 381, 386, 423, 428, 431–436]	2.8
	E (1722) [291, 295, 296]	1.9
	$\Delta\sigma_{31}$ (140) [70, 292]	0.8
	G (591) [301, 437–440]	0.9
	H (225) [370, 437, 438]	2.1
	F (397) [436]	3.1
	$C_{x'_L}$ (74) [366, 430, 441]	9.7
	$C_{z'_L}$ (26) [366, 430]	19
$\gamma p \to \pi^+ n$	$d\sigma/d\Omega$ (5670) [70, 331, 341, 351, 442–471]	2.2
	Σ (1456) [331, 374, 375, 392, 395, 467, 472–484]	3.5
	P (265) [476, 479, 485–489]	5.1
	T (718) [476, 479, 489–500]	4.3
	E (903) [70, 293, 298]	1.9
	$\Delta\sigma_{31}$ (231) [70, 293]	1.7
	G (303) [301, 439, 501, 502]	3.0
	H (128) [501–504]	7.4

Table 7: List of the χ^2 per number of data points for the reactions $\gamma p \to \pi N$ for each observable.

Reaction	Observable (# data points)	$\chi^2/\#$
$\gamma p \to \eta p$	$d\sigma/d\Omega$ (9442) [302, 505–526]	0.9
	Σ (615) [302, 513, 520, 527–529]	2.7
	P (63) [297, 510, 530]	4.7
	T (291) [297, 435, 531]	3.8
	E (306) [297, 299]	2.9
	G (47) [297]	2.7
	H (56) [297]	1.1
	F (144) [531]	2.1
$\gamma p \to K\Lambda$	$d\sigma/d\Omega$ (2563) [83, 532–552]	2.5
	Σ (459) [550, 553–556]	2.6
	P (1663) [83, 534, 536, 540, 541, 546–548, 551, 552, 555, 557–559]	1.7
	T (383) [556, 560, 561]	1.8
	$C_{x'}$ (123) [562]	1.2
	$C_{z'}$ (123) [562]	2.2
	$O_{x'}$ (66) [556, 561]	1.3
	$O_{z'}$ (66) [556, 561]	1.3
	O_x (314) [556, 561]	1.8
	O_z (314) [556, 561]	1.4

Table 8: List of the χ^2 per number of data points for the reactions $\gamma p \to \eta p$, $K\Lambda$ for each observable.

Reaction	Observable (# data points)	$\chi^2/\#$
$\gamma p \to K^+\Sigma^0$	$d\sigma/d\Omega$ (4381) [83, 533, 535, 538, 541–550, 563–566]	1.3
	Σ (280) [550, 553, 555, 556, 563]	2.6
	P (402) [83, 546–548, 555, 564]	2.7
	T (127) [556]	1.6
	$C_{x'}$ (94) [562]	2.1
	$C_{z'}$ (94) [562]	1.9
	O_x (127) [556]	2.5
	O_z (127) [556]	1.0
$\gamma p \to K^0\Sigma^+$	$d\sigma/d\Omega$ (281) [567–573]	2.5
	Σ (21) [303]	1.1
	P (188) [303, 567, 570, 572, 574]	2.3
	T (21) [303]	1.7
	O_x (21) [303]	3.8
	O_z (21) [303]	0.7

Table 9: List of the χ^2 per number of data points for the reactions $\gamma p \to K\Sigma$ for each observable.

points here, which were more than tripled. For the final-state $\pi^0 p$ shown in Fig. 10, we got slight improvements, especially at higher energies.

The new η-photoproduction data improved our description of backward angles at energies above 2 GeV as shown by the comparison to the previous solution in Figs. 12 and 13. For the observable Σ there was no data for energies above 2.1 GeV before, which explains the large overall improvement in this observable.

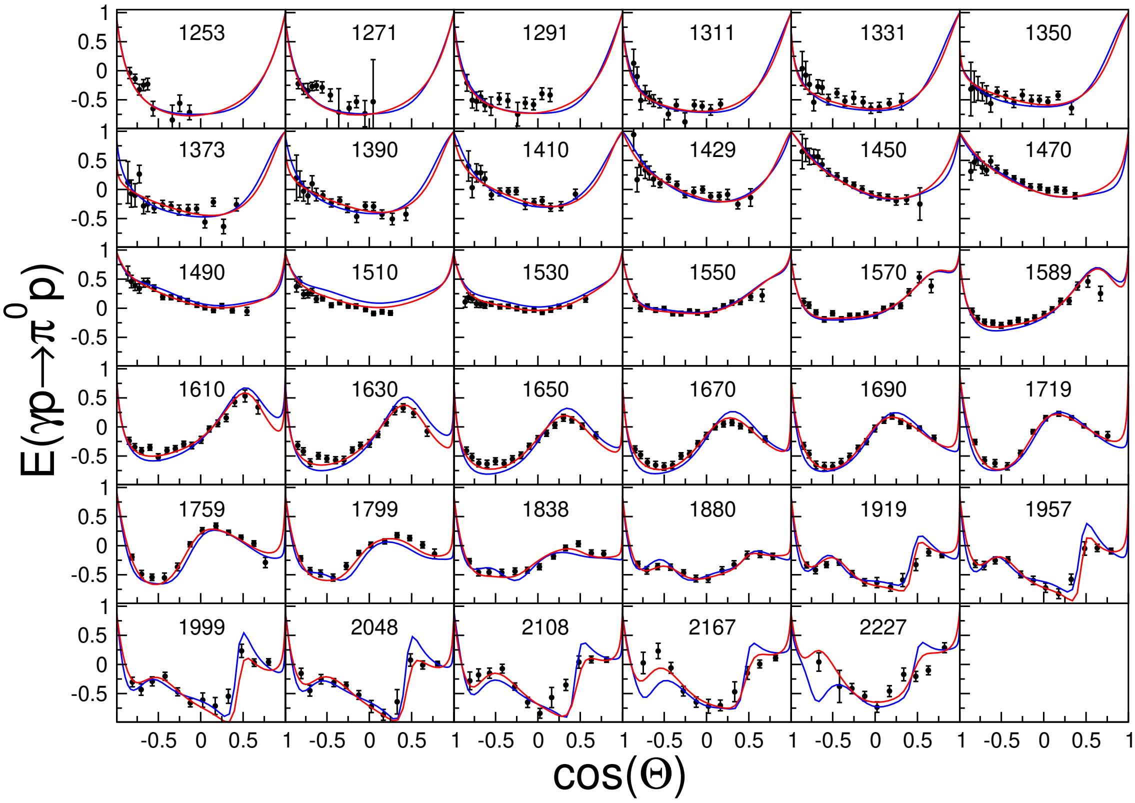

Figure 9: Current fit results (red) and 2022 fit [117] (blue) for comparison for the double spin polarization observable E for the process $\gamma p \to \pi^0 p$. The data was published by the CLAS collaboration in Ref. [291]. The numbers in each plot denote the center of mass energy in MeV.

4.4. Resonance spectrum

We already described the analytic properties of the amplitudes in Sec. 2.1 and the procedure to calculate the resonance parameters in our approach was explained in Sec. 3.6. We use the normalised residues to determine the coupling strengths of individual states to hadronic channels. The definition of normalised residues used in the model is in agreement with the Particle Data Group (PDG) [5]. For the coupling of the photo channel γp to the

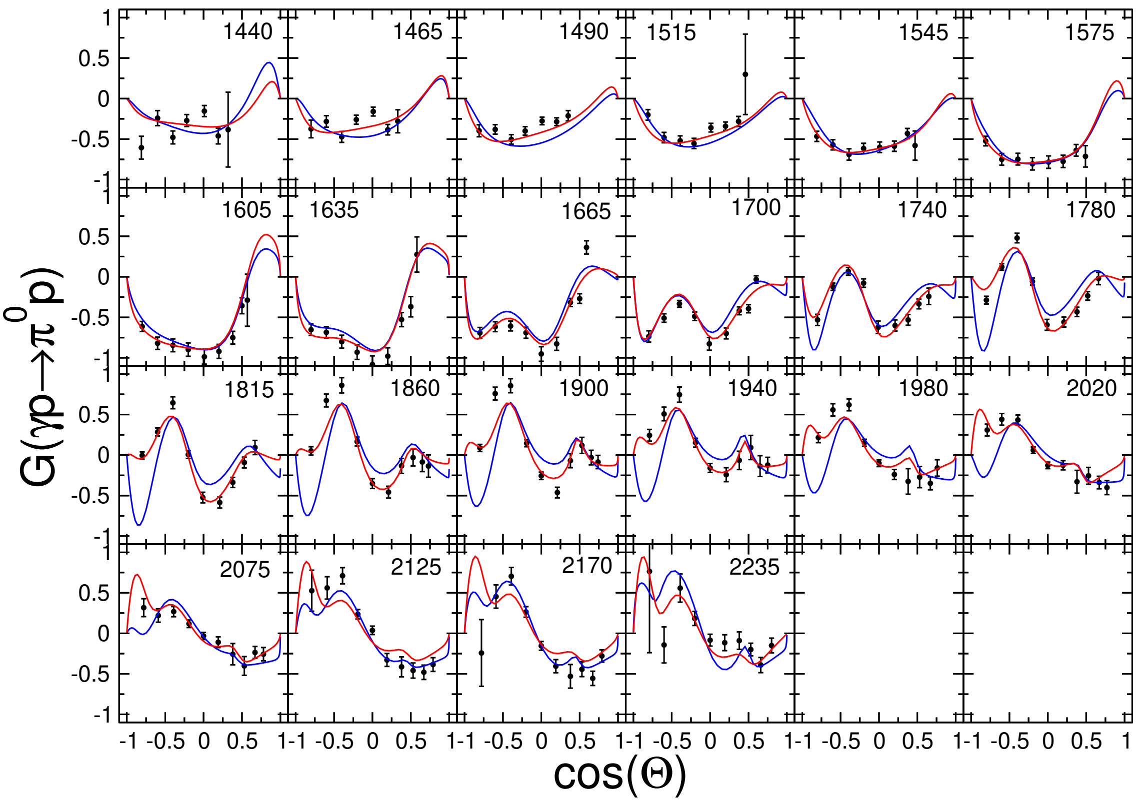

Figure 10: Current fit results (red) and 2022 fit [117] (blue) for comparison for the double polarization observable G for the process $\gamma p \to \pi^0 p$. The data was published by the CLAS collaboration in Ref. [301]. The numbers in each plot denote the center of mass energy in MeV.

resonances we use the PDG convention to define the so-called photocouplings at the pole A_p^h, where the subscript p labels the proton in the initial state here.

We present the resonance parameters in Tabs. 10 and 11. We list the pole positions W_0 and the residues of the states found in this study. We also present the photocouplings at the pole in Tab. 12. We further compare the values with the results from the JüBo2022 study [117] and we list PDG values [5], if an estimate is given. Within our analysis we find all 4-star resonances for $I = 1/2$ and $I = 3/2$ up to $J = 9/2$, except for the $N(1895)1/2^+$, which was not needed in our present study to get a good data description. This resonance was found to be important for the data near the $\eta' N$-threshold [575]. Once we extend the JüBo model to the $\eta' N$ channel, we can judge whether $N(1895)1/2^+$ has to be included within our approach. This kind of extension is planned for the future. A few further resonance states with less than a 4-star rating are also observed within our analysis. The

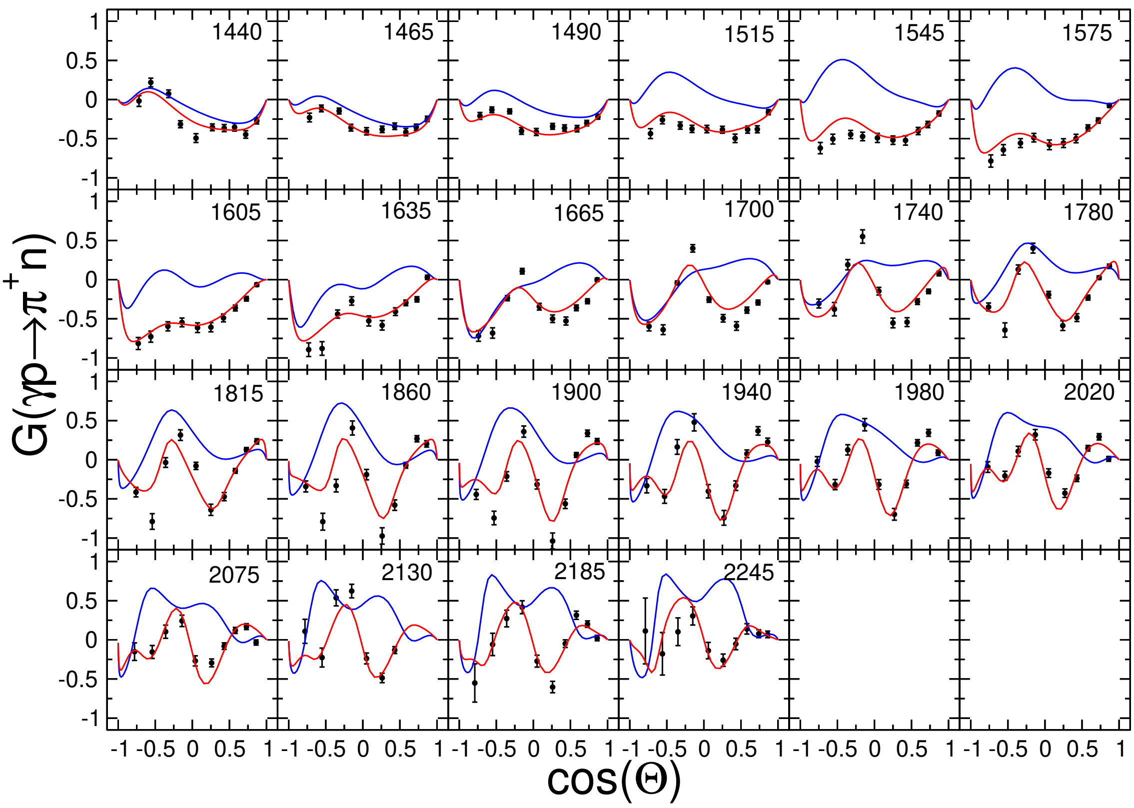

Figure 11: Current fit results (red) and 2022 fit [117] (blue) for comparison for the double polarization observable G for the process $\gamma p \to \pi^+ n$. The data was published by the CLAS collaboration in Ref. [301]. The numbers in each plot denote the center of mass energy in MeV.

full list of resonances found in the present study is given by:

$$\begin{gathered}
N(1535)1/2^-,\ N(1650)1/2^-,\ N(1440)1/2^+,\ N(1710)1/2^+,\\
N(1720)3/2^+,\ N(1900)3/2^+,\ N(1520)3/2^-,\ N(1675)5/2^-,\\
N(1680)5/2^+,\ N(1990)7/2^+,\ N(2190)7/2^-,\ N(2250)9/2^-,\\
N(2220)9/2^+,\ \Delta(1620)1/2^-,\ \Delta(1910)1/2^+,\ \Delta(1232)3/2^+,\\
\Delta(1600)3/2^+,\ \Delta(1920)3/2^+,\ \Delta(1700)3/2^-,\ \Delta(1930)5/2^-,\\
\Delta(1905)5/2^+,\ \Delta(1950)7/2^+,\ \Delta(2200)7/2^-,\ \Delta(2400)9/2^-\ .
\end{gathered}$$

We did not include any new resonance states as genuine s-channel states and did not find any new resonance in this study compared to the previous analysis JüBo2022 [117]. However, there were still some significant changes in the resonance parameters. We discuss the resonance spectrum within the JüBo model in the following part. A short overview of previous JüBo analyses, which we will refer to in the following, is given by:

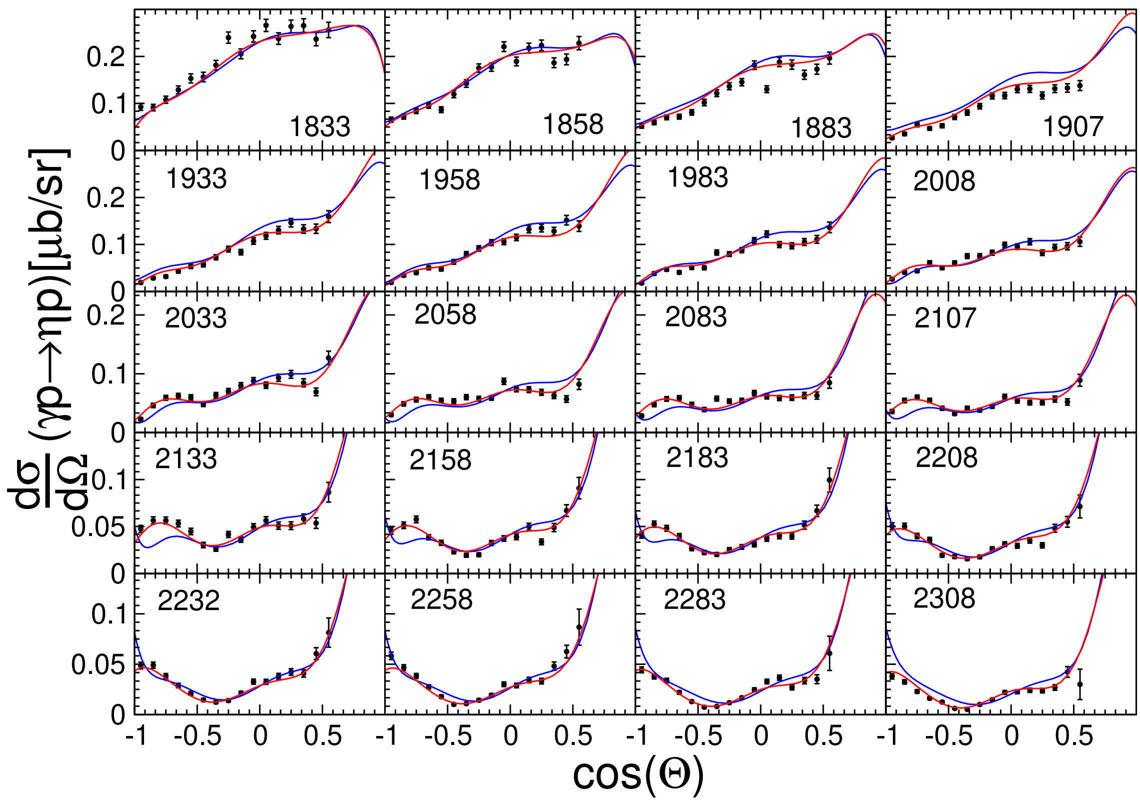

Figure 12: Current fit results (red) and 2022 fit [117] (blue) for comparison for the differential cross section for the process $\gamma p \to \eta p$. The data was published by the LEPS2/BGOegg collaboration in Ref. [302]. The numbers in each plot denote the center of mass energy in MeV.

- **JüBo2013**: Only pion-induced reaction are included in this study. This was the last analysis without photoproduction [113].

- **JüBo2014**: This is the first photoproduction fit of the Jülich-Bonn group. Here $\gamma p \to \pi N$ reactions were included and the γp-photocouplings A_p^h were determined for the first time in this framework. Note that the pole parameters were note varied in this study [114].

- **JüBo2015**: The model was extended to include the photoproduction process $\gamma p \to \eta p$. Different fits were performed in this analysis, but we will refer to the fit "B" here [115].

- **JüBo2017**: In this work the channel space for photoproduction was extended to include the $K\Lambda$ final-state [116].

- **JüBo2022**: This is the most recent study before the one presented in this chapter.

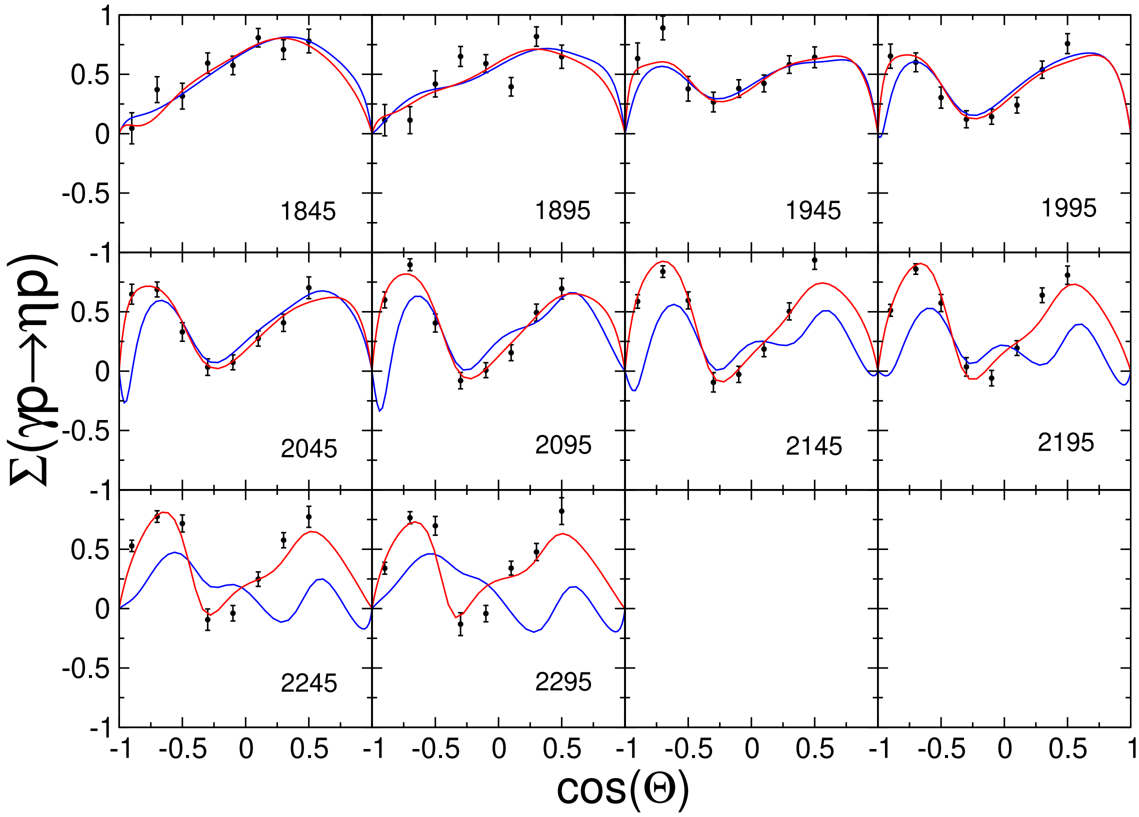

Figure 13: Current fit results (red) and 2022 fit [117] (blue) for comparison for the photon beam asymmetry Σ for the process $\gamma p \to \eta p$. The data was published by the LEPS2/BGOegg collaboration in Ref. [302]. The numbers in each plot denote the center of mass energy in MeV.

Data on the photoproduction reactions $\gamma p \to K\Sigma$ were included here [117].

- **JüBo2025**: This is the new analysis presented in this chapter. Here we included the new data sets and use the result to calculate the GDH sum rule contributions, which we will present in Chapter 6 [1].

We further show a graphical presentation for the pole positions of the different resonances for all of the above JüBo studies and the JüBo2026 analysis (presented in Chap. 5) in Figs. 14 and 15.

N^* resonance spectrum

<u>**$\mathbf{S_{11}}$**</u>: The two well known S_{11} resonance states $N(1535)1/2^-$ and $N(1650)1/2^-$ originate from bare s-channel states within the Jülich-Bonn model.

For the $N(1535)1/2^-$ the real part of the pole position remained stable throughout the different JüBo studies. It lies slightly above the ηN threshold. However, the width varied between the different analyses. In the JüBo2015 and JüBo2017 it was found to be above 100 MeV, but in the earlier analyses of 2013 and 2014 as well as in the recent JüBo2022 and the present JüBo2025 studies it was narrower (Γ = 74-78 MeV). The πN residue $|r_{\pi N}|$ remained around 20 MeV throughout the different analyses. The branching ratio into the ηN channel has been large in all studies ($\approx$ 50%) and even increased slightly in this work to 55%. The coupling to the $K\Lambda$ channel was less than 10% until the JüBo2017 analysis. After the inclusion of $\gamma p \to K\Sigma$ data in JüBo2022, the $K\Lambda$ residue increased significantly to 26%. Even though it decreased in the present study, it remains large at 22%. The normalised residue of the $K\Sigma$ increased significantly in the JüBo2022 study to 27%, while it was around 5% in the earlier photoproduction studies. However, in the current work, it was decreased significantly back to 6.7%. It should be noted, that the $N(1535)1/2^-$ lies relatively far below the $K\Sigma$ threshold, which makes the determination of the normalized residues difficult. The photocoupling $A_p^{1/2}$ was found to be small compared to other groups in the first photocoupling study JüBo2014 [114], but in the JüBo studies after it increased to values similar to the ones found in studies of other groups and remained stable.

For the $N(1650)1/2^-$ the pole position remains stable throughout all JüBo analyses and they agree with the PDG estimates. The real part only slightly decreased in the present result compared to JüBo2022. While the πN residue doubled its value in the JüBo2022 analysis, it decreased again in the current work and is now close to the PDG estimate. The ηN, $K\Lambda$ and $K\Sigma$ couplings increased significantly in the JüBo2022 study compared to earlier works. The change in the ηp channel was argued to origin from the inclusion of new data on the observables T, E, P, H and G [117]. In the present analysis we observe that all these couplings decreased again. It should further be noted, that the estimated uncertainties for the $N(1650)1/2^-$ are much smaller than in the JüBo2022 study, even though the same procedure was used. The γp photocoupling was slightly smaller than the values found by other groups in 2014, but increased slightly in subsequent studies and agrees with the results found by other groups.

$\underline{\mathbf{P_{11}}}$: In the P_{11} partial wave we find the two poles of the $N(1440)1/2^+$ and $N(1710)1/2^+$ resonances. The nucleon ground state is also included as a bare s-channel state, but we use a renormalization procedure, in which the bare mass and πN coupling are normalized so that the dressed quantities are fixed to the physical values [115]. Until the JüBo2017 study, we found another dynamically generated pole at $W_0 = 1750 - i\,159$ MeV labeled as $N(1750)1/2^+$ [116]. This resonance could not be identified with any listed in the PDG. However, in the JüBo2022 and JüBo2025 analyses this resonance is not seen anymore.

The $N(1440)1/2^+$ state is the famous Roper resonance. It is dynamically generated in the Jülich-Bonn model, predominantly by correlated 2π exchange with ρ quantum numbers and has strong contributions from the σN channel [33, 106]. The pole position remained stable throughout the different JüBo studies, but both the real part and width increased slightly in the present result. While the real part of the pole position agrees with the value listed in the PDG, the width within our study is marginally higher than the PDG estimate. The πN residue is stable throughout all analyses. The normalised residues into the channels ηN and KY were found to be small (1−2%), when only studying pion-induced data. The ηN residue increased to values $\approx 8\%$ over the course of the photoproduction studies. The $K\Lambda$ coupling also changed throughout the photoproduction analyses and is now 6.2%, while the $K\Sigma$ residue was found to be sub 1% for the Roper resonance. In the JüBo2014 study its photocoupling was found at $-54 \times 10^{-3}\text{GeV}^{-1/2}$ and it increased in magnitude over the course of the different photoproduction analyses. In the present work it was found at almost double the initial magnitude.

The $N(1710)1/2^+$ originated from the second s-channel pole (apart from the nucleon) in the P_{11} partial wave up to the JüBo2017 study. However, in the JüBo2022 analysis it was found that the s-channel state moved far into the complex plane and thus is not included in the resonance table. However, the $N(1710)1/2^+$ was still present and since then considered a dynamically generated pole. The pole position varied a lot within the JüBo studies. This is mainly explained by the change from it being an s-channel induced pole to a dynamically generated one and its interplay with the $N(1750)1/2^+$ resonance, which is not observed anymore. This shows that a pole cannot be assigned unambiguously to a specific s-channel term or to be fully dynamically generated, since our approach is highly nonlinear. Consequently, an interpretation of the nature of a state requires the use of other methods, e.g. compositeness or elementariness criteria as it was done within the JüBo framework in Refs. [218, 219]. In the present work the pole position of the $N(1710)1/2^+$ only changed slightly compared to JüBo2022 and is located at $1588(8) - i\ 56(4)$ MeV. This resonance couples weakly to the πN and $K\Sigma$ channels and dominantly to ηN and $K\Lambda$. The photocoupling remained stable at $\approx -20 \times 10^{-3}\text{GeV}^{-1/2}$ throughout the different studies.

P_{13}: For the P_{13} partial wave we observe two s-channel induced poles, the $N(1720)3/2^+$ and the $N(1900)3/2^+$.

For the $N(1720)3/2^+$ resonance the real part of the pole position varied between values below and above 1700 MeV, but it did not change significantly in the present work compared to JüBo2022 and we found a value of 1720(2) MeV. The width also changed throughout the different analyses. While the width was above 200 MeV until 2015, it decreased continuously in the more recent ones and has a value of 166(4) MeV in the present one. This agrees with the lower threshold of the PDG estimate. The πN residue and the normalised residues into the inelastic channels were stable in all analyses except for the JüBo2022 study. This increase of the residues in the JüBo2022 analysis could not be observed in the present one and all of them decreased again. The photocoupling $A_p^{1/2}$ decreased throughout the JüBo studies and in the present study it decreased even further to approximately half of the initial value of JüBo2014. For the $A_p^{3/2}$ photocoupling we found an increase from 2014 to 2015 and it was stable since then at a magnitude of approximately $25 \times 10^{-3}\text{GeV}^{-1/2}$.

The second P_{13} resonance is the $N(1900)3/2^+$, which was first included as a genuine s-channel state into the framework within the JüBo2017 study. Within the JüBo2017 work the width was found to be quite large at a value of 217(23) MeV, but it was significantly smaller in the JüBo2022 study ($<$ 100 MeV). In the present work it increased to 141(1) MeV, which agrees with the PDG estimate. The mass of this resonance

(1904(1) MeV) and the elastic residue $|r_{\pi N}|$ did not change significantly compared to the previous studies. We further observe a significant increase for the $N(1900)3/2^+$ residue into ηN and $K\Lambda$ in the present study. The $K\Sigma$ residue was 10% in the JüBo2017 analysis, but decreased significantly in the most recent and the current work to 1.5%. The photocouplings A_p^h decreased significantly from the JüBo2017 to the JüBo2022 study. In the present work we observe a decrease in the $A_p^{1/2}$ but a significantly increase for the magnitude of the $A_p^{3/2}$.

Within the JüBo2022 study we have already observed a high impact of the P_{13} resonances on the $\gamma p \to \eta p$ observables. In the present study we find the same influence. We visualized this influence on the $\gamma p \to \eta p$ data included in this study in the Appendix in Fig. 26.

D_{13}: We only observe the s-channel resonance $N(1520)3/2^-$ in the D_{13} partial wave.

In the studies until 2017 the mass of the $N(1520)3/2^-$ was found above 1500 MeV and decreased to values below in the JüBo2022 and the present works. The width varied between values of $89-126$ MeV throughout the studies. In the present analysis the width has a value of 102(6) MeV which agrees with the PDG estimate within the uncertainties. The elastic πN residue decreased throughout the studies from a value of ≈ 40 MeV in 2013 to 26(5) MeV in the present work. All inelastic residues had values of only a few % and only varied slightly throughout the analyses. The photocouplings A_p^h varied a lot since the JüBo2014 study and in the present analysis they decreased in magnitude, especially for the $A_p^{1/2}$.

As in the previous JüBo studies we see indications for a dynamically generated resonance $N(1875)3/2^-$ in the present analysis. The pole position is found at $1914(1) - i\,343(2)$ MeV. However, it has a width of 686 MeV, which is still significantly larger than the estimate of the PDG [5] of 160 ± 60 MeV. Such a broad state can only have a small influence on the physical axis. Consequently we do not include it in the resonance table.

D_{15}: We observe the $N(1675)5/2^-$ in the D_{15} partial wave which originates from an s-channel state.

The pole position of the $N(1675)5/2^-$ only varied slightly throughout the different JüBo analyses and is located at $W_0 = 1644(1) - i\,58(1)$ MeV in the present study. The elastic residue $|r_{\pi N}|$ was stable in the past analyses and varied only within values of $22-28$ MeV, but decreased in the current one to 14(5) MeV. The coupling to the ηN final-state has always been the largest one for the inelastic channels at $> 5\%$, but it decreased significantly in the JüBo2025 analysis to 3.5%. The $K\Lambda$ residue is very small throughout all analyses. The $K\Sigma$ coupling decreased slightly in the JüBo2017 study in which photoproduction to $K\Lambda$ was included and is stable at 2.2% since then.

The photocoupling $A_p^{1/2}$ increased in the photoproduction analyses until 2017. After the inclusion of the $K\Sigma$ final-state in the JüBo2022 there was a noticeable decrease in this photocoupling, but in the present work we find a similar value as in JüBo2017. For the $A_p^{3/2}$ we observed a significant increase after the inclusion of η photoproduction in the JüBo2015 analysis and its value was stable in all recent JüBo studies. In the present work the $A_p^{3/2}$ photocoupling decreased to a value similar to the initial one found in 2014 of

$35(5) \times 10^{-3}\mathrm{GeV}^{-1/2}$, which is likely explained by the lower residues for the final-states πN and ηN.

In the JüBo2017 analysis a dynamically generated pole was found in the D_{15} partial wave at $W_0 = 1924 - i\,100$ MeV. This pole could correspond to the 2 star resonance labeled $N(2060)5/2^-$ in the PDG. There were also inconclusive indications for this state by another study on the beam asymmetry for the process $\gamma p \to \eta p$ [528]. However, this pole was not observed in the JüBo2022 and the present study.

$\mathbf{F_{15}}$: In the F_{15} partial wave we only observe the s-channel resonance $N(1680)5/2^+$.

The mass of the $N(1680)5/2^+$ was stable throughout all JüBo studies and agrees with the PDG estimate. In contrast to this the width varied a lot in the different photoproduction studies. There were significant decreases of 20 MeV in both the JüBo2015 and JüBo2017 studies. However, after the inclusion of the $K\Sigma$ channel in 2022 the width of the $N(1680)5/2^+$ increased back to a value, which agrees with the PDG estimate. The πN residue was stable at ≈ 35 MeV throughout the JüBo studies. Even though we find a larger value in the present work, it is accompanied by a large uncertainty such that it agrees with the values of of previous analyses. The normalised residues for the inelastic channels were below 1% before including photoproduction data. We observed that the residues for both the ηN and the $K\Lambda$ final-states increased after their respective extensions in 2015 and 2017, but decreased in the following analyses again. In the present work the ηN coupling decreased further, which is likely caused by the inclusion of new data for $\gamma p \to \eta p$. However, the residues for the KY channels increased in the current result.

Within the JüBo studies the photocoupling $A_p^{1/2}$ has been much smaller in magnitude compared to $A_p^{3/2}$. This is further emphasized in the present result in which the modulus of $A_p^{1/2}$ decreased further to $-8(2) \times 10^{-3}\mathrm{GeV}^{-1/2}$ and we observe a significant increase for $A_p^{3/2}$ to $133(34) \times 10^{-3}\mathrm{GeV}^{-1/2}$.

$\mathbf{F_{17}}$: For the F_{17} partial wave we observe the $N(1990)7/2^+$, which has only a 2 star rating in the PDG.

The pole positions varied a lot throughout the different JüBo analyses. However, it did not change significantly in the present study compared to the JüBo2022. We observe a very small πN residue for the $N(1990)7/2^+$ in all studies, which is much narrower than the values found by other groups listed in the PDG [134, 143, 576]. All normalised residues were smaller than 2% until 2017, but we noticed a significant increase for the ηN residue in the JüBo2022 analysis. The $N(1990)7/2^+$ has a large influence on the forward peak in the beam asymmetry for the $\gamma p \to \eta p$ process. This large influence is also observed in the present study and we visualize this in the appendix in Fig. 27.

The photocouplings for the $N(1990)7/2^+$ had large uncertainties and varied in the different photoproduction analyses. However, in the present analysis the magnitudes of the photocouplings decreased and the uncertainties determined by the refits are much smaller compared to recent studies.

$\mathbf{G_{17}}$: The G_{17} features the 4-star resonance $N(2190)7/2^-$.

The mass of the $N(2190)7/2^-$ was found above 2050 MeV until the JüBo2017 analysis, but it decreased by 120 MeV after the inclusion of $K\Sigma$ data in 2022 and further decreased in the present study. The width of the $N(2190)7/2^-$ resonance was ≈ 280 MeV in the more recent analyses (and even above 300 MeV in 2014 and 2015), but we find a much lower width of 161(2) MeV in the present work. We already observed this change after the inclusion of the new polarization data for $K^0\Sigma^+$ photoproduction [303]. Our width is in clear disagreement with the PDG estimate. The $N(2190)7/2^-$ couples predominantly to the πN channel in all analyses, even though the corresponding residue decreased throughout the different studies.

The large change in the width is also reflected in the $A_p^{3/2}$ photocoupling, which reduced by 2/3 of the value found in JüBo2022.

<u>$\mathbf{G_{19}}$</u>: We observe the resonance $N(2250)9/2^-$ induced by a s-channel pole in the G_{19} partial wave.

We find large variations in the pole position of this resonance in the different JüBo studies. In the present work we find an increase by 99 MeV of the mass and the width decreased by 48 MeV compared to the JüBo2022 analysis. For the residues we observed very low values in the JüBo2017 study, in which the $K\Lambda$ final-state was included. However the residues increased again in the JüBo2022 analysis except for the $K\Lambda$ channel. In the present study we also find higher values for the residues than in 2022. We find large uncertainties within our estimation, but this is typical for higher lying resonances.

<u>$\mathbf{H_{19}}$</u>: In the H_{19} we find one s-channel pole, the $N(2220)9/2^+$.

The pole position of the $N(2220)9/2^+$ did not change significantly until the JüBo2017 analysis, but after the inclusion of $K\Sigma$ in 2022 we observe a much narrower width. In the present work we also find a significant smaller real part of the pole position. The $N(2220)9/2^+$ has a large coupling to πN, even though it decreased in the JüBo2022 and the present studies. The branching ratios into the inelastic channels have been small in past studies, but the ηN and $K\Lambda$ ones increased in 2022. In the present work the two respective residues decreased again.

We see large fluctuations in the photocouplings for the H_{19} resonance, but in the present work we find significant smaller values compares to past studies.

Δ resonance spectrum

<u>$\mathbf{S_{31}}$</u>: In the S_{31} partial wave we find the well-established resonance $\Delta(1620)1/2^-$.

The pole position was stable throughout all JüBo photoproduction analyses except for an increase in the width from 66(7) MeV to 85(5) MeV after the inclusion of $K\Sigma$ final-state data in the JüBo2022 study. We further observed a significant reduction of the normalised residues for both $K\Sigma$ and $\pi\Delta$ in 2022. The $\Delta(1620)1/2^-$ predominantly couples to the $\pi\Delta$ channel, which is further emphasized in the present result where the respective residue increased back to 51(9)%.

The photocoupling $A_p^{1/2}$ of the $\Delta(1620)1/2^-$ was small compared to the values of all other Δ resonances in recent JüBo studies, which could be explained by the small width and large inelastic residues. However, in the present analysis we observe an increase for photocoupling of the $\Delta(1620)1/2^-$ and we also find small photocouplings for other Δ resonances (e.g. $\Delta(1600)3/2^+$).

<u>$\mathbf{P_{31}}$</u>: The P_{31} features only the $\Delta(1910)1/2^+$, which originates from a genuine s-channel

pole.

The $\Delta(1910)1/2^+$ is a very wide resonance and couples weakly to πN channel. Furthermore, it is accompanied by a large, energy-dependent background. These problems lead to large uncertainties and variations for the extracted resonance parameters. In the JüBo2022 study we noticed a large decrease in the width and all residues. In the present analysis this trend can be observed again except for the $K\Sigma$ residue, which increased slightly. We also observe this for the photocoupling $A_p^{1/2}$, which significantly decreased in the present work compared to the value found in 2022.

$\mathbf{P_{33}}$: In the P_{33} we got the famous $\Delta(1232)3/2^+$ as well as the two resonances $\Delta(1600)3/2^+$ and the $\Delta(1920)3/2^+$. In this partial wave we observed a change in the analytic structure of the JüBo2022 analysis. The $\Delta(1600)3/2^+$ resonance was dynamically generated in older JüBo studies but was found to be induced by a s-channel pole in the P_{33} partial wave in 2022. For the $\Delta(1920)3/2^+$ this was the opposite. This shows the difficulties in understanding the nature of resonances in coupled-channel approaches, which is further discussed within the Jülich-Bonn framework in Refs. [218, 219].

The $\Delta(1232)3/2^+$ is stable throughout all different JüBo analyses and its resonance parameters are close to the PDG estimates.

The $\Delta(1600)3/2^+$ changed its pole position and πN residue significantly after the inclusion of the first strangeness channel $K\Lambda$ in 2017. Since the $I = 3/2$ resonances do not couple to the $K\Lambda$ channel, one may expect no major changes in the Δ resonances. However, we refit the whole data base in our JüBo analyses. Thus, changes in the $I = 1/2$ resonances due to a new channel (e.g. $K\Lambda$) will also lead to changes in $I = 3/2$ resonances for coupled channel approaches.

The mass of the $\Delta(1600)3/2^+$ increased, while the width was much narrower in the JüBo2017 analysis. These changes continued in the JüBo2022 and the present studies. Our width is much lower than the value suggested by the PDG.

The photocouplings of the $\Delta(1600)3/2^+$ resonance are relatively small when compared to the other $I = 3/2$ photocouplings. In the present study the value of the $A_p^{1/2}$ even decreased further.

The $\Delta(1920)3/2^+$ is very broad ($\Gamma > 800$ MeV). The mass underwent a significant change in the JüBo2017 analysis by increasing over 200 MeV compared 2015. Since then the real part of the pole position decreased again to a value of 1857(15) MeV in the present study. This resonance is very dominant in the $K\Sigma$ channel over a large energy range. This is further reflected by the large photocouplings of this resonance throughout all JüBo analyses. Note that in the present study the width and residues increased even further.

The large width of the $\Delta(1920)3/2^+$ may be an artifact of the parametrization of our amplitude, but it is certain that the P_{33} partial wave has a major influence on the $K\Sigma$ final-state.

$\mathbf{D_{33}}$: The D_{33} features only the s-channel pole $\Delta(1700)3/2^-$.

The pole position had no significant changes until the JüBo2022 study, in which the real part decreased by approximately 40 MeV. However, this change was accompanied with a large uncertainty. In the present work the mass increased to a value close to the ones found in earlier studies and agrees with the estimates of the PDG, but the width increased to 354(13) MeV. This width is in disagreement with the PDG estimate. We also observe that all residues in the present study are notable higher than in the past analyses. This is also reflected in the larger photocouplings.

In the JüBo2022 analysis we found indications of a dynamically generated pole located at $W_0 = 2118(10) - i356(73)$ MeV, which couples strongly to the $K\Sigma$ channel. This pole is again observed in the present analysis but with a smaller imaginary part of approximately 250 MeV. This pole may be associated with the 2-star resonance $\Delta(1940)3/2^-$ listed in the PDG, even though our pole position differs from the PDG estimate of $W_0 = 2000 \pm 60 - i(200 \pm 50)$ MeV.

<u>$\mathbf{D_{35}}$ & $\mathbf{F_{35}}$:</u> In the D_{35} we find the $\Delta(1930)5/2^-$ resonance and in the F_{35} we observe the $\Delta(1905)5/2^+$, which both originate from genuine s-channel diagrams.

In the $J = 5/2$ partial waves we can observe an interplay between the two delta resonances. Large changes for both resonances in the pole positions could be observed in the JüBo2017 and the JüBo2022 studies. It is also noteworthy that both had large uncertainties in the JüBo2017 analysis. In the present study we find a significant increase in the width of the $\Delta(1905)5/2^+$, which also lead to much larger photocouplings.

<u>$\mathbf{F_{37}}$:</u> For the F_{37} partial wave we have the s-channel pole $\Delta(1950)7/2^-$.

The mass of this resonance changed significantly in the 2017 analysis, in which the $K\Lambda$ channel was included. In the following extension to $K\Sigma$ this change in the mass was reverted, but the width was significantly narrower. In the present study there is no noteworthy change of the pole position. We also notice an increase in the πN and $\pi\Delta$ residue in the present work. The narrower width also lead to lower photocouplings A_p^h in the JüBo2022 and these have no noteworthy change in the present analysis. Even though the normalised residue for the $K\Sigma$ channel is only at 1.9(0.5)%, we already observed in the JüBo2013 study that this resonance is important for the reaction $\pi N \to K\Sigma$.

<u>$\mathbf{G_{37}}$:</u> We observe the 3-star resonance $\Delta(2200)7/2^-$ in the G_{37} partial wave.

We again see large changes in the pole position in 2017 and 2022, in which the strangeness channels were included. In the JüBo2022 and the present work we even find real parts below 2000 MeV. The πN coupling of this resonance is smaller than the ones of other Δ resonances. Furthermore, the residues of the inelastic channels decreased significantly in the JüBo2022 analysis and have no relevant changes in the present work. For the photocouplings we find a slightly lower value for $A_p^{1/2}$, but the $A_p^{3/2}$ photocoupling increased significantly.

<u>$\mathbf{G_{39}}$:</u> Our s-channel diagram in the G_{39} partial wave induces the $\Delta(2400)9/2^-$ pole. This resonance has a 2-star rating in the PDG.

The pole position of this resonance varies a lot throughout the different JüBo analyses. While both the real and imaginary part had large changes in the JüBo2017 analysis, we find a way larger mass in the JüBo2022 study, which increased further in the present result. It is also noteworthy that the width is much narrower in the new JüBo2025 solution ($\Gamma = 86(37)$ MeV). We also find significantly larger residues in the present analysis compared to 2022.

In the JüBo2022 study we found indications of a dynamically generated pole in the G_{39}

partial wave located at $W_0 = 1941(12) - i260(24)$ MeV, which is also found nearby in the present work. However, this pole is not listed in the resonance table for now, since more evidence is required to confirm its existence.

Table 10: For the $I = 1/2$ resonances we present the extracted resonance parameters of the new solution JüBo2025, namely the pole positions W_0 ($\Gamma_{\rm tot}$ defined as -2ImW_0), the elastic πN residues ($|r_{\pi N}|, \theta_{\pi N\to\pi N}$), and the normalized residues ($\sqrt{\Gamma_{\pi N}\Gamma_\mu}/\Gamma_{\rm tot}, \theta_{\pi N\to\mu}$) for the inelastic reactions $\pi N \to \mu$ with $\mu = \eta N$, $K\Lambda$, $K\Sigma$. In addition to the present study ("2025"), we list the JüBo2022 results ("2022") [117] and the estimates from the Particle Data Group [5] ("PDG"), if available, as well as the PDG star rating.

	fit	Re W_0 [MeV]	-2Im W_0 [MeV]	$\lvert r_{\pi N}\rvert$ [MeV]	$\theta_{\pi N\to\pi N}$ [deg]	$\frac{\Gamma^{1/2}_{\pi N}\Gamma^{1/2}_{\eta N}}{\Gamma_{\rm tot}}$ [%]	$\theta_{\pi N\to\eta N}$ [deg]	$\frac{\Gamma^{1/2}_{\pi N}\Gamma^{1/2}_{K\Lambda}}{\Gamma_{\rm tot}}$ [%]	$\theta_{\pi N\to K\Lambda}$ [deg]	$\frac{\Gamma^{1/2}_{\pi N}\Gamma^{1/2}_{K\Sigma}}{\Gamma_{\rm tot}}$ [%]	$\theta_{\pi N\to K\Sigma}$ [deg]
$N(1535)\ 1/2^-$	2025	1504 (1)	78 (2)	20 (1)	-27 (1)	55 (1)	128 (0)	22 (1)	-56 (1)	6.7 (1.3)	79 (9)
	2022	1504 (0)	74 (1)	18 (1)	-37 (3)	50 (3)	118 (3)	26 (2)	-67 (3)	28 (2)	92 (3)
****	PDG	1510 ± 10	110^{+20}_{-30}	25 ± 10	-20 ± 20	—	—	—	—	—	—
$N(1650)\ 1/2^-$	2025	1671 (2)	127 (3)	42 (1)	-54 (2)	24 (1)	39 (3)	17 (0)	-73 (2)	27 (1)	-61 (2)
	2022	1678 (3)	127 (3)	59 (21)	-18 (46)	34 (12)	71 (45)	26 (10)	-40 (46)	41 (15)	-21 (47)
****	PDG	1665 ± 15	135 ± 35	45^{+10}_{-20}	-70^{+20}_{-10}	—	—	—	—	—	—
$N(1440)\ 1/2^+$	2025	1359 (1)	213 (2)	61 (1)	-99 (1)	8.4 (0.4)	-32 (2)	6.2 (1.8)	140 (4)	0.9 (1.4)	-23 (9)
	2022	1353 (1)	203 (3)	59 (2)	-104 (4)	8.4 (0.4)	-28 (4)	2.5 (0.9)	-92 (86)	0.2 (0.5)	-32 (154)
****	PDG	1370 ± 10	190^{+15}_{-10}	55 ± 5	-90 ± 10	—	—	—	—	—	—
$N(1710)\ 1/2^+$	2025	1588 (5)	113 (9)	3.4 (0.7)	-115 (4)	21 (1)	86 (2)	14 (2)	-157 (4)	4.7 (0.4)	161 (3)
	2022	1605 (14)	115 (9)	5.5 (4.7)	-114 (57)	28 (26)	91 (63)	20 (19)	-144 (77)	5.5 (4.8)	162 (305)
****	PDG	1700 ± 50	120 ± 40	7^{+3}_{-4}	190^{+80}_{-70}	—	—	—	—	—	—
$N(1720)\ 3/2^+$	2025	1720 (2)	166 (4)	4.8 (3.7)	-16 (43)	2.5 (1.6)	99 (32)	1.2 (0.3)	-71 (31)	1.2 (0.9)	107 (37)
	2022	1726 (8)	185 (12)	15 (2)	-60 (5)	4.9 (0.9)	64 (10)	3.4 (0.4)	-101 (8)	5.9 (1)	82 (6)
****	PDG	1680^{+30}_{-20}	200^{+200}_{-50}	15 ± 10	-110 ± 50	—	—	—	—	—	—
$N(1900)\ 3/2^+$	2025	1904 (1)	141 (1)	1.1 (0.3)	-93 (4)	2.2 (0.2)	-2 (4)	4.2 (0.3)	-62 (3)	1.5 (0.2)	-79 (8)
	2022	1905 (3)	93 (4)	1.6 (0.3)	44 (21)	1.0 (0.3)	55 (29)	2.9 (0.6)	5.4 (18.6)	1.3 (0.3)	-40(18)
****	PDG	1920 ± 20	130^{+30}_{-40}	4 ± 2	-10 ± 30	—	—	—	—	—	—
$N(1520)\ 3/2^-$	2025	1496 (1)	102 (6)	26 (5.2)	-17 (4)	1.8 (0.8)	68 (9)	2.9 (7.4)	140 (15)	3.1 (20)	-36 (4)
	2022	1482 (6)	126 (18)	27 (21)	-36 (48)	2.1 (1.8)	34 (53)	2.6 (1.9)	127 (47)	1.0 (1.2)	94 (68)
****	PDG	1510 ± 5	110^{+10}_{-5}	35 ± 3	-10 ± 5	—	—	—	—	—	—
$N(1675)\ 5/2^-$	2025	1644 (1)	117 (2)	14 (5)	13 (16)	3.5 (1.0)	-9 (16)	< 0.1 (0.0)	-65 (49)	2.2 (0.5)	-144 (16)
	2022	1652 (3)	119 (1)	22 (1)	-17 (2)	6.3 (0.9)	-39 (2)	< 0.1 (0.2)	174 (161)	2.4 (0.2)	-166 (5)
****	PDG	1655 ± 5	135 ± 15	26^{+6}_{-4}	-22 ± 5	—	—	—	—	—	—
$N(1680)\ 5/2^+$	2025	1663 (5)	114 (3)	46 (18)	-41 (12)	0.1 (0.1)	-44 (110)	0.9 (0.3)	-121 (15)	0.1 (0.2)	-49 (196)
	2022	1657 (3)	120 (2)	36 (1)	-31 (1)	0.6 (0.7)	118 (2)	0.6 (0.1)	-119 (3)	< 0.1 (0.2)	-46 (29)
****	PDG	1670 ± 10	120^{+15}_{-10}	40 ± 5	-20 ± 10	—	—	—	—	—	—
$N(1990)\ 7/2^+$	2025	1851 (6)	82 (10)	0.18 (0.02)	-99 (4)	5.2 (0.4)	-50 (3)	0.1 (0.1)	-62 (190)	0.7 (0.3)	-64 (4)
	2022	1861 (9)	72 (5)	0.16 (0.01)	-119(4)	4.8 (0.2)	-43 (4)	0.4 (0.1)	133 (4)	1.0 (0.3)	-54 (4)
**	PDG	—	—	—	—	—	—	—	—	—	—
$N(2190)\ 7/2^-$	2025	1943 (8)	161 (2)	15 (1)	-45 (1)	2.9 (0.3)	-52 (1)	3.6 (0.5)	-62 (1)	1.1 (0.2)	-71 (2)
	2022	1965 (12)	287 (66)	18 (7)	-45 (27)	2.1 (1)	-65 (29)	2.6 (1.4)	-78 (30)	0.5 (0.2)	-92 (31)
****	PDG	2050 ± 100	400 ± 100	40 ± 20	0 ± 30	—	—	—	—	—	—
$N(2250)\ 9/2^-$	2025	2194 (43)	374 (65)	21 (10)	-45 (12)	3.8 (1.7)	-62 (14)	0.1 (0.1)	-76 (204)	1.1 (0.7)	-76 (13)
	2022	2095 (20)	422 (26)	14 (2)	-67 (17)	1.8 (0.2)	-89 (9)	0.3 (0.1)	80 (9)	0.4 (0.4)	-111 (9)
****	PDG	2150 ± 50	420^{+80}_{-70}	25^{+5}_{-10}	-40 ± 20	—	—	—	—	—	—
$N(2220)\ 9/2^+$	2025	2009 (46)	367 (41)	30 (4)	-52 (16)	2.3 (0.2)	-89 (13)	1.4 (0.3)	-106 (15)	0.2 (0.2)	-122 (199)
	2022	2131 (12)	388 (12)	48 (10)	-13 (3)	4.2 (1.1)	-48 (4)	2.0 (0.5)	-60 (4)	0.3 (1.6)	-70 (4)
****	PDG	2150^{+50}_{-20}	400^{+80}_{-40}	45^{+15}_{-10}	-40^{+30}_{-20}	—	—	—	—	—	—

Table 11: For the $I = 3/2$ resonances we present the extracted resonance parameters of the new solution JüBo2025, namely the pole positions W_0 (Γ_{tot} defined as -2ImW_0), elastic πN residues ($|r_{\pi N}|, \theta_{\pi N \to \pi N}$), and the normalized residues $\pi N \to K\Sigma$ and $\pi N \to \pi\Delta$ with the number in brackets indicating L of the $\pi\Delta$ state. In addition to the present study ("2025"), we list the JüBo2022 results ("2022") [117] and the estimates from the Particle Data Group [5] ("PDG"), if available, as well as the PDG star rating.

		Pole position		πN Residue		$K\Sigma$ channel		$\pi\Delta$, channel (6)		$\pi\Delta$, channel (7)	
		Re W_0 [MeV]	-2Im W_0 [MeV]	$\lvert r_{\pi N}\rvert$ [MeV]	$\theta_{\pi N\to\pi N}$ [deg]	$\frac{\Gamma^{1/2}_{\pi N}\Gamma^{1/2}_{K\Sigma}}{\Gamma_{\text{tot}}}$ [%]	$\theta_{\pi N\to K\Sigma}$ [deg]	$\frac{\Gamma^{1/2}_{\pi N}\Gamma^{1/2}_{\pi\Delta}}{\Gamma_{\text{tot}}}$ [%]	$\theta_{\pi N\to\pi\Delta}$ [deg]	$\frac{\Gamma^{1/2}_{\pi N}\Gamma^{1/2}_{\pi\Delta}}{\Gamma_{\text{tot}}}$ [%]	$\theta_{\pi N\to\pi\Delta}$ [deg]
	fit										
$\Delta(1620)$ $1/2^-$	2025	1601 (2)	79 (1)	17 (3)	-72 (19)	18 (3)	-65 (20)	—	—	51 (9) (D)	133 (19)
	2022	1607 (4)	85 (5)	12 (2)	126 (4)	11 (2)	-120 (5)	—	—	32 (2) (D)	81 (2)
****	PDG	1600 ± 10	110 ± 30	15 ± 5	-100 ± 20	—	—	—	—	—	—
$\Delta(1910)$ $1/2^+$	2025	1813 (6)	653 (25)	27 (21)	129 (306)	0.5 (1.4)	-100 (40)	15 (12) (P)	-3 (63)	—	—
	2022	1802 (11)	550 (22)	35 (25)	93 (14)	0.2 (0.4)	138 (19)	24 (18) (P)	-42(14)	—	—
****	PDG	1850 ± 50	350 ± 150	25 ± 5	-90^{+180}_{-90}	—	—	—	—	—	—
$\Delta(1232)$ $3/2^+$	2025	1215 (1)	92 (0)	48 (0)	-39 (0)						
	2022	1215 (2)	93 (1)	50 (2)	-39 (1)						
****	PDG	1210 ± 1	100 ± 2	50^{+2}_{-1}	-46^{+1}_{-2}						
$\Delta(1600)$ $3/2^+$	2025	1598 (1)	111 (1)	6.0 (0.8)	-110 (4)	9.5 (1.6)	8 (4)	22 (4) (P)	87 (5)	0.6 (0.1) (F)	-31 (9)
	2022	1590 (1)	136 (1)	11 (1)	-106 (2)	14 (1)	14 (2)	30 (3) (P)	87 (3)	0.4 (0.04) (F)	-62 (9)
****	PDG	1520^{+70}_{-50}	280^{+40}_{-30}	25 ± 15	210^{+40}_{-30}	—	—	—	—	1 ± 0.5	—
$\Delta(1920)$ $3/2^+$	2025	1857 (15)	875 (4)	60 (8)	-28 (19)	25 (2.1)	82 (13)	8.0 (0.8) (P)	-74 (13)	3.3 (0.5) (F)	96 (18)
	2022	1883 (4)	844 (10)	41 (5)	11 (7)	20 (2)	104 (4)	5.7 (0.5) (P)	-48 (5)	2.0 (0.3) (F)	147 (7)
***	PDG	1900 ± 50	300 ± 100	25 ± 10	-100 ± 50	—	—	—	—	—	—
$\Delta(1700)$ $3/2^-$	2025	1663 (4)	354 (13)	47 (13)	-11 (20)	3.1 (0.7)	-164 (15)	7.7 (1.7) (D)	148 (19)	59 (15) (S)	146 (19)
	2022	1637 (64)	295 (58)	15 (23)	-13 (147)	0.7 (1.5)	-176 (320)	3.8 (7.8) (D)	127 (254)	20 (29) (S)	146 (266)
****	PDG	1665 ± 25	250 ± 50	25 ± 15	-20 ± 20	—	—	—	—	—	—
$\Delta(1930)$ $5/2^-$	2025	1835 (11)	485 (20)	20 (2)	-123 (7)	0.7 (0.1)	28 (6)	11 (2.6) (D)	47 (6)	1.2 (0.1) (G)	147 (6)
	2022	1821 (4)	447 (13)	15 (3)	-108 (9)	1.0 (0.2)	49 (9)	12 (3) (D)	64 (7)	0.8 (0.2) (G)	148 (4)
***	PDG	1850 ± 30	320^{+130}_{-20}	14 ± 6	-50^{+40}_{-50}	—	—	—	—	—	—
$\Delta(1905)$ $5/2^+$	2025	1722 (4)	264 (11)	5.1 (3.5)	-65 (18)	0.3 (0.2)	-179 (356)	1.8 (1.3) (F)	47 (19)	9.4 (3.2) (P)	-105 (22)
	2022	1707 (1)	127 (8)	3.7 (1.0)	-92 (12)	0.2 (0.03)	154 (11)	1.7 (0.3) (F)	18 (15)	10 (1) (P)	-109 (14)
****	PDG	1770^{+30}_{-20}	300 ± 40	20 ± 5	-45^{+15}_{-75}	—	—	—	—	—	—
$\Delta(1950)$ $7/2^+$	2025	1871 (1)	170 (7)	38 (3.3)	8 (9)	1.9 (0.5)	-43 (8)	45 (4) (F)	168 (8)	2.9 (0.2) (H)	47 (9)
	2022	1875 (1)	166 (3)	27 (2)	1.1 (2.0)	2.0 (0.3)	-40 (7)	30 (54) (F)	166 (2)	5.1 (0.7) (H)	-11 (2)
****	PDG	1880 ± 10	240 ± 20	52 ± 8	-32 ± 8	—	—	—	—	—	—
$\Delta(2200)$ $7/2^-$	2025	1978 (7)	327 (12)	7.3 (0.5)	-76 (3)	0.0 (0.0)	64 (3)	0.4 (0.1) (G)	100 (18)	18 (1.1) (D)	100 (4)
	2022	1963 (2)	328 (3)	6.8 (0.6)	-80 (2)	< 0.1 (0.03)	-123 (2)	0.3 (0.1) (G)	152 (5)	16 (1) (D)	100 (2)
***	PDG	2100 ± 50	340 ± 80	—	—	—	—	—	—	—	—
$\Delta(2400)$ $9/2^-$	2025	2517 (49)	86 (37)	25 (2)	6 (6)	4.5 (3.4)	15 (7)	65 (29) (G)	16 (7)	12 (8) (I)	154 (11)
	2022	2458 (3)	280 (2)	5.4 (5)	8.4 (33)	0.4 (0.6)	17 (30)	10 (11) (G)	17 (23)	1.9 (0.5) (I)	-120 (49)
**	PDG	—	—	—	—	—	—	—	—	—	—

Table 12: Here we present the photocouplings at the pole (A^h_{pole}, ϑ^h) of the $I = 1/2$ (left) and $I = 3/2$ resonances (right). In addition to the present study ("2025"), we show the JüBo2022 results ("2022") [117] for comparison. The uncertainties quoted in parentheses provide a rather rough estimate as explained in the text.

	fit	$\mathbf{A^{1/2}_{pole}}$ [10^{-3} GeV$^{-1/2}$]	$\vartheta^{1/2}$ [deg]	$\mathbf{A^{3/2}_{pole}}$ [10^{-3} GeV$^{-1/2}$]	$\vartheta^{3/2}$ [deg]		fit	$\mathbf{A^{1/2}_{pole}}$ [10^{-3} GeV$^{-1/2}$]	$\vartheta^{1/2}$ [deg]	$\mathbf{A^{3/2}_{pole}}$ [10^{-3} GeV$^{-1/2}$]	$\vartheta^{3/2}$ [deg]
$N(1535)\ 1/2^-$	2025	90 (2)	−1 (2)			$\Delta(1620)\ 1/2^-$	2025	30 (11)	58 (12)		
	2022	84 (5)	−12 (3)				2022	11 (4)	57 (24)		
$N(1650)\ 1/2^-$	2025	34 (3)	−2 (5)			$\Delta(1910)\ 1/2^+$	2025	−164 (128)	−5 (352)		
	2022	39 (10)	−0.2 (27)				2022	−446 (72)	−70 (21)		
$N(1440)\ 1/2^+_{(a)}$	2025	−99 (15)	−18 (4)			$\Delta(1232)\ 3/2^+$	2025	−128 (5)	−18 (3)	−246 (3)	1 (1)
	2022	−90 (13)	−30 (5)				2022	−126 (4)	−18 (3)	−245 (7)	−0.7 (1.7)
$N(1710)\ 1/2^+$	2025	−18 (2)	37 (10)			$\Delta(1600)\ 3/2^+$	2025	9 (4)	11 (45)	−10 (6)	105 (43)
	2022	−18 (19)	40 (109)				2022	25 (10)	0.5 (5.9)	−6.0 (2.6)	62 (63)
$N(1720)\ 3/2^+$	2025	24 (10)	48 (13)	−26 (8)	−24 (13)	$\Delta(1920)\ 3/2^+_{(a)}$	2025	245 (30)	−28 (9)	475 (52)	10 (10)
	2022	39 (7)	60 (10)	−25 (7)	−5.7 (13)		2022	138 (12)	−8.9 (3.9)	252 (14)	14 (3)
$N(1900)\ 3/2^+$	2025	6 (1)	49 (21)	−39 (2)	−28 (3)	$\Delta(1700)\ 3/2^-$	2025	244 (53)	17 (11)	337 (67)	−4 (13)
	2022	9.1 (2.7)	80 (23)	−7.7 (3.4)	−42 (23)		2022	163 (120)	−4.4 (78)	221 (185)	−12 (79)
$N(1520)\ 3/2^-$	2025	−19 (3)	−34 (8)	102 (12)	17 (4)	$\Delta(1930)\ 5/2^-$	2025	218 (18)	162 (24)	240 (31)	173 (10)
	2022	−43 (25)	−47 (20)	112 (64)	1.8 (37)		2022	104 (18)	129 (16)	322 (44)	142 (7)
$N(1675)\ 5/2^-$	2025	35 (5)	17 (6)	36 (4)	15 (8)	$\Delta(1905)\ 5/2^+$	2025	75 (61)	−67 (40)	−373 (308)	94 (16)
	2022	25 (4)	−1.2 (7.8)	51 (4)	−1.0 (3.7)		2022	55 (8)	−159 (3)	−168 (40)	172 (1.7)
$N(1680)\ 5/2^+$	2025	−8 (2)	119 (23)	133 (34)	−31 (8)	$\Delta(1950)\ 7/2^+$	2025	−33 (7)	−67 (6)	−59 (8)	−70 (5)
	2022	−17 (6)	70 (14)	95 (6)	−57 (7)		2022	−31 (4)	−81 (7)	−45 (4)	−89 (4)
$N(1990)\ 7/2^+$	2025	−14 (3)	−74 (20)	−14 (3)	107 (15)	$\Delta(2200)\ 7/2^-$	2025	72 (17)	−134 (8)	65 (13)	−174 (7)
	2022	−30 (16)	−135 (25)	−18 (11)	53 (32)		2022	104 (22)	−139 (3)	21 (25)	−180 (39)
$N(2190)\ 7/2^-$	2025	−13 (2)	11 (15)	20 (7)	161 (15)	$\Delta(2400)\ 9/2^-$	2025	15 (9)	−102 (52)	22 (22)	156 (23)
	2022	−15 (8)	111 (17)	62 (22)	179 (26)		2022	21 (14)	−67 (23)	22 (14)	122 (14)
$N(2250)\ 9/2^-$	2025	−33 (8)	2 (19)	58 (20)	121 (20)						
	2022	−108 (14)	112 (7)	50 (22)	69 (16)						
$N(2220)\ 9/2^+$	2025	74 (46)	−78 (17)	−185 (37)	−14 (16)						
	2022	357 (39)	−91 (7)	−273 (50)	−102 (6)						

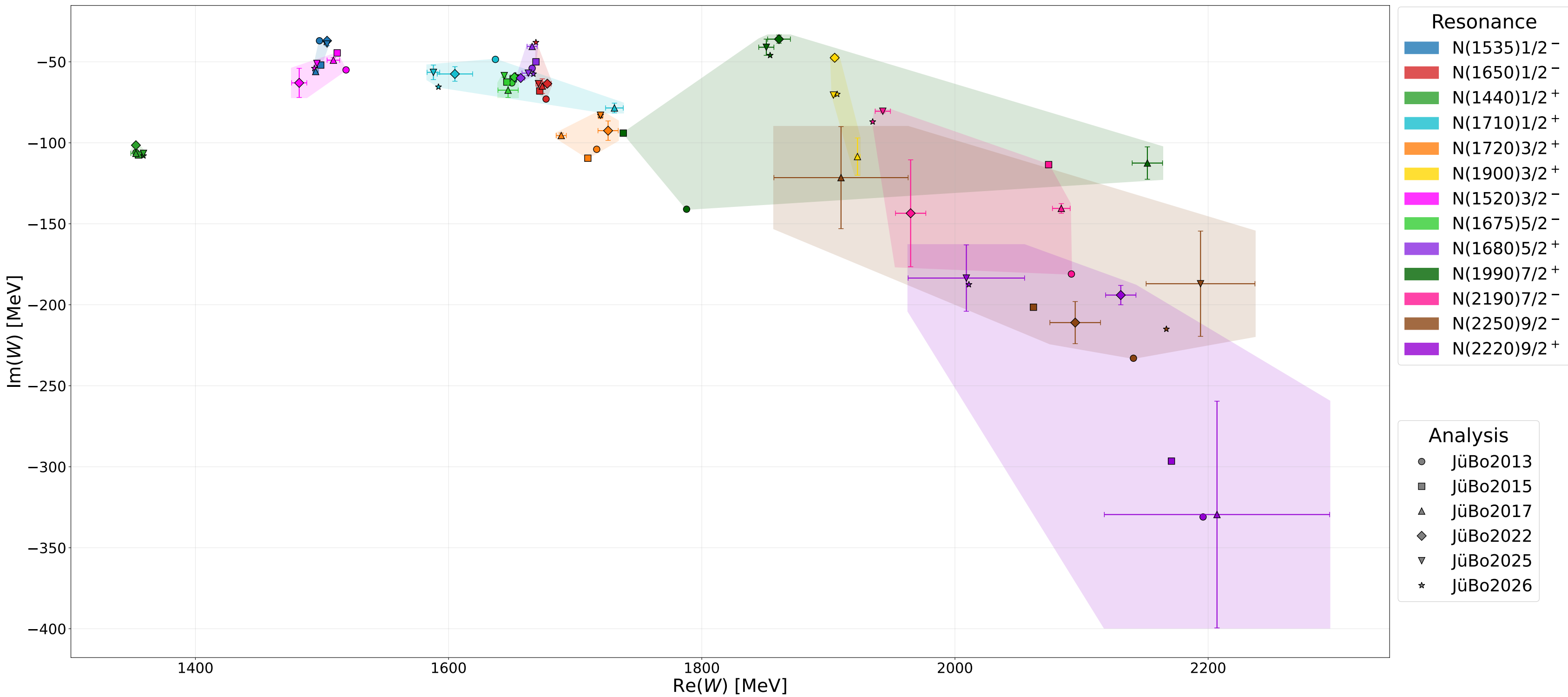

Figure 14: Pole positions of the $I = 1/2$ resonances in the different Jülich-Bonn analyses. The shaded regions indicate the uncertainty ranges of the pole positions for each resonance.

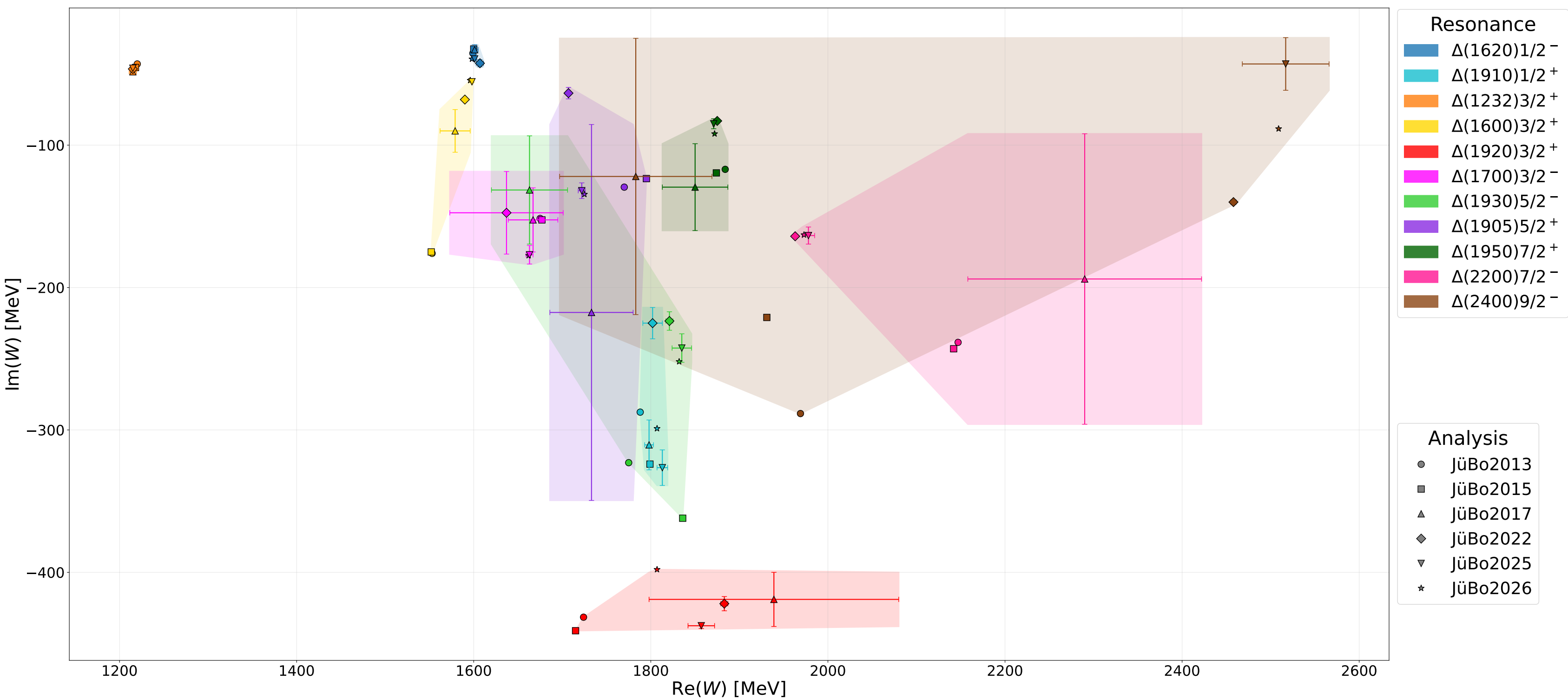

Figure 15: Pole positions of the $I = 3/2$ resonances in the different Jülich-Bonn analyses. The shaded regions indicate the uncertainty ranges of the pole positions for each resonance.

5. Extension of the Jülich-Bonn model to photoproduction off neutron targets

Information on the N and Δ resonances from photoproduction reactions is largely restricted to charged channels (final-states involving charged particles) and especially to photoproduction off protons. To extract all the isospin amplitudes and to disentangle the isoscalar and isovector electromagnetic couplings of the N and Δ resonances, one needs to analyze data for both neutron and proton targets. However, neutron targets pose a challenge for experiments, since the neutron is an unstable particle and one needs to use e.g. deuteron targets. To extract photoproduction data with neutron targets, one requires the use of a model-dependent nuclear correction, which comes from final-state interaction (FSI) effects within the target deuteron [577]. These final-state interactions are especially strong for np_s pair, where p_s is the spectator proton from the deuteron target. This is the case for the reaction $\gamma d \to \pi^0 n p_s$. The FSI effect for a two proton final-state in the process $\gamma d \to \pi^- p p_s$ is more suppressed [578]. These final-state interaction effects can be avoided by measuring the inverse reaction $\pi^- p \to \gamma n$ (e.g. [579, 580]), which also serves as an important test for the FSI corrections. Another unwanted effect is the Fermi motion, which can be avoided by a full reconstruction of the final-state to determine the momentum of the bound neutron.

As a result, observables from proton target photoproduction experiments are far more accessible and better studied than those from neutron target experiments. Increasing the number of neutron target data will give a more constrained study of the neutral states and allows groups to study the γn photocouplings of nucleon and Delta resonances.

In this chapter we describe the extensions made to the Jülich-Bonn model to include photoproduction processes with neutron targets. We further list the data base for pion photoproduction reactions off neutrons, which we all include in our fit. After that we present fit results of the current study "JüBo2026", in which we analyze photoproduction processes off neutron targets for first time within our framework and fit these simultaneously with the data included in past studies.

5.1. Extensions to the Photoproduction Amplitude

To include photoproduction processes off neutron targets $\gamma n \to X$, we need to investigate the difference in the amplitudes compared to a proton target. Thus, we study the couplings of isospins. For this we calculate the isospin factors for proton and neutron targets here.

As pointed out in Refs. [581, 582], the photon is composed of an isovector $I_\gamma = 1$ and an isoscalar $I_\gamma = 0$ component with its 3rd isospin component being $m_\gamma = 0$ for both cases. The isoscalar component can only couple with the target nucleon to $I = 1/2$, while the isovector component can couple to either $I = 1/2$ or $I = 3/2$. We define the isospin factor for initial $\gamma N \to X$ by:

$$C^{I_\gamma, I}_{\gamma N \to mb} = \langle I_N, m_N, I_\gamma, m_\gamma | I, M \rangle \cdot \langle I, M | I_b, m_b, I_m, m_m \rangle \ , \tag{5.1}$$

where m (b) in Eq. (5.1) denotes the final-state meson (baryon), $I_{m(b)}$ is the isospin of the final-state meson (baryon) and the $m_{m(b)}$ denotes the corresponding 3rd component of the isospin. Note that we use a "baryon first convention" in our model and this can lead to a sign switch for the Clebsch-Gordan coefficients

$$\langle I_m I_b m_m m_b | I_m I_b I M\rangle = (-1)^{I-I_m-I_b} \langle I_b I_m m_b m_m | I_b I_m I M\rangle \ . \tag{5.2}$$

We decompose the amplitude in the following way

$$\begin{aligned} T_\gamma^{mb} &= \langle I_b, m_b, I_m, m_m | \, T_{f\gamma} \, | I_\gamma, m_\gamma, I_N, m_N\rangle = \sum_{(I_\gamma, I)} C^{I_\gamma, I}_{\gamma N\to mb} \cdot T^{I_\gamma, I}_{f\gamma} \\ &= C^{1,\frac{3}{2}}_{\gamma N\to mb} \cdot T^{1,\frac{3}{2}}_{f\gamma} + C^{1,\frac{1}{2}}_{\gamma N\to mb} \cdot T^{1,\frac{1}{2}}_{f\gamma} + C^{0,\frac{1}{2}}_{\gamma N\to mb} \cdot T^{0,\frac{1}{2}}_{f\gamma} \ . \end{aligned} \tag{5.3}$$

where f denotes the corresponding isospin independant channel $f \in \{\pi N, \eta N, K\Lambda, K\Sigma\}$ and the subscript γ on the amplitude denotes the photo-channel.

The full calculations of the isospin factors is presented in Appendix C. Here we list the amplitudes for each reaction. The amplitudes for reactions with proton targets $\gamma p \to X$ are given by

$$T_\gamma^{\pi^0 p} = \frac{2}{3} T^{1,\frac{3}{2}}_{\pi N\gamma} + \frac{1}{3} T^{1,\frac{1}{2}}_{\pi N\gamma} + \frac{1}{\sqrt{3}} T^{0,\frac{1}{2}}_{\pi N\gamma} \tag{5.4}$$

$$T_\gamma^{\pi^+ n} = \frac{\sqrt{2}}{3} T^{1,\frac{3}{2}}_{\pi N\gamma} - \frac{\sqrt{2}}{3} T^{1,\frac{1}{2}}_{\pi N\gamma} - \sqrt{\frac{2}{3}} T^{0,\frac{1}{2}}_{\pi N\gamma} \tag{5.5}$$

$$T_\gamma^{\eta p} = \frac{1}{\sqrt{3}} T^{1,\frac{1}{2}}_{\eta N\gamma} + T^{0,\frac{1}{2}}_{\eta N\gamma} \tag{5.6}$$

$$T_\gamma^{K^+\Lambda} = \frac{1}{\sqrt{3}} T^{1,\frac{1}{2}}_{K\Lambda\gamma} + T^{0,\frac{1}{2}}_{K\Lambda\gamma} \tag{5.7}$$

$$T_\gamma^{K^0\Sigma^+} = \frac{\sqrt{2}}{3} T^{1,\frac{3}{2}}_{K\Sigma\gamma} + \frac{\sqrt{2}}{3} T^{1,\frac{1}{2}}_{K\Sigma\gamma} + \sqrt{\frac{2}{3}} T^{0,\frac{1}{2}}_{K\Sigma\gamma} \tag{5.8}$$

$$T_\gamma^{K^+\Sigma^0} = \frac{2}{3} T^{1,\frac{3}{2}}_{K\Sigma\gamma} - \frac{1}{3} T^{1,\frac{1}{2}}_{K\Sigma\gamma} - \frac{1}{\sqrt{3}} T^{0,\frac{1}{2}}_{K\Sigma\gamma} \ , \tag{5.9}$$

and for neutron targets $\gamma n \to X$ one finds

$$T_\gamma^{\pi^0 n} = \frac{2}{3} T^{1,\frac{3}{2}}_{\pi N\gamma} + \frac{1}{3} T^{1,\frac{1}{2}}_{\pi N\gamma} - \frac{1}{\sqrt{3}} T^{0,\frac{1}{2}}_{\pi N\gamma} \tag{5.10}$$

$$T_\gamma^{\pi^- p} = \frac{\sqrt{2}}{3} T^{1,\frac{3}{2}}_{\pi N\gamma} - \frac{\sqrt{2}}{3} T^{1,\frac{1}{2}}_{\pi N\gamma} + \sqrt{\frac{2}{3}} T^{0,\frac{1}{2}}_{\pi N\gamma} \tag{5.11}$$

$$T_\gamma^{\eta n} = -\frac{1}{\sqrt{3}} T^{1,\frac{1}{2}}_{\eta N\gamma} + T^{0,\frac{1}{2}}_{\eta N\gamma} \tag{5.12}$$

$$T_\gamma^{K^0\Lambda} = -\frac{1}{\sqrt{3}} T^{1,\frac{1}{2}}_{K\Lambda\gamma} + T^{0,\frac{1}{2}}_{K\Lambda\gamma} \tag{5.13}$$

$$T_\gamma^{K^+\Sigma^-} = \frac{\sqrt{2}}{3} T^{1,\frac{3}{2}}_{K\Sigma\gamma} + \frac{\sqrt{2}}{3} T^{1,\frac{1}{2}}_{K\Sigma\gamma} - \sqrt{\frac{2}{3}} T^{0,\frac{1}{2}}_{K\Sigma\gamma} \tag{5.14}$$

$$T_\gamma^{K^0\Sigma^0} = \frac{2}{3} T^{1,\frac{3}{2}}_{K\Sigma\gamma} - \frac{1}{3} T^{1,\frac{1}{2}}_{K\Sigma\gamma} + \frac{1}{\sqrt{3}} T^{0,\frac{1}{2}}_{K\Sigma\gamma} \ . \tag{5.15}$$

It is common to introduce different amplitudes for $I = 1/2$ as done in Ref. [583]. For example, the amplitudes with final-states πN are characterised by 3 amplitudes. Instead of the two $I = 1/2$ amplitudes resulting from the isoscalar and isovector components of the photon, one can define one $I = 1/2$ amplitude for proton target and neutron target reactions each. We define these in the following way for the πN channels:

$$T^{p,\frac{1}{2}}_{\pi N\gamma} = \frac{1}{3}T^{1,\frac{1}{2}}_{\pi N\gamma} + \frac{1}{\sqrt{3}}T^{0,\frac{1}{2}}_{\pi N\gamma} \;, \tag{5.16}$$

$$T^{n,\frac{1}{2}}_{\pi N\gamma} = -\frac{1}{3}T^{1,\frac{1}{2}}_{\pi N\gamma} + \frac{1}{\sqrt{3}}T^{0,\frac{1}{2}}_{\pi N\gamma} \;. \tag{5.17}$$

These relations show, that both the amplitudes for proton and neutron targets are needed to fully determine the isoscalar and isovector components of the photon. Now the pion photoproduction amplitudes can be rewritten as

$$T^{\pi^0 p}_{\gamma} = \frac{2}{3}T^{1,\frac{3}{2}}_{\pi N\gamma} + T^{p,\frac{1}{2}}_{\pi N\gamma} \tag{5.18}$$

$$T^{\pi^+ n}_{\gamma} = \frac{\sqrt{2}}{3}T^{1,\frac{3}{2}}_{\pi N\gamma} - \sqrt{2}\,T^{p,\frac{1}{2}}_{\pi N\gamma} \tag{5.19}$$

$$T^{\pi^0 n}_{\gamma} = \frac{2}{3}T^{1,\frac{3}{2}}_{\pi N\gamma} - T^{n,\frac{1}{2}}_{\pi N\gamma} \tag{5.20}$$

$$T^{\pi^- p}_{\gamma} = \frac{\sqrt{2}}{3}T^{1,\frac{3}{2}}_{\pi N\gamma} + \sqrt{2}\,T^{n,\frac{1}{2}}_{\pi N\gamma} \;, \tag{5.21}$$

where we now use the three amplitudes $T^{1,\frac{3}{2}}_{\pi N\gamma}$, $T^{p,\frac{1}{2}}_{\pi N\gamma}$ and $T^{n,\frac{1}{2}}_{\pi N\gamma}$ to characterise the πN amplitudes. This same procedure can be done for the other channels:

$$T^{p,\frac{1}{2}}_{\eta N\gamma} = \frac{1}{\sqrt{3}}T^{1,\frac{1}{2}}_{\eta N\gamma} + T^{0,\frac{1}{2}}_{\eta N\gamma} \tag{5.22}$$

$$T^{n,\frac{1}{2}}_{\eta N\gamma} = -\frac{1}{\sqrt{3}}T^{1,\frac{1}{2}}_{\eta N\gamma} + T^{0,\frac{1}{2}}_{\eta N\gamma} \tag{5.23}$$

$$T^{p,\frac{1}{2}}_{K\Lambda\gamma} = \frac{1}{\sqrt{3}}T^{1,\frac{1}{2}}_{K\Lambda\gamma} + T^{0,\frac{1}{2}}_{K\Lambda\gamma} \tag{5.24}$$

$$T^{n,\frac{1}{2}}_{K\Lambda\gamma} = -\frac{1}{\sqrt{3}}T^{1,\frac{1}{2}}_{K\Lambda\gamma} + T^{0,\frac{1}{2}}_{K\Lambda\gamma} \tag{5.25}$$

$$T^{p,\frac{1}{2}}_{K\Sigma\gamma} = \frac{1}{3}T^{1,\frac{1}{2}}_{K\Sigma\gamma} + \frac{1}{\sqrt{3}}T^{0,\frac{1}{2}}_{K\Sigma\gamma} \tag{5.26}$$

$$T^{n,\frac{1}{2}}_{K\Sigma\gamma} = -\frac{1}{3}T^{1,\frac{1}{2}}_{K\Sigma\gamma} + \frac{1}{\sqrt{3}}T^{0,\frac{1}{2}}_{K\Sigma\gamma} \;. \tag{5.27}$$

The resulting amplitudes are then given by

$$T_{\gamma}^{\eta p} = T_{\eta N\gamma}^{p,\frac{1}{2}} \tag{5.28}$$

$$T_{\gamma}^{\eta n} = T_{\eta N\gamma}^{n,\frac{1}{2}} \tag{5.29}$$

$$T_{\gamma}^{K^+\Lambda} = T_{K\Lambda\gamma}^{p,\frac{1}{2}} \tag{5.30}$$

$$T_{\gamma}^{K^0\Lambda} = T_{K\Lambda\gamma}^{n,\frac{1}{2}} \tag{5.31}$$

$$T_{\gamma}^{K^0\Sigma^+} = \frac{\sqrt{2}}{3}T_{K\Sigma\gamma}^{1,\frac{3}{2}} + \sqrt{2}\,T_{K\Sigma\gamma}^{p,\frac{1}{2}} \tag{5.32}$$

$$T_{\gamma}^{K^+\Sigma^0} = \frac{2}{3}T_{K\Sigma\gamma}^{1,\frac{3}{2}} - T_{K\Sigma\gamma}^{p,\frac{1}{2}} \tag{5.33}$$

$$T_{\gamma}^{K^+\Sigma^-} = \frac{\sqrt{2}}{3}T_{K\Sigma\gamma}^{1,\frac{3}{2}} - \sqrt{2}\,T_{K\Sigma\gamma}^{n,\frac{1}{2}} \tag{5.34}$$

$$T_{\gamma}^{K^0\Sigma^0} = \frac{2}{3}T_{K\Sigma\gamma}^{1,\frac{3}{2}} + T_{K\Sigma\gamma}^{n,\frac{1}{2}} \ . \tag{5.35}$$

In this work, we extended the Jülich-Bonn model to include the two πN final-states for reactions involving neutron targets. The other channels for photoproduction off neutrons will be included in the future. The pion photoproduction amplitudes are described by the set $(T_{\pi N\gamma}^{1,\frac{3}{2}}, T_{\pi N\gamma}^{p,\frac{1}{2}}, T_{\pi N\gamma}^{n,\frac{1}{2}})$. Note, the $I = 3/2$ amplitude is the same for reactions involving proton or neutron targets and we do not need to introduce new $I = 3/2$ parameters into our model. For the $I = 1/2$ amplitude for neutron targets $T_{\pi N\gamma}^{n,\frac{1}{2}}$, we introduce new parameters in the polynomial parametrization of the photoproduction amplitude presented in Eqs. (3.70) and (3.72):

$$P_i^{\mathrm{P}}(E) = \sum_{j=1}^{l_i} g_{i,j}^{\mathrm{P}} \left(\frac{E-E_s}{m_N}\right)^j e^{-\lambda_i^{\mathrm{P}}(E-E_s)} \ ,$$

$$P_\mu^{\mathrm{NP}}(E) = \sum_{j=0}^{l_\mu} g_{\mu,j}^{\mathrm{NP}} \left(\frac{E-E_s}{m_N}\right)^j e^{-\lambda_\mu^{\mathrm{NP}}(E-E_s)} \ .$$

The degree of the polynomials is chosen as demanded by the fit. The degree of polynomials chosen for the non pole part T^{NP} of this analysis are listed in Tab. 13. Here we get one polynomial for each partial wave and each final-state. The degrees for the pole part T^{P} are listed in Tab. 14 and in this case we get a polynomial for each N^* resonance. Note that the 0-th order term is not present in the pole part of the parametrization but it is used in the non-pole part (see Sec. 3.5). Each partial wave has a different set of parameters for the magnetic and electric multipole, except for the S_{11}, which only has an electric multipole, and P_{11}, which only has a magnetic multipole. We allow the polynomials for the electric and magnetic multipole to have different degrees. We start with a minimum degree of the polynomial and only increased this if it leads to a significant improvement of the χ^2. This resulted in some polynomials to only contain the 0-th order term.

For the non pole part we only consider the channels $\mu = (\pi N, \pi\Delta)$. We did not switch on the channels $(\eta N, K\Lambda, K\Sigma)$, since we only use πN final-state data in our analysis. Once the photoproduction off neutrons is extended to these channels, we will also turn on these parameters. In addition to the polynomial parameters, each term has one parameter λ in the exponential. Thus, we introduce 57 pole parameters and 98 non pole parameters, leading to a total of 155 new parameters. Note, that we additionally have the free parameters from the previous fit as listed in Sec. 4.2, which we also include in the fit procedure.

	S_{11}	P_{11}	P_{13}	D_{13}	D_{15}	F_{15}	F_{17}	G_{17}	G_{19}	H_{19}
$l^E_{\pi N}$	1	-	1	1	2	1	0	0	1	1
$l^E_{\pi\Delta}$	1	1	1	1	1	1	0	0	0	0
$l^M_{\pi N}$	-	2	1	1	1	1	0	0	1	1
$l^M_{\pi\Delta}$	-	1	1	1	1	1	0	0	0	0

Table 13: List of the chosen degrees l_μ for the non pole part of the polynomial parametrization P^{NP}_μ used in the $\gamma n \to \pi N$ fit. The superscript of the l_μ denotes the respective multipole.

	$N(1535)\ 1/2^-$	$N(1650)\ 1/2^-$	$N(939)\ 1/2^+$	$N(1710)\ 1/2^+$	$N(1720)\ 3/2^+$
l^E_i	2	2	-	-	1
l^M_i	-	-	1	1	1
	$N(1900)\ 3/2^+$	$N(1520)\ 3/2^-$	$N(1675)\ 5/2^-$	$N(1680)\ 5/2^+$	$N(1990)\ 7/2^+$
l^E_i	2	2	2	2	1
l^M_i	2	2	2	2	1
	$N(2190)\ 7/2^-$	$N(2250)\ 9/2^-$	$N(2220)\ 9/2^+$		
l^E_i	1	1	2		
l^M_i	1	2	2		

Table 14: List of the chosen degrees l_μ for the pole part of the polynomial parametrization P^{P}_i used in the $\gamma n \to \pi N$ fit. The superscript of the l_i denotes the respective multipole.

5.2. Database for $\gamma n \to \pi N$

The data sets used in the present analysis are taken from the SAID database [126] and HEP-data [584]. In Tab. 15 we give an overview of the data points used for the πN channels and list the total number together with the $\gamma p \to X$ data. Note that the main contribution for the data with neutron targets comes from the charged final-state $\pi^- p$, since the neutral channel $\pi^0 n$ is more difficult to measure. We further list the different data sets with their references, number of data points and the energy range in Tabs. 16-18. In Tab. 16 we list all observables for $\pi^0 n$ final-state. For the $\pi^- p$ channel we separated cross section data, shown in Tab. 17, and the polarization observables, which are listed in Tab. 18. The data base listed in Chapter 4 is also included in this study. We also added the data on $d\Delta\sigma/d\Omega$ published by the A2 Collaboration at MAMI [300] with 2052 data points in this analysis.

Data very close to threshold is not available yet for the process $\gamma n \to \pi^0 n$ and also very scarce for the final-state $\pi^- p$. We therefore used cross section predictions for $\gamma n \to \pi^0 n$ for the energies (1078, 1080, 1082, 1084) MeV from the chiral perturbation theory study of Ref. [585] to constrain the threshold behaviour of our amplitude. We further used values for the E_{0+} multipole of another ChPT study of Ref. [586] for the $\pi^0 n$ and $\pi^- p$ channels to restrict the S-wave multipole at threshold. The values for $\pi^- p$ are based on an experimental value of Ref. [587] and the leading order in the chiral expansion calculated in Ref. [588]. The value for $\pi^0 n$ is sourced from combined deuterium data with ChPT predictions of Ref. [589].

Reaction	Observables (# data points)	# data points/channel
$\gamma n \to \pi^0 n$	$d\sigma/d\Omega$ (1580), Σ (405), P (82), T(123)	
	E (541), H (82)	2813
$\gamma n \to \pi^- p$	$d\sigma/d\Omega$ (10,985), Σ (1609), P (82), T (104),	
	E (266)	12,860
	in total $\gamma n \to X$	15,673
	in total $\gamma p \to X$	73,171
	in total $\gamma N \to X$	88,844

Table 15: List of the number of data points for each observable used for the processes $\gamma n \to \pi^0 n$ and $\gamma n \to \pi^- p$.

5.3. Fit results for $\gamma n \to \pi N$

In the following we present and discuss the fit results of the current analysis which we label "JüBo2026". We present the χ^2 per data points for each observable in Tabs. 19-22. We further present the fit result for pion-induced and photoproduction processes off protons in the supplementary material of this thesis.

We present the results close to threshold for the differential cross section for the process $\gamma n \to \pi^0 n$ together with the ChPT predictions of Ref. [585] in Fig. 16.

Observable	# data p.	Energy range E_γ	Reference	Year	Weight
$d\sigma/d\Omega$	492	290–813 MeV	Briscoe et al. [590]	2019	15
$d\sigma/d\Omega$	931	450–1400 MeV	Dieterle et al. [591]	2018	30
$d\sigma/d\Omega$	9	208-373 MeV	Kossert et al. [592]	2004	4
$d\sigma/d\Omega$	43	299-889 MeV	Ando [593]	1976	4
$d\sigma/d\Omega$	42	455-905 MeV	Hemmi et al. [594]	1973	4
$d\sigma/d\Omega$	35	462-784 MeV	Bacci et al. [595]	1972	4
$d\sigma/d\Omega$	28	911-1390 MeV	Klinesmith PhD thesis [596]	1967	4
Σ	492	390-610 MeV	Mullen et al. [597]	2021	30
Σ	216	600-1500 MeV	Di Salvo et al. [598]	2009	40
E	390	250-1480 MeV	Cividini et al. [599]	2022	100
E	151	450-1400 MeV	Dieterle et al. [600]	2017	70
T	123	680-2685 MeV	Jermann et al. [601]	2023	20
P	82	680-1332 MeV	Jermann et al. [601]	2023	20
H	82	680-1332 MeV	Jermann et al. [601]	2023	20

Table 16: List of the data sets used in the current analysis for the process $\gamma n \to \pi^0 n$. If no reference could be found for a data set, we refer to the SAID data base and mention the author listed there.

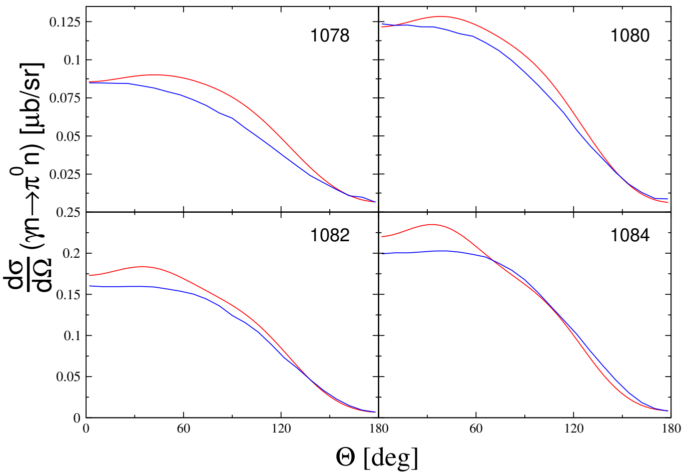

Figure 16: Fit results for the differential cross sections close to threshold for the $\pi^0 n$ final-state are shown in red and the ChPT predictions of Ref. [585] are shown in blue for comparison. The numbers in each plot denotes the center of mass energy in MeV.

Observable	# data p.	Energy range E_γ	Reference	Year	Weight
$d\sigma/d\Omega$	8428	445–2510 MeV	Mattione et al. [602]	2017	4
$d\sigma/d\Omega$	577	1050–2500 MeV	Chen et al. [603]	2012	2
$d\sigma/d\Omega$	104	301–455 MeV	Briscoe et al. [604]	2012	2
$d\sigma/d\Omega$	11	1104–2484 MeV	Zhu et al. [469]	2005	2
$d\sigma/d\Omega$	300	285–769 MeV	Shafi et al. [605]	2004	2
$d\sigma/d\Omega$	12	158–168 MeV	Liu, PhD thesis [580]	1994	2
$d\sigma/d\Omega$	39	194–379 MeV	Wang, PhD thesis [126]	1989	2
$d\sigma/d\Omega$	12	458–648 MeV	Kim et al. [606]	1989	2
$d\sigma/d\Omega$	50	194–270 MeV	Bagheri et al. [607]	1988	2
$d\sigma/d\Omega$	16	175–187 MeV	Salomon et al. [579]	1984	2
$d\sigma/d\Omega$	119	900–1800 MeV	Besch et al. [608]	1982	2
$d\sigma/d\Omega$	12	900–1650 MeV	Abrahamian et al. [609]	1980	2
$d\sigma/d\Omega$	48	260–418 MeV	Tran et al. [610]	1979	2
$d\sigma/d\Omega$	16	231–446 MeV	Argan et al. [611]	1978	2
$d\sigma/d\Omega$	291	250–815 MeV	Fuji et al. [459]	1977	2
$d\sigma/d\Omega$	18	530–907 MeV	Weiss et al. [612]	1975	2
$d\sigma/d\Omega$	28	285–409 MeV	Comiso et al. [613]	1975	2
$d\sigma/d\Omega$	343	600–1250 MeV	Scheffler et al. [614]	1974	2
$d\sigma/d\Omega$	35	240–400 MeV	Hotley et al. [615]	1974	2
$d\sigma/d\Omega$	14	480–870 MeV	Beneventano et al. [616]	1974	2
$d\sigma/d\Omega$	19	355–519 MeV	Berardo et al. [616]	1974	2
$d\sigma/d\Omega$	39	250–403 MeV	Boucrout et al. [617]	1973	2
$d\sigma/d\Omega$	220	210–1900 MeV	Benz et al. [618]	1973	2
$d\sigma/d\Omega$	309	190–935 MeV	Rossi et al. [619]	1973	2
$d\sigma/d\Omega$	50	290–1180 MeV	Fujii et al. [456]	1971	2
$d\sigma/d\Omega$	24	500–1000 MeV	Neugebauer et al. [620]	1960	2

Table 17: List of the data sets for the differential cross section $d\sigma/d\Omega$ used in the current analysis for the process $\gamma n \to \pi^- p$. If no reference could be found for a data set, we refer to the SAID data base and mention the author listed there.

Observable	# data p.	Energy range E_γ	Reference	Year	Weight
Σ	1293	947–2498 MeV	Sokhan [126]	2017	30
Σ	99	753–1438 MeV	Mandaglio et al. [621]	2010	50
Σ	9	850–1790 MeV	Sandorfi [126]	1995	30
Σ	60	280–322 MeV	Adamyan et al. [622]	1989	30
Σ	12	900–1500 MeV	Abrahamian et al. [623]	1980	30
Σ	45	250–500 MeV	Ganenko et al. [126, 624]	1976	30
Σ	45	630–790 MeV	Knies et al. [375]	1974	30
Σ	20	260–500 MeV	Kondo et al. [625]	1974	30
Σ	13	700–2000 MeV	Alspector et al. [374]	1970	30
Σ	5	357–555 MeV	Kondo et al. [626]	1970	30
Σ	8	225–450 MeV	Liu et al. [627]	1964	30
P	4	348-398 MeV	Stasko et al. [628]	1994	50
P	45	340-648 MeV	Kim et al. [629]	1991	50
P	6	458 MeV	Alder et al. [630]	1983	50
P	19	717-1186 MeV	Takeda et al. [631]	1980	50
P	7	515-714 MeV	Benebentano et al. [632]	1970	50
P	1	715 MeV	Kenemuth et al. [633]	1963	50
T	14	300-400 MeV	Agranovich [126]	1989	50
T	60	563-900 MeV	Fujii et al. [634]	1981	50
T	9	850 MeV	Althoff et al. [496]	1977	50
T	10	700 MeV	Althoff et al. [635]	1976	50
T	11	450-2000 MeV	Althoff et al. [636]	1975	50
E	266	727–2345 MeV	Ho et al. [637]	2017	100

Table 18: List of the data sets for the polarization observables for the process $\gamma n \to \pi^- p$. If no reference could be found for a data set, we refer to the SAID data base and mention the author listed there.

Reaction	Observable (# data points)	$\chi^2/\#$
$\gamma n \to \pi^0 n$	$d\sigma/d\Omega$ (1580)	2.0
	Σ (405)	2.4
	P (82)	2.6
	T(123)	4.1
	E (541)	2.4
	H (82)	3.1
$\gamma n \to \pi^- p$	$d\sigma/d\Omega$ (10,985)	1.8
	Σ (1609)	2.5
	P (82)	1.4
	T (104)	1.9
	E (266)	2.2

Table 19: List of the χ^2 per number of data points for the $\gamma N \to \pi N$ channels for each observable.

Reaction	Observable (# data points)	$\chi^2/\#$
$\gamma p \to \pi^0 p$	$d\sigma/d\Omega$ (18,721) [70, 72, 292, 311–370]	2.3
	Σ (3287) [72, 331, 348, 359, 361, 363, 367, 371–395]	2.2
	P (768) [332, 376, 380, 381, 386, 396–430]	2.9
	T (1404) [348, 368, 370, 376, 380, 381, 386, 423, 428, 431–436]	3.7
	E (1722) [291, 295, 296]	3.0
	$\Delta\sigma_{31}$ (2192) [70, 292, 300]	1.1
	G (591) [301, 437–440]	1.6
	H (225) [370, 437, 438]	2.1
	F (397) [436]	3.4
	$C_{x'_L}$ (74) [366, 430, 441]	7.0
	$C_{z'_L}$ (26) [366, 430]	15
$\gamma p \to \pi^+ n$	$d\sigma/d\Omega$ (5670) [70, 331, 341, 351, 442–471]	2.4
	Σ (1456) [331, 374, 375, 392, 395, 467, 472–484]	3.3
	P (265) [476, 479, 485–489]	5.1
	T (718) [476, 479, 489–500]	5.1
	E (903) [70, 293, 298]	2.4
	$\Delta\sigma_{31}$ (231) [70, 293]	1.5
	G (303) [301, 439, 501, 502]	5.4
	H (128) [501–504]	4.5

Table 20: List of the χ^2 per number of data points for the reactions $\gamma p \to \pi N$ for each observable.

Reaction	Observable (# data points)	$\chi^2/\#$
$\gamma p \to \eta p$	$d\sigma/d\Omega$ (9442) [302, 505–526]	1.0
	Σ (615) [302, 513, 520, 527–529]	2.9
	P (63) [297, 510, 530]	7.0
	T (291) [297, 435, 531]	3.4
	E (306) [297, 299]	2.7
	G (47) [297]	3.3
	H (56) [297]	1.5
	F (144) [531]	1.6
$\gamma p \to K\Lambda$	$d\sigma/d\Omega$ (2563) [83, 532–552]	2.5
	Σ (459) [550, 553–556]	2.8
	P (1663) [83, 534, 536, 540, 541, 546–548, 551, 552, 555, 557–559]	1.5
	T (383) [556, 560, 561]	1.7
	$C_{x'}$ (123) [562]	1.2
	$C_{z'}$ (123) [562]	2.0
	$O_{x'}$ (66) [556, 561]	1.4
	$O_{z'}$ (66) [556, 561]	1.4
	O_x (314) [556, 561]	1.7
	O_z (314) [556, 561]	1.2

Table 21: List of the χ^2 per number of data points for the reactions $\gamma p \to \eta p$, $K\Lambda$ for each observable.

Reaction	Observable (# data points)	$\chi^2/\#$
$\gamma p \to K^+\Sigma^0$	$d\sigma/d\Omega$ (4381) [83, 533, 535, 538, 541–550, 563–566]	1.2
	Σ (280) [550, 553, 555, 556, 563]	3.2
	P (402) [83, 546–548, 555, 564]	3.3
	T (127) [556]	1.5
	$C_{x'}$ (94) [562]	2.1
	$C_{z'}$ (94) [562]	2.1
	O_x (127) [556]	2.6
	O_z (127) [556]	1.1
$\gamma p \to K^0\Sigma^+$	$d\sigma/d\Omega$ (281) [567–573]	2.6
	Σ (21) [303]	0.7
	P (188) [303, 567, 570, 572, 574]	2.1
	T (21) [303]	1.7
	O_x (21) [303]	4.3
	O_z (21) [303]	0.6

Table 22: List of the χ^2 per number of data points for the reactions $\gamma p \to K\Sigma$ for each observable.

For the fitting procedure we started from the JüBo2025 fit result and fixed the parameters used in that analysis. For the initial steps, we varied only the new parameters relevant for photoproduction on neutron targets. After constraining the threshold behaviour with the ChPT predictions, we fitted to the multipole amplitudes from the latest SAID analysis [132] to obtain starting values for these new photoproduction parameters. The SAID amplitudes were then excluded from the subsequent fitting procedure. In a next step, we included the data for the final-states $\pi^0 n$ and $\pi^- p$ in neutron photoproduction, as listed in Tabs. 16-18. Note, we continued to constain the threshold values using the ChPT predictions throughout the entire fit. Once the new parameters had stabilized, we included all data listed in Tab. 4.1 of the previous study presented in Sec. 4 and also allowed the parameters of the JüBo2025 study to vary.

We present our results for the multipoles for neutron targets in Fig. 17 and also include the SAID solution [132] for comparison. Even though we used this solution in the beginning of the fit procedure, our multipole amplitudes differ from the SAID results in some partial waves.

The ChPT values for the E_{0+} multipole at threshold of Ref. [586] together with our result close to threshold are given by

$$E_{0+}^{\text{JüBo}}(\pi^0 n) = 1.7 \times 10^{-3} m_\pi^{-1} \ , \quad E_{0+}^{\text{ChPT}}(\pi^0 n) = (2.1 \pm 0.5) \times 10^{-3} m_\pi^{-1} \ , \tag{5.36}$$

$$E_{0+}^{\text{JüBo}}(\pi^- p) = -31.2 \times 10^{-3} m_\pi^{-1} \ , \ E_{0+}^{\text{ChPT}}(\pi^- p) = (-31.5 \pm 0.8) \times 10^{-3} m_\pi^{-1} \ . \tag{5.37}$$

Our result agrees with the ChPT values within the respective uncertainties.

5.3.1. Results for $\gamma n \to \pi^0 n$

Fit results for the $\pi^0 n$ final-state data listed in Tab. 16 can be found in the Appendix in Sec. E. We discuss our results for the different data sets in the following.

In Fig. 28 and 29 we present the fit results for the data sets up to the year 2004. These data sets consist of only few data points each, making it hard to constrain the amplitude from just these alone. There are also no data points very close to threshold, since the lowest energy is given at $W = 1130.20$ MeV with only one data point. That is why we decided to put a lower weight on these older data points in the fit procedure.

In Fig. 30 we present the data from a MAMI study published in 2018 [591]. This cross section data covers a large range of $W = 1312 - 1888$ MeV and covers a large angular range. The fit result describes these data points well.

The data shown in Fig. 31 was published in 2019 by the MAMI collaboration [590]. Energies of $W = 1195 - 1553$ MeV was covered and the fit result describes the data sets well until around 1500 MeV. However, there is a discrepancy between the data of both MAMI publication in the energy region 1500-1553 MeV, which makes it hard to get a good description of both data sets.

For the beam asymmetry Σ we included a data set from a 2009 study of GRAAL [598] as well as data from a MAMI study from 2021 [597]. These are presented with our fit results in Fig. 32 and the result describes the data well. One noteworthy remark is that

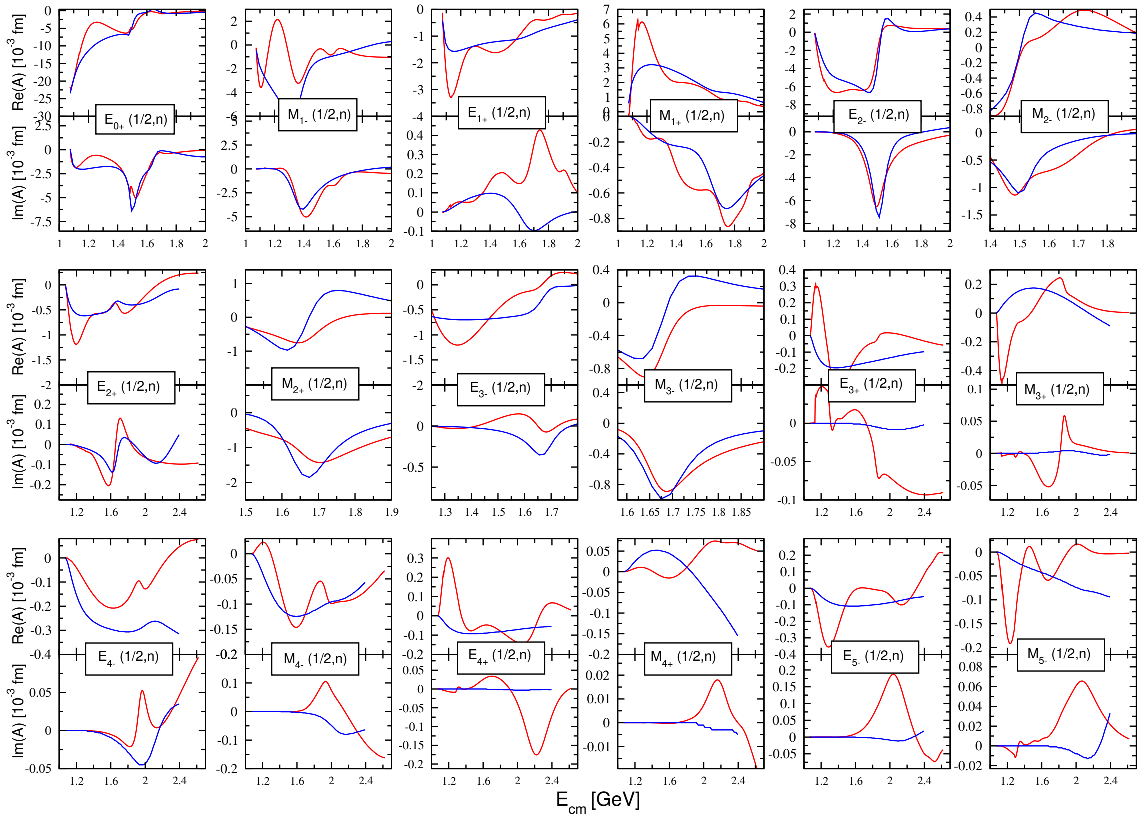

Figure 17: Fit results for the multipole amplitudes are shown in red and the SAID 2022 solution [132] is shown in blue for comparison.

there is a significant dip visible in our solution, which starts to emerge above 1870 MeV and for angles of 60-90°.

The only data on the observables H, P and T was measured recently by CBELSA/TAPS and published in Ref. [601] in 2023. Our fit result with the observables P and H data are shown in Fig. 33. The uncertainties are relatively large for this data and thus the curve describes the data well. For the observable T (shown in Fig. 34) the uncertainties in the lower energy bins are much smaller. Here our solution gets a good description of the data. However, for energies above 1715 MeV our solution still has much room for improvement.

For the double polarization observable E we have two data sets published by the MAMI collaboration. The earlier one published in 2017 [600] is shown in Fig. 35. Our solution describes this data well until 1744 MeV and afterwards differs from the data point with the lowest angle θ. For the more recent data from 2022 [599] (presented in Fig. 36), we see a similar behaviour. The results of the current study are in good agreement with the data except for the lowest angle points above 1753 MeV, which have large error bars.

5.3.2. Results for $\gamma n \to \pi^- p$

The fit results for the $\pi^- p$ final-state data sets, that are listed in Tab. 17 and 18, are presented in the Appendix in Sec. F.

We present cross section data up until the year 1994 together with the fit results of the current analysis in Figs. 37-41. Difficulties in the fitting process arise from inconsistencies between some data sets and some measurements only having a few (or even one) data points per energy bin. Still our analysis describes most of these data sets satisfactorily. The most prominent deviations from the data can be observed in the energy range 1233-1328 MeV, for forward angles above 1520 MeV and for the highest energies of the data set of Besch et al. [608] with the abbreviation BX(82).

We further included a data set from the Crystal Ball Collaboration for the cross section from 2004 [605]. This data is presented in the upper plot of Fig. 42 together with our results. Even though the two lowest energy bins are described well by the present solution, it underestimates the differential cross section for all other bins slightly.

Another data set with only a few data points is given by the one published by JLAB in 2005 [469], which is shown in the lower plot in Fig. 42. Our solution is consistent with these data points.

The data published in 2012 by the CLAS collaboration [603] is shown in Fig. 43. It covers a center of mass energy range of 1690-2362 MeV. For these energies the fit result from the current analysis agrees well with the data points.

Another data set for the differential cross section was published by the MAMI collaboration in 2012 [604]. This set covers the energies from 1203 MeV to 1318 MeV. The result of the current study clearly underestimates the cross section when compared to these data points.

The last cross section data set for $\pi^- p$ covers about 75% of the data points. It was published by CLAS in the year 2017 [602] and has a very fine angle binning, but does not cover the most forward angles or the backward angles. The data points with our result are presented in Figs. 44-47. The measured data lies within the energy range of

1311-2366 MeV. We observe that our amplitude underestimates the cross section below 1360 MeV. For higher energies, the current solution agrees mostly with the data except for the lowest angle bins. This means the forward peak is not as prominent in our solution as measured in the experiment.

For the beam asymmetry Σ data we grouped all data sets up to the year 1995 together and present them with our results in Figs. 48-50. Here, we again face the problem of some data sets having only single data points. We observe that our result differs from the data a lot around 1300 MeV. For higher energies the solution agrees with the data well.

Another data set for Σ was published by GRAAL [621] and covers center of mass energies from 1515 MeV to 1893 MeV. Our result agrees well with this data set.

The major portion of Σ data available from the SAID data base [126] covers the center of mass energies from 1631 MeV to 2361 MeV. Our result agrees well with these data points, which is to be expected since it has a large influence on the fit procedure.

We present the data on the observable P in Fig. 55. Unfortunately, many energy bins only have single data points, there is no large angle coverage and there is no data above 1763 MeV. Thus the data can not restrict the amplitude very much.

For the observable T we have a similar situation. Our results and the data sets are shown in Figs. 56 and 57. Even though there are energy bins for energies up to 2154 MeV, most of the higher energy bins only have a single data point. We notice a lot of structure in our solution at higher energies in the observable T, but to confirm this behaviour more data is needed.

The last data set included in the present study is for the double polarization observable E. It was recently published by CLAS [637] and covers the energies 1500-2300 MeV. Our results agrees well with this data set.

5.4. Influence on the resonance spectrum

In Tabs. 23-26 we list the resonance parameters from the fit results of the analysis including photoproduction off neutrons. We further list the values from the previous JüBo2025 analysis presented in Chapter 4 for comparison. A graphical presentation for the pole positions of the different resonances for the JüBo2026 analysis together with the past JüBo studies (discussed in Chap. 4) is shown in Figs. 14 and 15. Note, an uncertainty estimation for this analysis using neutron photoproduction data is currently planned in a different project, which uses Bayesian parameter estimation within the Jülich-Bonn framework.

Since this analysis covers photoproduction data off neutron targets for the first time, we can also calculate the corresponding γn photocouplings A_n^h. We further list values from other analyses for these photocouplings with neutron targets for comparison in Tab. 23. These values for comparison are from the SAID analysis from 2023 [132], the 2017 Bonn-Gatchina analysis [638] and from a different DCC analysis of the ANL-Osaka group [124].

For the resonance $N(1535)1/2^-$ our result agrees with the one found by the SAID analysis, while the studies of BnGa and ANL find higher photocouplings.

The photocouplings for the $N(1620)1/2^-$ is very small in our analysis as well as for the work of the ANL-Osaka group. In contrast to this the SAID and BnGa group find higher photocouplings for this resonance.

For the Roper resonance $N(1440)1/2^+$ we find a large photocoupling compared to the other groups. We noticed a deviation of our result from the $\pi^- p$ data in the energy range around the pole position of the $N(1440)1/2^+$. This deviation may be connected to the high photocoupling to the γn channel of the $N(1440)1/2^+$.

The photocoupling for the $N(1710)1/2^+$ is smaller than the one of the Roper. In the BnGa analysis it was only half as large as our value, but the ANL-Osaka group find a much larger coupling.

For the $N(1720)3/2^+$ we find only find very small photocouplings $\left|A_n^h\right|$, while all other groups find larger ones. The other P_{13} resonance $N(1900)3/2^+$ has a much larger value for $\left|A_n^{1/2}\right|$ (similar size as for the Roper).

All other groups find similar values for both photocouplings $\left|A_n^h\right|$ for the $N(1520)3/2^-$ resonance. In our case, the $\left|A_n^{1/2}\right|$ is only half as large and for the $\left|A_n^{3/2}\right|$ about 2/3 of the values found by other groups.

The $\left|A_n^{1/2}\right|$ photocoupling for the $N(1675)5/2^-$ found in the present work is very small. The other groups find much larger values. For the $\left|A_n^{3/2}\right|$ coupling our result agrees with the one of ANL-Osaka, but the SAID and BnGa groups find values about twice as large.

For the resonance $N(1680)5/2^+$ all groups find similar values for $A_n^{1/2}$, while the $A_n^{3/2}$ photocouplings are vary more.

For the resonances $N(1990)7/2^+$ and $N(2190)7/2^-$ we find smaller values again for $A_n^{1/2}$, while we have similar ones for $A_n^{3/2}$.

Note that none of the other analysis groups included our highest partial wave resonances $N(2250)9/2^-$ and $N(2220)9/2^+$. Our current analysis found the largest photocoupling for the resonance $N(2220)9/2^+$ in the H_{19} partial wave, which indicates a large influence of this resonance on the γn amplitude. To illustrate this, we present some plots in the Appendix in Sec. F.2.1, in which we did not allow the H_{19} resonance $N(2220)9/2^+$ to couple to the πN channels. In these examples, one can observe this large influence on the amplitude for higher energies. This large photocoupling of the $N(2220)9/2^+$ may be an artifact of the local minimum found in our fit result and has to be investigated further in future analyses.

We do not find any new resonance state and included no new s-channel state in this study compared to the JüBo2025 analysis. For almost all resonance states we do not observe large changes in the pole positions. In the following we discuss the changes of the resonance parameters compared to the JüBo2025 solution.

For the S_{11} partial wave we do not find any significant changes to the pole positions or the residues. For the $N(1650)1/2^-$ the $A_p^{1/2}$ photocoupling decreased slightly.

The only change we observe in the P_{11} partial wave is that the width of the $N(1710)1/2^+$ increased slightly. All other resonance parameters do not have significant changes.

In the P_{13} the only change is visible for the residues of the $N(1900)3/2^+$.

The only resonance in the D_{13} partial wave is the $N(1520)3/2^-$. It has an increased πN residue and the other residues increased slightly but within the uncertainties of the

JüBo2025 results.

For the D_{15} resonance $N(1675)5/2^-$ we find a small increase in the real part of the pole position. We further see an increase in the residues as well as in the γp photocouplings for this resonance.

In the F_{15} partial wave we observe a decrease in the elastic residue $|r_{\pi N}|$ and in the normalised residue into the channel $K\Lambda$ for the $N(1680)5/2^+$. We also find a small increase in the modulus of the $A_p^{1/2}$ photocoupling.

The only two star nucleon resonance in our analysis $N(1990)7/2^-$ lies in the F_{17} partial wave. The only significant changes compared to the JüBo2025 solution is found in the $A_p^{1/2}$ parameter, of which the absolute value decreased.

For the G_{17} resonance $N(2190)7/2^+$ the pole position changes slightly and the residues changed within the uncertainties of the previous study. We also observe an increase in the modulus of the photocoupling $A_p^{3/2}$.

The $N(2250)9/2^-$ resonance is included in the G_{19} partial wave. Its pole position changed and is closer to the PDG values. The residues also changed slightly but all changes are within the uncertainties. For the γp photocouplings we observe a decrease in the absolute values.

The H_{19} resonance $N(2220)9/2^+$ does not have any significant changes in the pole position or residues. However, the $A_p^{1/2}$ photocoupling is only half of the result from the JüBo2025 result, but it had a large uncertainty.

For the only S_{31} resonance $\Delta(1620)1/2^-$ we find a smaller residue for the $\pi\Delta$ channel compared to the JüBo2025 solution as well as a smaller photocoupling $A^{1/2}$.

The P_{31} resonance $\Delta(1910)1/2^+$ we find a smaller width, but it is still larger than the PDG estimate. We further find that all residues increased significantly in the current study. We also find a larger γN photocoupling.

The P_{33} partial wave features three resonances. The $\Delta(1232)$ has no noteworthy change in the resonance parameters. For the $\Delta(1600)3/2^+$ we observe a decrease in all residues, but the moduli of the γp photocouplings only changed within the uncertainties of the previous analysis. The third resonance is the $\Delta(1920)3/2^+$ and both the real and imaginary parts of the pole position changed in the JüBo2026 result. We also observe that some residues decreased slightly compared to the JüBo2025 solution. For the photocouplings we find that the $A^{1/2}$ increased while the $A^{3/2}$ decreased.

The only D_{33} resonance in our model is given by the $\Delta(1700)3/2^-$. The only resonance parameters that significantly changed are the γN photocouplings, which both decreased.

For the $\Delta(1930)5/2^-$ resonance in the D_{35} partial wave we only find changes of the resonance parameters within the uncertainties of the previous study.

The F_{35} partial wave features the $\Delta(1905)5/2^+$. For this resonance all residues as well as the moduli of the γN photocouplings decreased. For this resonance we already found large uncertainties on the resonance parameters in the JüBo2025 study.

In the F_{37} partial wave we find the $\Delta(1950)7/2^+$. Here we observe a slight increase in the width, the πN residue and the modulus of the photocoupling $A^{1/2}$.

For the resonance $\Delta(2200)7/2^-$ in the G_{37} partial wave we find an increase in the $K\Sigma$ residue, which was very small in the previous studies. We also find a smaller $A^{3/2}$

photocoupling.

The G_{39} partial wave features the two star resonance $\Delta(2400)9/2^-$. In the current study its width increased significantly and all residues decreased. We also find larger photocouplings than in the JüBo2025 study.

Table 23: Here we present the photocouplings at the pole for neutron targets (A_n^h, ϑ_n^h) of the nucleon resonances. In addition to the present study ("2026"), we list the values from the 2023 SAID study [132] as "SAID", from the 2017 BnGa analysis [638] as "BnGa" and from a study from 2016 of ANL-Osaka [124] as "ANL" for comparison.

	fit	$\mathbf{A_n^{1/2}}$ [10^{-3} GeV$^{-1/2}$]	$\vartheta_n^{1/2}$ [deg]	$\mathbf{A_n^{3/2}}$ [10^{-3} GeV$^{-1/2}$]	$\vartheta_n^{3/2}$ [deg]		fit	$\mathbf{A_n^{1/2}}$ [10^{-3} GeV$^{-1/2}$]	$\vartheta_n^{1/2}$ [deg]	$\mathbf{A_n^{3/2}}$ [10^{-3} GeV$^{-1/2}$]	$\vartheta_n^{3/2}$ [deg]
$N(1535)\ 1/2^-$	2026	64	-76			$N(1650)\ 1/2^-$	2026	7	-145		
	SAID	67 (9)	-174 (22)				SAID	26 (5)	-72 (13)		
	BnGa	88 (4)	-175 (4)				BnGa	16 (4)	-28 (10)		
	ANL	112	-164				ANL	1	-47		
$N(1440)\ 1/2^+$	2026	166	-17			$N(1710)\ 1/2^+$	2026	64	10		
	SAID	80 (5)	1.25 (0.08)				SAID	–	–		
	BnGa	41 (5)	23 (10)				BnGa	29 (7)	80 (20)		
	ANL	95	-15				ANL	195	-8		
$N(1720)\ 3/2^+$	2026	6	121	6	-94	$N(1900)\ 3/2^+$	2026	-162	122	32	18
	SAID	56 (21)	-21 (8)	65 (24)	169 (64)		SAID	–	–	–	–
	BnGa	$-(25^{+40}_{-15})$	-75 (35)	100 (35)	-80 (35)		BnGa	-98 (20)	-13 (20)	74 (15)	5 (15)
	ANL	-59	6	-28	-19		ANL	–	–	–	–
$N(1520)\ 3/2^-$	2026	25	0	82	-154						
	SAID	44 (4)	-175 (15)	121 (10)	-170 (14)						
	BnGa	45 (5)	175 (4)	119 (5)	-175 (4)						
	ANL	43	179	-110	5						
$N(1675)\ 5/2^-$	2026	7	-133	40	139	$N(1680)\ 5/2^+$	2026	30	-33	33	152
	SAID	123 (27)	-19 (4)	84 (18)	-170 (38)		SAID	37 (6)	-15 (3)	40 (7)	-176 (29)
	BnGa	53 (4)	177 (5)	73 (5)	168 (5)		BnGa	32 (3)	-7 (5)	63 (4)	170 (5)
	ANL	76	-177	38	176		ANL	34	-12	56	176
$N(1990)\ 7/2^+$	2026	11	55	65	38	$N(2190)\ 7/2^-$	2026	18	100	-20	162
	SAID	37 (6)	-15 (3)	40 (7)	-176 (29)		SAID	–	–	–	–
	BnGa	32 (3)	-7 (5)	63 (4)	170 (5)		BnGa	30 (7)	5 (15)	-23 (8)	13 (20)
	ANL	–	–	–	–		ANL	–	–	–	–
$N(2250)\ 9/2^-$	2026	99	175	108	16	$N(2220)\ 9/2^+$	2026	-609	26	-610	13
	SAID	–	–	–	–		SAID	–	–	–	–
	BnGa	–	–	–	–		BnGa	–	–	–	–
	ANL	–	–	–	–		ANL	–	–	–	–

Table 24: For the $I = 1/2$ resonances we present the extracted resonance parameters, namely the pole positions W_0 ($\Gamma_{\rm tot}$ defined as -2ImW_0), the elastic πN residues ($|r_{\pi N}|, \theta_{\pi N\to\pi N}$), and the normalized residues ($\sqrt{\Gamma_{\pi N}\Gamma_\mu}/\Gamma_{\rm tot}, \theta_{\pi N\to\mu}$) for the inelastic reactions $\pi N \to \mu$ with $\mu = \eta N$, $K\Lambda$, $K\Sigma$. In addition to the present study ("2026"), we list the JüBo2025 results ("2025") [1] from Chapter 4 and the estimates from the Particle Data Group [5] ("PDG"), if available, as well as the PDG star rating.

	fit	Re W_0 [MeV]	-2Im W_0 [MeV]	$\lvert r_{\pi N}\rvert$ [MeV]	$\theta_{\pi N\to\pi N}$ [deg]	$\frac{\Gamma^{1/2}_{\pi N}\Gamma^{1/2}_{\eta N}}{\Gamma_{\rm tot}}$ [%]	$\theta_{\pi N\to\eta N}$ [deg]	$\frac{\Gamma^{1/2}_{\pi N}\Gamma^{1/2}_{K\Lambda}}{\Gamma_{\rm tot}}$ [%]	$\theta_{\pi N\to K\Lambda}$ [deg]	$\frac{\Gamma^{1/2}_{\pi N}\Gamma^{1/2}_{K\Sigma}}{\Gamma_{\rm tot}}$ [%]	$\theta_{\pi N\to K\Sigma}$ [deg]
$N(1535)\ 1/2^-$	2026	1503	76	19	-28	56	127	21	-56	4.4	64
	2025	1504 (1)	78 (2)	20 (1)	-27 (1)	55 (1)	128 (0)	22 (1)	-56 (1)	6.7 (1.3)	79 (9)
****	PDG	1510 ± 10	110^{+20}_{-30}	25 ± 10	-20 ± 20	—	—	—	—	—	—
$N(1650)\ 1/2^-$	2026	1669	124	39	-55	25	33	16	-73	26	-63
	2025	1671 (2)	127 (3)	42 (1)	-54 (2)	24 (1)	39 (3)	17 (0)	-73 (2)	27 (1)	-61 (2)
****	PDG	1665 ± 15	135 ± 35	45^{+10}_{-20}	-70^{+20}_{-10}	—	—	—	—	—	—
$N(1440)\ 1/2^+$	2026	1359	216	62	-99	8.2	-35	6.4	134	0.8	-18
	2025	1359 (1)	213 (2)	61 (1)	-99 (1)	8.4 (0.4)	-32 (2)	6.2 (1.8)	140 (4)	0.9 (1.4)	-23 (9)
****	PDG	1370 ± 10	190^{+15}_{-10}	55 ± 5	-90 ± 10	—	—	—	—	—	—
$N(1710)\ 1/2^+$	2026	1592	131	4.1	-119	20	78	13	-158	3.9	157
	2025	1588 (5)	113 (9)	3.4 (0.7)	-115 (4)	21 (1)	86 (2)	14 (2)	-157 (4)	4.7 (0.4)	161 (3)
****	PDG	1700 ± 50	120 ± 40	7^{+3}_{-4}	190^{+80}_{-70}	—	—	—	—	—	—
$N(1720)\ 3/2^+$	2026	1720	166	3.8	-17	2.5	95	1.5	-71	1.1	103
	2025	1720 (2)	166 (4)	4.8 (3.7)	-16 (43)	2.5 (1.6)	99 (32)	1.2 (0.3)	-71 (31)	1.2 (0.9)	107 (37)
****	PDG	1680^{+30}_{-20}	200^{+100}_{-50}	15 ± 10	-110 ± 50	—	—	—	—	—	—
$N(1900)\ 3/2^+$	2026	1907	140	0.4	-148	1.6	-2	3.2	-58	1.4	-72
	2025	1904 (1)	141 (1)	1.1 (0.3)	-93 (4)	2.2 (0.2)	-2 (4)	4.2 (0.3)	-62 (3)	1.5 (0.2)	-79 (8)
****	PDG	1920 ± 20	130^{+30}_{-40}	4 ± 2	-10 ± 30	—	—	—	—	—	—
$N(1520)\ 3/2^-$	2026	1494	108	40	-16	2.6	66	3.7	141	6.1	-36
	2025	1496 (1)	102 (6)	26 (5.2)	-17 (4)	1.8 (0.8)	68 (9)	2.9 (7.4)	140 (15)	3.1 (20)	-36 (4)
****	PDG	1510 ± 5	110^{+10}_{-5}	35 ± 3	-10 ± 5	—	—	—	—	—	—
$N(1675)\ 5/2^-$	2026	1653	117	19	-13	5.1	-34	0.1	-90	3.1	-162
	2025	1644 (1)	117 (2)	14 (5)	13 (16)	3.5 (1.0)	-9 (16)	< 0.1 (0.0)	-65 (49)	2.2 (0.5)	-144 (16)
****	PDG	1655 ± 5	135 ± 15	26^{+6}_{-4}	-22 ± 5	—	—	—	—	—	—
$N(1680)\ 5/2^+$	2026	1667	115	30	-31	0.2	130	0.5	-109	0.2	142
	2025	1663 (5)	114 (3)	46 (18)	-41 (12)	0.1 (0.1)	-44 (110)	0.9 (0.3)	-121 (15)	0.1 (0.2)	-49 (196)
****	PDG	1670 ± 10	120^{+15}_{-10}	40 ± 5	-20 ± 10	—	—	—	—	—	—
$N(1990)\ 7/2^+$	2026	1854	92	0.2	-102	4.8	-52	0.1	-62	0.3	-68
	2025	1851 (6)	82 (10)	0.18 (0.02)	-99 (4)	5.2 (0.4)	-50 (3)	0.1 (0.1)	-62 (190)	0.7 (0.3)	-64 (4)
**	PDG	—	—	—	—	—	—	—	—	—	—
$N(2190)\ 7/2^-$	2026	1935	174	16	-47	2.6	-55	3.1	-65	0.9	-76
	2025	1943 (8)	161 (2)	15 (1)	-45 (1)	2.9 (0.3)	-52 (1)	3.6 (0.5)	-62 (1)	1.1 (0.2)	-71 (2)
****	PDG	2050 ± 100	400 ± 100	40 ± 20	0 ± 30	—	—	—	—	—	—
$N(2250)\ 9/2^-$	2026	2167	430	17	-62	2.9	-83	0.2	-94	0.7	-101
	2025	2194 (43)	374 (65)	21 (10)	-45 (12)	3.8 (1.7)	-62 (14)	0.1 (0.1)	-76 (204)	1.1 (0.7)	-76 (13)
****	PDG	2150 ± 50	420^{+80}_{-70}	25^{+5}_{-10}	-40 ± 20	—	—	—	—	—	—
$N(2220)\ 9/2^+$	2026	2011	375	30	-49	2.1	-87	1.3	-103	0.1	64
	2025	2009 (46)	367 (41)	30 (4)	-52 (16)	2.3 (0.2)	-89 (13)	1.4 (0.3)	-106 (15)	0.2 (0.2)	-122 (199)
****	PDG	2150^{+50}_{-20}	400^{+80}_{-40}	45^{+15}_{-10}	-40^{+30}_{-20}	—	—	—	—	—	—

Table 25: For the $I = 3/2$ resonances we present the extracted resonance parameters, namely the pole positions W_0 (Γ_{tot} defined as -2ImW_0), elastic πN residues $(|r_{\pi N}|, \theta_{\pi N\to\pi N})$, and the normalized residues $\pi N \to K\Sigma$ and $\pi N \to \pi\Delta$ with the number in brackets indicating L of the $\pi\Delta$ state. In addition to the present study ("2026"), we list the JüBo2025 results ("2025") [1] from Chapter 4 and the estimates from the Particle Data Group [5] ("PDG"), if available, as well as the PDG star rating.

		Pole position		πN Residue		$K\Sigma$ channel		$\pi\Delta$, channel (6)		$\pi\Delta$, channel (7)	
		Re W_0 [MeV]	-2Im W_0 [MeV]	$\lvert r_{\pi N}\rvert$ [MeV]	$\theta_{\pi N\to\pi N}$ [deg]	$\frac{\Gamma^{1/2}_{\pi N}\Gamma^{1/2}_{K\Sigma}}{\Gamma_{\text{tot}}}$ [%]	$\theta_{\pi N\to K\Sigma}$ [deg]	$\frac{\Gamma^{1/2}_{\pi N}\Gamma^{1/2}_{\pi\Delta}}{\Gamma_{\text{tot}}}$ [%]	$\theta_{\pi N\to\pi\Delta}$ [deg]	$\frac{\Gamma^{1/2}_{\pi N}\Gamma^{1/2}_{\pi\Delta}}{\Gamma_{\text{tot}}}$ [%]	$\theta_{\pi N\to\pi\Delta}$ [deg]
	fit										
$\Delta(1620)$ $1/2^-$	2026	1598	79	13	-104	14	-99	—	—	39 (D)	102
	2025	1601 (2)	79 (1)	17 (3)	-72 (19)	18 (3)	-65 (20)	—	—	51 (9) (D)	133 (19)
****	PDG	1600 ± 10	110 ± 30	15 ± 5	-100 ± 20	—	—	—	—	—	—
$\Delta(1910)$ $1/2^+$	2026	1807	598	101	156	7.0	-138	64 (P)	25	—	—
	2025	1813 (6)	653 (25)	27 (21)	129 (306)	0.5 (1.4)	-100 (40)	15 (12) (P)	-3 (63)	—	—
****	PDG	1850 ± 50	350 ± 150	25 ± 5	-90^{+180}_{-90}	—	—	—	—	—	—
$\Delta(1232)$ $3/2^+$	2026	1215	95	49	-40						
	2025	1215 (1)	92 (0)	48 (0)	-39 (0)						
****	PDG	1210 ± 1	100 ± 2	50^{+2}_{-1}	-46^{+1}_{-2}						
$\Delta(1600)$ $3/2^+$	2026	1596	109	2.4	-111	3.0	13	7.6 (P)	89	0.3 (F)	-48
	2025	1598 (1)	111 (1)	6.0 (0.8)	-110 (4)	9.5 (1.6)	8 (4)	22 (4) (P)	87 (5)	0.6 (0.1) (F)	-31 (9)
****	PDG	1520^{+70}_{-50}	280^{+40}_{-30}	25 ± 15	210^{+40}_{-30}	—	—	—	—	1 ± 0.5	—
$\Delta(1920)$ $3/2^+$	2026	1807	796	48	-96	24	38	6.8 (P)	-129	2.3 (F)	25
	2025	1857 (15)	875 (4)	60 (8)	-28 (19)	25 (2.1)	82 (13)	8.0 (0.8) (P)	-74 (13)	3.3 (0.5) (F)	96 (18)
***	PDG	1900 ± 50	300 ± 100	25 ± 10	-100 ± 50	—	—	—	—	—	—
$\Delta(1700)$ $3/2^-$	2026	1662	355	42	-21	3.1	-171	7.2 (D)	139	52 (S)	138
	2025	1663 (4)	354 (13)	47 (13)	-11 (20)	3.1 (0.7)	-164 (15)	7.7 (1.7) (D)	148 (19)	59 (15) (S)	146 (19)
****	PDG	1665 ± 25	250 ± 50	25 ± 15	-20 ± 20	—	—	—	—	—	—
$\Delta(1930)$ $5/2^-$	2026	1832	504	23	-127	0.8	25	12 (D)	44	1.2 (G)	139
	2025	1835 (11)	485 (20)	20 (2)	-123 (7)	0.7 (0.1)	28 (6)	11 (2.6) (D)	47 (6)	1.2 (0.1) (G)	147 (6)
***	PDG	1850 ± 30	320^{+130}_{-20}	14 ± 6	-50^{+40}_{-50}	—	—	—	—	—	—
$\Delta(1905)$ $5/2^+$	2026	1725	269	1.7	-29	0.1	-137	0.7 (F)	38	3.9 (P)	-62
	2025	1722 (4)	264 (11)	5.1 (3.5)	-65 (18)	0.3 (0.2)	-179 (356)	1.8 (1.3) (F)	47 (19)	9.4 (3.2) (P)	-105 (22)
****	PDG	1770^{+30}_{-20}	300 ± 40	20 ± 5	-45^{+15}_{-75}	—	—	—	—	—	—
$\Delta(1950)$ $7/2^+$	2026	1872	184	44	-6	1.7	-62	51 (F)	156	2.3 (H)	24
	2025	1871 (1)	170 (7)	38 (3.3)	8 (9)	1.9 (0.5)	-43 (8)	45 (4) (F)	168 (8)	2.9 (0.2) (H)	47 (9)
****	PDG	1880 ± 10	240 ± 20	52 ± 8	-32 ± 8	—	—	—	—	—	—
$\Delta(2200)$ $7/2^-$	2026	1973	326	7.0	-72	0.3	-114	0.3 (G)	114	18 (D)	104
	2025	1978 (7)	327 (12)	7.3 (0.5)	-76 (3)	0.0 (0.0)	64 (3)	0.4 (0.1) (G)	100 (18)	18 (1.1) (D)	100 (4)
***	PDG	2100 ± 50	340 ± 80	—	—	—	—	—	—	—	—
$\Delta(2400)$ $9/2^-$	2026	2509	177	21	11	0.7	29	47 (G)	28	7.4 (I)	-175
	2025	2517 (49)	86 (37)	25 (2)	6 (6)	4.5 (3.4)	15 (7)	65 (29) (G)	16 (7)	12 (8) (I)	154 (11)
**	PDG	—	—	—	—	—	—	—	—	—	—

Table 26: Here we present the photocouplings at the pole for proton targets (A_p^h, ϑ_p^h) of the $I = 1/2$ resonances (left). We also list the photocouplings at the pole for $I = 3/2$ resonances (right) as (A^h, ϑ^h) because they are the same for proton and neutron targets. In addition to the present study ("2026"), we show the JüBo2025 results ("2025") [1] from Sec. 4 for comparison.

	fit	$\mathbf{A_p^{1/2}}$ [10^{-3} GeV$^{-1/2}$]	$\vartheta_p^{1/2}$ [deg]	$\mathbf{A_p^{3/2}}$ [10^{-3} GeV$^{-1/2}$]	$\vartheta_p^{3/2}$ [deg]		fit	$\mathbf{A^{1/2}}$ [10^{-3} GeV$^{-1/2}$]	$\vartheta^{1/2}$ [deg]	$\mathbf{A^{3/2}}$ [10^{-3} GeV$^{-1/2}$]	$\vartheta^{3/2}$ [deg]
$N(1535)\ 1/2^-$	2026	87	−1			$\Delta(1620)\ 1/2^-$	2026	17	57		
	2025	90 (2)	−1 (2)				2025	30 (11)	58 (12)		
$N(1650)\ 1/2^-$	2026	26	−4			$\Delta(1910)\ 1/2^+$	2026	−288	24		
	2025	34 (3)	−2 (5)				2025	−164 (128)	−5 (352)		
$N(1440)\ 1/2^+$	2026	−87	−12			$\Delta(1232)\ 3/2^+$	2026	−128	−17	−238	1
	2025	−99 (15)	−18 (4)				2025	−128 (5)	−18 (3)	−246 (3)	1 (1)
$N(1710)\ 1/2^+$	2026	−24	44			$\Delta(1600)\ 3/2^+$	2026	11	110	−12	167
	2025	−18 (2)	37 (10)				2025	9 (4)	11 (45)	−10 (6)	105 (43)
$N(1720)\ 3/2^+$	2026	24	47	−35	−13	$\Delta(1920)\ 3/2^+_{(a)}$	2026	295	−41	364	−15
	2025	24 (10)	48 (13)	−26 (8)	−24 (13)		2025	245 (30)	−28 (9)	475 (52)	10 (10)
$N(1900)\ 3/2^+$	2026	7	91	−42	0	$\Delta(1700)\ 3/2^-$	2026	163	8	276	−1
	2025	6 (1)	49 (21)	−39 (2)	−28 (3)		2025	244 (53)	17 (11)	337 (67)	−4 (13)
$N(1520)\ 3/2^-$	2026	−24	−45	116	11	$\Delta(1930)\ 5/2^-$	2026	240	2	215	166
	2025	−19 (3)	−34 (8)	102 (12)	17 (4)		2025	218 (18)	162 (24)	240 (31)	173 (10)
$N(1675)\ 5/2^-$	2026	48	16	51	3	$\Delta(1905)\ 5/2^+$	2026	28	−178	−155	148
	2025	35 (5)	17 (6)	36 (4)	15 (8)		2025	75 (61)	−67 (40)	−373 (308)	94 (16)
$N(1680)\ 5/2^+$	2026	−12	110	110	−31	$\Delta(1950)\ 7/2^+$	2026	−48	−73	−59	−84
	2025	−8 (2)	119 (23)	133 (34)	−31 (8)		2025	−33 (7)	−67 (6)	−59 (8)	−70 (5)
$N(1990)\ 7/2^+$	2026	−8	−38	−11	136	$\Delta(2200)\ 7/2^-$	2026	60	−141	38	−165
	2025	−14 (3)	−74 (20)	−14 (3)	107 (15)		2025	72 (17)	−134 (8)	65 (13)	−174 (7)
$N(2190)\ 7/2^-$	2026	−12	18	38	167	$\Delta(2400)\ 9/2^-$	2026	53	−104	39	159
	2025	−13 (2)	11 (15)	20 (7)	161 (15)		2025	15 (9)	−102 (52)	22 (22)	156 (23)
$N(2250)\ 9/2^-$	2026	−12	28	38	167						
	2025	−33 (8)	2 (19)	58 (20)	121 (20)						
$N(2220)\ 9/2^+$	2026	38	−36	−192	−12						
	2025	74 (46)	−78 (17)	−185 (37)	−14 (16)						

6. GDH sum rule contributions in the Jülich-Bonn model

The experimental confirmation of the GDH sum rule (introduced in Sec. 2.4) poses a considerable challenge. To measure the observable $\Delta\sigma$, which is directly connected to the GDH sum rule one requires circularly polarized photon beams and longitudinally polarized nucleon targets. One further has to include data over a large energy range. Inclusive measurements of all possible outgoing channels is not feasible in photoproduction. However, this is possible in electroproduction processes, as it was presented in Refs. [639, 640], where the proton spin structure was studied with polarized electron beams by the CLAS Collaboration. One then extrapolates these measurements to the photon point at zero momentum transfer by using the generalized GDH integrals. These generalized GDH integrals are derived from chiral effective field theory [641–645]. Many experimental programs were dedicated to the GDH sum rule directly in photoproduction processes. There was also the GDH Collaboration at MAMI and ELSA [646–648]. To this day photoproduction data for $\Delta\sigma$ and the observable E, which is directly linked to $\Delta\sigma$, are only available for πN, $\pi\pi N$ and ηN final-states (see Tabs. 7, 8 and 9). To get information on the missing channels or energies, one can only rely on predictions from theory or phenomenological models. Coupled-channel approaches are especially useful to get information on contributions of different hadronic final-states, since they analyze multiple initial and final-states simultaneously. Different calculations were done for the single-pion contributions to the GDH integral, e.g. by the GWU/SAID [649, 650] or the MAID [138] frameworks. For the $K\Sigma$ channel contribution there was a study from Ref. [651] using an isobar model for $K\Sigma$ photoproduction off proton and neutron targets.

In this chapter, we calculate the individual channel contributions to the GDH sum rule from the Jülich-Bonn DCC model. In Sec. 6.1 we discuss the results from the JüBo2025 solution presented in Sec. 4. Here we calculate the GDH sum rule contributions from photoproduction processes off proton targets for the final-states $\pi^0 p$, $\pi^+ n$, ηp, $K^+\Lambda^0$, $K^0\Sigma^+$, and $K^+\Sigma^0$. These results were already published within Ref. [1]. After that we present the GDH sum rule contributions from the analysis presented in Sec. 6.2, in which we extended the model to include $\gamma n \to \pi N$ processes. This allows us to also calculate the contributions to the finals states $\pi^0 n$ and $\pi^- p$.

6.1. GDH sum rule contributions for photoproduction with only proton targets

In Ref. [1] we used the JüBo coupled-channel approach to extract the contributions to the GDH sum rule of the πN, ηN, $K\Lambda$ and $K\Sigma$ channels individually for photoproduction reactions off proton targets. Similar analyses were done in Ref. [650] for single pion photoproduction channels, and there are also analyses considering ηN, $\pi\pi N$ or KY channels such as Refs. [195, 651, 652]. While the JüBo approach includes the $\pi\pi N$ channels effectively in the purely hadronic amplitude, no $\pi\pi N$ photoproduction data are taken into account yet. Consequently, we cannot determine the contribution of this channel to the GDH sum rule directly.

We derived the GDH sum rule in Sec. 2.4. Since a numerical evaluation of the left-hand side of the integral in Eq. (2.63) with an upper limit of infinity is not possible, one defines the so-called "running" GDH integral as

$$I^p_{\mathrm{GDH}}(E_\gamma) = \int_{E^0_\gamma}^{E_\gamma} \mathrm{d}E'_\gamma \, \frac{\Delta\sigma^p(E'_\gamma)}{E'_\gamma} \ . \tag{6.1}$$

where I^p_{GDH} is now a function of the upper limit of the integral E_γ. The superscript p labels the proton target here. We will also consider neutron target processes in Sec. 6.2.

We present the individual channel contributions to this running GDH integral from the JüBo2025 analysis in Fig. 18 and also show the corresponding uncertainties extracted from the refits described in Sec. 4.2. The black dashed line represents the sum of all channels, and the horizontal line denotes the right hand side value of the GDH sum rule of $I^p_{\mathrm{GDH}} = 204.78\,\mu\mathrm{b}$, which is calculated with the corresponding PDG values. The main contribution is given by the $\pi^0 p$ channel, followed by $\pi^+ n$.

The 6 channel contributions to the GDH sum rule for the highest energy $E_\gamma = 2.5$ GeV are given by the following values:

$$\begin{aligned}
I^p_{\mathrm{GDH}}(\pi^0 p) &= 147 \pm 7 \ \mu\mathrm{b} \ , \\
I^p_{\mathrm{GDH}}(\pi^+ n) &= 29 \pm 15 \ \mu\mathrm{b} \ , \\
I^p_{\mathrm{GDH}}(\eta p) &= -8.8 \pm 0.1 \ \mu\mathrm{b} \ , \\
I^p_{\mathrm{GDH}}(K^+ \Lambda^0) &= 0.80 \pm 0.05 \ \mu\mathrm{b} \ , \\
I^p_{\mathrm{GDH}}(K^0 \Sigma^+) &= -0.12 \pm 0.05 \ \mu\mathrm{b} \ , \\
I^p_{\mathrm{GDH}}(K^+ \Sigma^0) &= 1.42 \pm 0.05 \ \mu\mathrm{b} \ , \\
I^p_{\mathrm{GDH}}(\mathrm{all}) &= 170 \pm 19 \ \mu\mathrm{b} \ .
\end{aligned} \tag{6.2}$$

As for the resonance parameters we determine the uncertainties of the contributions to the GDH sum rule for the different channels from refits as explained in 4.2. Consequently, the uncertainties of the individual channel contributions are necessarily correlated. Therefore, the uncertainty of the sum of all channels is determined by the respective spread of the sum of the integrals.

The contribution of the two single pion channels determined in a recent SAID analysis [650] was 183.4 µb. The $\pi^0 p$-channel contribution was ~ 155 µb and the $\pi^+ n$-channel contributed ~ 30 µb. Comparing this with our calculated contributions, we observe that our $\pi^+ n$ contribution is in good agreement while our $\pi^0 p$ channel is giving a slightly smaller contribution. We also observe a relatively large uncertainty in these two channels, especially for $\pi^+ n$. This can be explained by the fact, that less data is available for the $\pi^+ n$ final-state.

To get a better visualization, we added a zoomed-in version for GDH sum rule contributions in Fig. 19, which allows to observe the small contributions of the channels ηp, $K^+\Lambda^0$, $K^0\Sigma^+$ and $K^+\Sigma^0$ in more detail. We further present the running GDH integral for the individual channels separately in the Appendix in Sec. G.1. For the ηp channel we find a negative contribution for all energies. This final-state provides a larger contribution than the KY channels. However, compared to the πN channels the other four have only a marginal contribution of $\sim -6.69\,\mu b$ and they even lower the sum of all channels. Some other studies as, e.g. Refs. [195, 651–653], found negative contributions for all the final-states ηp, $K^+\Lambda^0$, $K^0\Sigma^+$ and $K^+\Sigma^0$. In our study this is not the case, as can be seen for $K^+\Lambda^0$ and $K^+\Sigma^0$, which give positive contributions. Note that no data on $\Delta\sigma$ or E is available for the KY channels yet. Consequently, the corresponding predicted values for the GDH integral may be subject to even greater uncertainties than suggested by the error band.

In the JüBo2025 analysis the full sum of all channels saturates to a value $I^p_{\mathrm{GDH}}(\mathrm{all}) = 170 \pm 19$ µb. This leaves a difference to the right hand side value of $\Delta I^p_{\mathrm{GDH}} = 35 \pm 19$ µb compared to the central value of our sum presented by a black dashed line in Fig. 18. This difference most likely corresponds to contributions of channels not considered explicitly in the JüBo model. Most important is the $\pi\pi N$ channel, which exhibits a large total cross section at energies beyond the $\Delta(1232)$ region. Contributions from other missing channels like ωN or $\eta' N$ are less significant as other analyses suggest. An example is given by the study in Ref. [653], in which a contribution of less than 1 µb was found for the ωN channel.

This hypothesis is also supported by other works. In a direct measurement of two-pion photoproduction from Ref. [654], the contribution of the channel $\gamma p \to \pi^0\pi^+ n$ was found to be only $(11.3 \pm 0.7 \pm 0.7)$ µb. However, the photon energies were only measured up to $E_\gamma = 800$ MeV. As mentioned by the authors, this contribution did not saturate yet at that energy. Furthermore, the analyses of Refs. [195, 655] found a contribution of the $\pi\pi N$ channel over the full energy range of $I^p_{\mathrm{GDH}}(\pi\pi N) = 28\,\mu b$ and in Ref. [653] $I^p_{\mathrm{GDH}}(\pi\pi N) = 21\,\mu b$. Considering our uncertainties on $I^p_{\mathrm{GDH}}(\mathrm{all})$ these values would be enough to reproduce the right hand side of the GDH sum rule of $I^p_{\mathrm{GDH}} = 204.78\,\mu b$ in our analysis. We conclude that the missing contribution in the present analysis is indeed originating from the missing $\pi\pi N$-channel. Once the framework is extended to 2π photoproduction off the nucleon, we will be able to verify this assumption quantitatively.

In the JüBo2025 study the GDH integrals for all channels with significant contributions, namely πN and ηN, are converged already at 2 GeV, which is still in the range where data are available. While the predicted integral for the strangeness channels, $K\Lambda$ and $K\Sigma$, seems not to be converged to full extent, their overall contribution is only marginal compared to πN. The convergence of the integral is in contrast to various studies of the contribution to the GDH integral from the energy range beyond 2.5 GeV employing Regge theory [197, 656–658]. The last of these references quotes a value as large as (-15 ± 2) µb. This suggests that the full sum of the contributions has to be even larger than the value of right-hand side $I^p_{\mathrm{GDH}} = 204.78\,\mu b$.

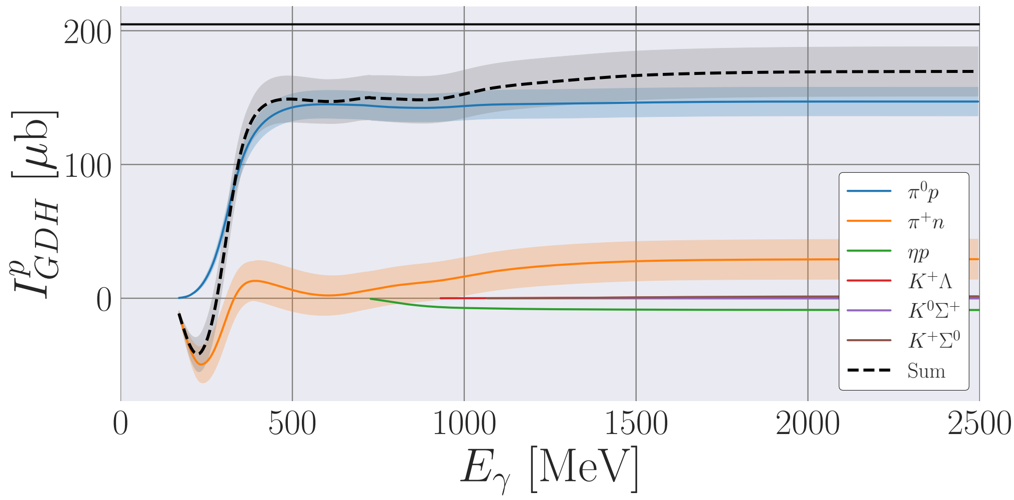

Figure 18: Running GDH integral I^p_{GDH} as in Eq. (6.1) for the different channels with their respective errorbands. The black horizontal line shows the value of $I^p_{\mathrm{GDH}} = 204.78\,\mu\mathrm{b}$ calculated from PDG values. The black dashed line with the grey errorband shows the sum of all channels.

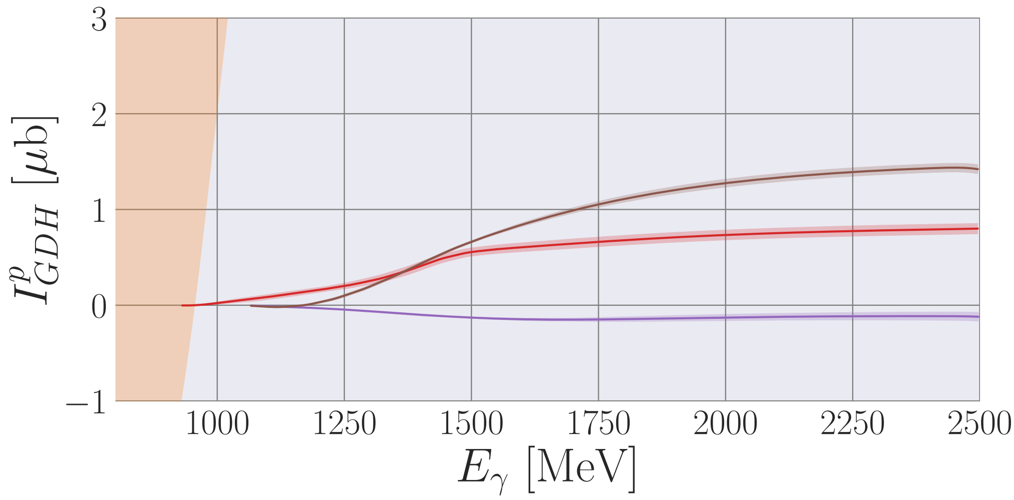

Figure 19: Zoom into the running GDH integral I^p_{GDH} as in Eq. (6.1) for the different channels for better visualization of the higher lying channels.

6.2. GDH sum rule contributions for photoproduction off proton and neutron targets

In Chapter 5 we presented the "JüBo2026" solution, in which we extended the Jülich-Bonn model to include photoproduction processes involving neutron targets and produced fit results for $\gamma n \to \pi N$. This allows us to calculate the GDH sum rule contributions for the final-states $\pi^0 n$ and $\pi^- p$ for neutron targets. The running GDH integral is analogously defined as the one for proton targets as:

$$I^n_{\mathrm{GDH}}(E_\gamma) = \int_{E^0_\gamma}^{E_\gamma} \mathrm{d}E'_\gamma \, \frac{\Delta\sigma^n(E'_\gamma)}{E'_\gamma} \; . \tag{6.3}$$

where the superscript n now denotes that processes with neutron targets $\gamma n \to X$ are considered. We present the GDH sum rule contributions and the sum of all channels for neutron and proton targets in Fig. 20. Note that the contributions for proton targets also changed compared to the ones presented in Sec. 6.1, since we performed a fit in the JüBo2026 analysis for the full data base and also varied the parameters for photoproduction off protons. In Fig. 20 the horizontal lines denote the right hand side of Eqs. (2.63) and (2.64) which are given by

$$I^p_{\mathrm{GDH}} = 204.78\,\mu\mathrm{b}\,, \tag{6.4}$$
$$I^n_{\mathrm{GDH}} = 232.25\,\mu\mathrm{b}\,. \tag{6.5}$$

In this study we find the GDH sum rule contributions for proton targets at the largest energy $E_\gamma = 2.5$ GeV to be given by:

$$\begin{aligned}
I^p_{\mathrm{GDH}}(\pi^0 p) &= 142 \;\mu\mathrm{b} \;, \\
I^p_{\mathrm{GDH}}(\pi^+ n) &= 32 \;\mu\mathrm{b} \;, \\
I^p_{\mathrm{GDH}}(\eta p) &= -8.8 \;\mu\mathrm{b} \;, \\
I^p_{\mathrm{GDH}}(K^+\Lambda^0) &= 0.85 \;\mu\mathrm{b} \;, \\
I^p_{\mathrm{GDH}}(K^0\Sigma^+) &= -0.11 \;\mu\mathrm{b} \;, \\
I^p_{\mathrm{GDH}}(K^+\Sigma^0) &= 1.37 \;\mu\mathrm{b} \;, \\
I^p_{\mathrm{GDH}}(\mathrm{all}) &= 168 \;\mu\mathrm{b} \;.
\end{aligned} \tag{6.6}$$

We notice that the $\pi^0 p$ channel contribution decreased by 5 µb compared to the JüBo2025 result, while the $\pi^+ n$ final-state has increased by 3 µb. There are also small changes in the KY channels, but these still give marginal contributions to the full sum and there is still no $\Delta\sigma$ or E data for these final-states. It is expected that the πN channels are influenced the most by the inclusion of the $\gamma n \to \pi N$ data in the JüBo2026 analysis, since the $I = 3/2$ photoproduction parameters for the πN final state are used both for photoproduction off proton and neutron targets (see Sec. 5.1). Consequently, these parameters must change for proton targets if they are adjusted to describe photoproduction data with neutron targets. However, the change of the full sum is still only 2 µb and thus our hypothesis, that the missing contribution most likely originates from the $\pi\pi N$ channels, remains. For

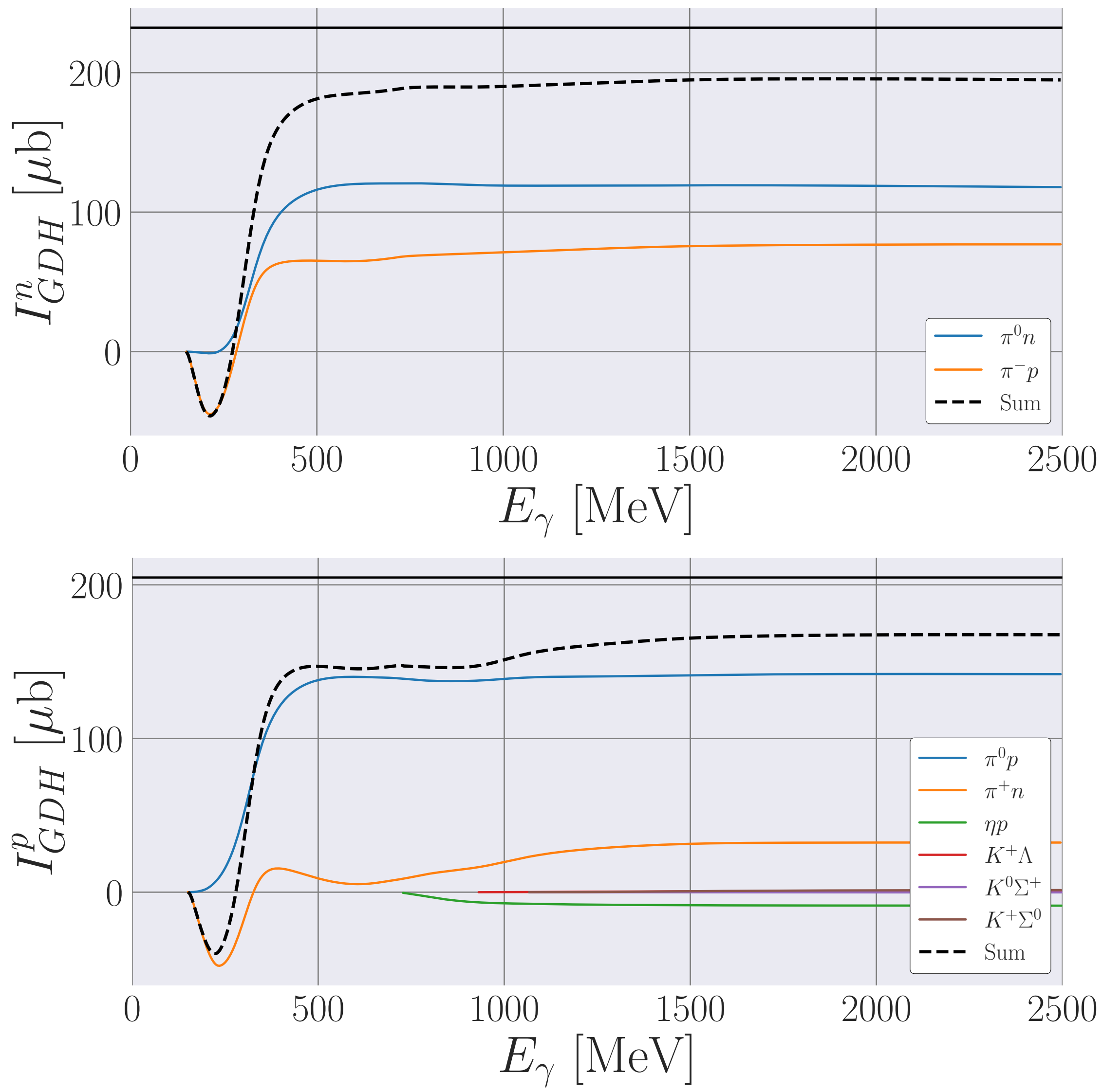

Figure 20: Running GDH integrals I^n_{GDH} and I^p_{GDH} for the different channels from the analysis with neutron targets. The black horizontal lines show the value of $I^n_{\text{GDH}} = 232.25\,\mu\text{b}$ and $I^p_{\text{GDH}} = 204.78\,\mu\text{b}$ calculated from PDG values. The black dashed lines show the sums of all respective channels.

photoproduction processes with neutron targets we find GDH sum rule contributions at the largest energy $E_\gamma = 2.5$ GeV to be given by

$$\begin{aligned} I^n_{\rm GDH}(\pi^0 n) &= 118\ \mu\text{b}\ , \\ I^n_{\rm GDH}(\pi^- p) &= 77\ \mu\text{b}\ , \\ I^n_{\rm GDH}(\pi N) &= 195\ \mu\text{b}\ . \end{aligned} \tag{6.7}$$

We list our values with the ones from other groups for comparison in Tab. 27. In an analysis from 2022 of Strakovsky et al. [650] phenomenological amplitudes obtained in partial wave analyses of the SAID and MAID groups have been used to determine the GDH sum rule contributions. We further show a graphical comparison of our solution with the one from Strakovsky et al. [650] in Fig. 21. The second work from the year 2002 of Zhao et al. [652] used a quark model approach with an effective Lagrangian to evaluate contributions to the GDH sum rule. The last study used for comparison was published by the GDH/A2 collaboration in 2001 [646], in which only a value for all channels was presented.

It is directly noticeable that our $\pi^0 n$ component is smaller than the ones from Refs. [650, 652], while our $\pi^- p$ contribution is much larger and gives a positive value in contrast to the negative ones from the other groups. In Fig. 21 one observes that the contribution for $\pi^- p$ is negative for all energies in the study of Strakovsky et al. [650], while in our result it is only negative up until $E_\gamma \approx 300$ MeV. In the JüBo2026 analysis we observe a large rise to values $> 60\,\mu$b until around ≈ 400 MeV after the minimum. In contrast to this the result from Strakovsky et al. [650] only rises slightly to about $\approx -20\,\mu$b in the same energy range. Another difference between the analyses is that for our work the curve does decrease further. But for the GDH contribution presented in Ref. [650] it decreases.

The main difference to the results found by Strakovsky et al. [650] for the $\pi^- p$ channel contribution lies in the energy range of $E_\gamma = 250 - 550$ MeV, which corresponds to center of mass energies of around $W = 1150 - 1400$ MeV. As stated in Sec. 5.3.2, starting from 1220 MeV up to energies around 1350 MeV our solution underestimates the cross section. This might explain the discrepancy between the solutions and could be the reason for the large rise of the JüBo2026 curve. However, it should be noted that there is only one data set from CLAS [637] on the observable E or $\Delta\sigma$ for the final-state $\pi^- p$, which is included in both our analysis and the one from Strakovsky et al. [650]. Especially for energies below 1500 MeV there is no data at all, which makes it difficult to get reliable predictions or to verify the behaviour of the GDH integral. As listed in Tab. 27, there is another study from Zhao et al. from 2002 [652] that suggest a negative saturated value.

For the final-state $\pi^0 n$ both the JüBo2026 result and the one from Strakovsky et al. [650] rise in the aforementioned energy region. However, the one in Ref. [650] increases further up to a value of $150\,\mu$b while our contribution already saturates at around $120\,\mu$b. In this study we included a data set for the observable $E \propto \Delta\sigma$ from 2022 [599] for the $\pi^0 n$ channel, which includes energies as low as 1165 MeV. The data points of the lowest energy bins have large uncertainties, especially towards the most forward angles. However, the JüBo2026 result describes most of these data points well. Our contribution to the GDH integral does not rise to a value as high as $150\,\mu$b found in Ref. [650]. A similar value was found by Zhao et al. [652]. Since the new data set of Ref. [599] was published after the study of Strakovsky et al. [650], it could not be used for their analysis and it would be interesting to see whether its inclusion would lead to a similar result as found in our current study.

For the values of $I^n_{\mathrm{GDH}}(\mathrm{all})$ it should be noted that in the JüBo2026 analysis and the study from Strakovsky et al. [650] only πN final-states were considered, while in the work of Zhao et al. [652] also contributions from $\pi\pi N$, ηn, KY, ωn and ρN were used. The work of the GDH/A2 collaboration [646] determined the GDH sum rule contribution directly from the measurement of $\Delta\sigma$ in the energy region $E_\gamma = 200 - 800$ MeV. All groups still miss a major contribution to the right hand side value of $I^n_{\mathrm{GDH}} = 232\,\mu\mathrm{b}$. The study of Zhao et al. [652] finds a contribution for the $\pi\pi N$ channels of $50\,\mu\mathrm{b}$ while all other channels apart from πN only give marginal contributions of about $-6\,\mu\mathrm{b}$. This is similar to the case of proton targets where the missing contribution likely originates from the $\pi\pi N$ channels. However, if the $\pi^- p$ contribution is indeed found to have a negative value as suggested by the other groups, our value for the sum of all channels $I^n_{\mathrm{GDH}}(\mathrm{all}) = 195\,\mu\mathrm{b}$ will also decrease significantly. This gives us a larger discrepancy to the value of $232\,\mu\mathrm{b}$, similar as for the other groups. Furthermore, a contribution of the $\pi\pi N$ channel of about $50\,\mu\mathrm{b}$ may not be enough to explain the missing part in such a case. More data for the photoproduction off neutrons is needed to fully understand the large discrepancy.

Reference	$I^n_{\mathrm{GDH}}(\pi^0 n)$	$I^n_{\mathrm{GDH}}(\pi^- p)$	$I^n_{\mathrm{GDH}}(\mathrm{all})$
JüBo2026	118	77	195
Strakovsky et al. [650]	150	-20	130
Zhao et al. [652]	154	-30	168
GDH/A2 [646]	-	-	187±8±10
PDG [5]	-	-	232

Table 27: List of GDH sum rule contributions for neutron targets from different References. Values are given in µb. We list our current results from the JüBo2026 solution. For comparison we also include a recent study of Strakovsky et al. [650]. We also compare to values from works of the early 2000s from Zhao et al. [652] and from the GDH/A2 collaboration published Ref. [646] and list the calcualted right hand side value as PDG [5].

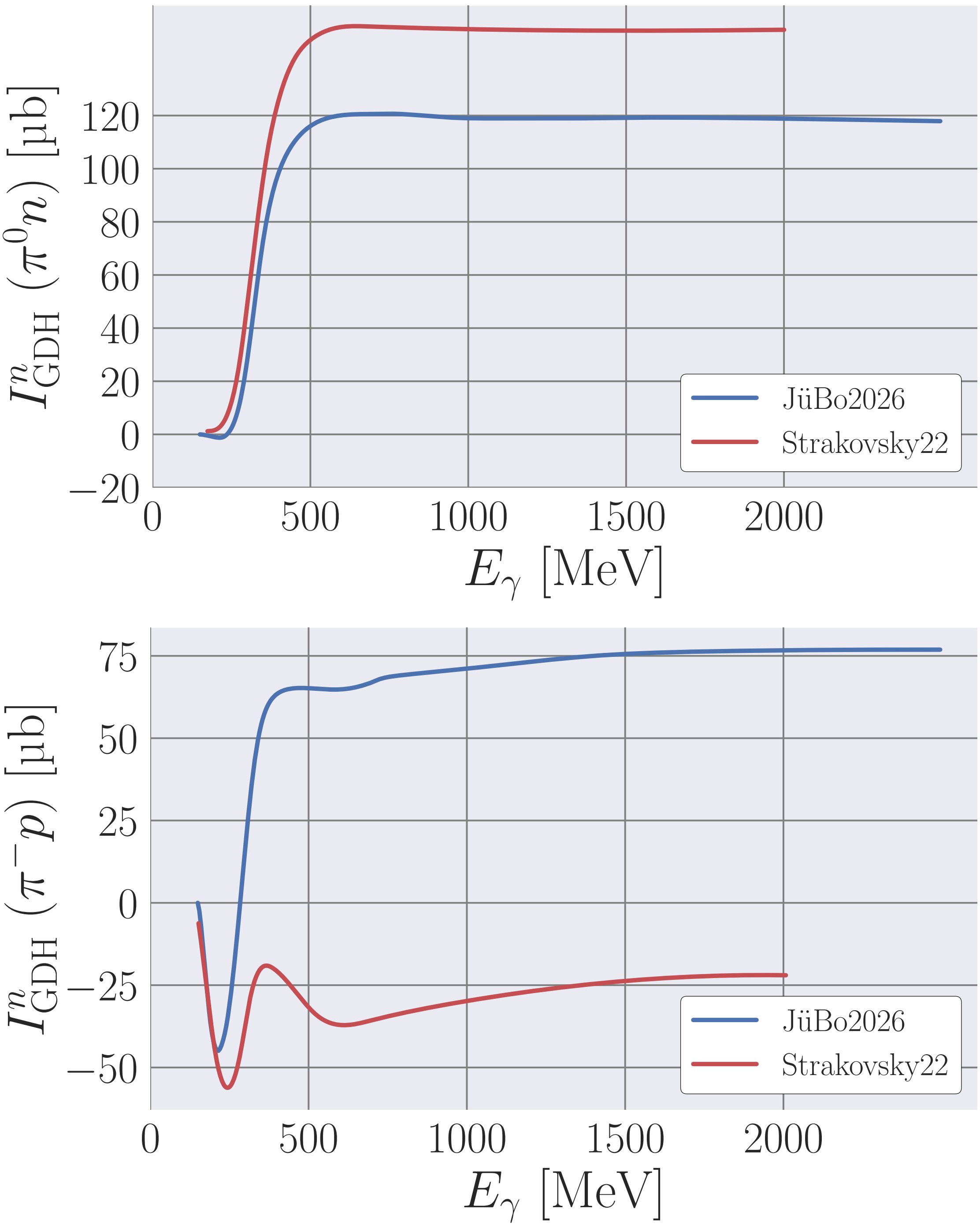

Figure 21: Running GDH integrals I^n_{GDH} for the channels $\pi^0 n$ (upper) and $\pi^- p$ (lower) from the present analysis with neutron targets (blue) and the study of Strakovsky et al. [650] (red) labeled as Strakovsky22 for comparison.

7. Conclusion and Outlook

In this thesis, the Jülich-Bonn dynamical coupled-channel framework was employed to perform a fit to newly available photoproduction data for the reactions $\gamma p \to \pi^0 p$, $\pi^+ n$ and ηp, in addition to the existing data base. Within this coupled-channel study we analyzed pion-induced reactions $\pi N \to \pi N$, ηN and KY as well as the photoproduction processes $\gamma p \to \pi^0 p$, $\pi^+ n$, ηp, $K^0\Lambda^+$, $K^+\Sigma^0$ and $K^0\Sigma^+$ simultaneously. The newly included ηp measurements of $d\sigma/d\Omega$ and Σ extend to center-of-mass energies above 2.1 GeV together with a large-angle region for the first time. The inclusion of this data improved the description of the backward-angle peak in the ηp cross section. In addition, new data on the double-polarization observable G for the $\pi^0 p$ and $\pi^+ n$ channels were incorporated. For the $\pi^+ n$ final state the available database for this observable was more than tripled. Furthermore, recent measurements of the observable E in the $\pi^0 p$ channel were included. This data set is particularly important for constraining the helicity-dependent cross-section difference $\Delta\sigma$, since E is directly related to this quantity. This is essential for obtaining reliable GDH sum rule contributions from the present fit, which are presented in Sec. 6.1.

A further important achievement of this thesis is the extension of the Jülich-Bonn framework to photoproduction processes on neutron targets. Up to now, the photoproduction sector of the model had been applied to proton-target reactions only, so that the inclusion of $\gamma n \to \pi^0 n$ and $\gamma n \to \pi^- p$ constitutes a significant step toward a more complete description of meson photoproduction. The neutron data provide different constraints, which helps to disentangle the isospin dependence of the photocouplings and resonance contributions. In particular, the simultaneous treatment of proton and neutron channels within the same coupled-channel framework strengthens the consistency of the analysis and enhances its relevance for the extraction of resonance properties. This extension is therefore essential for a more comprehensive understanding of baryon spectroscopy and for future studies of spin-dependent observables and sum rules.

The produced fit achieves a good overall description of the included data base with more than $15,000$ data points for the reactions $\gamma n \to \pi^0 n$ and $\gamma n \to \pi^- p$. Despite the overall good description of the data, there are some differences between our solution and the experimental data. The most pronounced discrepancies are observed in the differential cross section for the $\pi^- p$ final-state in the energy region $W = 1.2 - 1.35$ GeV. The inclusion of these neutron-target data allowed for the first extraction of neutron photocouplings within the Jülich-Bonn framework. The pole positions of most resonances remained stable compared to the previous JüBo2025 solution, but we observe some changes in the residues as well as the proton photocouplings. Some neutron photocouplings found in the analysis are particularly large (i.e. $N(1440)1/2^+$, $N(1900)3/2^+$ and $N(2220)9/2^+$), which reflect the that neutron observables are sensitive to the electromagnetic structure of nucleon resonances.

Another important result of this thesis is the determination of the individual channel contributions to the GDH sum rule within the Jülich-Bonn framework. Since the GDH sum rule links the anomalous magnetic moment of the nucleon to the helicity dependence of the photoabsorption cross section, it provides a direct link between experimental photoproduction data and fundamental properties of the nucleon spin structure. By evaluating the contributions of the individual channels within the JüBo framework, it becomes possible to identify the relative importance of the different final states and to assess how the sum rule is approached in a channel-resolved manner. This demonstrates that the model is not only suited for spectroscopy, but also for studies of spin-dependent sum rules and nucleon structure. We observe a large discrepancy for the $\pi^- p$ channel compared to the results of other groups. In a direct comparison of the running GDH-integrals, we find the main difference to be in the energy region $W = 1.2 - 1.35$ GeV, for which we already observed a discrepancy of our solution with the experimental data. However, it is noteworthy that there is no data on the observable E or $\Delta\sigma$, which is closely related to the GDH-sum rule, in this energy region for the $\pi^- p$ final-state. But this discrepancy indicates that additional constraints from future measurements or further refinements of the photoproduction amplitudes are required for future analyses.

The results of the present work show that the inclusion of the new photoproduction data leads to a refined description of several observables and provides better constraints on the corresponding amplitudes. In particular, polarization observables play a crucial role, since they are sensitive to interference effects and therefore carry important information on the underlying reaction dynamics. In this way, the present work contributes to a more complete understanding of the light baryon spectrum and allows for the evaluation of individual GDH sum-rule channel contributions.

Future extensions of this work may address several directions. Another natural extension of the present framework is the inclusion of additional final states, such as $\gamma n \to \eta n$ and KY, as well as $\eta' N$ or ωN channels in the full photoproduction model. Furthermore, a more systematic statistical treatment of uncertainties including correlations of data sets would also be highly desirable in future analyses. Especially the statistics of elastic πN channel has to be improved [309]. The inclusion of further statistical techniques such as the LASSO method [306–308] could also help to systematically reduce the number of parameters to find a "minimal model". Such developments would further strengthen the predictive power of the model and improve the reliability of the extracted resonance parameters. Moreover, a project using a Hamiltonian Monte Carlo (HMC) algorithm in the No-U-Turn Sampler variant acting on the untempered posterior distribution is planned for the future [659, 660]. This will be applied to the analysis presented in Chapter 5. Such a study is important, since it allows for a more rigorous uncertainty estimation than the one currently used within the JüBo framework.

Appendix

A. Definitions and Conventions

In this part we list the different definitions, conventions and notations relevant for this work.

We use the metric tensor $g^{\mu\nu}$ with the convention

$$g^{\mu\nu} = \begin{pmatrix} 1 & 0 & 0 & 0 \\ 0 & -1 & 0 & 0 \\ 0 & 0 & -1 & 0 \\ 0 & 0 & 0 & -1 \end{pmatrix} . \tag{A.1}$$

The totally antisymmetric Levi-Civita tensor is given by

$$\epsilon_{\mu\nu\kappa\lambda} = \begin{cases} -1 & \text{for even permutations} \\ 1 & \text{for odd permutations} \\ 0 & \end{cases} . \tag{A.2}$$

For the γ-matrices we use the Dirac-representation

$$\gamma^0 = \begin{pmatrix} \mathbb{1}_2 & 0 \\ 0 & -\mathbb{1}_2 \end{pmatrix} , \quad \vec{\gamma} = \begin{pmatrix} 0 & \vec{\sigma} \\ -\vec{\sigma} & 0 \end{pmatrix} ,$$
$$\gamma^5 = i\gamma^0\gamma^1\gamma^2\gamma^3 = \begin{pmatrix} \mathbb{1}_2 & 0 \\ 0 & -\mathbb{1}_2 \end{pmatrix} , \tag{A.3}$$

where $\mathbb{1}_2$ is the 2-dimensional identity matrix and σ_i are the Pauli matrices given by

$$\sigma_1 = \begin{pmatrix} 0 & 1 \\ 1 & 0 \end{pmatrix} , \sigma_2 = \begin{pmatrix} 0 & -i \\ i & 0 \end{pmatrix} , \sigma_3 = \begin{pmatrix} 1 & 0 \\ 0 & -1 \end{pmatrix} . \tag{A.4}$$

In our framework we consider the spin-1/2 spinors in the helicity basis:

$$u(\vec{p}, \lambda) = \sqrt{\frac{m + E_p}{2E_p}} \begin{pmatrix} 1 \\ \frac{2\lambda p}{m+E_p} \end{pmatrix} \chi_\lambda , \tag{A.5}$$

$$v(\vec{p}, \lambda) = \sqrt{\frac{m + E_p}{2E_p}} \begin{pmatrix} \frac{-p}{m+E_p} \\ 2\lambda \end{pmatrix} \chi_{-\lambda} . \tag{A.6}$$

Here m and $\vec{p}$ denote the mass and momentum of the particle and the energy is given by $E_p = \sqrt{\vec{p}^2 + m^2}$. The spinors χ_λ are eigenstate of the helicity operator

$$\frac{\vec{\sigma} \cdot \vec{p}}{2p} \chi_\lambda = \lambda \chi_\lambda , \tag{A.7}$$

where $\lambda \in \{-1/2, +1/2\}$. For these spinors we have the explicit forms given by

$$\chi_{+1/2} = \begin{pmatrix} \cos\left(\frac{\theta}{2}\right)\exp\left(-i\frac{\phi}{2}\right) \\ \sin\left(\frac{\theta}{2}\right)\exp\left(i\frac{\phi}{2}\right) \end{pmatrix} , \tag{A.8}$$

$$\chi_{-1/2} = \begin{pmatrix} -\sin\left(\frac{\theta}{2}\right)\exp\left(-i\frac{\phi}{2}\right) \\ \cos\left(\frac{\theta}{2}\right)\exp\left(i\frac{\phi}{2}\right) \end{pmatrix} . \tag{A.9}$$

For the spin-1 polarization vectors we use the phase convention from Ref. [202]. The polarization 4-vector with spin 1 in the helicity basis with momentum $\vec{p}$ is defined by

$$\epsilon^\mu(\vec{p}, \lambda = \pm 1) = \frac{1}{\sqrt{2}} \begin{pmatrix} 0 \\ \mp\cos\theta\cos\phi + i\sin\phi \\ \mp\cos\theta\sin\phi - i\cos\phi \\ \pm\sin\theta \end{pmatrix} , \tag{A.10}$$

$$\epsilon^\mu(\vec{p}, \lambda = 0) = \frac{1}{m} \begin{pmatrix} p \\ E_p\sin\theta\cos\phi \\ E_p\sin\theta\sin\phi \\ E_p\cos\theta \end{pmatrix} . \tag{A.11}$$

The Rarita-Schwinger spinor for a spin-3/2 is defined via a spin-1/2 spinor and a spin-1 polarization vector by [33]

$$u^\mu(\vec{p}, \lambda) = \sum_{\lambda_1,\lambda_2} \langle 1\lambda_1, 1/2\lambda_2 | 3/2\lambda\rangle\, \epsilon^\mu(\vec{p}, \lambda_1) u(\vec{p}, \lambda_2) . \tag{A.12}$$

We use the Rarita-Schwinger propagator for the Δ-exchange, where the numerator has the form

$$P^{\mu\nu}(p) = (\not{p} + m)\left[-g^{\mu\nu} + \frac{\gamma^\mu\gamma^\nu}{3} + \frac{2p^\mu p^\nu}{3m^2} - \frac{p^\mu\gamma^\nu - p^\nu\gamma^\mu}{3m}\right] . \tag{A.13}$$

The definitions of the field operators for the nucleon and Δ (all other spin-1/2 and spin-3/2 are analogously defined) are given by

$$\Psi_N(x) = (2\pi)^{-3/2}\int \mathrm{d}^3q \sum_\lambda \left(b_N(\vec{q}, \lambda)u(\vec{q}, \lambda)e^{-iq^\mu x_\mu} + d_N^\dagger(\vec{q}, \lambda)v(\vec{q}, \lambda)e^{ik^\mu x_\mu}\right) , \tag{A.14}$$

$$\Delta^\mu(x) = (2\pi)^{-3/2}\int \mathrm{d}^3q \sum_\lambda \left(b_\Delta(\vec{q}, \lambda)u^\mu(\vec{q}, \lambda)e^{-iq^\nu x_\nu} + d_\Delta^\dagger(\vec{q}, \lambda)v^\mu(\vec{q}, \lambda)e^{ik^\nu x_\nu}\right) . \tag{A.15}$$

For the pseudoscalar, scalar, vector and axial vector mesons we have

$$\Psi_p(x) = (2\pi)^{-3/2} \int \mathrm{d}^3q \, \frac{1}{\sqrt{2\omega_q}} \left(a_p(\vec{q}) e^{-iq^\mu x_\mu} + a_p^\dagger(\vec{q}) e^{ik^\mu x_\mu} \right) \ , \tag{A.16}$$

$$\Psi_s(x) = (2\pi)^{-3/2} \int \mathrm{d}^3q \, \frac{1}{\sqrt{2\omega_q}} \left(a_s(\vec{q}) e^{-iq^\mu x_\mu} + a_s^\dagger(\vec{q}) e^{ik^\mu x_\mu} \right) \ , \tag{A.17}$$

$$\Psi_v^\mu(x) = (2\pi)^{-3/2} \int \mathrm{d}^3q \sum_\lambda \frac{1}{\sqrt{2\omega_q}} \left(\epsilon^\mu(\vec{q},\lambda) a_v(\vec{q},\lambda) e^{-iq^\nu x_\nu} \right) + \text{h.c.} \ , \tag{A.18}$$

$$\Psi_a^\mu(x) = (2\pi)^{-3/2} \int \mathrm{d}^3q \sum_\lambda \frac{1}{\sqrt{2\omega_q}} \left(\epsilon^\mu(\vec{q},\lambda) a_a(\vec{q},\lambda) e^{-iq^\nu x_\nu} \right) + \text{h.c.} \ , \tag{A.19}$$

where the on-shell energy of the meson is given by $\omega_q = \sqrt{\vec{q}^2 + m^2}$. The annihilation operators obey the following (anti-)commutation relations

$$\left[a(\vec{q},\lambda), a^\dagger(\vec{q}\,',\lambda') \right]_- = \delta^{(3)}(\vec{q} - \vec{q}) \delta_{\lambda,\lambda'} \ , \tag{A.20}$$

$$\left[b(\vec{q},\lambda), b^\dagger(\vec{q}\,',\lambda') \right]_+ = \delta^{(3)}(\vec{q} - \vec{q}) \delta_{\lambda,\lambda'} \ , \tag{A.21}$$

$$\left[d(\vec{q},\lambda), d^\dagger(\vec{q}\,',\lambda') \right]_+ = \delta^{(3)}(\vec{q} - \vec{q}) \delta_{\lambda,\lambda'} \ . \tag{A.22}$$

For calculations in isospin space we use the following notation for the nucleon, pion and Δ wave functions

$$N = \begin{pmatrix} p \\ n \end{pmatrix}, \quad \vec{\pi} = \begin{pmatrix} -\pi^+ \\ \pi^0 \\ \pi^- \end{pmatrix}, \quad \Delta = \begin{pmatrix} \Delta^{++} \\ \Delta^+ \\ \Delta^0 \\ \Delta^- \end{pmatrix} \ . \tag{A.23}$$

The other particles with isospin $I = 1/2$, 1 or $3/2$ are defined analogously. The isospin matrices for the nucleon are defined by

$$\tau_{-1} = \sqrt{2} \begin{pmatrix} 0 & 0 \\ -1 & 0 \end{pmatrix} \ , \quad \tau_0 = \begin{pmatrix} 1 & 0 \\ 0 & -1 \end{pmatrix} \ , \quad \tau_{+1} = \sqrt{2} \begin{pmatrix} 0 & 1 \\ 0 & 0 \end{pmatrix} \ , \tag{A.24}$$

For the pion we have

$$t_{-1} = \begin{pmatrix} 0 & 0 & 0 \\ -1 & 0 & 0 \\ 0 & -1 & 0 \end{pmatrix} \ , \quad t_0 = \begin{pmatrix} 1 & 0 & 0 \\ 0 & 0 & 0 \\ 0 & 0 & -1 \end{pmatrix} \ , \quad t_{+1} = \begin{pmatrix} 0 & 1 & 0 \\ 0 & 0 & 1 \\ 0 & 0 & 0 \end{pmatrix} \ , \tag{A.25}$$

and the transition from $I = 3/2$ to $I = 1/2$ is defined by

$$S_{-1} = \begin{pmatrix} 1 & 0 & 0 & 0 \\ 0 & \frac{1}{\sqrt{3}} & 0 & 0 \end{pmatrix} \ , \ S_0 = \begin{pmatrix} 0 & \sqrt{\frac{2}{3}} & 0 & 0 \\ 0 & 0 & \sqrt{\frac{2}{3}} & 0 \end{pmatrix} \ , \ S_{+1} = \begin{pmatrix} 0 & 0 & \frac{1}{\sqrt{3}} & 0 \\ 0 & 0 & 0 & 1 \end{pmatrix} \ . \tag{A.26}$$

Lastly, the isospin matrices for the Δ are given by

$$T_{-1} = \begin{pmatrix} 0 & 0 & 0 & 0 \\ -\sqrt{\frac{2}{3}} & 0 & 0 & 0 \\ 0 & -\frac{2\sqrt{2}}{3} & 0 & 0 \\ 0 & 0 & -\sqrt{\frac{2}{3}} & 0 \end{pmatrix} , \tag{A.27}$$

$$T_0 = \begin{pmatrix} 1 & 0 & 0 & 0 \\ 0 & \frac{1}{3} & 0 & 0 \\ 0 & 0 & -\frac{1}{3} & 0 \\ 0 & 0 & 0 & -1 \end{pmatrix} , \tag{A.28}$$

$$T_{+1} = \begin{pmatrix} 0 & \sqrt{\frac{2}{3}} & 0 & 0 \\ 0 & 0 & \frac{2\sqrt{2}}{3} & 0 \\ 0 & 0 & 0 & \sqrt{\frac{2}{3}} \\ 0 & 0 & 0 & 0 \end{pmatrix} . \tag{A.29}$$

B. Further details on the JüBo framework

In this section we give further details on parts of the JüBo model presented in Chapter 3.

B.1. Coupling scheme of the different channels

In the coupled channel framework of the JüBo model we include the stable channels πN, ηN, $K\Lambda$ and $K\Sigma$ as well as the inelastic channels ρN, $\pi\Delta$ and σN for the effective 3-body channel $\pi\pi N$. In Tab. 28 we show the coupling scheme for these channels in the Jülich-Bonn model. Note that for the $\pi\Delta$ and ρN channels there are different possibilities to couple to J^P, which we list as separate channels. Here, the total spin $S_{\rho N} = |\vec{S}_N + \vec{S}_\rho|$ is defined by the ρ spin and the nucleon spin and the respective orbital angular momentum is given by $L_{\rho N}$. The notation $L_{2I;2J}$ is defined with respect to the πN channel, e.g. S_{11}.

Table 28: Angular momentum structure of the different channels in the JüBo framework for isospin $I = 1/2$ up to a total spin $J = 9/2$. The isospin $I = 3/2$ sector is analogous up to some isospin selection rules.

$J^P =$	$\frac{1}{2}^-$	$\frac{1}{2}^+$	$\frac{3}{2}^+$	$\frac{3}{2}^-$	$\frac{5}{2}^-$	$\frac{5}{2}^+$	$\frac{7}{2}^+$	$\frac{7}{2}^-$	$\frac{9}{2}^-$	$\frac{9}{2}^+$
πN	S_{11}	P_{11}	P_{13}	D_{13}	D_{15}	F_{15}	F_{17}	G_{17}	G_{19}	H_{19}
$\rho N(S_{\rho N} = 1/2)$	S_{11}	P_{11}	P_{13}	D_{13}	D_{15}	F_{15}	F_{17}	G_{17}	G_{19}	H_{19}
$\rho N(S_{\rho N} = 3/2, \|J_{\rho N} - L_{\rho N}\| = 1/2)$	—	P_{11}	P_{13}	D_{13}	D_{15}	F_{15}	F_{17}	G_{17}	G_{19}	H_{19}
$\rho N(S_{\rho N} = 3/2, \|J_{\rho N} - L_{\rho N}\| = 3/2)$	D_{11}	—	F_{13}	S_{13}	G_{15}	P_{15}	H_{17}	D_{17}	I_{19}	F_{19}
ηN	S_{11}	P_{11}	P_{13}	D_{13}	D_{15}	F_{15}	F_{17}	G_{17}	G_{19}	H_{19}
$\pi\Delta(\|J_{\pi\Delta} - L_{\pi\Delta}\| = 1/2)$	—	P_{11}	P_{13}	D_{13}	D_{15}	F_{15}	F_{17}	G_{17}	G_{19}	H_{19}
$\pi\Delta(\|J_{\pi\Delta} - L_{\pi\Delta}\| = 3/2)$	D_{11}	—	F_{13}	S_{13}	G_{15}	P_{15}	H_{17}	D_{17}	I_{19}	F_{19}
σN	P_{11}	S_{11}	D_{13}	P_{13}	F_{15}	D_{15}	G_{17}	F_{17}	H_{19}	G_{19}
$K\Lambda$	S_{11}	P_{11}	P_{13}	D_{13}	D_{15}	F_{15}	F_{17}	G_{17}	G_{19}	H_{19}
$K\Sigma$	S_{11}	P_{11}	P_{13}	D_{13}	D_{15}	F_{15}	F_{17}	G_{17}	G_{19}	H_{19}

B.2. Resonance vertex functions

Within our framework the partial wave projected bare resonance vertices $\gamma^{a,c}$ in Eq. (3.25) are defined as

$$\gamma^{a,c} = v\, I_R\, F(k)\sqrt{\frac{m_B + E}{\omega E}}\ . \tag{B.1}$$

Here, $k = \left|\vec{k}\right|$ is the center of mass meson-baryon momentum, I_R is the isospin factor, which is listed in Tab. 29 and E (ω) are the baryon (meson) on-shell center of mass energies:

$$E = \sqrt{\vec{p}_B^{\,2} + m_B^2}, \quad \omega = \sqrt{\vec{p}_m^{\,2} + m_m^2}\ . \tag{B.2}$$

	πN	ηN	ρN	$\pi\Delta$	$K\Lambda$	$K\Sigma$
$I=1/2$	$\sqrt{3}$	1	$\sqrt{3}$	$-\sqrt{2}$	1	$-\sqrt{3}$
$I=3/2$	1	0	1	$\sqrt{5/3}$	0	-1

Table 29: Isospin factors I_R for the bare resonance vertex functions $\gamma^{a,c}$.

The form factors $F(k)$ for the resonance vertices have the form

$$F(k) = \left(\frac{\Lambda^4 + m_R^4}{\Lambda^4 + (E(k) + \omega(k))^4}\right)^n \tag{B.3}$$

where m_R is the nominal mass of the respective resonance. For $J \leq 3/2$ we choose $n = 1$ for all channels except for $\pi\Delta$, which has $n = 2$. For $J > 3/2$ we have $n = 2$ except for $\pi\Delta$, for which we take $n = 3$. The cut-off parameters Λ is set to 2 GeV for all resonances.

For resonances with $J > 3/2$ we do not derive the bare resonance vertices from Lagrangians. We construct them in such a way that they have the correct orbital angular momentum dependence (centrifugal barrier):

$$\begin{aligned}
(\gamma^{a,c})_{\frac{5}{2}^-} &= \frac{k}{m_b}\,(\gamma^{a,c})_{\frac{3}{2}^+} \;, & (\gamma^{a,c})_{\frac{5}{2}^+} &= \frac{k}{m_b}\,(\gamma^{a,c})_{\frac{3}{2}^-} \;, \\
(\gamma^{a,c})_{\frac{7}{2}^+} &= \frac{k^2}{m_b^2}\,(\gamma^{a,c})_{\frac{3}{2}^+} \;, & (\gamma^{a,c})_{\frac{7}{2}^-} &= \frac{k^2}{m_b^2}\,(\gamma^{a,c})_{\frac{3}{2}^-} \;, \\
(\gamma^{a,c})_{\frac{9}{2}^-} &= \frac{k^3}{m_b^3}\,(\gamma^{a,c})_{\frac{3}{2}^+} \;, & (\gamma^{a,c})_{\frac{9}{2}^+} &= \frac{k^3}{m_b^3}\,(\gamma^{a,c})_{\frac{3}{2}^-} \;.
\end{aligned} \tag{B.4}$$

The partial wave projected vertex functions v and the explicit expressions for $J \leq 3/2$ are given by:

- S_{11}, S_{31}, $J^P = \frac{1}{2}^-$ partial wave
  - πN-channel
$$v = -i\frac{f}{m_\pi}\frac{1}{\sqrt{8}\pi}(\omega_\pi + E_N - m_N) \tag{B.5}$$
  - ηN-channel
$$v = -i\frac{f}{m_\pi}\frac{1}{\sqrt{8}\pi}(\omega_\eta + E_N - m_N) \tag{B.6}$$
  - ρN-channel ($L_{\rho N} = 0$, $S_{\rho N} = 1/2$)
$$v = -f\frac{1}{\sqrt{24}\pi}\frac{1}{m_\rho}(\omega_\rho + E_N - m_N + 2m_\rho) \tag{B.7}$$
  - ρN-channel ($L_{\rho N} = 2$, $S_{\rho N} = 3/2$)
$$v = -f\frac{1}{\sqrt{12}\pi}\frac{1}{m_\rho}(\omega_\rho + E_N - m_N - m_\rho) \tag{B.8}$$

– $\pi\Delta$-channel

$$v = -i\frac{f}{m_\pi}\frac{1}{\sqrt{12}\pi}\frac{E_\Delta + \omega_\pi}{m_\Delta}(E_\Delta - m_\Delta) \tag{B.9}$$

– $K\Lambda$-channel

$$v = -if\frac{1}{\sqrt{8}\pi}\left(\omega_K + \frac{\vec{k}^2}{E_\Lambda + m_\Lambda}\right) \tag{B.10}$$

– $K\Sigma$-channel

$$v = -if\frac{1}{\sqrt{8}\pi}\left(\omega_K + \frac{\vec{k}^2}{E_\Sigma + m_\Sigma}\right) \tag{B.11}$$

- P_{11}, P_{31}, $J^P = \frac{1}{2}^+$ partial wave
  – πN-channel

$$v = -i\frac{f}{m_\pi}\frac{k}{\sqrt{8}\pi}\left(1 + \frac{\omega_\pi}{E_N + m_N}\right) \tag{B.12}$$

  – ηN-channel

$$v = i\frac{f}{m_\pi}\frac{k}{\sqrt{8}\pi}\left(1 + \frac{\omega_\eta}{E_N + m_N}\right) \tag{B.13}$$

  – ρN-channel ($L_{\rho N} = 1$, $S_{\rho N} = 1/2$)

$$v = f\frac{1}{\sqrt{24}\pi}\frac{k}{m_\rho}\left(1 + \frac{\omega_\rho}{E_N + m_N} - \frac{2m_\rho}{E_N + m_N}\right) \tag{B.14}$$

  – ρN-channel ($L_{\rho N} = 1$, $S_{\rho N} = 3/2$)

$$v = f\frac{1}{\sqrt{12}\pi}\frac{k}{m_\rho}\left(1 + \frac{\omega_\rho}{E_N + m_N} + \frac{m_\rho}{E_N + m_N}\right) \tag{B.15}$$

  – $\pi\Delta$-channel

$$v = i\frac{f}{m_\pi}\frac{1}{\sqrt{12}\pi}\frac{k}{m_\Delta}(E_\Delta + \omega_\pi) \tag{B.16}$$

  – $K\Lambda$-channel

$$v = if\frac{k}{\sqrt{8}\pi}\left(1 + \frac{\omega_K}{E_\Lambda + m_\Lambda}\right) \tag{B.17}$$

  – $K\Sigma$-channel

$$v = if\frac{k}{\sqrt{8}\pi}\left(1 + \frac{\omega_K}{E_\Sigma + m_\Sigma}\right) \tag{B.18}$$

- P_{13}, P_{33}, $J^P = \frac{3}{2}^+$ partial wave
  – πN-channel

$$v = i\frac{f}{m_\pi}\frac{k}{\sqrt{24}\pi} \tag{B.19}$$

– ηN-channel

$$v = i\frac{f}{m_\pi}\frac{k}{\sqrt{24\pi}} \tag{B.20}$$

– ρN-channel ($L_{\rho N} = 1,\ S_{\rho N} = 1/2$)

$$v = \frac{f}{m_\rho}\frac{1}{\sqrt{72\pi}}\frac{k}{E_N + m_N}\left(E_N + m_N - \omega_\rho - m_\rho\right) \tag{B.21}$$

– ρN-channel ($L_{\rho N} = 1,\ S_{\rho N} = 3/2$)

$$v = \frac{f}{m_\rho}\frac{1}{\sqrt{360\pi}}\frac{k}{E_N + m_N}\left(5E_N + 5m_N + 4\omega_\rho + m_\rho\right) \tag{B.22}$$

– ρN-channel ($L_{\rho N} = 3,\ S_{\rho N} = 3/2$)

$$v = \frac{f}{m_\rho}\frac{1}{\sqrt{40\pi}}\frac{k}{E_N + m_N}\left(\omega_\rho - m_\rho\right) \tag{B.23}$$

– $\pi\Delta$-channel ($L_{\pi\Delta} = 1$)

$$v = i\frac{f}{m_\pi}\frac{1}{\sqrt{360\pi}}\frac{k}{m_\Delta}(E_\Delta + 4m_\Delta)\left(1 + \frac{\omega_\pi}{E_\Delta + m_\Delta}\right) \tag{B.24}$$

– $\pi\Delta$-channel ($L_{\pi\Delta} = 3$)

$$v = -i\frac{f}{m_\pi}\frac{1}{\sqrt{40\pi}}\frac{k}{m_\Delta}(E_\Delta - m_\Delta)\left(1 + \frac{\omega_\pi}{E_\Delta + m_\Delta}\right) \tag{B.25}$$

– $K\Lambda$-channel

$$v = if\frac{k}{\sqrt{24\pi}} \tag{B.26}$$

– $K\Sigma$-channel

$$v = if\frac{k}{\sqrt{24\pi}} \tag{B.27}$$

- D_{13}, D_{33}, $J^P = \frac{3}{2}^-$ partial wave
  – πN-channel

$$v = i\frac{f}{m_\pi^2}\frac{k^2}{\sqrt{24\pi}}\left(1 + \frac{\omega_\pi}{E_N + m_N}\right) \tag{B.28}$$

  – ηN-channel

$$v = i\frac{f}{m_\pi^2}\frac{1}{\sqrt{24\pi}}\left(1 + \frac{\omega_\eta}{E_N + m_N}\right) \tag{B.29}$$

– ρN-channel ($L_{\rho N}=0,\ S_{\rho N}=3/2$)

$$v=-i\frac{f}{m_\rho}\frac{1}{\sqrt{72}\pi}\left(E_N+m_\rho+2\omega_\rho-m_N\right) \tag{B.30}$$

– ρN-channel ($L_{\rho N}=2,\ S_{\rho N}=1/2$)

$$v=-i\frac{f}{m_\rho}\frac{1}{\sqrt{72}\pi}\left(\omega_\rho-m_\rho-E_N+m_N\right) \tag{B.31}$$

– ρN-channel ($L_{\rho N}=2,\ S_{\rho N}=3/2$)

$$v=-i\frac{f}{m_\rho}\frac{1}{\sqrt{72}\pi}\left(2E_N+\omega_\rho-m_\rho-2m_N\right) \tag{B.32}$$

– $\pi\Delta$-channel ($L_{\pi\Delta}=0$)

$$v=\frac{f}{m_\pi}\frac{1}{\sqrt{72}\pi}\frac{1}{m_\Delta}(E_\Delta+2m_\Delta)\left(\omega_\pi+\frac{\vec{k}^2}{E_\Delta+m_\Delta}\right) \tag{B.33}$$

– $\pi\Delta$-channel ($L_{\pi\Delta}=2$)

$$v=-\frac{f}{m_\pi}\frac{1}{\sqrt{72}\pi}\frac{1}{m_\Delta}(E_\Delta-m_\Delta)\left(\omega_\pi+\frac{\vec{k}^2}{E_\Delta+m_\Delta}\right) \tag{B.34}$$

– $K\Lambda$-channel

$$v=f\frac{k^2}{\sqrt{24}\pi}\left(1+\frac{\omega_K}{E_\Lambda+m_\Lambda}\right) \tag{B.35}$$

– $K\Sigma$-channel

$$v=f\frac{k^2}{\sqrt{24}\pi}\left(1+\frac{\omega_K}{E_\Sigma+m_\Sigma}\right)\ . \tag{B.36}$$

Here, the bare couplings f are free parameters of the model and are fitted to data. We further list effective Lagrangians for s-channel diagrams in Tab. 30.

B.3. Details on the exchange potentials

In this part we are going to list the explicit expressions for the exchange potentials. The interaction terms from the Lagrangian are listed in Tab. 31. The vertices that are not listed in Tab. 31 can be related to the ones in the table via SU(3) flavor symmetry. Explicit expressions for the couplings g_a are listed later in this section.

For the explicit expressions of the exchange potentials given in Eqs. (B.46)-(B.73), we need to define the notation. We label the incoming (outgoing) baryon with the index 1 (3)

Vertex	$\mathcal{L}_{\text{eff}}$	Vertex	$\mathcal{L}_{\text{eff}}$
$\pi N N^*(S_{11})$	$\frac{f_{\pi N N^*}}{m_\pi}\bar{\Psi}_{N^*}\gamma^\mu\vec{\tau}\partial_\mu\vec{\pi}\Psi$ + h.c.	$K\Sigma N^*(D_{13})$	$\frac{f_{K\Sigma N^*}}{m_\pi^2}\bar{\Psi}^\mu_{N^*}\vec{\tau}\gamma^5\gamma^\nu\partial_\mu\partial_\nu\phi_K\Psi_\Sigma$ + h.c.
$\eta N N^*(S_{11})$	$\frac{f_{\eta N N^*}}{m_\pi}\bar{\Psi}_{N^*}\gamma^\mu\partial_\mu\eta\Psi$ + h.c.	$\pi N\Delta^*(S_{31})$	$\frac{f_{\pi N\Delta^*}}{m_\pi}\bar{\Delta}^*\gamma^\mu\vec{S}^\dagger\Psi\partial_\mu\vec{\pi}$ + h.c.
$\rho N N^*(S_{11})$	$f_{\rho N N^*}\bar{\Psi}_{N^*}\gamma^5\gamma^\mu\vec{\tau}\vec{\rho}_\mu\Psi$ + h.c.	$\rho N\Delta^*(S_{31})$	$f_{\rho N\Delta^*}\bar{\Delta}^*\vec{S}^\dagger\gamma^5(\gamma^\mu - \frac{\kappa}{2m_0}\sigma^{\mu\nu}\partial_\nu)\vec{\rho}_\mu\Psi$ + h.c.
$\pi\Delta N^*(S_{11})$	$-\frac{f_{\pi\Delta N^*}}{m_\pi}\bar{\Psi}_{N^*}\gamma^5\vec{S}\Delta^\mu\partial_\mu\vec{\pi}$ + h.c.	$\pi\Delta\Delta^*(S_{31})$	$-\frac{f_{\pi\Delta\Delta^*}}{m_\pi}\bar{\Delta}^*\gamma^5\vec{T}\Delta^\mu\partial_\mu\vec{\pi}$ + h.c.
$K\Lambda N^*(S_{11})$	$\frac{f_{K\Lambda N^*}}{m_\pi}\bar{\Psi}_{N^*}\gamma^\mu\partial_\mu\phi_K\Psi_\Lambda$ + h.c.	$K\Sigma\Delta^*(S_{31})$	$\frac{f_{K\Sigma\Delta^*}}{m_\pi}\bar{\Delta}^*\gamma^\mu\vec{S}^\dagger\partial_\mu\phi_K\Psi_\Sigma$ + h.c.
$K\Sigma N^*(S_{11})$	$\frac{f_{K\Sigma N^*}}{m_\pi}\bar{\Psi}_{N^*}\gamma^\mu\vec{\tau}\partial_\mu\phi_K\Psi_\Sigma$ + h.c.	$\pi N\Delta^*(P_{31})$	$-\frac{f_{\pi N\Delta^*}}{m_\pi}\bar{\Delta}^*\gamma^5\gamma^\mu\vec{S}^\dagger\Psi\partial_\mu\vec{\pi}$ + h.c.
$\pi N N^*(P_{13})$	$\frac{f_{\pi N N^*}}{m_\pi}\bar{\Psi}^\mu_{N^*}\vec{\tau}\Psi\partial_\mu\vec{\pi}$ + h.c.	$\rho N\Delta^*(P_{31})$	$-f_{\rho N\Delta^*}\bar{\Delta}^*\vec{S}^\dagger(\gamma^\mu - \frac{\kappa}{2m_0}\sigma^{\mu\nu}\partial_\nu)\vec{\rho}_\mu\Psi$ + h.c.
$\eta N N^*(P_{13})$	$\frac{f_{\eta N N^*}}{m_\pi}\bar{\Psi}^\mu_{N^*}\Psi\partial_\mu\eta$ + h.c.	$\pi\Delta\Delta^*(P_{31})$	$-\frac{f_{\pi\Delta\Delta^*}}{m_\pi}\bar{\Delta}^*\vec{T}\Delta^\mu\partial_\mu\vec{\pi}$ + h.c.
$\pi\Delta N^*(P_{13})$	$\frac{f_{\pi\Delta N^*}}{m_\pi}\bar{\Psi}^\mu_{N^*}\gamma^5\gamma^\nu\vec{S}\Delta_\mu\partial_\nu\vec{\pi}$ + h.c.	$K\Sigma\Delta^*(P_{31})$	$\frac{f_{K\Sigma\Delta^*}}{m_\pi}\bar{\Delta}^*\vec{S}^\dagger\gamma^5\gamma^\mu\partial_\mu\phi_K\Psi_\Sigma$ + h.c.
$K\Lambda N^*(P_{13})$	$\frac{f_{K\Lambda N^*}}{m_\pi}\bar{\Psi}^\mu_{N^*}\partial_\mu\phi_K\Psi_\Lambda$ + h.c.	$\pi N\Delta^*(P_{33})$	$\frac{f_{\pi N\Delta^*}}{m_\pi}\bar{\Delta}^*_\mu\vec{S}^\dagger\Psi\partial^\mu\vec{\pi}$ + h.c.
$K\Sigma N^*(P_{13})$	$\frac{f_{K\Sigma N^*}}{m_\pi}\bar{\Psi}^\mu_{N^*}\partial_\mu\vec{\tau}\phi_K\Psi_\Sigma$ + h.c.	$\rho N\Delta^*(P_{33})$	$-i\frac{f_{\rho N\Delta^*}}{m_\rho}\bar{\Delta}^*_\mu\gamma^5\gamma_\nu\vec{S}^\dagger\vec{\rho}^{\mu\nu}\Psi$ + h.c.
$\pi N N^*(D_{13})$	$\frac{f_{\pi N N^*}}{m_\pi^2}\bar{\Psi}^\mu_{N^*}\gamma^5\gamma^\nu\vec{\tau}\Psi\partial_\mu\partial_\nu\vec{\pi}$ + h.c.	$K\Sigma\Delta^*(P_{33})$	$\frac{f_{K\Sigma\Delta^*}}{m_\pi^2}\bar{\Delta}^*_\mu\vec{S}^\dagger\gamma^\mu\partial_\mu\phi_K\Psi_\Sigma$ + h.c.
$\eta N N^*(D_{13})$	$\frac{f_{\eta N N^*}}{m_\pi}\bar{\Psi}^\mu_{N^*}\gamma^5\gamma^\nu\Psi\partial_\nu\partial_\mu\eta$ + h.c.	$\pi N\Delta^*(D_{33})$	$\frac{f_{\pi N\Delta^*}}{m_\pi^2}\bar{\Psi}\gamma^5\gamma_\nu\vec{S}^\dagger\Delta^*_\mu\partial^\nu\partial^\mu\vec{\pi}$ + h.c.
$\rho N N^*(D_{13})$	$\frac{f_{\rho N N^*}}{m_\rho}\bar{\Psi}^\mu_{N^*}\gamma^\nu\vec{\tau}\vec{\rho}_{\mu\nu}\Psi$ + h.c.	$\rho N\Delta^*(D_{33})$	$\frac{f_{\rho N\Delta^*}}{m_\rho}\bar{\Delta}^*_\mu\gamma_\nu\vec{S}^\dagger\vec{\rho}^{\mu\nu}\Psi$ + h.c.
$\pi\Delta N^*(D_{13})$	$i\frac{f_{\pi\Delta N^*}}{m_\pi}\bar{\Psi}^\mu_{N^*}\vec{S}\gamma^\nu\Delta_\mu\partial_\nu\vec{\pi}$ + h.c.	$\pi\Delta\Delta^*(D_{33})$	$\frac{f_{\pi\Delta\Delta^*}}{m_\pi}\bar{\Delta}^*_\mu\vec{T}\gamma^\nu\Delta^\mu\partial_\nu\vec{\pi}$ + h.c.
$K\Lambda N^*(D_{13})$	$\frac{f_{K\Lambda N^*}}{m_\pi^2}\bar{\Psi}^\mu_{N^*}\gamma^5\gamma^\nu\partial_\nu\partial_\mu\phi_K\Psi_\Lambda$ + h.c.	$K\Sigma\Delta^*(D_{33})$	$\frac{f_{K\Sigma\Delta^*}}{m_\pi^2}\Psi_\Sigma\gamma^5\gamma^\nu\vec{S}^\dagger\Delta^*_\mu\partial^\mu\partial_\nu\phi_K$ + h.c.

Table 30: Here we list the effective Lagrangians for s-channel diagrams up to $J = 3/2$. Note that spin-3/2 field operators are equipped with a Rarita-Schwinger spinor as defined in Eq. (A.12) and consequently have a Lorentz index μ. The vector notation refers to isospin space here. Some field operators have their isospin matrices defined implicitly. We also use the notation $\vec{\rho}_{\mu\nu} = \partial_\mu\vec{\rho}_\nu - \partial_\nu\vec{\rho}_\mu$.

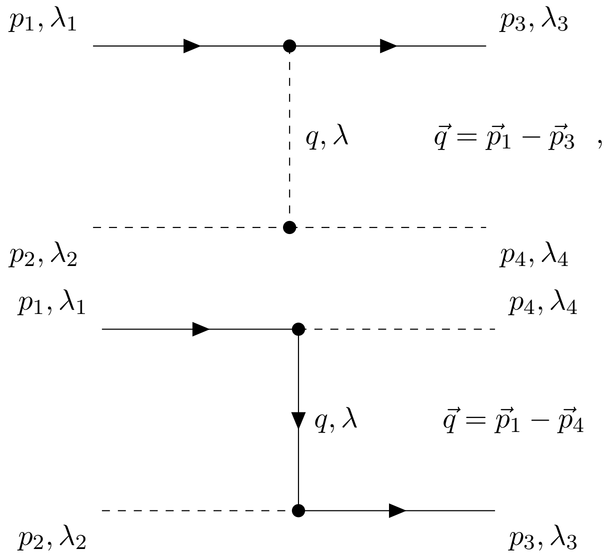

Figure 22: Notation for t- and u-channel exchange diagrams. Time flows from left to right.

and for the incoming (outgoing) meson with 2 (4). The on-shell energies for the baryon and meson are given by

$$E_i = \sqrt{\vec{p}_i^{\,2} + m_i^2}, \quad \omega_i = \sqrt{\vec{p}_i^{\,2} + m_i^2} \ , \tag{B.37}$$

where m_i are the respective masses. Within the TOPT framework the 0-th component of the inital and final momenta are equal to their on-shell energies. The intermediate particle carries the three momentum $\vec{q}$ and the 0-th component of the four vector q is $q^0 = E_q$ for a baryon exchange and $q^0 = \omega_q$ for a meson exchange in the first time ordering. In the second time ordering we label the four momentum with $\bar{q}$ and the 0-th component takes for values $\bar{q}^0 = -E_q$ for a baryon exchange and $\bar{q}^0 = -\omega_q$ for a meson exchange.

The potential for t- and u-exchanges in the helicity basis is defined by

$$V^{\vec{p}_1,\vec{p}_2,\vec{p}_3,\vec{p}_4}_{\lambda_1,\lambda_2,\lambda_3,\lambda_4} = N \cdot F_1 F_2 \cdot I_{\mathrm{NP}} \cdot \mathcal{V} \ , \tag{B.38}$$

where we introduced a kinematic normalization factor N

$$N = \frac{1}{(2\pi)^3} \frac{1}{2\sqrt{\omega_2 \omega_4}} \ , \tag{B.39}$$

which is included in each exchange diagram. We also included the isospin factor I_{NP} for the exchange process. To obtain the contributions to the non-pole part of the potential V^{NP}, one needs to again transform in the JLS-basis.

We also multiply the exchange potentials $\mathcal{V}$ with form factors F_1 and F_2, which depend on the exchanged momentum $\vec{q}$. For the form factors of t- and u-channel exchanges we use

$$F(q) = \left(\frac{\Lambda^2 - m_{ex}^2}{\Lambda^2 + \vec{q}^{\,2}} \right)^n \ , \tag{B.40}$$

Vertex	$\mathcal{L}_{int}$	Vertex	$\mathcal{L}_{int}$
πNN	$-\frac{g_{\pi NN}}{m_\pi}\bar{\Psi}\gamma^5\gamma^\mu\vec{\tau}\cdot\partial_\mu\vec{\pi}\Psi$	ωNN	$-g_{\omega NN}\bar{\Psi}[\gamma^\mu - \frac{\kappa_\omega}{2m_N}\sigma^{\mu\nu}\partial_\nu]\omega_\mu\Psi$
$\pi N\Delta$	$\frac{g_{\pi N\Delta}}{m_\pi}\bar{\Delta}^\mu\vec{S}^\dagger\cdot\partial_\mu\vec{\pi}\Psi\ +\ \text{h.c.}$	$\pi\omega\rho$	$\frac{g_{\pi\omega\rho}}{m_\omega}\epsilon_{\alpha\beta\mu\nu}\partial^\alpha\vec{\rho}^\beta\cdot\partial^\mu\vec{\pi}\omega^\nu$
$\pi\pi\rho$	$-g_{\pi\pi\rho}(\vec{\pi}\times\partial_\mu\vec{\pi})\cdot\vec{\rho}^\mu$	$\rho N\Delta$	$-i\frac{g_{\rho N\Delta}}{m_\rho}\bar{\Delta}^\mu\gamma^5\gamma^\mu\vec{S}^\dagger\cdot\vec{\rho}_{\mu\nu}\Psi\ +\ \text{h.c.}$
ρNN	$-g_{\rho NN}\Psi[\gamma^\mu - \frac{\kappa_\rho}{2m_N}\sigma^{\mu\nu}\partial_\nu]\vec{\tau}\cdot\vec{\rho}_\mu\Psi$	$\rho\rho\rho$	$g_{\rho NN}(\vec{\rho}_\mu\times\vec{\rho}_\nu)\cdot\vec{\rho}^{\mu\nu}$
$NN\sigma$	$-g_{NN\sigma}\bar{\Psi}\Psi\sigma$	$\rho\rho NN$	$\frac{\kappa_\rho g^2_{\rho NN}}{2m_N}\bar{\Psi}\sigma^{\mu\nu}\vec{\tau}\Psi(\vec{\rho}_\mu\times\vec{\rho}_\nu)$
$\pi\pi\sigma$	$\frac{g_{\pi\pi\sigma}}{2m_\pi}\partial_\mu\vec{\pi}\cdot\partial^\mu\vec{\pi}\sigma$	$\pi\Delta\Delta$	$\frac{g_{\pi\Delta\Delta}}{m_\pi}\bar{\Delta}_\mu\gamma^5\gamma^\nu\vec{T}\Delta^\mu\partial_\nu\vec{\pi}$
$\sigma\sigma\sigma$	$-g_{\sigma\sigma\sigma}m_\sigma\sigma\sigma\sigma$	$\rho\Delta\Delta$	$-g_{\rho\Delta\Delta}\bar{\Delta}_\tau(\gamma^\mu - i\frac{\kappa_{\rho\Delta\Delta}}{2m_\Delta}\sigma^{\mu\nu}\partial_\nu)\vec{\rho}_\mu\cdot\vec{T}\Delta^\tau$
$\pi\rho NN$	$\frac{g_{\pi NN}}{m_\pi}2g_{\rho NN}\bar{\Psi}\gamma^5\gamma^\mu\vec{\tau}\Psi(\vec{\rho}_\mu\times\vec{\pi})$	ηNN	$-\frac{g_{\eta NN}}{m_\pi}\bar{\Psi}\gamma^5\gamma^\mu\partial_\mu\eta\Psi$
a_1NN	$-\frac{g_{\pi NN}}{m_\pi}m_{a_1}\bar{\Psi}\gamma^5\gamma^\mu\vec{\tau}\Psi\vec{a}_\mu$	a_0NN	$g_{a_0NN}m_\pi\bar{\Psi}\vec{\tau}\Psi\vec{a_0}$
$\pi a_1\rho$	$-\frac{2g_{\pi a_1\rho}}{m_{a_1}}[\partial_\mu\vec{\pi}\times\vec{a}_\nu - \partial_\nu\vec{\pi}\times\vec{a}_\mu]\cdot[\partial^\mu\vec{\rho}^\nu - \partial^\nu\vec{\rho}^\mu]$	$\pi\eta a_0$	$g_{\pi\eta a_0}m_\pi\eta\vec{\pi}\cdot\vec{a}_0$
	$+\frac{2g_{\pi a_1\rho}}{2m_{a_1}}[\vec{\pi}\times(\partial_\mu\vec{\rho}_\nu - \partial_\nu\vec{\rho}_\mu)]\cdot[\partial^\mu\vec{a}^\nu - \partial^\nu\vec{a}^\mu]$		

Table 31: Here we list the interaction terms of the effective Lagrangians used for the exchange potential. The vector notation refers to isospin space here. Some field operators have their isospin matrices defined implicitly. We also use the notation $\vec{\rho}_{\mu\nu} = \partial_\mu\vec{\rho}_\nu - \partial_\nu\vec{\rho}_\mu$.

where m_{ex} denotes the mass of the exchanged particle. The different powers are used to ensure the convergence of the integrals over off-shell momenta and the powers $n = 1, 2$ correspond to monopole or dipole form factors, respectively. For the vertices with ρ, ω, ϕ, Δ, K^* and Σ^* we use the dipole type, except for the Δ exchange in $\rho N \to \rho N$ (where we use $n = 4$) and the $\pi\pi\rho$ vertex in $\pi\Delta \to \pi\Delta$ with a ρ exchange (where we use $n = 1$). For all other we use the monopole form factor.

Another special case is the u-exchange at the πNN vertex for the processes $\pi N \to \pi N$, ρN, $\pi\Delta$ and σN. Here the monopole form factor is modified to be normalized to unity at the Cheng-Dashen point

$$F(q) = \frac{\Lambda^2 - m_N^2}{\Lambda^2 - \left(\frac{m_N^2 - m_\pi^2}{m_N}\right)^2 + \vec{q}^2} \ . \tag{B.41}$$

For contact terms we use the form factor

$$F(p_2, p_4) = \left(\frac{\Lambda^2 - m_2^2}{\Lambda^2 + \vec{p}_2^2}\right)^2 \left(\frac{\Lambda^2 - m_4^2}{\Lambda^2 + \vec{p}_4^2}\right)^2 \ , \tag{B.42}$$

where the momenta and masses are from the incoming and outgoing mesons respectively.

For the correlated $\pi\pi$ exchange potentials we include form factors of the form [103, 109]

$$F(p_2, p_4) = \frac{\Lambda^2}{\Lambda^2 + \vec{p}_2^2}\frac{\Lambda^2}{\Lambda^2 + \vec{p}_4^2} \ . \tag{B.43}$$

This kind of form factor does not depend on the energy and does not modify the on-shell potential in a strong way, which is assumed to be fully determined by the dispersion integrals.

The cut-off parameters Λ in the form factors for t- and u-channel exchanges are fit parameters in our model. These were not fitted in the studies presented in this work, since the non-pole parameters largely increase computation time. However, the values were fitted in earlier JüBo-studies and values on these can be found in Refs. [33, 110, 112, 113].

For spin-3/2 particles we use the Rarita-Schwinger spinor u^μ as defined in Eq. (A.12) and the Rarita-Schwinger tensor $P^{\mu\nu}$ from Eq. (A.13) [33]. If the argument of $P^{\mu\nu}$ is q_{B^*} in the potential expression, this then denotes the exchange of a $J = 3/2^+$ baryon $B^* = \Delta(1232)$, $\Sigma^*(1385)$ or $\Xi^*(1530)$. For this we adopt the simplified prescription from Ref. [104] to avoid issues associated with constructing contact graphs in TOPT. The 0-th component of the exchanged momentum is

$$q^0_{B^*} = E_1^{\text{on}} - \omega_4^{\text{on}} \ , \tag{B.44}$$

with

$$E_1^{\text{on}} = \frac{W^2 + m_1^2 - m_2^2}{2W} \ , \quad \omega_4^{\text{on}} = \frac{W^2 - m_3^2 + m_4^2}{2W} \ . \tag{B.45}$$

We denote the tensor coupling for vector mesons coupling to octet baryons by $f_{VBB} = g_{VBB} \cdot \kappa_V$, where g_{VBB} is the vector coupling. We use correlated two-pion exchange for the exchange of ρ and σ quantum numbers in the reaction $\pi N \to \pi N$. However, there is no pseudo data to fix the parameters for the exchange of these quantum numbers in other channels. Consequently, we use the exchange of stable particles with masses $m_\rho = 770$ MeV and $m_\sigma = 650$ MeV. The masses of the exchange particles for other t-channel processes are

$$\begin{aligned} m_\omega &= 783 \text{ MeV}, & m_{f_0} &= 974 \text{ MeV}, \\ m_{a_0} &= 983 \text{ MeV}, & m_{a_1} &= 1260 \text{ MeV}, \\ m_{K^*} &= 892 \text{ MeV}, & m_\phi &= 1020 \text{ MeV}. \end{aligned}$$

For the exchanged baryons we take their PDG values [5], except for the unstable $\Xi^*(1530)$ for which we use $m_{\Xi^*} = 1533$ MeV.

In the following we are going to list the explicit expression for the exchange pseudo-potentials $\mathcal{V}$ as defined in Eq. (B.38). We label the different kind of potentials as "types" with numbers.

Type 1: u-exchange of an $J^P = 1/2^+$ octet baryon

$$\mathcal{V} = \frac{g_a g_b}{m_\pi^2} \bar{u}(\vec{p}_3, \lambda_3) \frac{\not{p}_2}{2E_q} \left(\frac{\not{q} + m_{ex}}{W - E_q - \omega_2 - \omega_4} + \frac{\tilde{\not{q}} + m_{ex}}{W - E_q - E_1 - E_3} \right) \gamma^5 \not{p}_4 u(\vec{p}_1, \lambda_1) \tag{B.46}$$

Type 2: u-exchange of a decuplet baryon

$$\mathcal{V} = \frac{g_a g_b}{m_\pi^2} \bar{u}(\vec{p}_3, \lambda_3) \frac{p_{2\mu} P^{\mu\nu}(q_{B^*})}{2E_q} \left(\frac{1}{W - E_q - \omega_2 - \omega_4} + \frac{1}{W - E_q - E_1 - E_3} \right) p_{4\nu} u(\vec{p}_1, \lambda_1) \tag{B.47}$$

Type 3: t-exchange of a scalar meson (f_0)

$$\mathcal{V} = \frac{g_a g_b}{2m_\pi}(-2p_{2\mu}p_4^\mu)\frac{1}{2\omega_q}\left(\frac{1}{W-\omega_q-\omega_2-E_3}+\frac{1}{W-\omega_q-\omega_4-E_1}\right)\bar{u}(\vec{p}_3,\lambda_3)u(\vec{p}_1,\lambda_1) \tag{B.48}$$

Type 4: t-exchange of a vector meson

$$\mathcal{V} = g_a\bar{u}(\vec{p}_3,\lambda_3)\left(\frac{g_b\gamma^\mu - i\frac{f_b}{2m_N}\sigma^{\mu\nu}q_\nu}{W-\omega_q-E_3-\omega_2}+\frac{g_b\gamma^\mu - i\frac{f_b}{2m_N}\sigma^{\mu\nu}\tilde{q}_\nu}{W-\omega_q-E_1-\omega_4}\right)u(\vec{p}_1,\lambda_1)\frac{(p_2+p_4)_\mu}{2\omega_q} \tag{B.49}$$

Type 5: Contact interaction in $\pi N \to \rho N$

$$\mathcal{V} = -2\frac{g_a}{m_\pi}g_b\bar{u}(\vec{p}_3,\lambda_3)\gamma^5\not{\epsilon}^*(\vec{p}_4,\lambda_4)u(\vec{p}_1,\lambda_1) \tag{B.50}$$

Type 6: t-exchange of a scalar meson (a_0) (scalar coupling)

$$\mathcal{V} = g_a g_b m_\pi \bar{u}(\vec{p}_3,\lambda_3)u(\vec{p}_1,\lambda_1)\frac{1}{2\omega_q}\left(\frac{1}{W-\omega_q-\omega_2-E_3}+\frac{1}{W-\omega_q-\omega_4-E_1}\right) \tag{B.51}$$

Type 7: u-exchange of N in $\pi N \to \rho N$

$$\begin{aligned}\mathcal{V} =& -i\frac{g_a g_b}{m_\pi}\bar{u}(\vec{p}_3,\lambda_3)\gamma^5\not{p}_2\left(\frac{\not{q}+m_N}{W-E_q-\omega_2-\omega_4}+\frac{\tilde{\not{q}}+m_N}{W-E_q-E_1-E_3}\right)\\ &\times\frac{1}{2E_q}\left(\not{\epsilon}^*(\vec{p}_4,\lambda_4)-i\frac{\kappa_\rho}{2m_N}\sigma^{\mu\nu}p_{4\nu}\epsilon^*_\mu(\vec{p}_4,\lambda_4)\right)u(\vec{p}_1,\lambda_1)\end{aligned} \tag{B.52}$$

Type 8: t-exchange of a π in $\pi N \to \rho N$

$$\begin{aligned}\mathcal{V} =& -\frac{g_a g_b}{m_\pi}\bar{u}(\vec{p}_3,\lambda_3)\gamma^5\left(\frac{\not{q}(p_2-q)_\nu}{2\omega_q(W-\omega_q-E_3-\omega_2)}\right.\\ &\left.+\frac{\tilde{\not{q}}(p_2-\tilde{q})_\nu}{2\omega_q(W-\omega_q-E_1-\omega_4)}-\gamma^0\delta^0_\nu\right)\epsilon^{*,\nu}(\vec{p}_4,\lambda_4)u(\vec{p}_1,\lambda_1)\end{aligned} \tag{B.53}$$

Type 9: t-exchange of a pseudovector meson

$$\begin{aligned}\mathcal{V} =& \frac{4g_a g_b}{m_\pi}\bar{u}(\vec{p}_3,\lambda_3)\gamma^5\gamma_\mu\left(\frac{-g^{\mu\nu}+\frac{q^\mu q^\nu}{m_{a1}^2}}{2\omega_q(W-\omega_q-E_3-\omega_2)}\left[\left(p_2+\frac{q}{2}\right)_\tau p_4^\tau\epsilon^*_\nu(\vec{p}_4,\lambda_4)-\left(p_2+\frac{q}{2}\right)^\tau\epsilon^*_\tau(\vec{p}_4,\lambda_4)p_{4\nu}\right]\right.\\ &+\left[\left(p_2+\frac{\tilde{q}}{2}\right)_\tau p_4^\tau\epsilon^*_\nu(\vec{p}_4,\lambda_4)-\left(p_2+\frac{\tilde{q}}{2}\right)^\tau\epsilon^*_\tau(\vec{p}_4,\lambda_4)p_{4\nu}\right]\frac{-g^{\mu\nu}+\frac{\tilde{q}^\mu\tilde{q}^\nu}{m_{a1}^2}}{2\omega_q(W-\omega_q-E_1-\omega_4)}\\ &\left.+\frac{1}{m_{a1}^2}\delta^0_\mu\left[p_{2\nu}p_4^\nu\epsilon^*_0(\vec{p}_4,\lambda_4)-p_2^\nu\epsilon^*_\nu(\vec{p}_4,\lambda_4)p_{4_0}\right]\right)u(\vec{p}_1,\lambda_1)\end{aligned} \tag{B.54}$$

Type 10: t-exchange of ω in $\pi N \to \rho N$

$$\mathcal{V} = \frac{g_a}{m_\omega}\bar{u}(\vec{p}_3,\lambda_3)\left(\frac{g_b\gamma^\nu - i\frac{f_b}{2m_N}\sigma^{\nu\tau}q_\tau}{W-\omega_q-E_3-\omega_2} + \frac{g_b\gamma^\nu - i\frac{f_b}{2m_N}\sigma^{\nu\tau}\tilde{q}_\tau}{W-\omega_q-E_1-\omega_4}\right)u(\vec{p}_1,\lambda_1)\epsilon_{\alpha\beta\mu\nu}p_4^\alpha\epsilon^{*,\beta}(\vec{p}_4,\lambda_4)p_2^\mu\frac{1}{2\omega_q} \tag{B.55}$$

Type 11: u-exchange of N in $\pi N \to \pi\Delta$

$$\mathcal{V} = -\frac{g_a g_b}{m_\pi^2}\bar{u}^\mu(\vec{p}_3,\lambda_3)\frac{p_{2\mu}}{2E_q}\left(\frac{\not{q}+m_{ex}}{W-E_q-\omega_2-\omega_4} + \frac{\tilde{\not{q}}+m_{ex}}{W-E_q-E_1-E_3}\right)\gamma^5\not{p}_4 u(\vec{p}_1,\lambda_1) \tag{B.56}$$

Type 12: t-exchange of ρ in $\pi\Delta \to \pi\Delta$

$$\mathcal{V} = -i\frac{g_a g_b}{m_\rho}\bar{u}^\mu(\vec{p}_3,\lambda_3)\gamma^5(q_\mu\gamma_\nu - \not{q}g_{\mu\nu})u(\vec{p}_1,\lambda_1)\frac{1}{2\omega_q}\left(\frac{1}{W-\omega_q-\omega_2-E_3} + \frac{1}{W-\omega_q-\omega_4-E_1}\right)(p_2+p_4)^\nu \tag{B.57}$$

Type 13: u-exchange of Δ in $\pi N \to \pi\Delta$

$$\mathcal{V} = \frac{g_a g_b}{m_\pi^2}\bar{u}_\mu(\vec{p}_3,\lambda_3)\gamma^5\not{p}_2\frac{P^{\mu\nu}(q_{B^*})}{2E_q}\left(\frac{1}{W-E_q-\omega_2-\omega_4} + \frac{1}{W-E_q-E_1-E_3}\right)p_{4\nu}u(\vec{p}_1,\lambda_1) \tag{B.58}$$

Type 14: u-exchange of N in $\pi N \to \sigma N$

$$\mathcal{V} = -i\frac{g_a g_b}{m_\pi}\bar{u}(\vec{p}_3,\lambda_3)\gamma^5\frac{\not{p}_2}{2E_q}\left(\frac{\not{q}+m_{ex}}{W-E_q-\omega_2-\omega_4} + \frac{\tilde{\not{q}}+m_{ex}}{W-E_q-E_1-E_3}\right)u(\vec{p}_1,\lambda_1) \tag{B.59}$$

Type 15: t-exchange of π in $\pi N \to \sigma N$

$$\mathcal{V} = i\frac{g_a g_b}{m_\pi^2}\bar{u}(\vec{p}_3,\lambda_3)\frac{1}{2\omega_q}\left(\frac{\gamma^5\not{q}q_\mu}{W-\omega_q-\omega_2-E_3}p_2^\mu + \frac{\gamma^5\tilde{\not{q}}\tilde{q}_\mu}{W-\omega_q-\omega_4-E_1}p_2^\mu + 2\omega_q\gamma^5\gamma^0p_2^0\right)u(\vec{p}_1,\lambda_1) \tag{B.60}$$

Type 16: u-exchange of Δ in $\pi N \to \rho N$

$$\begin{aligned}\mathcal{V} =& i\frac{g_a g_b}{m_\pi m_\rho}\bar{u}(\vec{p}_3,\lambda_3)p_{2\mu}\left(\frac{P^{\mu\nu}(q)}{2E_q(W-E_q-\omega_2-\omega_4)} + \frac{P^{\mu\nu}(\tilde{q})}{2E_q(W-E_q-E_1-E_3)}\right)\\ &\times\gamma^5(\not{\epsilon}^*(\vec{p}_4,\lambda_4)p_{4\nu} - \not{p}_4\epsilon_\nu^*(\vec{p}_4,\lambda_4))u(\vec{p}_1,\lambda_1)\end{aligned} \tag{B.61}$$

Type 17: u-exchange of N in $\rho N \to \rho N$

$$\begin{aligned}\mathcal{V} =& g_a\bar{u}(\vec{p}_3,\lambda_3)\left[g_b\gamma^\mu + i\frac{f_b}{2m_N}\sigma^{\mu\nu}p_{2\nu}\right]\epsilon_\mu(\vec{p}_2,\lambda_2)\frac{1}{2E_q}\left(\frac{\not{q}+m_{ex}}{W-E_q-\omega_2-\omega_4} + \frac{\tilde{\not{q}}+m_{ex}}{W-E_q-E_1-E_3}\right)\\ &\times\left[\gamma^\tau - i\frac{\kappa_\rho}{2m_N}\sigma^{\tau\nu}p_{4\nu}\right]\epsilon_\tau^*(\vec{p}_4,\lambda_4)u(\vec{p}_1,\lambda_1)\end{aligned} \tag{B.62}$$

Type 18: Contact interaction in $\rho N \to \rho N$

$$\mathcal{V} = \frac{g_a}{m_N}f_b\bar{u}(\vec{p}_3,\lambda_3)\sigma^{\mu\nu}\epsilon_\mu(\vec{p}_2,\lambda_2)\epsilon_\nu^*(\vec{p}_4,\lambda_4)u(\vec{p}_1,\lambda_1) \tag{B.63}$$

Type 19: t-exchange of ρ in $\rho N \to \rho N$

$$\begin{aligned}\mathcal{V} =& - ig_a\Bigg(\bar{u}(\vec{p}_3,\lambda_3)\frac{\Big[g_b\gamma^\mu - i\frac{f_b}{2m_N}\sigma^{\mu\nu}q_\nu\Big]}{2\omega_q(W-\omega_q-E_3-\omega_2)} \\ &\times\Big[\epsilon^\tau(\vec{p}_2,\lambda_2)\epsilon^*_\tau(\vec{p}_4,\lambda_4)(-p_4-p_2)_\mu + (q+p_4)^\tau\epsilon_\tau(\vec{p}_2,\lambda_2)\epsilon^*_\mu(\vec{p}_4,\lambda_4) + (p_2-q)^\tau\epsilon^*_\tau(\vec{p}_4,\lambda_4)\epsilon_\mu(\vec{p}_2,\lambda_2)\Big] \\ &+\Big[\epsilon^\tau(\vec{p}_2,\lambda_2)\epsilon^*_\tau(\vec{p}_4,\lambda_4)(-p_4-p_2)_\mu + (\tilde{q}+p_4)^\tau\epsilon_\tau(\vec{p}_2,\lambda_2)\epsilon^*_\mu(\vec{p}_4,\lambda_4) + (p_2-\tilde{q})^\tau\epsilon^*_\tau(\vec{p}_4,\lambda_4)\epsilon_\mu(\vec{p}_2,\lambda_2)\Big] \\ &\times\bar{u}(\vec{p}_3,\lambda_3)\frac{\Big[g_b\gamma^\mu - i\frac{f_b}{2m_N}\sigma^{\mu\nu}\tilde{q}_\nu\Big]}{2\omega_q(W-\omega_q-E_1-\omega_4)}\Bigg)u(\vec{p}_1,\lambda_1)\end{aligned} \tag{B.64}$$

Type 20: u-exchange of Δ in $\rho N \to \rho N$

$$\begin{aligned}\mathcal{V} =& \frac{g_a g_b}{m_\rho^2}\bar{u}(\vec{p}_3,\lambda_3)\gamma^5(\gamma_\kappa p_{4\mu} - \not{p}_4 g_{\mu\kappa})\epsilon^{\kappa *}(\vec{p}_4,\lambda_4)\left(\frac{P^{\mu\nu}(q)}{2E_q(W-E_q-\omega_2-\omega_4)} + \frac{P^{\mu\nu}(\tilde{q})}{2E_q(W-E_q-E_1-E_3)}\right) \\ &\times\gamma^5(\gamma_\tau p_{2\nu} - \not{p}_2 g_{\nu\tau})\epsilon^\tau(\vec{p}_2,\lambda_2)u(\vec{p}_1,\lambda_1)\end{aligned} \tag{B.65}$$

Type 21: u-exchange of N in $\pi\Delta \to \pi\Delta$

$$\mathcal{V} = \frac{g_a g_b}{m_\pi^2}\bar{u}^\mu(\vec{p}_3,\lambda_3)\frac{p_{2\mu}}{2E_q}\left(\frac{\not{q}+m_{ex}}{W-E_q-\omega_2-\omega_4} + \frac{\tilde{\not{q}}+m_{ex}}{W-E_q-E_1-E_3}\right)p_{4\nu}u^\nu(\vec{p}_1,\lambda_1) \tag{B.66}$$

Type 22: t-exchange of ρ in $\pi\Delta \to \pi\Delta$

$$\mathcal{V} = ig_a\bar{u}^\tau(\vec{p}_3,\lambda_3)\left(\frac{g_b\gamma_\mu - i\frac{f_b}{2m_\Delta}\sigma_{\mu\nu}q^\nu}{W-\omega_q-E_3-\omega_2} + \frac{g_b\gamma_\mu - i\frac{f_b}{2m_\Delta}\sigma_{\mu\nu}\tilde{q}^\nu}{W-\omega_q-E_1-\omega_4}\right)u_\tau(\vec{p}_1,\lambda_1)\frac{(p_2+p_4)^\mu}{2\omega_q} \tag{B.67}$$

Type 23: u-exchange of Δ in $\pi\Delta \to \pi\Delta$

$$\mathcal{V} = \frac{g_a g_b}{m_\pi^2}\bar{u}_\mu(\vec{p}_3,\lambda_3)\gamma^5\not{p}_2\frac{P^{\mu\nu}(q_{B^*})}{2E_q}\left(\frac{1}{W-E_q-\omega_2-\omega_4} + \frac{1}{W-E_q-E_1-E_3}\right)\gamma^5\not{p}_4 u_\nu(\vec{p}_1,\lambda_1) \tag{B.68}$$

Type 24: t-exchange of π in $\rho N \to \pi\Delta$

$$\begin{aligned}\mathcal{V} =& \frac{g_a g_b}{m_\pi}\bar{u}_\mu(\vec{p}_3,\lambda_3)\frac{1}{2\omega_q}\Bigg(\frac{q^\mu(p_4-q)_\nu}{W-\omega_q-E_3-\omega_2}\epsilon^\nu(\vec{p}_1,\lambda_1) \\ &+\frac{\tilde{q}^\mu(p_4-\tilde{q})_\nu}{W-\omega_q-E_1-\omega_4}\epsilon^\nu(\vec{p}_2,\lambda_2) - \delta^\mu_0\epsilon^0(\vec{p}_2,\lambda_2)2\omega_q\Bigg)u(\vec{p}_1,\lambda_1)\end{aligned} \tag{B.69}$$

Type 25: u-exchange of N in $\rho N \to \pi\Delta$

$$\begin{aligned}\mathcal{V} =& - i\frac{g_a g_b}{m_\pi m_\rho}\bar{u}^\mu(\vec{p}_3,\lambda_3)\Big[p_{2\mu}\gamma^5\not{\epsilon}(-\vec{p}_2,\lambda_2) - \epsilon_\mu(\vec{p}_2,\lambda_2)\gamma^5\not{p}_2\Big] \\ &\times\frac{1}{2E_q}\left(\frac{\not{q}+m_N}{W-E_q-\omega_2-\omega_4} + \frac{\tilde{\not{q}}+m_N}{W-E_q-E_1-E_3}\right)\gamma^5\not{p}_2 u(\vec{p}_1,\lambda_1)\end{aligned} \tag{B.70}$$

Type 26: t-exchange of π in $\sigma N \to \pi\Delta$

$$\mathcal{V} = i\frac{g_a g_b}{m_\pi^2}\bar{u}^\mu(\vec{p}_3,\lambda_3)\frac{1}{2\omega_q}\left(\frac{q_\mu q_\nu p_4^\nu}{W-\omega_q-\omega_2-E_3}+\frac{\tilde{q}_\mu\tilde{q}_\nu p_4^\nu}{W-\omega_q-\omega_4-E_1}+\delta_\mu^0 p_{4_0}2\omega_q\right)u(\vec{p}_1,\lambda_1) \tag{B.71}$$

Type 27: u-exchange of N in $\sigma N \to \sigma N$

$$\mathcal{V} = g_a g_b\bar{u}(\vec{p}_3,\lambda_3)\frac{1}{2E_q}\left(\frac{\not{q}+m_{ex}}{W-E_q-\omega_2-\omega_4}+\frac{\tilde{\not{q}}+m_{ex}}{W-E_q-E_1-E_3}\right)u(\vec{p}_1,\lambda_1) \tag{B.72}$$

Type 28: t-exchange of σ in $\sigma N \to \sigma N$

$$\mathcal{V} = 6g_a g_b m_\sigma\bar{u}(\vec{p}_3,\lambda_3)u(\vec{p}_1,\lambda_1)\left(\frac{1}{W-\omega_q-E_3-\omega_2}+\frac{1}{W-\omega_q-E_1-\omega_4}\right) \tag{B.73}$$

For the correlated $\pi\pi$ exchange in the ρ-channel we use the definition from Ref. [33] and for the σ-channel we use the one from Ref. [110]. For the latter one we use the same subtraction constant $A_0 = 25\text{MeV}/F_\pi^2$ as it was used in Ref. [110].

Couplings for t- and u-channel diagrams

Many of the coupling constants of t- and u-channel exchanges are related to each other by $SU(3)$ flavor symmetry [661]. The coupling of a meson nonet to an octet baryon current $(8_B\otimes 8_B)$ results in two products: $8_B\otimes 8_B\otimes 1_M$ and $8_B\otimes 8_B\otimes 8_M$. The coupling to the meson octet 8_M is governed by two parameters, g_1 and g_2, which correspond to the symmetric and antisymmetric representations of $8_B\otimes 8_B$. We use the notation of Ref. [661] to rewrite this in terms of a coupling constant g and a mixing parameter α

$$g = \frac{\sqrt{30}}{40}g_1+\frac{\sqrt{6}}{24}g_2, \quad \alpha = \frac{\sqrt{6}}{24}\frac{g_2}{g}\ . \tag{B.74}$$

In the case of the baryon octets coupling to the meson singlet one need another independent coupling constant.

For vertices involving pseudoscalar mesons, we adopt the values from Ref. [228], namely $\alpha_{PBB} = 0.4$ and $\alpha_{PPV} = 1$. Here, P denotes a pseudoscalar meson and V a vector meson. We use η to label the octet η_8 and assume the singlet coupling to be zero. This results in a difference of approximately 10% for $g_{\eta\Sigma\Sigma}$ and $g_{\eta\Lambda\Lambda}$, where we assumed a mixing angle of $\theta_p \approx -10°$. For the coupling constant $g_{\eta KK^*}$ we find a difference of only 2%. We use a phenomenological small value for $g_{\eta NN} = 0.147$ from Ref. [662] instead of the $SU(3)$ value $g_{\eta NN} = 0.343$. As mentioned before, we have a tensor and vector coupling for vertices of vector meson with octet baryons related by $f_{VBB} = g_{VBB}\kappa_V$. For the ρ-meson we use $\kappa_\rho = 6.1$ from Ref. [228].

We determine the couplings of the physical ω and ϕ mesons by assuming ideal mixing of the $SU(3)$ singlet and octet, i.e. ω_1 and ω_8. To fix the singlet coupling constant, we assume that the ϕ meson does not couple to the nucleon, which is in accordance with

Table 32: Here we list the coupling constants for the calculation of the t- and u-channel diagrams and contact (ct) diagrams used in this study. The first two columns specify the diagram and the exchange particle (ex). The third column specifies the diagram type as defined in Eqs. (B.46)-(B.73). The columns 4-6 denote which coupling constants is used in these expressions. The values of these coupling constants are quoted in. We further list the isospin factors $I_{\rm NP}$ used in Eq. (B.38) in columns 7 and 8.

Reaction	ex	Type	g_a	g_b	f_b	$I_{\rm NP}(\frac{1}{2})$	$I_{\rm NP}(\frac{3}{2})$
$\pi N \to \pi N$	N	1	$g_{\pi NN}$	$g_{\pi NN}$		-1	2
	σ	$(\pi\pi)_{\rm corr}$				1	1
	ρ	$(\pi\pi)_{\rm corr}$				$2i$	$-i$
	Δ	2	$g_{\pi\Delta N}$	$g_{\pi\Delta N}$		$\frac{4}{3}$	$\frac{1}{3}$
$\pi N \to \rho N$	N	7	$g_{\pi NN}$	$g_{\rho NN}$		-1	2
	ct	5	$g_{\pi NN}$	$g_{\rho NN}$		$-2i$	i
	π	8	$g_{\pi NN}$	$g_{\pi\pi\rho}$		$-2i$	i
	ω	10	$g_{\pi\omega\rho}$	$g_{\omega NN}$	$f_{\omega NN}$	1	1
	a_1	9	$g_{a_1 NN}$	$g_{\pi a_1 \rho}$		$-2i$	i
	Δ	16	$g_{\pi N\Delta}$	$g_{\rho N\Delta}$		$\frac{4}{3}$	$\frac{1}{3}$
$\pi N \to \eta N$	N	1	$g_{\pi NN}$	$g_{\eta NN}$		$\sqrt{3}$	0
	a_0	6	$g_{\pi\eta a_0}$	$g_{a_0 NN}$		$\sqrt{3}$	0
$\pi N \to \pi\Delta$	N	11	$g_{\pi NN}$	$g_{\pi N\Delta}$		$-\sqrt{\frac{8}{3}}$	$\sqrt{\frac{5}{3}}$
	ρ	12	$g_{\pi\pi\rho}$	$g_{\rho N\Delta}$		$\sqrt{\frac{2}{3}}$	$\sqrt{\frac{5}{3}}$
	Δ	13	$g_{\pi N\Delta}$	$g_{\pi\Delta\Delta}$		$-\frac{5}{3}\sqrt{\frac{2}{3}}$	$-\frac{10}{3\sqrt{15}}$
$\pi N \to \sigma N$	N	14	$g_{\sigma NN}$	$g_{\pi NN}$		$\sqrt{3}$	0
	π	15	$g_{\pi\pi\sigma}$	$g_{\pi NN}$		$\sqrt{3}$	0
$\pi N \to \Lambda K$	K^*	4	$g_{\pi KK^*}$	$g_{NK^*\Lambda}$	$f_{NK^*\Lambda}$	$\sqrt{3}$	0
	Σ	1	$g_{\pi\Sigma\Lambda}$	$g_{KN\Sigma}$		$\sqrt{3}$	0
	Σ^*	2	$g_{\pi\Lambda\Sigma^*}$	$g_{KN\Sigma^*}$		$\sqrt{3}$	0
$\Lambda K \to \Lambda K$	f_0	3	$g_{f_0 KK}$	$g_{f_0\Lambda\Lambda}$		1	0
	ω	4	$g_{KK\omega}$	$g_{\omega\Lambda\Lambda}$	$f_{\omega\Lambda\Lambda}$	1	0
	ϕ	4	$g_{KK\phi}$	$g_{\phi\Lambda\Lambda}$	$f_{\phi\Lambda\Lambda}$	1	0
	Ξ	1	$g_{K\Lambda\Xi}$	$g_{K\Lambda\Xi}$		1	0
	Ξ^*	2	$g_{K\Lambda\Xi^*}$	$g_{K\Lambda\Xi^*}$		1	0
$\pi N \to \Sigma K$	K^*	4	$g_{\pi KK^*}$	$g_{K^*N\Sigma}$	$f_{NK^*\Sigma}$	1	2
	Σ	1	$g_{\pi\Sigma\Sigma}$	$g_{KN\Sigma}$		2	1
	Λ	1	$g_{\pi\Lambda\Sigma}$	$g_{KN\Lambda}$		-1	1
	Σ^*	2	$g_{\pi\Sigma\Sigma^*}$	$g_{KN\Sigma^*}$		2	1

Table 33: Continuation of Table 32.

Transition	ex	Type	g_a	g_b	f_b	$I_{\rm NP}(\frac{1}{2})$	$I_{\rm NP}(\frac{3}{2})$
$\Lambda K \to \Sigma K$	ρ	4	$g_{K\rho K}$	$g_{\Lambda\rho\Sigma}$	$f_{\Lambda\rho\Sigma}$	$-\sqrt{3}$	0
	Ξ	1	$g_{K\Xi\Sigma}$	$g_{\Lambda\Xi K}$		$\sqrt{3}$	0
	Ξ^*	2	$g_{K\Xi^*\Sigma}$	$g_{\Lambda\Xi^* K}$		$\sqrt{3}$	0
$\Sigma K \to \Sigma K$	f_0	3	g_{KKf_0}	$g_{\Sigma\Sigma f_0}$		1	1
	ω	4	$g_{K\omega K}$	$g_{\Sigma\omega\Sigma}$	$f_{\Sigma\omega\Sigma}$	1	1
	ϕ	4	$g_{K\phi K}$	$g_{\Sigma\phi\Sigma}$	$f_{\Sigma\phi\Sigma}$	1	1
	ρ	4	$g_{K\rho K}$	$g_{\Sigma\rho\Sigma}$	$f_{\Sigma\rho\Sigma}$	2	-1
	Ξ	1	$g_{K\Xi\Sigma}$	$g_{K\Xi\Sigma}$		-1	2
	Ξ^*	2	$g_{K\Xi^*\Sigma}$	$g_{K\Xi^*\Sigma}$		-1	2
$\rho N \to \rho N$	N	17	$g_{\rho NN}$	$g_{\rho NN}$	$f_{\rho NN}$	-1	2
	ct	18	$g_{\rho NN}$		$f_{\rho NN}$	$-2i$	i
	ρ	19	$g_{\rho\rho\rho}$	$g_{\rho NN}$	$f_{\rho NN}$	$2i$	$-i$
	Δ	20	$g_{N\Delta\rho}$	$g_{N\Delta\rho}$		$\frac{4}{3}$	$\frac{1}{3}$
$\rho N \to \pi\Delta$	π	24	$g_{\pi\pi\rho}$	$g_{\Delta N\pi}$		$-\sqrt{\frac{2}{3}}i$	$-\sqrt{\frac{5}{3}}i$
	N	25	$g_{NN\pi}$	$g_{\Delta N\rho}$		$-\sqrt{\frac{8}{3}}$	$\sqrt{\frac{5}{3}}$
$\eta N \to \eta N$	N	1	$g_{\eta NN}$	$g_{\eta NN}$		1	0
	f_0	6	$g_{\eta\eta f_0}$	g_{NNf_0}		1	0
$\eta N \to K\Lambda$	K^*	4	$g_{\eta K^* K}$	$g_{NK^*\Lambda}$	$f_{NK^*\Lambda}$	1	0
	Λ	1	$g_{\eta\Lambda\Lambda}$	$g_{N\Lambda K}$		1	0
$\eta N \to K\Sigma$	K^*	4	$g_{\eta K^* K}$	$g_{NK^*\Sigma}$	$f_{KK^*\Sigma}$	$-\sqrt{3}$	0
	Σ	1	$g_{\eta\Sigma\Sigma}$	$g_{N\Sigma K}$		$-\sqrt{3}$	0
	Σ^*	2	$g_{\eta\Sigma^*\Sigma}$	$g_{N\Sigma^* K}$		$-\sqrt{3}$	0
$\pi\Delta \to \pi\Delta$	N	21	$g_{\pi N\Delta}$	$g_{\pi N\Delta}$		$\frac{1}{3}$	$-\frac{2}{3}$
	ρ	22	$g_{\pi\pi\rho}$	$g_{\Delta\Delta\rho}$	$f_{\Delta\Delta\rho}$	$\frac{5}{3}i$	$\frac{2}{3}i$
	Δ	23	$g_{\Delta\Delta\pi}$	$g_{\Delta\Delta\pi}$		$-\frac{10}{9}$	$\frac{11}{9}$
$\sigma N \to \pi\Delta$	π	26	$g_{\pi\pi\sigma}$	$g_{\Delta\pi N}$		$-\sqrt{2}$	0
$\sigma N \to \sigma N$	N	27	$g_{NN\sigma}$	$g_{NN\sigma}$		1	0
	σ	28	$g_{\sigma\sigma\sigma}$	$g_{NN\sigma}$		1	0

the OZI-rule. However, it should be noted that kaon loops generate a small but nonzero effective ϕNN coupling [663, 664], which is neglected in our model.

In the vector-meson sector, the coupling constants are chosen with explicit $SU(3)$-breaking effects in mind, which arise in several ways. Firstly, we do not include a genuine ρ-exchange in the elastic πN channel, but instead account its effect through a correlated $\pi\pi$-exchange. In addition, the commonly found value of $g_{\omega NN}$ in NN interaction studies lies above the $SU(3)$-symmetric prediction [228, 665]. To reflect this, we use $\alpha_{VBB} = 1.5$ rather than the symmetric value $\alpha_{VBB} = 1$, based on the ω coupling constant from Ref. [228], which introduces a small $SU(3)$ breaking in vector meson couplings. For the sake of simplicity, we also set $f_{\omega NN} = 0$.

The relations used for the different coupling constants are listed in the following, and their appearance in the different t- and u-channel expressions in $\mathcal{V}$ (see Eqs. (B.46)-(B.73)) is listed in Tab. 32.
The couplings of a pseudoscalar meson with octet baryons are given by

$$
\begin{aligned}
g_{\pi NN} &= g_{PBB} \,, & g_{KN\Sigma} &= g_{PBB}(1-2\alpha_{PBB}) \,, \\
g_{KN\Lambda} &= -\frac{\sqrt{3}}{3}\, g_{PBB}(1+2\alpha_{PBB}) \,, & g_{\pi\Sigma\Sigma} &= 2\, g_{PBB}\alpha_{PBB} \,, \\
g_{\pi\Lambda\Sigma} &= \frac{2}{\sqrt{3}}\, g_{PBB}(1-\alpha_{PBB}) \,, & g_{K\Xi\Sigma} &= -g_{PBB} \,, \\
g_{K\Xi\Lambda} &= \frac{1}{\sqrt{3}}\, g_{PBB}(4\alpha_{PBB}-1) \,, & g_{\eta\Lambda\Lambda} &= -\frac{2}{\sqrt{3}}\, g_{PBB}(1-\alpha_{PBB}) \,, \\
& & g_{\eta\Sigma\Sigma} &= \frac{2}{\sqrt{3}}\, g_{PBB}(1-\alpha_{PBB}) \,.
\end{aligned}
\tag{B.75}
$$

where $g_{PBB} = 0.989$ [228]. The relations of vector couplings for a vector meson with octet baryons are listed below

$$
\begin{aligned}
g_{\rho NN} &= g_{VBB} \,, & g_{\omega NN} &= g_{VBB}(4\alpha_{VBB}-1) \,, \\
g_{K^*N\Lambda} &= -\frac{1}{\sqrt{3}} g_{VBB}(1+2\alpha_{VBB}) \,, & g_{K^*N\Sigma} &= g_{VBB}(1-2\alpha_{VBB}) \,, \\
g_{\omega\Lambda\Lambda} &= \frac{2}{3} g_{VBB}(5\alpha_{VBB}-2) \,, & g_{\omega\Sigma\Sigma} &= 2 g_{VBB}\alpha_{VBB} \,, \\
g_{\phi\Lambda\Lambda} &= -\frac{\sqrt{2}}{3} g_{VBB}(2\alpha_{VBB}+1) \,, & g_{\phi\Sigma\Sigma} &= -\sqrt{2} g_{VBB}(2\alpha_{VBB}-1) \,, \\
g_{\rho\Sigma\Sigma} &= 2 g_{VBB}\alpha_{VBB} \,, & g_{\rho\Lambda\Sigma} &= \frac{2}{\sqrt{3}} g_{VBB}(1-\alpha_{VBB}) \,,
\end{aligned}
\tag{B.76}
$$

with $g_{VBB} = 3.25$ [228]. The tensor couplings for these vertices are given by

$$\begin{aligned}
f_{\rho NN} &= g_{\rho NN}\kappa_\rho \ , & f_{K^*N\Lambda} &= -\frac{1}{2\sqrt{3}}f_{\omega NN} - \frac{\sqrt{3}}{2}f_{\rho NN} \ , \\
f_{K^*N\Sigma} &= -\frac{1}{2}f_{\omega NN} + \frac{1}{2}f_{\rho NN} \ , & f_{\omega\Lambda\Lambda} &= \frac{5}{6}f_{\omega NN} - \frac{1}{2}f_{\rho NN} \ , \\
f_{\omega\Sigma\Sigma} &= \frac{1}{2}f_{\omega NN} + \frac{1}{2}f_{\rho NN} \ , & f_{\phi\Lambda\Lambda} &= -\frac{1}{3\sqrt{2}}f_{\omega NN} - \frac{1}{\sqrt{2}}f_{\rho NN} \ , \\
f_{\phi\Sigma\Sigma} &= -\frac{1}{\sqrt{2}}f_{\omega NN} + \frac{1}{\sqrt{2}}f_{\rho NN} \ , & f_{\rho\Sigma\Sigma} &= \frac{1}{2}f_{\omega NN} + \frac{1}{2}f_{\rho NN} \ , \\
& & f_{\rho\Lambda\Sigma} &= -\frac{1}{2\sqrt{3}}f_{\omega NN} + \frac{\sqrt{3}}{2}f_{\rho NN} \ ,
\end{aligned} \tag{B.77}$$

where $\kappa_\rho = 6.1$ [228] and $f_{\omega NN} = 0$. The relations for the couplings for a vector meson coupling to pseudoscalar mesons are

$$\begin{aligned}
g_{\pi\pi\rho} &= 2\, g_{PPV} \ , & g_{KK\rho} &= g_{PPV} \ , \\
g_{\pi KK^*} &= -g_{PPV} \ , & g_{KK\omega} &= g_{PPV} \ , \\
g_{KK\phi} &= \sqrt{2}\, g_{PPV} \ , & g_{K\eta K^*} &= -\sqrt{3}\, g_{PPV} \ ,
\end{aligned} \tag{B.78}$$

with $g_{PPV} = 3.02$ [666]. Lastly, we have the couplings for a vertex with a decuplet baryon, an octet baryon and a pseudoscalar meson:

$$\begin{aligned}
g_{\pi N\Delta} &= g_{PBD} \ , & g_{KN\Sigma^*} &= -\frac{1}{\sqrt{6}}g_{PBD} \ , \\
g_{\pi\Sigma\Sigma^*} &= \frac{1}{\sqrt{6}}g_{PBD} \ , & g_{\pi\Lambda\Sigma^*} &= \frac{1}{\sqrt{2}}g_{PBD} \ , \\
g_{K\Lambda\Xi^*} &= \frac{1}{\sqrt{2}}\, g_{PBD} \ , & g_{K\Sigma\Xi^*} &= \frac{1}{\sqrt{6}}\, g_{PBD} \ , \\
& & g_{\eta\Sigma\Sigma^*} &= -\frac{1}{\sqrt{2}}\, g_{PBD} \ ,
\end{aligned} \tag{B.79}$$

with $g^2_{\pi N\Delta}/4\pi = 0.36$ [228] and $g_{PBD} = g_{\Delta N\pi}$. $SU(3)$ symmetry does not fix the couplings for the scalar mesons f_0 and σ. For the g_{f_0KK} coupling we take a value obtained from hyperon-nucleon interaction from Refs. [667, 668]. We treat the couplings $g_{\sigma NN}$, $g_{\sigma\sigma\sigma}$, $g_{f_0\Sigma\Sigma}$ and $g_{f_0\Lambda\Lambda}$ as free parameters in our model. We did not include these parameters in the fits of the JüBo2025 and JüBo2026 studies, but values on these can be found in past studies [33, 110, 112, 113].

B.4. Observables

In this section we review how the amplitudes in the Jülich-Bonn model relate to the observables measured in experiments. We start with pion-induced reactions in Sec. B.4.1 and go to photoproduction processes in Sec. B.4.2.

B.4.1. Observables for Pion-induced Reactions

For pion-induced processes we are dealing with the scattering of a spin-0 off a spin-1/2 particle. We consider a reaction $(\vec{k}_i, \nu) \to (\vec{k}_f, \nu')$, where ν and ν' are the z-projections of the nucleon spin. The differential cross section can then be expressed as [669]

$$\frac{\mathrm{d}\sigma}{\mathrm{d}\Omega} = \left|\langle s', \nu' | \, M \, | s, v\rangle\right|^2 \,, \tag{B.80}$$

where the initial and final polarizations are given by

$$\vec{P}_i = \langle \chi_\nu | \, \vec{\sigma} \, | \chi_\nu \rangle \quad \vec{P}_f = \frac{\langle M\chi_\nu | \, \vec{\sigma} \, | M\chi_\nu \rangle}{\langle M\chi_\nu | M\chi_\nu \rangle} \,. \tag{B.81}$$

χ_ν is the initial spin-1/2 eigenvector and $\vec{\sigma}$ is the Pauli spin-vector. M can be expressed in terms of the non-spin-flip and spin-flip amplitudes g and h by

$$M = g(k, \theta) \; \mathbb{1} + h(k, \theta) \; \vec{\sigma} \cdot \hat{n} \tag{B.82}$$

where g and h are complex function of the energy, scattering angle θ and $\hat{n} = \frac{\vec{k}_i \times \vec{k}_f}{\left|\vec{k}_i \times \vec{k}_f\right|}$. The final state polarization $\vec{P}_f$ can then be expressed as

$$\vec{P}_f = \frac{(|g|^2 - |h|^2)\vec{P}_i + (gh^* + g^*h + 2|h|^2 \vec{P}_i \cdot \hat{n})\hat{n} + i(gh^* - g^*h)\vec{P}_i \times \hat{n}}{|g|^2 + |h|^2 + (gh^* + g^*h)\hat{n} \cdot \vec{P}_i} \tag{B.83}$$

and the differential cross section is given by

$$\frac{\mathrm{d}\sigma}{\mathrm{d}\Omega} = \left(|g|^2 + |h|^2 + (gh^* + g^*h)\hat{n} \cdot \vec{P}_i \right) \frac{k_f}{k_i} \,. \tag{B.84}$$

For the case of an unpolarized target ($\vec{P}_i = 0$), these relations simplify to

$$\frac{\mathrm{d}\sigma}{\mathrm{d}\Omega} = \left(|g|^2 + |h|^2 \right) \frac{k_f}{k_i}, \quad \vec{P}_f = \frac{(gh^* + g^*h)}{|g|^2 + |h|^2}\hat{n} = \frac{2\,\mathrm{Re}(gh^*)}{|g|^2 + |h|^2}\hat{n} \,. \tag{B.85}$$

The amplitudes g and h can be expressed by the partial wave amplitudes τ in the following way:

$$\begin{aligned} g = \frac{1}{2\sqrt{k_f k_i}} \sum_J (2J+1) \Big(& d^J_{\frac{1}{2}\frac{1}{2}}(\theta) \left[\tau^{J(J-\frac{1}{2})\frac{1}{2}} + \tau^{J(J+\frac{1}{2})\frac{1}{2}} \right] \cos\frac{\theta}{2} \\ & + d^J_{-\frac{1}{2}\frac{1}{2}}(\theta) \left[\tau^{J(J-\frac{1}{2})\frac{1}{2}} - \tau^{J(J+\frac{1}{2})\frac{1}{2}} \right] \sin\frac{\theta}{2} \Big) \,, \end{aligned} \tag{B.86}$$

$$\begin{aligned} h = \frac{-i}{2\sqrt{k_f k_i}} \sum_J (2J+1) \Big(& d^J_{\frac{1}{2}\frac{1}{2}}(\theta) \left[\tau^{J(J-\frac{1}{2})\frac{1}{2}} + \tau^{J(J+\frac{1}{2})\frac{1}{2}} \right] \sin\frac{\theta}{2} \\ & - d^J_{-\frac{1}{2}\frac{1}{2}}(\theta) \left[\tau^{J(J-\frac{1}{2})\frac{1}{2}} - \tau^{J(J+\frac{1}{2})\frac{1}{2}} \right] \cos\frac{\theta}{2} \Big) \,. \end{aligned} \tag{B.87}$$

Thus, we have the following explicit expression for the differential cross section:

$$\frac{\mathrm{d}\sigma}{\mathrm{d}\Omega} = \frac{1}{2k_i^2}\frac{1}{2}\left|\sum_J (2J+1)\left(\tau^{J(J-\frac{1}{2})\frac{1}{2}} + \tau^{J(J+\frac{1}{2})\frac{1}{2}}\right) d^J_{\frac{1}{2}\frac{1}{2}}(\theta)\right|^2$$
$$+ \frac{1}{2k_i^2}\frac{1}{2}\left|\sum_J (2J+1)\left(\tau^{J(J-\frac{1}{2})\frac{1}{2}} - \tau^{J(J+\frac{1}{2})\frac{1}{2}}\right) d^J_{-\frac{1}{2}\frac{1}{2}}(\theta)\right|^2 , \tag{B.88}$$

and the total cross section is given by

$$\sigma = \frac{1}{2}\frac{4\pi}{k_i^2}\sum_{JLS,L'S'}(2J+1)\left|\tau^{JL'S'}_{LS}\right|^2 . \tag{B.89}$$

The spin-rotation parameter β is the rotation angle of the spin projection on the scattering plane and is given by

$$\beta = \arctan\left(\frac{2\,\mathrm{Im}(h^* g)}{|g|^2 - |h|^2}\right) . \tag{B.90}$$

B.4.2. Observables for Photoproduction Reactions

In Sec. 3.5 we introduced the photoproduction amplitude. In our model we consider partial waves with $J \leq 9/2$ corresponding to orbital angular momenta $L \leq 5$. Note that this excludes E_{5+} and M_{5+}. The expressions for the amplitudes F_i resulting from Eqs. (3.64) and (3.65) are given by [114]:

$$\begin{aligned} F_1 =& - i\frac{4\pi W}{\sqrt{m_N m_B}}\frac{1}{128}\Big[32(4E_{0+} + 9E_{2+} + 4M_{2-} + 9M_{4-}) + 450E_{4+} + 2\cos(\theta)(192E_{1+} \\ &+ 360E_{3+} + 525E_{5+} - 64M_{1-} + 64M_{1+} + 168M_{3-} + 24M_{3+} + 345M_{5-} + 15M_{5+}) \\ &+ 8\cos(2\theta)(60E_{2+} + 105E_{4+} - 48M_{2-} + 48M_{2+} + 40M_{4-} + 20M_{4+}) \\ &+ 5\cos(3\theta)(112E_{3+} + 189E_{5+} - 144M_{3-} + 144M_{3+} + 49M_{5-} + 63M_{5+}) \\ &+ 70\cos(4\theta)(9E_{4+} + 16(M_{4+} - M_{4-})) + 63\cos(5\theta)(11E_{5+} + 25(M_{5+} - M_{5-}))\Big] , \end{aligned}$$

$$\begin{aligned} F_2 =& - i\frac{4\pi W}{\sqrt{m_N m_B}}\frac{1}{64}\Big[64M_{1-} + 128M_{1+} + 9(48M_{3-} + 64M_{3+} + 125M_{5-} + 150M_{5+}) \\ &+ 24\cos(\theta)(16M_{2-} + 24M_{2+} + 60M_{4-} + 75M_{4+}) + 60\cos(2\theta)(12M_{3-} + 16M_{3+} \\ &+ 35M_{5-} + 42M_{5+}) + 280\cos(3\theta)(4M_{4-} + 5M_{4+}) + 315\cos(4\theta)(5M_{5-} + 6M_{5+})\Big] , \end{aligned}$$

$$F_3 = -i\frac{4\pi W}{\sqrt{m_N m_B}}\frac{1}{64}\Big[192E_{1+} + 1200E_{3+} + 3675E_{5+} + 64M_{1-} - 64M_{1+}$$
$$+ 816M_{3-} - 624M_{3+} + 3525M_{5-} - 2325M_{5+}$$
$$+ 24\cos(\theta)(40E_{2+} + 172E_{4+} + 4(4M_{2-} - 4M_{2+} + 35M_{4-} - 25M_{4+}))$$
$$+ 60\cos(2\theta)(28E_{3+} + 105E_{5+} + 12M_{3-} - 12M_{3+} + 91M_{5-} - 63M_{5+})$$
$$+ 280\cos(3\theta)(9E_{4+} + 4M_{4-} - 4M_{4+}) + 315\cos(4\theta)(11E_{5+} + 5M_{5-} - 5M_{5+}\Big] ,$$

$$F_4 = -i\frac{4\pi W}{\sqrt{m_N m_B}}\frac{3}{8}\Big[-2(4E_{2+} + 25E_{4+} + 8M_{2-} - 4M_{2+} + 50M_{4-} - 25M_{4+})$$
$$- 5\cos(\theta)(8E_{3+} + 35E_{5+} + 16M_{3-} - 8M_{3+} + 70M_{5-} - 35M_{5+})$$
$$- 70\cos(2\theta)(E_{4+} + 2M_{4-} - M_{4+}) - 105\cos(3\theta)(E_{5+} + 2M_{5-} - M_{5+})\Big] ,$$

where m_B is the mass of the outgoing baryon. We consider the reaction for the pseudoscalar meson photoproduction process:

$$\gamma(k) + N(p) \to M(q) + B(p') , \tag{B.91}$$

where k, p, q and p' define the four momenta of the incident photon, target nucleon, emitted meson and recoil baryon, respectively. In the following we will explain our convention in the Jülich-Bonn model and give the definitions of the observables in terms of the multipole amplitude $\hat{\mathcal{M}}$ and in terms of the amplitudes F_i.

We introduce a set of coordinate independent unit vectors:

$$\hat{n}_3 = \hat{k}, \quad \hat{n}_2 = \frac{\hat{k}\times\hat{q}}{\left|\hat{k}\times\hat{q}\right|}, \quad \hat{n}_1 = \hat{n}_2 \times \hat{n}_3 . \tag{B.92}$$

The center-of-momentum (c.m.) Cartesian coordinate system $\{\hat{x},\hat{y},\hat{z}\}$, with $\vec{k}+\vec{p} = \vec{q}+\vec{p}' = 0$, and the laboratory (lab) Cartesian coordinate system $\{\hat{x}_L,\hat{y}_L,\hat{z}_L\}$, with $\vec{p}=0$, are given in terms of $\{\hat{n}_1,\hat{n}_2,\hat{n}_3\}$ by:

$$\{\hat{x},\hat{y},\hat{z}\} = \{\hat{n}_1,\hat{n}_2,\hat{n}_3\}_{\mathrm{cm}} , \tag{B.93}$$
$$\{\hat{x}_L,\hat{y}_L,\hat{z}_L\} = \{\hat{n}_1,\hat{n}_2,\hat{n}_3\}_{\mathrm{lab}} , \tag{B.94}$$

where the subscripts indicate the frame in which $\{\hat{n}_1,\hat{n}_2,\hat{n}_3\}$ is to be evaluated. The reaction plane is then defined by the $\hat{n}_1\hat{n}_3$-plane and $\hat{n}_2$ is perpendicular to it.

For a real photon one has two independent polarizations. A linearly polarized photon is characterised by the two photon polarization vectors parallel $\vec{\epsilon}_\parallel$ and perpendicular $\vec{\epsilon}_\perp$ to the reaction plane. We further define the polarized photon states obtained by rotating by an angle ϕ about the $\hat{n}_3$-axis by

$$\begin{aligned}\vec{\epsilon}_{\parallel'} &= \cos\phi\;\vec{\epsilon}_\parallel + \sin\phi\;\vec{\epsilon}_\perp ,\\ \vec{\epsilon}_{\perp'} &= -\sin\phi\;\vec{\epsilon}_\parallel + \cos\phi\;\vec{\epsilon}_\perp .\end{aligned} \tag{B.95}$$

Circularly polarized photons are characterized by

$$\vec{\epsilon}_\pm = \mp\frac{1}{\sqrt{2}}(\vec{\epsilon}_\parallel \pm i\vec{\epsilon}_\perp) \ . \tag{B.96}$$

We introduce the projection operator $\hat{P}_\lambda$ which projects onto the photon polarization state $\hat{P}_\lambda\vec{\epsilon} \equiv \vec{\epsilon}_\lambda$. Since these are projection operators, the relations $\hat{P}_{\lambda'}\hat{P}_\lambda = \delta_{\lambda'\lambda}$ and $\sum_\lambda \hat{P}_\lambda = 1$ hold. These projection operators $\hat{P}_\lambda$ are associated with the Stokes vector $\vec{P}^S$ (see e.g. [670]), which is used to specify the direction and degree of the photon polarization. The differences of projection operators can also be expressed in terms of Pauli spin matrices in the photon helicity space such as $\hat{P}_+ - \hat{P}_- = \sigma_{n_3}$ or $\hat{P}_\perp - \hat{P}_\parallel = \sigma_{n_1}$.

Now we can define coordinate-independent observables in terms of $\hat{\mathcal{M}}$. Note, with a Lorentz invariant amplitude $\hat{\mathcal{M}}$ the observables themselves are also Lorentz invariants. One defines the cross section by:

$$\frac{\mathrm{d}\sigma}{\mathrm{d}\Omega} = \frac{1}{4}\,\mathrm{Tr}\left[\hat{\mathcal{M}}\hat{\mathcal{M}}^\dagger\right] \ , \tag{B.97}$$

where the trace runs over the nucleon spin and photon polarizations. The factor 1/4 originates from the averaging over the target-nucleon spin and the incident photon-beam polarization.

Next we define the single polarization observables, labeled beam (Σ), target (T) and recoil (P) polarization asymmetries, by:

$$\begin{aligned}
\frac{\mathrm{d}\sigma}{\mathrm{d}\Omega}\Sigma &\equiv \frac{1}{4}\,\mathrm{Tr}\left[\hat{\mathcal{M}}(\hat{P}_\perp - \hat{P}_\parallel)\hat{\mathcal{M}}^\dagger\right] \ , \\
\frac{\mathrm{d}\sigma}{\mathrm{d}\Omega}T &\equiv \frac{1}{4}\,\mathrm{Tr}\left[\hat{\mathcal{M}}\sigma_{n_2}\hat{\mathcal{M}}^\dagger\right] \ , \\
\frac{\mathrm{d}\sigma}{\mathrm{d}\Omega}P &\equiv \frac{1}{4}\,\mathrm{Tr}\left[\hat{\mathcal{M}}\hat{\mathcal{M}}^\dagger\sigma_{n_2}\right] \ .
\end{aligned} \tag{B.98}$$

For the beam-target asymmetries (E, F, G, H) we have the definitions:

$$\begin{aligned}
\frac{\mathrm{d}\sigma}{\mathrm{d}\Omega}E &\equiv -\frac{1}{4}\,\mathrm{Tr}\left[\hat{\mathcal{M}}(\hat{P}_+ - \hat{P}_-)\sigma_{n_3}\hat{\mathcal{M}}^\dagger\right] \ , \\
\frac{\mathrm{d}\sigma}{\mathrm{d}\Omega}F &\equiv \frac{1}{4}\,\mathrm{Tr}\left[\hat{\mathcal{M}}(\hat{P}_+ - \hat{P}_-)\sigma_{n_1}\hat{\mathcal{M}}^\dagger\right] \ , \\
\frac{\mathrm{d}\sigma}{\mathrm{d}\Omega}G &\equiv -\frac{1}{4}\,\mathrm{Tr}\left[\hat{\mathcal{M}}(\hat{P}_{\perp'} - \hat{P}_{\parallel'})\sigma_{n_3}\hat{\mathcal{M}}^\dagger\right] \ , \\
\frac{\mathrm{d}\sigma}{\mathrm{d}\Omega}H &\equiv \frac{1}{4}\,\mathrm{Tr}\left[\hat{\mathcal{M}}(\hat{P}_{\perp'} - \hat{P}_{\parallel'})\sigma_{n_1}\hat{\mathcal{M}}^\dagger\right] \ .
\end{aligned} \tag{B.99}$$

The projection operators $\hat{P}_{\parallel'}$ and $\hat{P}_{\perp'}$ correspond to the photon polarizations of Eq. (B.95) with $\phi = \pi/4$. Note that we introduced a minus sign in the definitions of E and G to match the convention of the SAID group in the c.m. frame.

The beam-recoil asymmetries labeled as $C_{n'_i}$ and $O_{n'_i}$ with $i = (1,3)$ are given by:

$$\begin{aligned}
\frac{\mathrm{d}\sigma}{\mathrm{d}\Omega} C_{n'_i} &\equiv -\frac{1}{4} \operatorname{Tr}\left[\hat{\mathcal{M}}(\hat{P}_+ - \hat{P}_-)\hat{\mathcal{M}}^\dagger \sigma_{n'_i}\right] \;, \\
\frac{\mathrm{d}\sigma}{\mathrm{d}\Omega} O_{n'_i} &\equiv \frac{1}{4} \operatorname{Tr}\left[\hat{\mathcal{M}}(\hat{P}_{\perp'} - \hat{P}_{\parallel'})\hat{\mathcal{M}}^\dagger \sigma_{n'_i}\right] \;.
\end{aligned} \tag{B.100}$$

One obtains $\{\hat{n}'_1, \hat{n}'_2, \hat{n}'_3\}$ by rotating $\{\hat{n}_1, \hat{n}_2, \hat{n}_3\}$ counterclockwise by an angle θ (defined by $\cos\theta = \hat{q} \cdot \hat{n}_3$) about the $\hat{n}_2$-axis such that $\hat{n}'_3$ is in the direction of the emitted meson momentum $\vec{q}$. The full relations are given by:

$$\begin{aligned}
\hat{n}'_1 &= \cos\theta \hat{n}_1 - \sin\theta \hat{n}_3 \;, \\
\hat{n}'_3 &= \sin\theta \hat{n}_1 + \cos\theta \hat{n}_3 \\
\hat{n}'_2 &= \hat{n}_2 \;.
\end{aligned} \tag{B.101}$$

Lastly we have the target-recoil asymmetries $L_{n'_i}$ and $T_{n'_i}$ with $i = (1,3)$. These are defined by:

$$\begin{aligned}
\frac{\mathrm{d}\sigma}{\mathrm{d}\Omega} L_{n'_i} &\equiv \xi_i \frac{1}{4} \operatorname{Tr}\left[\hat{\mathcal{M}}\sigma_{n_3}\hat{\mathcal{M}}^\dagger \sigma_{n'_i}\right] \;, \\
\frac{\mathrm{d}\sigma}{\mathrm{d}\Omega} T_{n'_i} &\equiv \frac{1}{4} \operatorname{Tr}\left[\hat{\mathcal{M}}\sigma_{n_1}\hat{\mathcal{M}}^\dagger \sigma_{n'_i}\right] \;,
\end{aligned} \tag{B.102}$$

where $\xi_1 = -1$ and $\xi_3 = +1$ were introduced to match the SAID convention in the c.m. frame. A list of different conventions used by the various groups in the field may be found in Ref. [671].

We can further write these observables in terms of the amplitudes F_i. The differential cross section then reads:

$$\frac{\mathrm{d}\sigma}{\mathrm{d}\Omega} = |F_1|^2 + \frac{1}{2}\Big(|F_2|^2 + {F_3}^2 + {F_4}^2 + 2\,\mathrm{Re}\left[(F_1 + F_3\cos\theta)F_4^*\right]\Big)\sin^2\theta \;. \tag{B.103}$$

To get the physical cross section $d\sigma_0/d\Omega$, one needs to multiply the incident flux and the final state phase-space density factors which have been omitted in Eq. (B.103):

$$\frac{\mathrm{d}\sigma_0}{\mathrm{d}\Omega} \equiv \left(\frac{m_N}{4\pi W}\right)^2 \frac{|\vec{q}|}{\left|\vec{k}\right|} \frac{\mathrm{d}\sigma}{\mathrm{d}\Omega} \;. \tag{B.104}$$

The single polarization observables in terms of F_i are given by:

$$\begin{aligned}
\frac{\mathrm{d}\sigma}{\mathrm{d}\Omega}\Sigma &= \frac{1}{2}\left[|F_2|^2 - |F_3|^2 - |F_4|^2 - 2\,\mathrm{Re}\left[(F_1 + F_3\cos\theta)F_4^*\right]\right]\sin^2\theta \;, \\
\frac{\mathrm{d}\sigma}{\mathrm{d}\Omega}T &= \mathrm{Im}\left[(-F_2 + F_3 + F_4\cos\theta)F_1^* + (F_3 + F_4\cos\theta)F_4^*\sin^2\theta\right]\sin\theta \;, \\
\frac{\mathrm{d}\sigma}{\mathrm{d}\Omega}P &= -\,\mathrm{Im}\left[(F_2 + F_3 + F_4\cos\theta)F_1^* + (F_3 + F_4\cos\theta)F_4^*\sin^2\theta\right]\sin\theta \;.
\end{aligned} \tag{B.105}$$

The double-polarization observables are then rewritten as:

$$
\begin{aligned}
\frac{\mathrm{d}\sigma}{\mathrm{d}\Omega}E &= |F_1|^2 + \mathrm{Re}\,[F_2^*(F_3+F_4\cos\theta)+F_1^*F_4]\sin^2\theta \ , \\
\frac{\mathrm{d}\sigma}{\mathrm{d}\Omega}F &= -\,\mathrm{Re}\left[F_2^*(F_1+F_4\sin^2\theta)-F_1^*(F_3+F_4\cos\theta)\right]\sin\theta \ , \\
\frac{\mathrm{d}\sigma}{\mathrm{d}\Omega}G &= \mathrm{Im}\,[F_2^*(F_3+F_4\cos\theta)+F_1^*F_4]\sin^2\theta \ , \\
\frac{\mathrm{d}\sigma}{\mathrm{d}\Omega}H &= -\,\mathrm{Im}\left[F_2^*(F_1+F_4\sin^2\theta)-F_1^*(F_3+F_4\cos\theta)\sin\theta\right]\sin\theta \ .
\end{aligned}
\tag{B.106}
$$

The beam-recoil polarizations then become:

$$
\begin{aligned}
\frac{\mathrm{d}\sigma}{\mathrm{d}\Omega}C_{n_1'} &= \left\{|F_1|^2+\mathrm{Re}\left[F_1^*(F_2+F_3)\cos\theta+(F_1^*F_4-F_2^*F_3\sin^2\theta)\right]\right\}\sin\theta \ , \\
\frac{\mathrm{d}\sigma}{\mathrm{d}\Omega}C_{n_3'} &= -|F_1|^2\cos\theta+\mathrm{Re}\,[F_1^*(F_2+F_3)+F_2^*(F_3\cos\theta+F_4)]\sin^2\theta \ .
\end{aligned}
\tag{B.107}
$$

In our case we determine $C_{n_1'} = C_{x'}$ and $C_{n_3'} = C_{z'}$ in the c.m. frame, where the Cartesian coordinates $\{\hat{x}', \hat{y}', \hat{z}'\}$ are identifies with $\{\hat{n}_1', \hat{n}_2', \hat{n}_3'\}_{\mathrm{cm}}$. However, experimentalists usually report the beam-target asymmetries in the lab frame and different groups use different lab coordinate frames. We then define the coordinates for $C_{x_L'}$ and $C_{z_L'}$ by a rotation of $\{\hat{x}_L, \hat{y}_L, \hat{z}_L\}$ by an angle $\pi - \theta_{p_L'}$ about the $\hat{y}_L$-axis, where $\theta_{p_L'}$ denotes the recoil nucleon scattering angle $\cos\theta_{p_L'} \equiv \hat{p}_L' \cdot \hat{z}_L$. To obtain the beam-recoil polarization observables in the lab frame, one has to perform a combination of Lorentz boosts and rotations [430]:

$$
\begin{aligned}
C_{x_L'} &= \cos\theta_r C_{x'} - \sin\theta_r C_{z'} \ , \\
C_{z_L'} &= \sin\theta_r C_{x'} + \cos\theta_r C_{z'} \ ,
\end{aligned}
\tag{B.108}
$$

with the rotation angle θ_r defined by:

$$
\begin{aligned}
\cos\theta_r &= -\cos\theta\cos\theta_{p_L'} - \gamma_3\sin\theta\sin\theta_{p_L'} \ , \\
\sin\theta_r &= \gamma_1\left[\cos\theta_{p_L'}\sin\theta + \gamma_3\sin\theta_{p_L'}(\beta_1\beta_3-\cos\theta)\right] \ ,
\end{aligned}
\tag{B.109}
$$

and with the Lorentz boost parameters

$$
\beta_1 = \frac{|\vec{q}|}{\sqrt{\vec{q}^2+m_N^2}}, \quad \beta_3 = \frac{\left|\vec{k}_L\right|}{\sqrt{\vec{k}_L^2+m_N^2}}, \quad \gamma_i = \frac{1}{\sqrt{1-\beta_i^2}} \ . \tag{B.110}
$$

The meson momentum in the c.m. frame is given by $\vec{q}$ and the photon momentum in the lab frame is denoted as $\vec{k}_L$. We further want to introduce the difference of helicity cross sections:

$$
\frac{\mathrm{d}\Delta\sigma}{\mathrm{d}\Omega} = \frac{\mathrm{d}\sigma_{3/2}}{\mathrm{d}\Omega} - \frac{\mathrm{d}\sigma_{1/2}}{\mathrm{d}\Omega} \ , \tag{B.111}
$$

where the subscript for the cross sections denotes parallel ($\lambda_N - \lambda_\gamma = \pm 3/2$) or anti-parallel ($\lambda_N - \lambda_\gamma = \pm 1/2$) initial state helicities. This quantity is closely related to the helicity asymmetry E by:

$$\frac{\mathrm{d}\Delta\sigma}{\mathrm{d}\Omega} = -2\frac{\mathrm{d}\sigma_0}{\mathrm{d}\Omega}E \ , \tag{B.112}$$

where the factor 2 is introduced because $d\sigma_0/d\Omega$ contains a factor for averaging over initial spins of 1/4 but $d\Delta\sigma/d\Omega$ only has a factor of 1/2.

C. Isospin factors for photoproduction reactions

In this section we calculate the isospin factors for the amplitudes of the photoproduction processes in detail. For this we defined the factors in Sec. 5.1 as

$$C^{I_\gamma,I}_{\gamma N\to mb} = \langle I_N, m_N, I_\gamma, m_\gamma | I, M\rangle \cdot \langle I, M | I_b, m_b, I_m, m_m\rangle \ , \tag{C.1}$$

and we also defined the photoproduction amplitudes by

$$\begin{aligned} T^{mb}_\gamma &= \langle I_b, m_b, I_m, m_m | \, T_{f\gamma} \, | I_\gamma, m_\gamma, I_N, m_N\rangle \\ &= \sum_{(I_\gamma,I)} C^{I_\gamma,I}_{\gamma N\to mb} \cdot T^{I_\gamma,I}_{f\gamma} = C^{1,\frac{3}{2}}_{\gamma N\to mb} \cdot T^{1,\frac{3}{2}}_{f\gamma} + C^{1,\frac{1}{2}}_{\gamma N\to mb} \cdot T^{1,\frac{1}{2}}_{f\gamma} + C^{0,\frac{1}{2}}_{\gamma N\to mb} \cdot T^{0,\frac{1}{2}}_{f\gamma} \ . \end{aligned}$$

Let us start with the reaction $\gamma p \to \pi^0 p$ in detail. If we consider the case of an isoscalar photon $|I_\gamma, m_\gamma\rangle = |0,0\rangle$, we can only couple it with the proton $|I_p, m_p\rangle = |1/2, +1/2\rangle$ to the state $|I, M\rangle = |1/2, +1/2\rangle$. With the final state of $|\pi^0 p\rangle = |1/2, +1/2, 1, 0\rangle$ we can derive the isospin factor:

$$\begin{aligned} C^{0,\frac{1}{2}}_{\gamma p\to\pi^0 p} &= \left\langle \frac{1}{2}, +\frac{1}{2}, 0, 0 \middle| \frac{1}{2}, +\frac{1}{2} \right\rangle \left\langle \frac{1}{2}, +\frac{1}{2} \middle| \frac{1}{2}, +\frac{1}{2}, 1, 0 \right\rangle \\ &= (-1)^{\frac{1}{2}-\frac{1}{2}-0} \cdot 1 \cdot (-1)^{\frac{1}{2}-\frac{1}{2}-1} \cdot \left(-\frac{1}{\sqrt{3}}\right) \\ &= \frac{1}{\sqrt{3}} \ . \end{aligned} \tag{C.2}$$

Now we consider the isovector component of the photon $|I_\gamma, m_\gamma\rangle = |1,0\rangle$. Here we have to calculate two isospin factors for $I = 1/2$ and $I = 3/2$:

$$\begin{aligned} C^{1,\frac{1}{2}}_{\gamma p\to\pi^0 p} &= \left\langle \frac{1}{2}, +\frac{1}{2}, 1, 0 \middle| \frac{1}{2}, +\frac{1}{2} \right\rangle \left\langle \frac{1}{2}, +\frac{1}{2} \middle| \frac{1}{2}, +\frac{1}{2}, 1, 0 \right\rangle \\ &= (-1)^{\frac{1}{2}-\frac{1}{2}-1} \cdot \left(-\frac{1}{\sqrt{3}}\right) \cdot (-1)^{\frac{1}{2}-\frac{1}{2}-1} \cdot \left(-\frac{1}{\sqrt{3}}\right) \\ &= \frac{1}{3} \ , \end{aligned} \tag{C.3}$$

$$\begin{aligned} C^{1,\frac{3}{2}}_{\gamma p\to\pi^0 p} &= \left\langle \frac{1}{2}, +\frac{1}{2}, 1, 0 \middle| \frac{3}{2}, +\frac{1}{2} \right\rangle \left\langle \frac{3}{2}, +\frac{1}{2} \middle| \frac{1}{2}, +\frac{1}{2}, 1, 0 \right\rangle \\ &= (-1)^{\frac{3}{2}-\frac{1}{2}-1} \cdot \left(\sqrt{\frac{2}{3}}\right) \cdot (-1)^{\frac{3}{2}-\frac{1}{2}-1} \cdot \left(\sqrt{\frac{2}{3}}\right) \\ &= \frac{2}{3} \ . \end{aligned} \tag{C.4}$$

This leads to the amplitude:

$$T^{\pi^0 p}_\gamma = \frac{2}{3} T^{1,\frac{3}{2}}_{\pi N\gamma} + \frac{1}{3} T^{1,\frac{1}{2}}_{\pi N\gamma} + \frac{1}{\sqrt{3}} T^{0,\frac{1}{2}}_{\pi N\gamma} \ . \tag{C.5}$$

For the process $\gamma p \to \pi^+ n$, we find the following isospin factors:

$$\begin{aligned}
C^{0,\frac{1}{2}}_{\gamma p\to\pi^+ n} &= \left\langle \frac{1}{2},+\frac{1}{2},0,0 \middle| \frac{1}{2},+\frac{1}{2} \right\rangle \left\langle \frac{1}{2},+\frac{1}{2} \middle| \frac{1}{2},-\frac{1}{2},1,1 \right\rangle \\
&= (-1)^{\frac{1}{2}-\frac{1}{2}-0} \cdot 1 \cdot (-1)^{\frac{1}{2}-\frac{1}{2}-1} \cdot \left(\sqrt{\frac{2}{3}}\right) \\
&= -\sqrt{\frac{2}{3}} \ , \qquad \text{(C.6)}
\end{aligned}$$

$$\begin{aligned}
C^{1,\frac{1}{2}}_{\gamma p\to\pi^+ n} &= \left\langle \frac{1}{2},+\frac{1}{2},1,0 \middle| \frac{1}{2},+\frac{1}{2} \right\rangle \left\langle \frac{1}{2},+\frac{1}{2} \middle| \frac{1}{2},-\frac{1}{2},1,1 \right\rangle \\
&= (-1)^{\frac{1}{2}-\frac{1}{2}-1} \cdot \left(-\frac{1}{\sqrt{3}}\right) \cdot (-1)^{\frac{1}{2}-\frac{1}{2}-1} \cdot \left(\sqrt{\frac{2}{3}}\right) \\
&= -\frac{\sqrt{2}}{3} \ , \qquad \text{(C.7)}
\end{aligned}$$

$$\begin{aligned}
C^{1,\frac{3}{2}}_{\gamma p\to\pi^+ n} &= \left\langle \frac{1}{2},+\frac{1}{2},1,0 \middle| \frac{3}{2},+\frac{1}{2} \right\rangle \left\langle \frac{3}{2},+\frac{1}{2} \middle| \frac{1}{2},-\frac{1}{2},1,1 \right\rangle \\
&= (-1)^{\frac{3}{2}-\frac{1}{2}-1} \cdot \left(\sqrt{\frac{2}{3}}\right) \cdot (-1)^{\frac{3}{2}-\frac{1}{2}-1} \cdot \left(\frac{1}{\sqrt{3}}\right) \\
&= \frac{\sqrt{2}}{3} \ . \qquad \text{(C.8)}
\end{aligned}$$

Thus, the full amplitude can be written as:

$$T^{\pi^+ n}_{\gamma} = \frac{\sqrt{2}}{3} T^{1,\frac{3}{2}}_{\pi N\gamma} - \frac{\sqrt{2}}{3} T^{1,\frac{1}{2}}_{\pi N\gamma} - \sqrt{\frac{2}{3}} T^{0,\frac{1}{2}}_{\pi N\gamma} \ . \qquad \text{(C.9)}$$

Here we can use the phase definition of π^+ again to get $T^{\pi^+ n}_{f\gamma} \to -T^{\pi^+ n}_{f\gamma}$.

The next reaction is $\gamma p \to \eta p$. The η-meson is an isospin singlet $|0,0\rangle$ and thus the state can only couple to an isospin 1/2-state with the proton. Thus, we have

$$C^{1,\frac{3}{2}}_{\gamma p\to\eta p} = 0 \ .$$

The other two isospin factors are then given by:

$$\begin{aligned}
C^{0,\frac{1}{2}}_{\gamma p\to\eta p} &= \left\langle \frac{1}{2},+\frac{1}{2},0,0 \middle| \frac{1}{2},+\frac{1}{2} \right\rangle \left\langle \frac{1}{2},+\frac{1}{2} \middle| \frac{1}{2},\frac{1}{2},0,0 \right\rangle \\
&= (-1)^{\frac{1}{2}-\frac{1}{2}-0} \cdot 1 \cdot (-1)^{\frac{1}{2}-\frac{1}{2}-0} \cdot 1 \\
&= 1 \ , \qquad \text{(C.10)}
\end{aligned}$$

$$
\begin{aligned}
C^{1,\frac{1}{2}}_{\gamma p\to\eta p} &= \left\langle \frac{1}{2},+\frac{1}{2},1,0\middle|\frac{1}{2},+\frac{1}{2}\right\rangle \left\langle \frac{1}{2},+\frac{1}{2}\middle|\frac{1}{2},\frac{1}{2},0,0\right\rangle \\
&= (-1)^{\frac{1}{2}-\frac{1}{2}-1}\cdot\left(-\frac{1}{\sqrt{3}}\right)\cdot(-1)^{\frac{1}{2}-\frac{1}{2}-0}\cdot 1 \\
&= \frac{1}{\sqrt{3}}\ ,
\end{aligned} \tag{C.11}
$$

and the amplitude

$$
T^{\eta p}_{\gamma} = \frac{1}{\sqrt{3}}T^{1,\frac{1}{2}}_{\eta N\gamma} + T^{0,\frac{1}{2}}_{\eta N\gamma}\ . \tag{C.12}
$$

For the final state $K^+\Lambda$, we again have the combination of an isosinglet $|\Lambda\rangle = |0,0\rangle$ and an isospin 1/2 as $|K^+\rangle = |1/2,+1/2\rangle$. This leads to the same isospin factors as for the ηp final state and we find the amplitude:

$$
T^{K^+\Lambda}_{\gamma} = \frac{1}{\sqrt{3}}T^{1,\frac{1}{2}}_{K\Lambda\gamma} + T^{0,\frac{1}{2}}_{K\Lambda\gamma}\ . \tag{C.13}
$$

For the process $\gamma p \to K^0\Sigma^+$ we are dealing with the isovector $|\Sigma^+\rangle = |1,1\rangle$ as the final state baryon and the meson $|K^0\rangle = |1/2,-1/2\rangle$. The isospin factors are then determined in the following way:

$$
\begin{aligned}
C^{0,\frac{1}{2}}_{\gamma p\to K^0\Sigma^+} &= \left\langle \frac{1}{2},+\frac{1}{2},0,0\middle|\frac{1}{2},+\frac{1}{2}\right\rangle \left\langle \frac{1}{2},+\frac{1}{2}\middle|1,1,\frac{1}{2},-\frac{1}{2}\right\rangle \\
&= (-1)^{\frac{1}{2}-\frac{1}{2}-0}\cdot 1\cdot\left(\sqrt{\frac{2}{3}}\right) \\
&= \sqrt{\frac{2}{3}}\ ,
\end{aligned} \tag{C.14}
$$

$$
\begin{aligned}
C^{1,\frac{1}{2}}_{\gamma p\to K^0\Sigma^+} &= \left\langle \frac{1}{2},+\frac{1}{2},1,0\middle|\frac{1}{2},+\frac{1}{2}\right\rangle \left\langle \frac{1}{2},+\frac{1}{2}\middle|1,1,\frac{1}{2},-\frac{1}{2}\right\rangle \\
&= (-1)^{\frac{1}{2}-\frac{1}{2}-1}\cdot\left(-\frac{1}{\sqrt{3}}\right)\cdot\left(\sqrt{\frac{2}{3}}\right) \\
&= \frac{\sqrt{2}}{3}\ ,
\end{aligned} \tag{C.15}
$$

$$
\begin{aligned}
C^{1,\frac{3}{2}}_{\gamma p\to K^0\Sigma^+} &= \left\langle \frac{1}{2},+\frac{1}{2},1,0\middle|\frac{3}{2},+\frac{1}{2}\right\rangle \left\langle \frac{3}{2},+\frac{1}{2}\middle|1,1,\frac{1}{2},-\frac{1}{2}\right\rangle \\
&= (-1)^{\frac{3}{2}-\frac{1}{2}-1}\cdot\left(\sqrt{\frac{2}{3}}\right)\cdot\left(\frac{1}{\sqrt{3}}\right) \\
&= \frac{\sqrt{2}}{3}\ .
\end{aligned} \tag{C.16}
$$

This leads to the amplitude

$$T_\gamma^{K^0\Sigma^+} = \frac{\sqrt{2}}{3}T^{1,\frac{3}{2}}_{K\Sigma\gamma} + \frac{\sqrt{2}}{3}T^{1,\frac{1}{2}}_{K\Sigma\gamma} + \sqrt{\frac{2}{3}}T^{0,\frac{1}{2}}_{K\Sigma\gamma} \ . \tag{C.17}$$

The last process with a proton target is $\gamma p \to K^+\Sigma^0$. Here we are dealing with the final state hadrons $|\Sigma^0\rangle = |1,0\rangle$ and $|K^+\rangle = |1/2, +1/2\rangle$ and get the isospin factors:

$$\begin{aligned} C^{0,\frac{1}{2}}_{\gamma p\to K^+\Sigma^0} &= \left\langle \frac{1}{2},+\frac{1}{2},0,0\middle|\frac{1}{2},+\frac{1}{2}\right\rangle \left\langle \frac{1}{2},+\frac{1}{2}\middle|1,0,\frac{1}{2},+\frac{1}{2}\right\rangle \\ &= (-1)^{\frac{1}{2}-\frac{1}{2}-0}\cdot 1\cdot\left(-\frac{1}{\sqrt{3}}\right) \\ &= -\frac{1}{\sqrt{3}} \ , \end{aligned} \tag{C.18}$$

$$\begin{aligned} C^{1,\frac{1}{2}}_{\gamma p\to K^+\Sigma^0} &= \left\langle \frac{1}{2},+\frac{1}{2},1,0\middle|\frac{1}{2},+\frac{1}{2}\right\rangle \left\langle \frac{1}{2},+\frac{1}{2}\middle|1,0,\frac{1}{2},+\frac{1}{2}\right\rangle \\ &= (-1)^{\frac{1}{2}-\frac{1}{2}-1}\cdot\left(-\frac{1}{\sqrt{3}}\right)\cdot\left(-\frac{1}{\sqrt{3}}\right) \\ &= -\frac{1}{3} \ , \end{aligned} \tag{C.19}$$

$$\begin{aligned} C^{1,\frac{3}{2}}_{\gamma p\to K^+\Sigma^0} &= \left\langle \frac{1}{2},+\frac{1}{2},1,0\middle|\frac{3}{2},+\frac{1}{2}\right\rangle \left\langle \frac{3}{2},+\frac{1}{2}\middle|1,0,\frac{1}{2},+\frac{1}{2}\right\rangle \\ &= (-1)^{\frac{3}{2}-\frac{1}{2}-1}\cdot\left(\sqrt{\frac{2}{3}}\right)\cdot\left(\sqrt{\frac{2}{3}}\right) \\ &= \frac{2}{3} \ . \end{aligned} \tag{C.20}$$

This gives us the amplitude

$$T_\gamma^{K^+\Sigma^0} = \frac{2}{3}T^{1,\frac{3}{2}}_{K\Sigma\gamma} - \frac{1}{3}T^{1,\frac{1}{2}}_{K\Sigma\gamma} - \frac{1}{\sqrt{3}}T^{0,\frac{1}{2}}_{K\Sigma\gamma} \ . \tag{C.21}$$

Next we calculate the isospin factors for photoproduction processes with neutron target $\gamma n \to X$. The difference is that the intermediate state Here we start with the $\pi^0 n$ final state:

$$\begin{aligned} C^{0,\frac{1}{2}}_{\gamma n\to \pi^0 n} &= \left\langle \frac{1}{2},-\frac{1}{2},0,0\middle|\frac{1}{2},-\frac{1}{2}\right\rangle \left\langle \frac{1}{2},-\frac{1}{2}\middle|\frac{1}{2},-\frac{1}{2},1,0\right\rangle \\ &= (-1)^{\frac{1}{2}-\frac{1}{2}-0}\cdot 1\cdot(-1)^{\frac{1}{2}-\frac{1}{2}-1}\cdot\left(\frac{1}{\sqrt{3}}\right) \\ &= -\frac{1}{\sqrt{3}} \ , \end{aligned} \tag{C.22}$$

$$\begin{aligned}
C^{1,\frac{1}{2}}_{\gamma n\to\pi^0 n} &= \left\langle\frac{1}{2},-\frac{1}{2},1,0\middle|\frac{1}{2},-\frac{1}{2}\right\rangle\left\langle\frac{1}{2},-\frac{1}{2}\middle|\frac{1}{2},-\frac{1}{2},1,0\right\rangle \\
&= (-1)^{\frac{1}{2}-\frac{1}{2}-1}\cdot\left(\frac{1}{\sqrt{3}}\right)\cdot(-1)^{\frac{1}{2}-\frac{1}{2}-1}\cdot\left(\frac{1}{\sqrt{3}}\right) \\
&= \frac{1}{3}\ ,
\end{aligned} \tag{C.23}$$

$$\begin{aligned}
C^{1,\frac{3}{2}}_{\gamma n\to\pi^0 n} &= \left\langle\frac{1}{2},-\frac{1}{2},1,0\middle|\frac{3}{2},-\frac{1}{2}\right\rangle\left\langle\frac{3}{2},-\frac{1}{2}\middle|\frac{1}{2},-\frac{1}{2},1,0\right\rangle \\
&= (-1)^{\frac{3}{2}-\frac{1}{2}-1}\cdot\left(\sqrt{\frac{2}{3}}\right)\cdot(-1)^{\frac{3}{2}-\frac{1}{2}-1}\cdot\left(\sqrt{\frac{2}{3}}\right) \\
&= \frac{2}{3}\ .
\end{aligned} \tag{C.24}$$

This leads to the amplitude

$$T^{\pi^0 n}_{\gamma} = \frac{2}{3}T^{1,\frac{3}{2}}_{\pi N\gamma} + \frac{1}{3}T^{1,\frac{1}{2}}_{\pi N\gamma} - \frac{1}{\sqrt{3}}T^{0,\frac{1}{2}}_{\pi N\gamma}\ . \tag{C.25}$$

For the final state $\pi^- p$ we are dealing with $|\pi^-\rangle = |1,-1\rangle$ and $|p\rangle = |1/2,+1/2\rangle$. This gives us the following isospin factors:

$$\begin{aligned}
C^{0,\frac{1}{2}}_{\gamma n\to\pi^- p} &= \left\langle\frac{1}{2},-\frac{1}{2},0,0\middle|\frac{1}{2},-\frac{1}{2}\right\rangle\left\langle\frac{1}{2},-\frac{1}{2}\middle|\frac{1}{2},+\frac{1}{2},1,-1\right\rangle \\
&= (-1)^{\frac{1}{2}-\frac{1}{2}-0}\cdot 1\cdot(-1)^{\frac{1}{2}-\frac{1}{2}-1}\cdot\left(-\sqrt{\frac{2}{3}}\right) \\
&= \sqrt{\frac{2}{3}}\ ,
\end{aligned} \tag{C.26}$$

$$\begin{aligned}
C^{1,\frac{1}{2}}_{\gamma n\to\pi^- p} &= \left\langle\frac{1}{2},-\frac{1}{2},1,0\middle|\frac{1}{2},-\frac{1}{2}\right\rangle\left\langle\frac{1}{2},-\frac{1}{2}\middle|\frac{1}{2},+\frac{1}{2},1,-1\right\rangle \\
&= (-1)^{\frac{1}{2}-\frac{1}{2}-1}\cdot\left(\frac{1}{\sqrt{3}}\right)\cdot(-1)^{\frac{1}{2}-\frac{1}{2}-1}\cdot\left(-\sqrt{\frac{2}{3}}\right) \\
&= -\frac{\sqrt{2}}{3}\ ,
\end{aligned} \tag{C.27}$$

$$\begin{aligned}
C^{1,\frac{3}{2}}_{\gamma n\to\pi^- p} &= \left\langle\frac{1}{2},-\frac{1}{2},1,0\middle|\frac{3}{2},-\frac{1}{2}\right\rangle\left\langle\frac{3}{2},-\frac{1}{2}\middle|\frac{1}{2},+\frac{1}{2},1,-1\right\rangle \\
&= (-1)^{\frac{3}{2}-\frac{1}{2}-1}\cdot\left(\sqrt{\frac{2}{3}}\right)\cdot(-1)^{\frac{3}{2}-\frac{1}{2}-1}\cdot\left(\frac{1}{\sqrt{3}}\right) \\
&= \frac{\sqrt{2}}{3}\ ,
\end{aligned} \tag{C.28}$$

and we find

$$T_{\gamma}^{\pi^- p} = \frac{\sqrt{2}}{3} T_{\pi N\gamma}^{1,\frac{3}{2}} - \frac{\sqrt{2}}{3} T_{\pi N\gamma}^{1,\frac{1}{2}} + \sqrt{\frac{2}{3}} T_{\pi N\gamma}^{0,\frac{1}{2}} \ . \tag{C.29}$$

For the final-state ηn we get

$$\begin{aligned} C_{\gamma n\to\eta n}^{0,\frac{1}{2}} &= \left\langle \frac{1}{2}, -\frac{1}{2}, 0, 0 \middle| \frac{1}{2}, -\frac{1}{2} \right\rangle \left\langle \frac{1}{2}, -\frac{1}{2} \middle| \frac{1}{2}, -\frac{1}{2}, 0, 0 \right\rangle \\ &= (-1)^{\frac{1}{2}-\frac{1}{2}-0} \cdot 1 \cdot (-1)^{\frac{1}{2}-\frac{1}{2}-0} \cdot 1 \\ &= 1 \ , \end{aligned} \tag{C.30}$$

$$\begin{aligned} C_{\gamma n\to\eta n}^{1,\frac{1}{2}} &= \left\langle \frac{1}{2}, -\frac{1}{2}, 1, 0 \middle| \frac{1}{2}, -\frac{1}{2} \right\rangle \left\langle \frac{1}{2}, -\frac{1}{2} \middle| \frac{1}{2}, -\frac{1}{2}, 0, 0 \right\rangle \\ &= (-1)^{\frac{1}{2}-\frac{1}{2}-1} \cdot \left(\frac{1}{\sqrt{3}} \right) \cdot (-1)^{\frac{1}{2}-\frac{1}{2}-0} \cdot 1 \\ &= -\frac{1}{\sqrt{3}} \ , \end{aligned} \tag{C.31}$$

$$C_{\gamma n\to\eta n}^{1,\frac{3}{2}} = 0 \ . \tag{C.32}$$

This leads to the amplitude

$$T_{\gamma}^{\eta n} = -\frac{1}{\sqrt{3}} T_{\eta N\gamma}^{1,\frac{1}{2}} + T_{\eta N\gamma}^{0,\frac{1}{2}} \ . \tag{C.33}$$

For the process $\gamma n \to K^0\Lambda$ we have the final state meson $|K^0\rangle = |1/2, -1/2\rangle$ and baryon $|\Lambda\rangle = |0, 0\rangle$. This gives us the isospin factors

$$\begin{aligned} C_{\gamma n\to K^0\Lambda}^{0,\frac{1}{2}} &= \left\langle \frac{1}{2}, -\frac{1}{2}, 0, 0 \middle| \frac{1}{2}, -\frac{1}{2} \right\rangle \left\langle \frac{1}{2}, -\frac{1}{2} \middle| 0, 0, \frac{1}{2}, -\frac{1}{2} \right\rangle \\ &= (-1)^{\frac{1}{2}-\frac{1}{2}-0} \cdot 1 \cdot (-1)^{\frac{1}{2}-\frac{1}{2}-0} \cdot 1 \\ &= 1 \ , \end{aligned} \tag{C.34}$$

$$\begin{aligned} C_{\gamma n\to K^0\Lambda}^{1,\frac{1}{2}} &= \left\langle \frac{1}{2}, -\frac{1}{2}, 1, 0 \middle| \frac{1}{2}, -\frac{1}{2} \right\rangle \left\langle \frac{1}{2}, -\frac{1}{2} \middle| 0, 0, \frac{1}{2}, -\frac{1}{2} \right\rangle \\ &= (-1)^{\frac{1}{2}-\frac{1}{2}-1} \cdot \left(\frac{1}{\sqrt{3}} \right) \cdot (-1)^{\frac{1}{2}-\frac{1}{2}-0} \cdot 1 \\ &= -\frac{1}{\sqrt{3}} \ , \end{aligned} \tag{C.35}$$

$$C_{\gamma n\to K^0\Lambda}^{1,\frac{3}{2}} = 0 \ , \tag{C.36}$$

and one finds the analogous amplitude as for ηn

$$T_{\gamma}^{K^0\Lambda} = -\frac{1}{\sqrt{3}} T_{K\Lambda\gamma}^{1,\frac{1}{2}} + T_{K\Lambda\gamma}^{0,\frac{1}{2}} \ . \tag{C.37}$$

Next we calculate the isospin factors for the channel $K^+\Sigma^-$. The final state states are given by $|K^+\rangle = |1/2, +1/2\rangle$ and $|\Sigma^-\rangle = |1, -1\rangle$. This results in the following isospin factors

$$\begin{aligned} C^{0,\frac{1}{2}}_{\gamma n \to K^+\Sigma^-} &= \left\langle \frac{1}{2}, -\frac{1}{2}, 0, 0 \middle| \frac{1}{2}, -\frac{1}{2} \right\rangle \left\langle \frac{1}{2}, -\frac{1}{2} \middle| 1, -1, \frac{1}{2}, +\frac{1}{2} \right\rangle \\ &= (-1)^{\frac{1}{2}-\frac{1}{2}-0} \cdot 1 \cdot \left(-\sqrt{\frac{2}{3}} \right) \\ &= -\sqrt{\frac{2}{3}} \,, \end{aligned} \tag{C.38}$$

$$\begin{aligned} C^{1,\frac{1}{2}}_{\gamma n \to K^+\Sigma^-} &= \left\langle \frac{1}{2}, -\frac{1}{2}, 1, 0 \middle| \frac{1}{2}, -\frac{1}{2} \right\rangle \left\langle \frac{1}{2}, -\frac{1}{2} \middle| 1, -1, \frac{1}{2}, +\frac{1}{2} \right\rangle \\ &= (-1)^{\frac{1}{2}-\frac{1}{2}-1} \cdot \left(\frac{1}{\sqrt{3}} \right) \cdot \left(-\sqrt{\frac{2}{3}} \right) \\ &= \frac{\sqrt{2}}{3} \,, \end{aligned} \tag{C.39}$$

$$\begin{aligned} C^{1,\frac{3}{2}}_{\gamma n \to K^+\Sigma^-} &= \left\langle \frac{1}{2}, -\frac{1}{2}, 1, 0 \middle| \frac{3}{2}, -\frac{1}{2} \right\rangle \left\langle \frac{3}{2}, -\frac{1}{2} \middle| 1, -1, \frac{1}{2}, +\frac{1}{2} \right\rangle \\ &= (-1)^{\frac{3}{2}-\frac{1}{2}-1} \cdot \left(\sqrt{\frac{2}{3}} \right) \cdot \left(\frac{1}{\sqrt{3}} \right) \\ &= \frac{\sqrt{2}}{3} \,. \end{aligned} \tag{C.40}$$

The resulting amplitude is given by

$$T_\gamma^{K^+\Sigma^-} = \frac{\sqrt{2}}{3} T^{1,\frac{3}{2}}_{K\Sigma\gamma} + \frac{\sqrt{2}}{3} T^{1,\frac{1}{2}}_{K\Sigma\gamma} - \sqrt{\frac{2}{3}} T^{0,\frac{1}{2}}_{K\Sigma\gamma} \,. \tag{C.41}$$

The last process we are investigating is $\gamma n \to K^0\Sigma^0$. Here we find the isospin factors

$$\begin{aligned} C^{0,\frac{1}{2}}_{\gamma n \to K^0\Sigma^0} &= \left\langle \frac{1}{2}, -\frac{1}{2}, 0, 0 \middle| \frac{1}{2}, -\frac{1}{2} \right\rangle \left\langle \frac{1}{2}, -\frac{1}{2} \middle| 1, 0, \frac{1}{2}, -\frac{1}{2} \right\rangle \\ &= (-1)^{\frac{1}{2}-\frac{1}{2}-0} \cdot 1 \cdot \left(\frac{1}{\sqrt{3}} \right) \\ &= \frac{1}{\sqrt{3}} \,, \end{aligned} \tag{C.42}$$

$$\begin{aligned} C^{1,\frac{1}{2}}_{\gamma n \to K^0\Sigma^0} &= \left\langle \frac{1}{2}, -\frac{1}{2}, 1, 0 \middle| \frac{1}{2}, -\frac{1}{2} \right\rangle \left\langle \frac{1}{2}, -\frac{1}{2} \middle| 1, 0, \frac{1}{2}, -\frac{1}{2} \right\rangle \\ &= (-1)^{\frac{1}{2}-\frac{1}{2}-1} \cdot \left(\frac{1}{\sqrt{3}} \right) \cdot \left(\frac{1}{\sqrt{3}} \right) \\ &= -\frac{1}{3} \,, \end{aligned} \tag{C.43}$$

$$
\begin{aligned}
C^{1,\frac{3}{2}}_{\gamma n \to K^0\Sigma^0} &= \left\langle \frac{1}{2}, -\frac{1}{2}, 1, 0 \middle| \frac{3}{2}, -\frac{1}{2} \right\rangle \left\langle \frac{3}{2}, -\frac{1}{2} \middle| 1, 0, \frac{1}{2}, -\frac{1}{2} \right\rangle \\
&= (-1)^{\frac{3}{2}-\frac{1}{2}-1} \cdot \left(\sqrt{\frac{2}{3}}\right) \cdot \left(\sqrt{\frac{2}{3}}\right) \\
&= \frac{2}{3} \qquad \text{(C.44)}
\end{aligned}
$$

and get the amplitude

$$
T_\gamma^{K^0\Sigma^0} = \frac{2}{3} T^{1,\frac{3}{2}}_{K\Sigma\gamma} - \frac{1}{3} T^{1,\frac{1}{2}}_{K\Sigma\gamma} + \frac{1}{\sqrt{3}} T^{0,\frac{1}{2}}_{K\Sigma\gamma} \ . \qquad \text{(C.45)}
$$

In summary, we found the following amplitudes:

$$
\begin{aligned}
T_\gamma^{\pi^0 p} &= \frac{2}{3} T^{1,\frac{3}{2}}_{\pi N\gamma} + \frac{1}{3} T^{1,\frac{1}{2}}_{\pi N\gamma} + \frac{1}{\sqrt{3}} T^{0,\frac{1}{2}}_{\pi N\gamma} && \text{(C.46)} \\
T_\gamma^{\pi^+ n} &= \frac{\sqrt{2}}{3} T^{1,\frac{3}{2}}_{\pi N\gamma} - \frac{\sqrt{2}}{3} T^{1,\frac{1}{2}}_{\pi N\gamma} - \sqrt{\frac{1}{3}} T^{0,\frac{1}{2}}_{\pi N\gamma} && \text{(C.47)} \\
T_\gamma^{\eta p} &= \frac{1}{\sqrt{3}} T^{1,\frac{1}{2}}_{\eta N\gamma} + T^{0,\frac{1}{2}}_{\eta N\gamma} && \text{(C.48)} \\
T_\gamma^{K^+ \Lambda} &= \frac{1}{\sqrt{3}} T^{1,\frac{1}{2}}_{K\Lambda\gamma} + T^{0,\frac{1}{2}}_{K\Lambda\gamma} && \text{(C.49)} \\
T_\gamma^{K^0 \Sigma^+} &= \frac{\sqrt{2}}{3} T^{1,\frac{3}{2}}_{K\Sigma\gamma} + \frac{\sqrt{2}}{3} T^{1,\frac{1}{2}}_{K\Sigma\gamma} + \sqrt{\frac{2}{3}} T^{0,\frac{1}{2}}_{K\Sigma\gamma} && \text{(C.50)} \\
T_\gamma^{K^+ \Sigma^0} &= \frac{2}{3} T^{1,\frac{3}{2}}_{K\Sigma\gamma} - \frac{1}{3} T^{1,\frac{1}{2}}_{K\Sigma\gamma} - \frac{1}{\sqrt{3}} T^{0,\frac{1}{2}}_{K\Sigma\gamma} && \text{(C.51)}
\end{aligned}
$$

$$
\begin{aligned}
T_\gamma^{\pi^0 n} &= \frac{2}{3} T^{1,\frac{3}{2}}_{\pi N\gamma} + \frac{1}{3} T^{1,\frac{1}{2}}_{\pi N\gamma} - \frac{1}{\sqrt{3}} T^{0,\frac{1}{2}}_{\pi N\gamma} && \text{(C.52)} \\
T_\gamma^{\pi^- p} &= \frac{\sqrt{2}}{3} T^{1,\frac{3}{2}}_{\pi N\gamma} - \frac{\sqrt{2}}{3} T^{1,\frac{1}{2}}_{\pi N\gamma} + \sqrt{\frac{2}{3}} T^{0,\frac{1}{2}}_{\pi N\gamma} && \text{(C.53)} \\
T_\gamma^{\eta n} &= -\frac{1}{\sqrt{3}} T^{1,\frac{1}{2}}_{\eta N\gamma} + T^{0,\frac{1}{2}}_{\eta N\gamma} && \text{(C.54)} \\
T_\gamma^{K^0 \Lambda} &= -\frac{1}{\sqrt{3}} T^{1,\frac{1}{2}}_{K\Lambda\gamma} + T^{0,\frac{1}{2}}_{K\Lambda\gamma} && \text{(C.55)} \\
T_\gamma^{K^+ \Sigma^-} &= \frac{\sqrt{2}}{3} T^{1,\frac{3}{2}}_{K\Sigma\gamma} + \frac{\sqrt{2}}{3} T^{1,\frac{1}{2}}_{K\Sigma\gamma} - \sqrt{\frac{2}{3}} T^{0,\frac{1}{2}}_{K\Sigma\gamma} && \text{(C.56)} \\
T_\gamma^{K^0 \Sigma^0} &= \frac{2}{3} T^{1,\frac{3}{2}}_{K\Sigma\gamma} - \frac{1}{3} T^{1,\frac{1}{2}}_{K\Sigma\gamma} + \frac{1}{\sqrt{3}} T^{0,\frac{1}{2}}_{K\Sigma\gamma} \ . && \text{(C.57)}
\end{aligned}
$$

D. Additional material for the JüBo2025 study

D.1. New Data for $\Delta\sigma$ from A2/MAMI-collaboration

In Fig. 24-25 one can see the new data from the A2/MAMI-collaboration [300] and the solution of the present study. Note that this dataset was not included in the fit. Still, the data are described well.

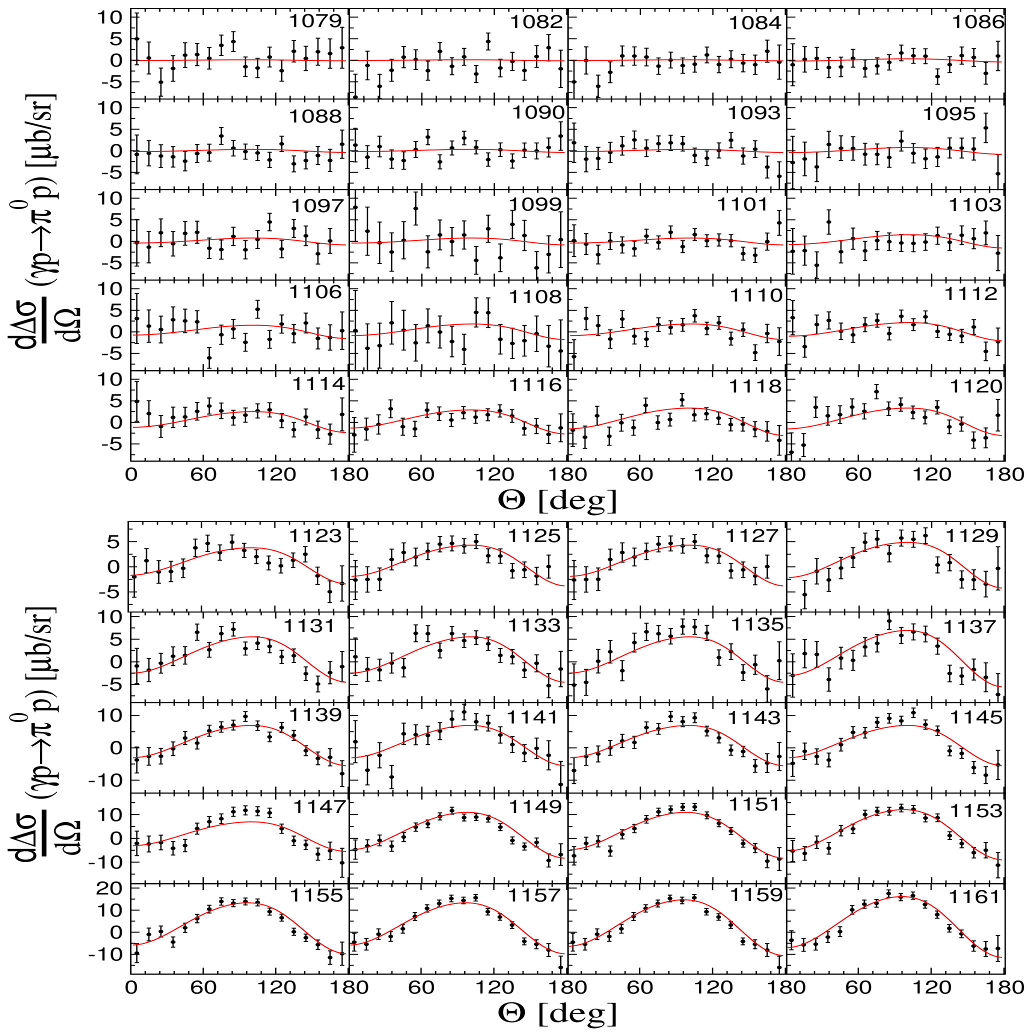

Figure 23: Solution JüBo2025 (red) for the helicity dependent differential cross section from Ref. [300] for the process $\gamma p \to \pi^0 p$. (Data not included in the fit.) The numbers in each plot denote the center of mass energy in MeV.

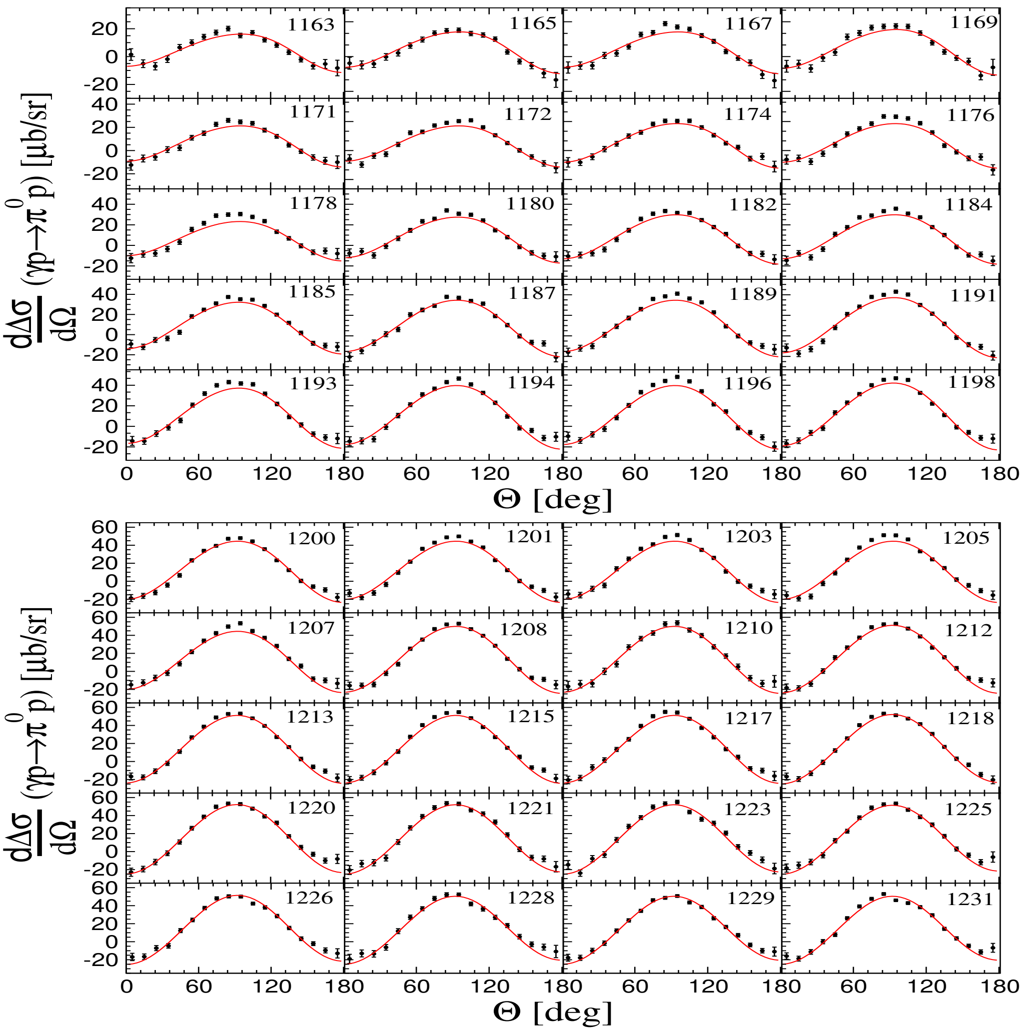

Figure 24: Solution JüBo2025 (red) for the helicity dependent differential cross section from Ref. [300] for the process $\gamma p \to \pi^0 p$. (Data not included in the fit.) The numbers in each plot denote the center of mass energy in MeV.

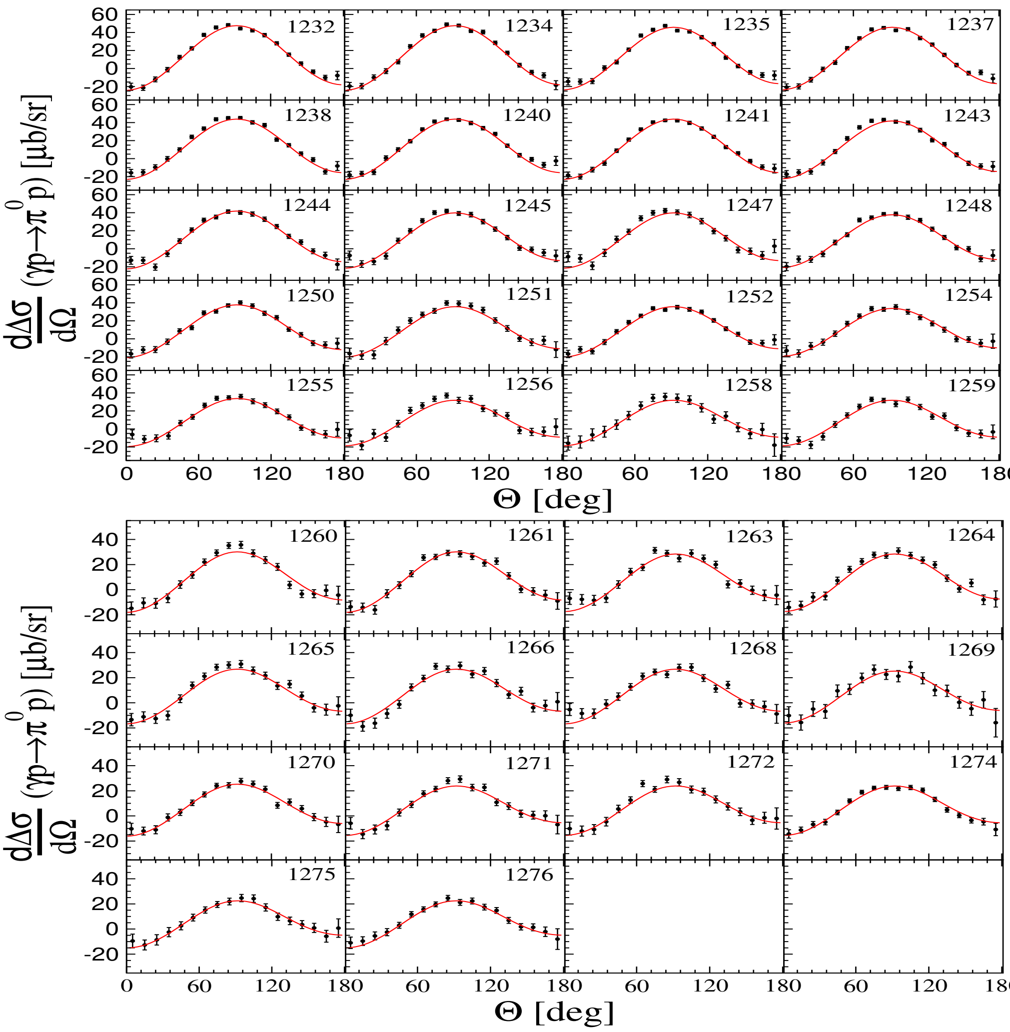

Figure 25: Solution JüBo2025 (red) for the helicity dependent differential cross section from Ref. [300] for the process $\gamma p \to \pi^0 p$. (Data not included in the fit.) The numbers in each plot denote the center of mass energy in MeV.

D.2. Influence of specific poles on newly included ηp data sets

For the two P_{13} poles we observe a large impact on the ηp data sets that were newly included in the current study. This is shown in Fig. 26. We show analogously the effect of the F_{17} pole $N(1990)\ 7/2^+$ on the new ηp-dataset in Fig. 27. Note that the scale for the observable $\mathrm{d}\sigma/\mathrm{d}\Omega$ in the first two rows is set to logarithmic scale such that the impact of the $N(1990)\ 7/2^+$ can actually be seen. This large impact for the lowest energy bins is explained by the pole position of the $N(1990)\ 7/2^+$ at 1851 MeV.

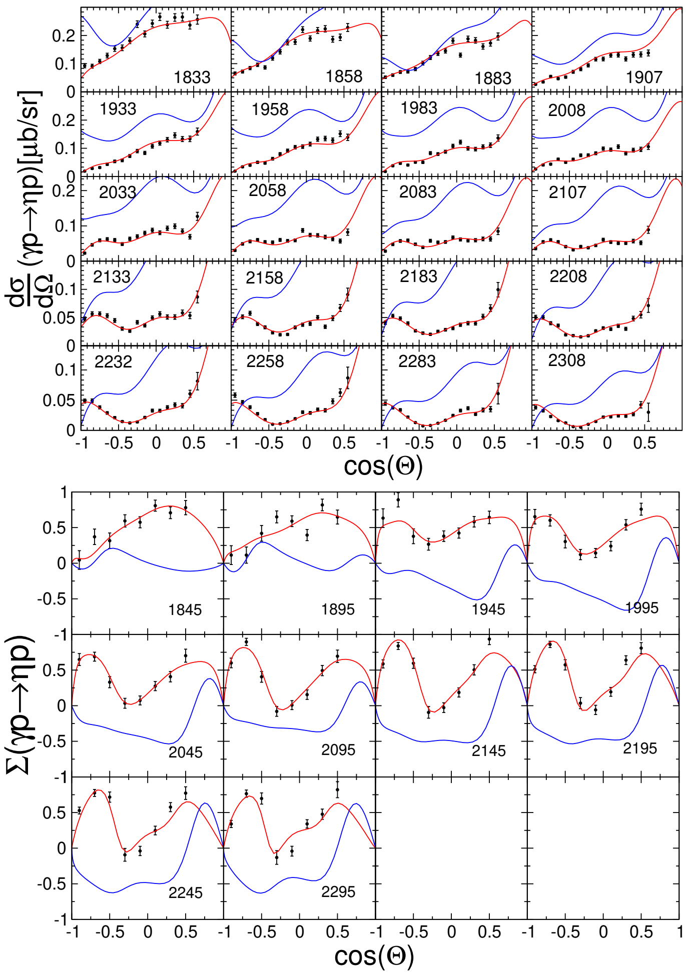

Figure 26: Current fit results (red) and the same solution without allowing P_{13} poles to couple to ηN (blue) for the newly included data sets from Ref. [302]. The numbers in each plot denote the center of mass energy in MeV.

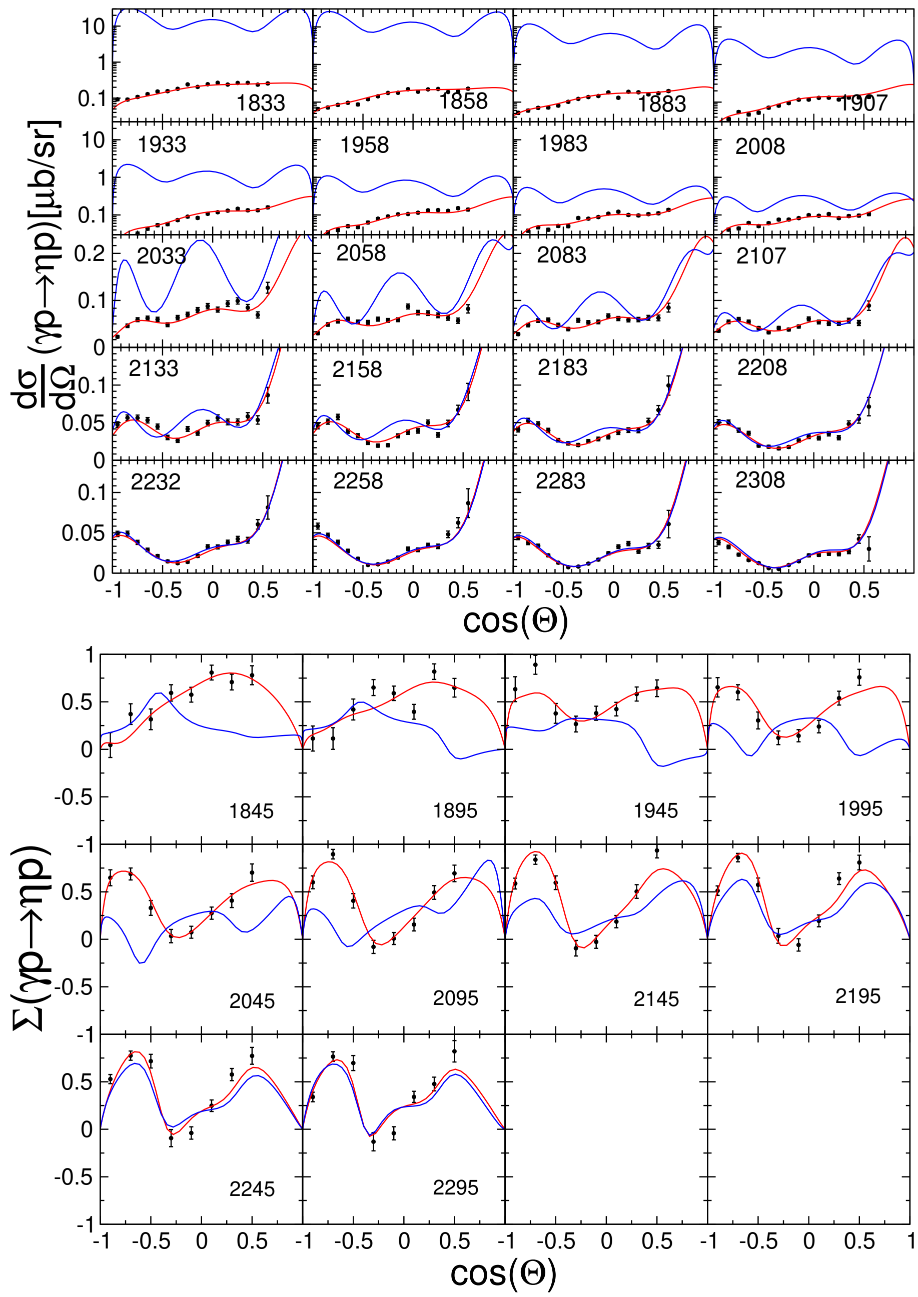

Figure 27: Current fit results (red) and the same solution without allowing the F_{17} pole to couple to ηN (blue) for the newly included data sets from Ref. [302]. Note that the scale for the observable $d\sigma/d\Omega$ in the first two rows is set to log-scale. The numbers in each plot denote the center of mass energy in MeV.

E. Fit results for $\gamma n \to \pi^0 n$

In this section we are presenting the fit results to the data sets included in the analysis of Chapter 5 for the final state $\pi^0 n$.

E.1. Differential cross section

We start by presenting the fit results to the different differential cross section $d\sigma/d\Omega$ data sets in Figs. 28-31. The references for the data sets can be found in Tab. 16.

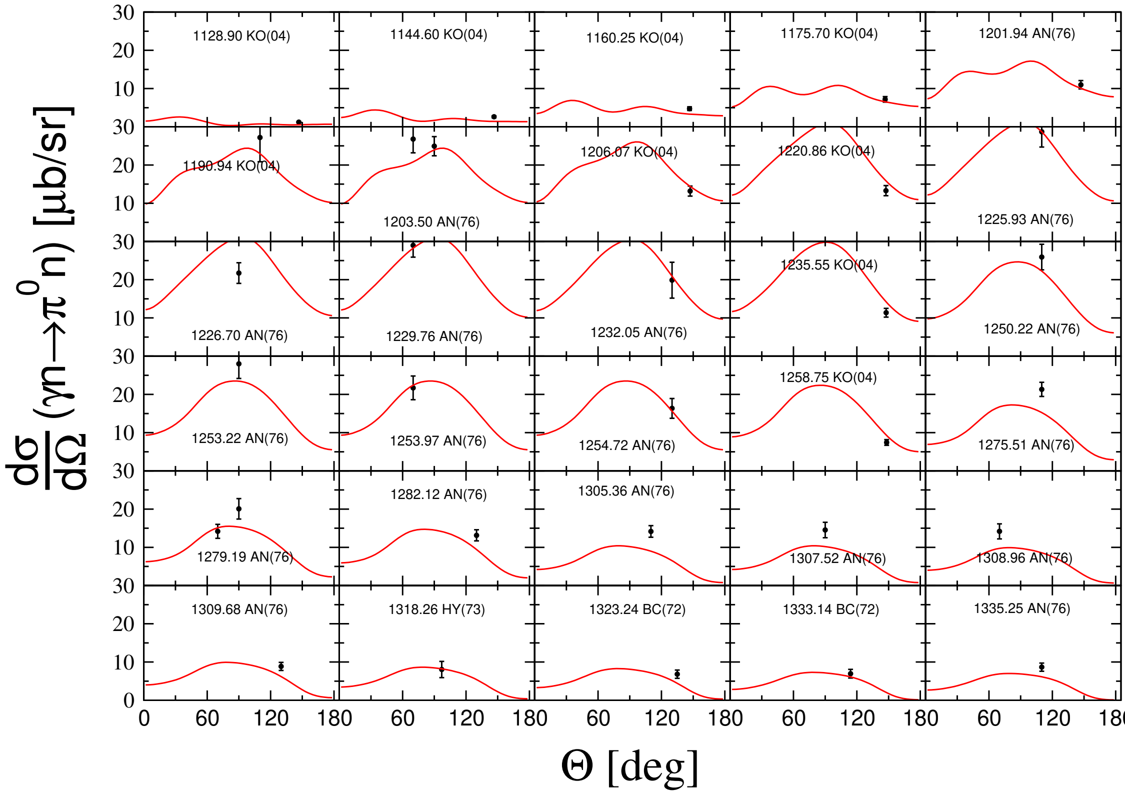

Figure 28: Fit results for the differential cross section for the process $\gamma n \to \pi^0 n$ are shown in red. The abbreviations are taken from the first author and year of the data sets up to 2004 as listed in Tab. 16. The numbers in each plot denote the center of mass energy in MeV.

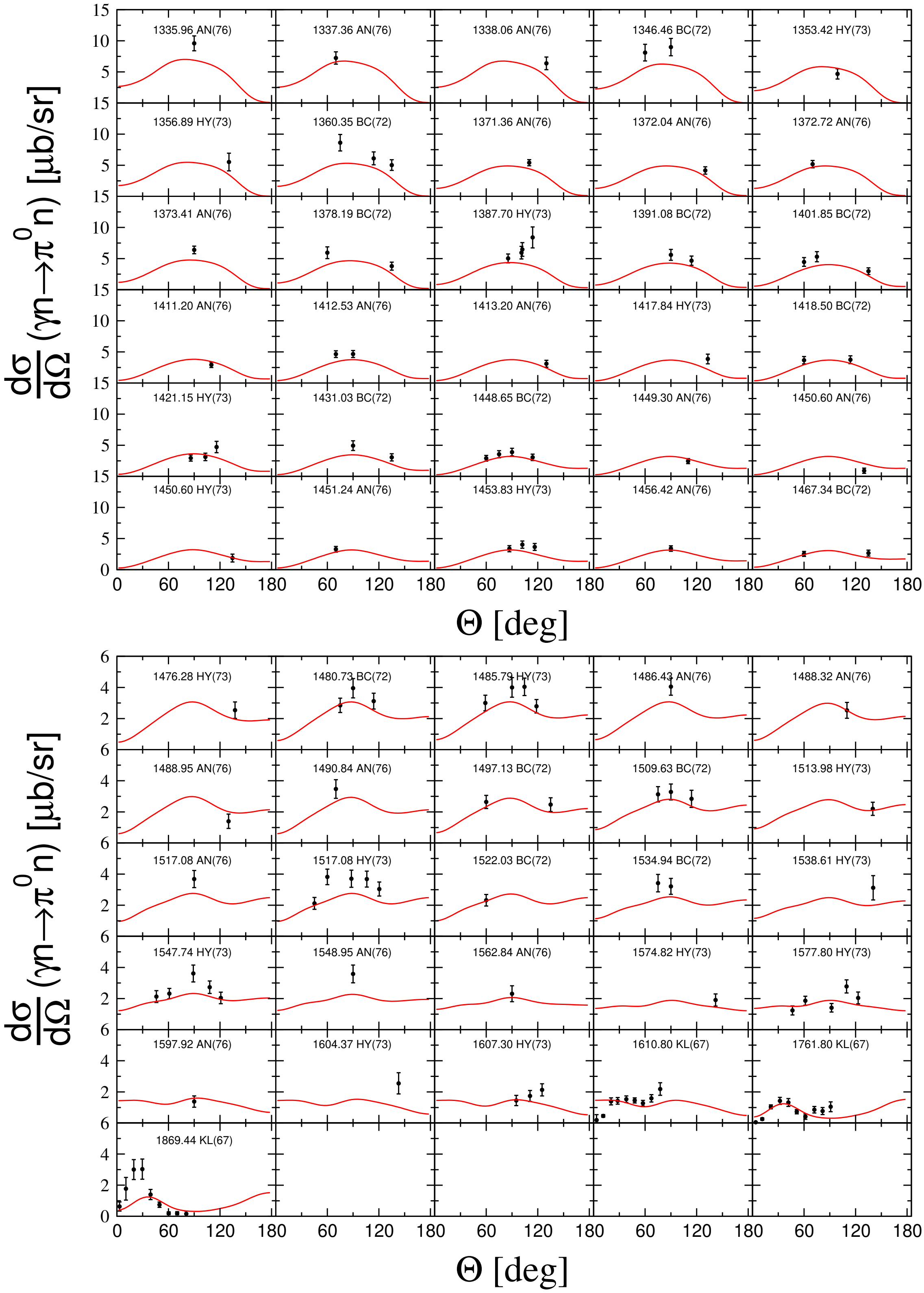

Figure 29: Fit results for the differential cross section for the process $\gamma n \rightarrow \pi^0 n$ are shown in red. The abbreviations are taken from the first author and year of the data sets up to 2004 as listed in Tab. 16. The numbers in each plot denote the center of mass energy in MeV.

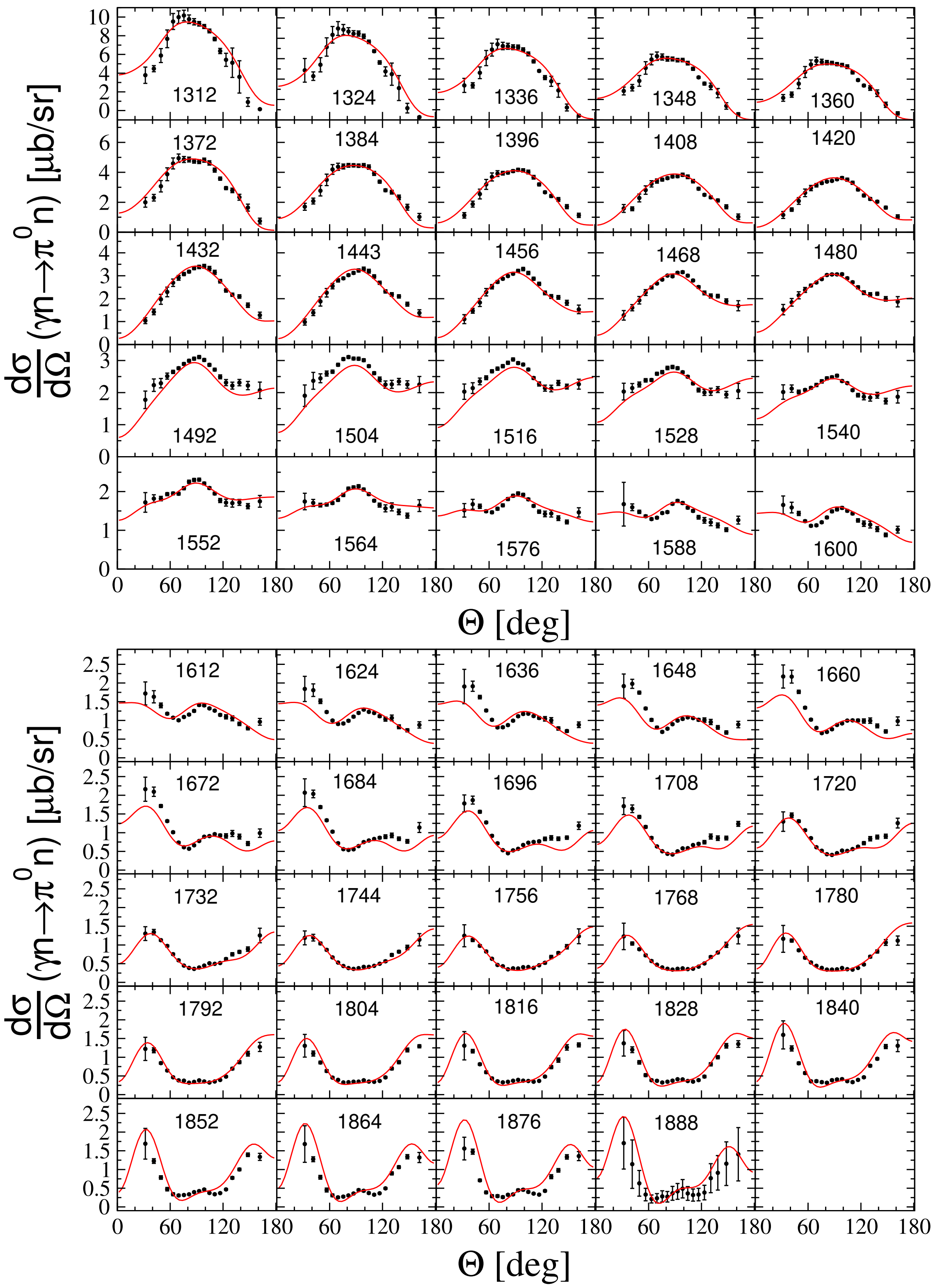

Figure 30: Fit results for the differential cross section for the process $\gamma n \rightarrow \pi^0 n$ are shown in red. The data shown is from MAMI [591]. The numbers in each plot denote the center of mass energy in MeV.

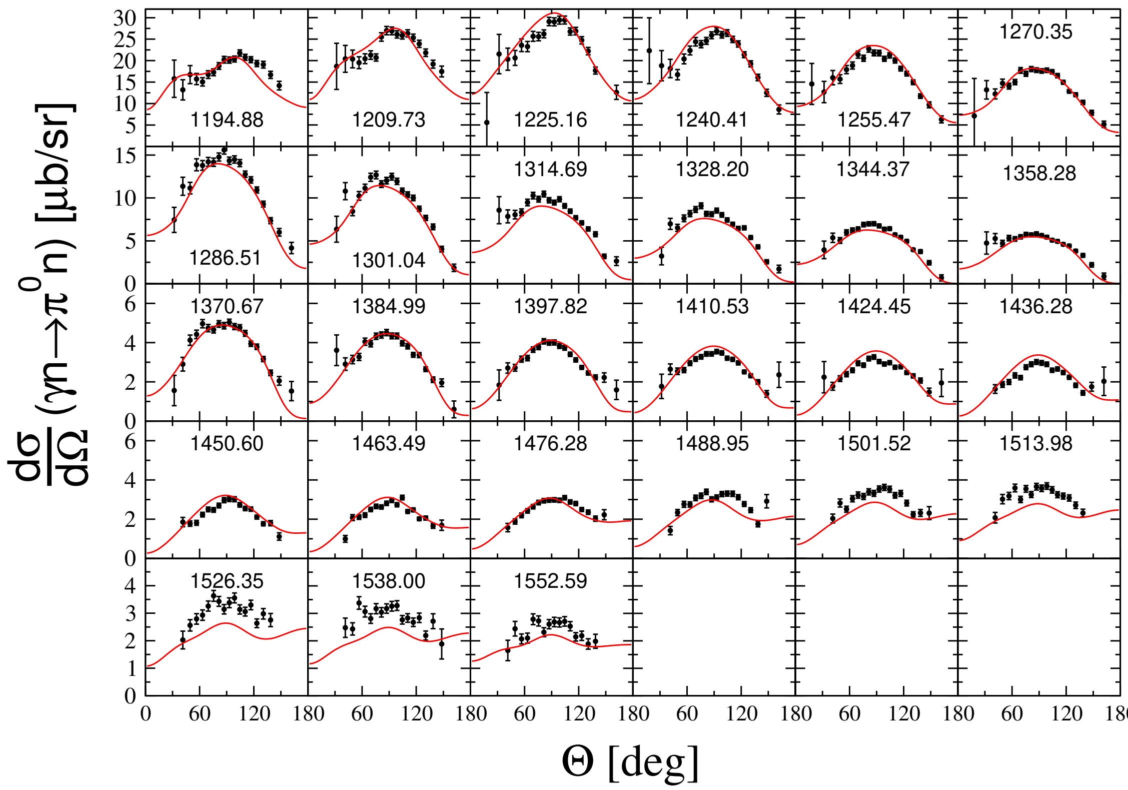

Figure 31: Fit results for the differential cross section for the process $\gamma n \to \pi^0 n$ are shown in red. The data shown is from MAMI [590]. The numbers in each plot denote the center of mass energy in MeV.

E.2. Polarization observables

Here we present the fit results to the polarization data sets. One can find the Σ data in Fig. 32, the data for polarizations H and P in Fig. 33, the T data in Fig. 34 and the E data in Figs. 35-36. The references for the data sets can be found in Tab. 16.

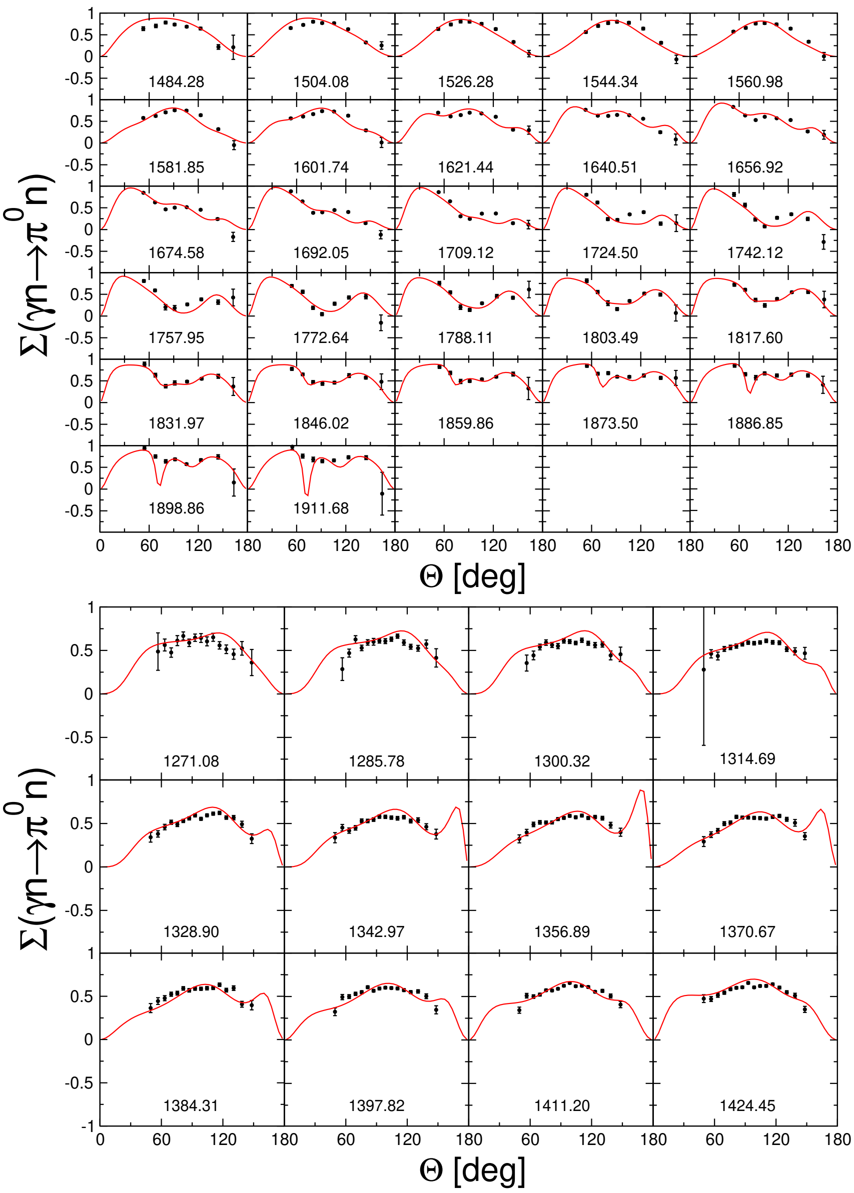

Figure 32: Fit results for the beam asymmetry Σ of the process $\gamma n \to \pi^0 n$ are shown in red. The data shown in the upper plot is from GRAAL [598] and in the lower from MAMI [597]. The numbers in each plot denote the center of mass energy in MeV.

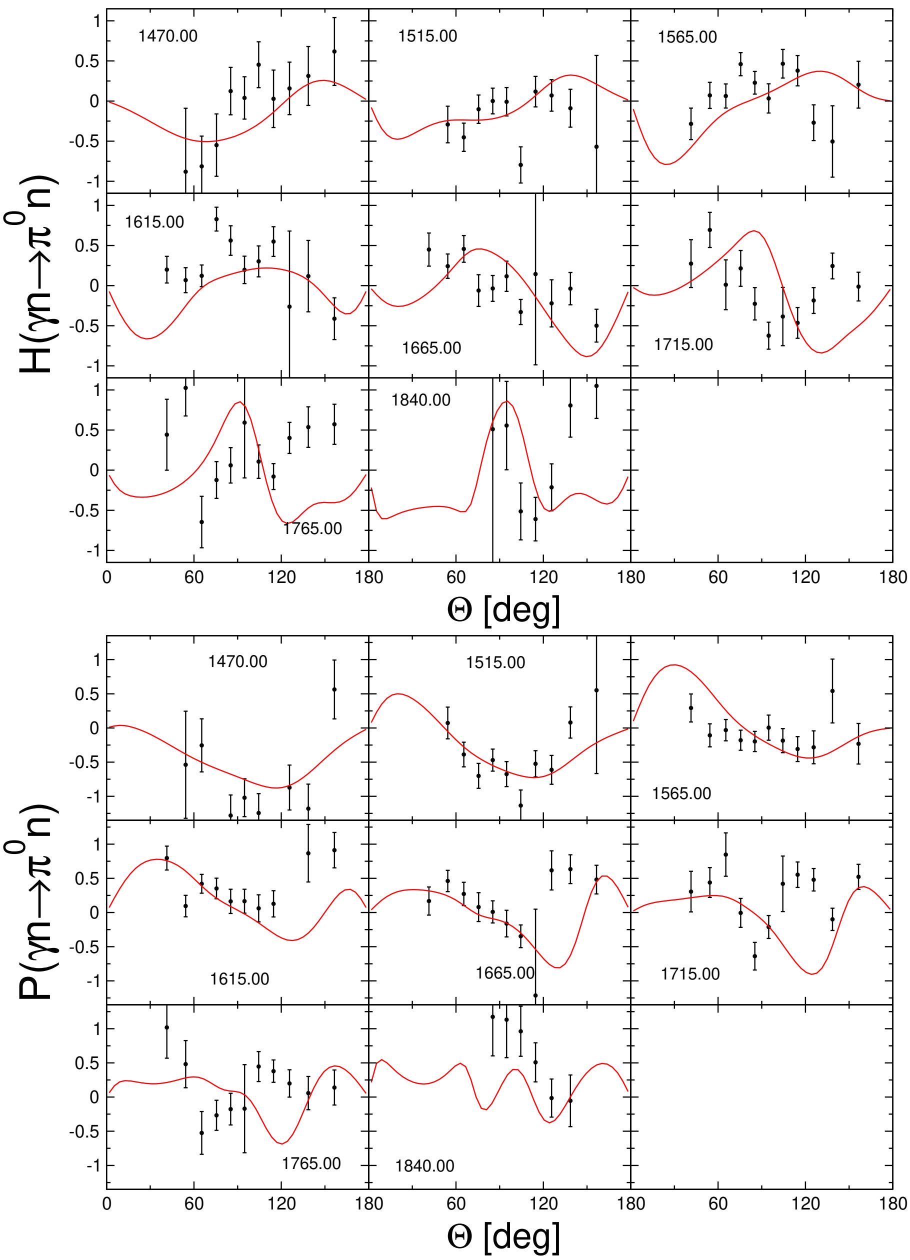

Figure 33: Fit results for the beam-target asymmetry H and recoil asymmetry P of the process $\gamma n \to \pi^0 n$ are shown in red. The data shown is from CBELSA/TAPS [601]. The numbers in each plot denote the center of mass energy in MeV.

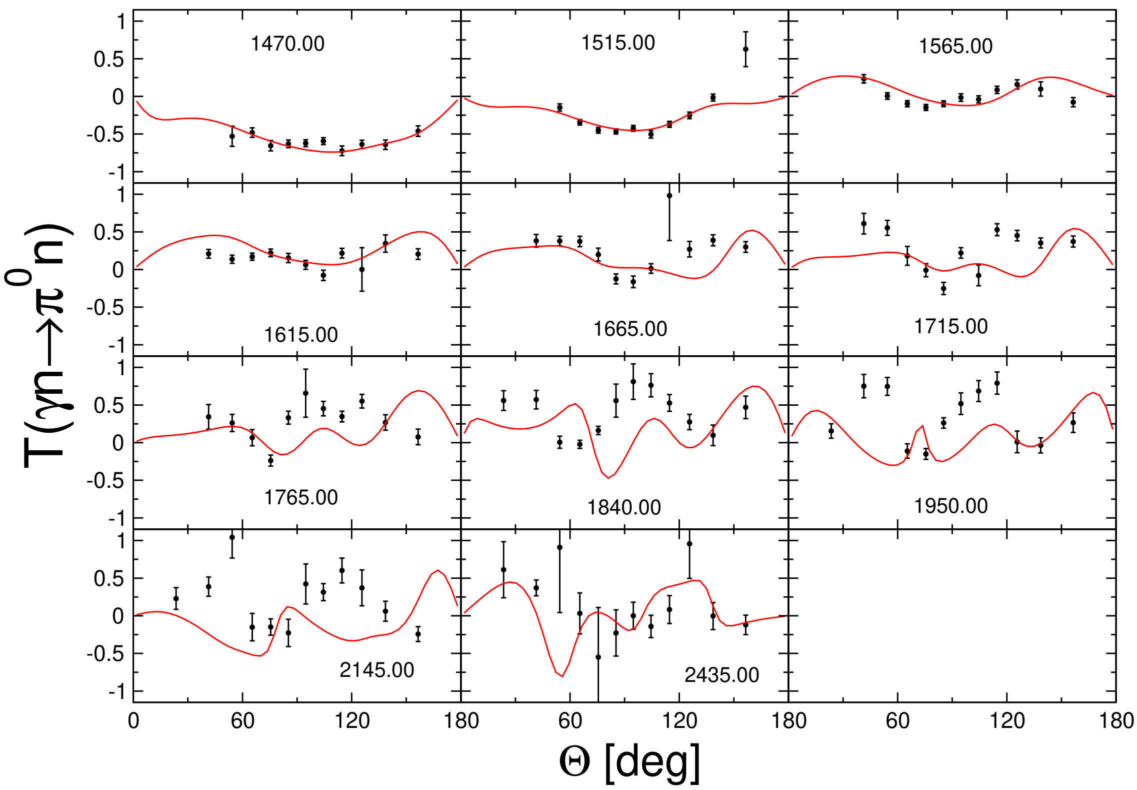

Figure 34: Fit results for the target asymmetry T of the process $\gamma n \to \pi^0 n$ are shown in red. The data shown is from CBELSA/TAPS [601]. The numbers in each plot denote the center of mass energy in MeV.

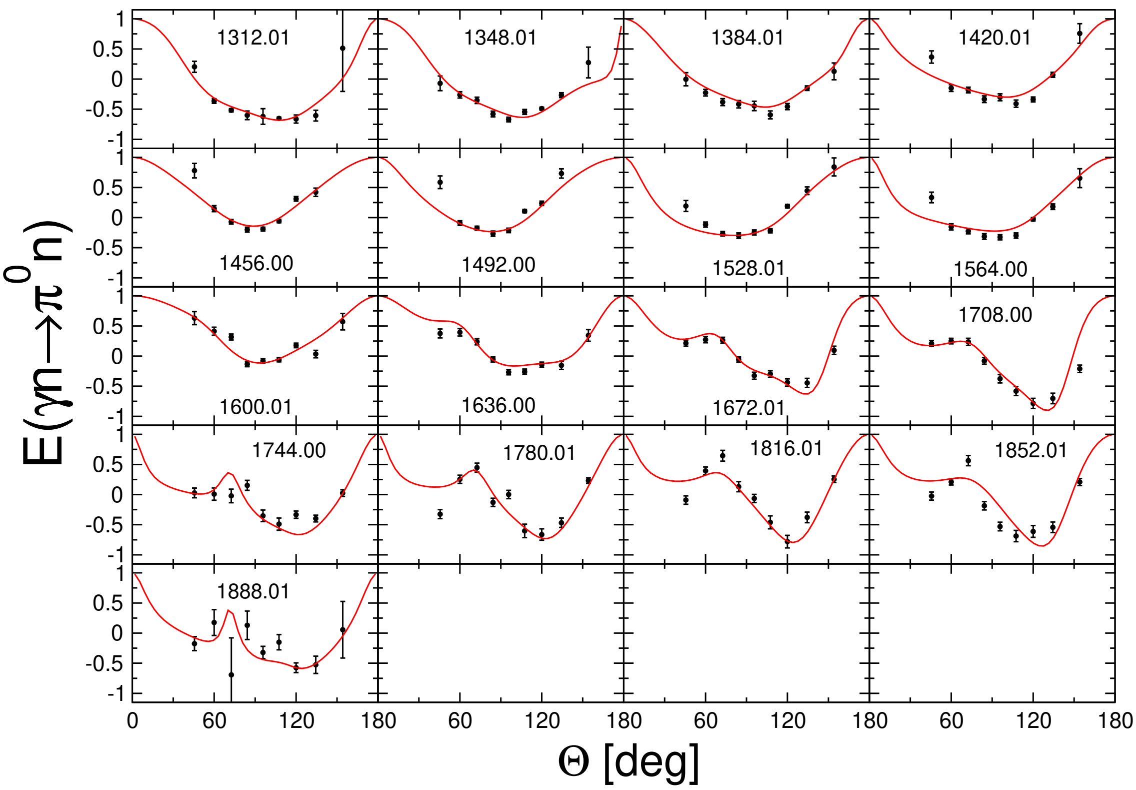

Figure 35: Fit results for the double polarization observable E of the process $\gamma n \to \pi^0 n$ are shown in red. The data shown is from 2017 of the MAMI collaboration [600]. The numbers in each plot denote the center of mass energy in MeV.

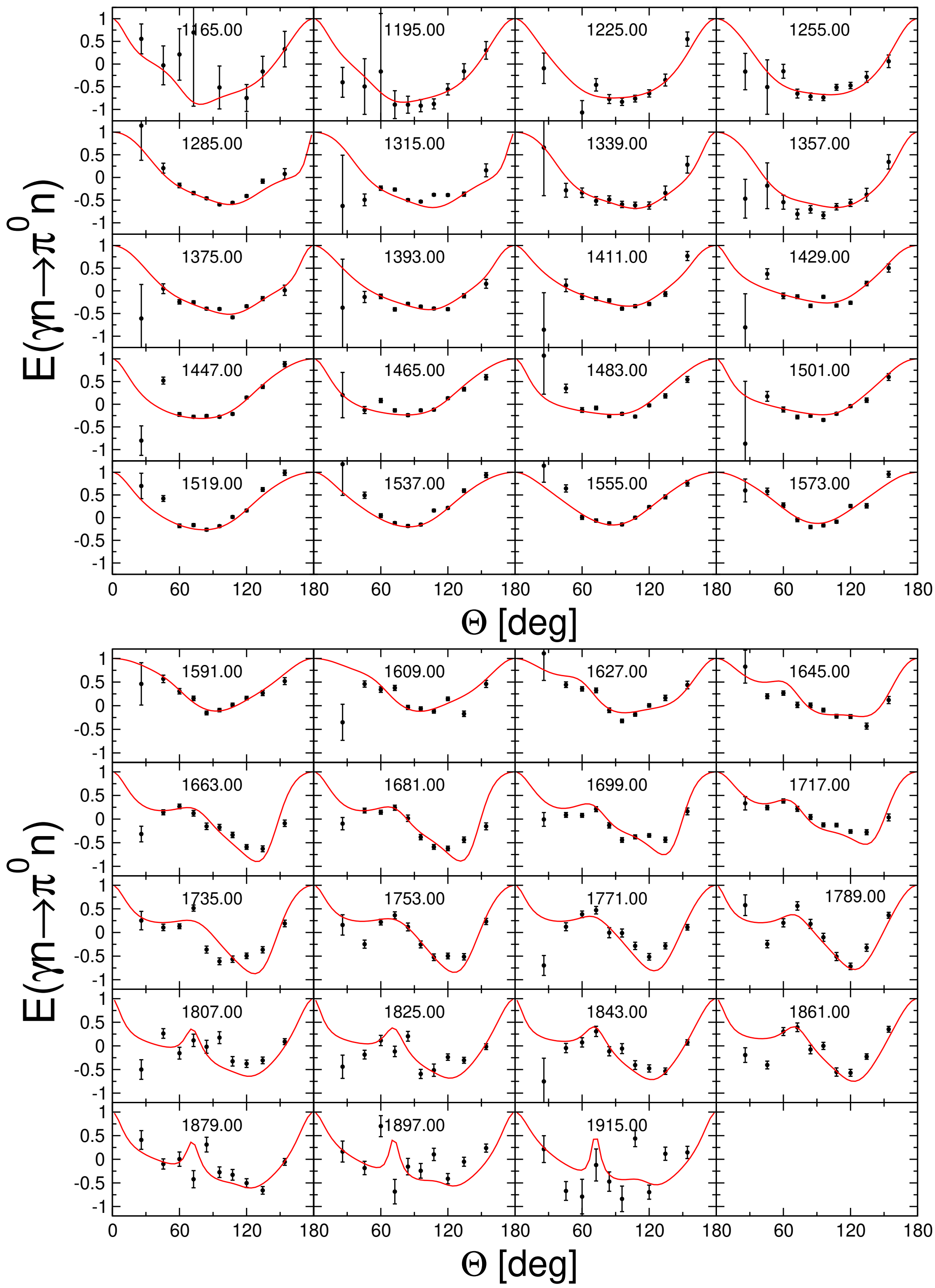

Figure 36: Fit results for the double polarization observable E of the process $\gamma n \rightarrow \pi^0 n$ are shown in red. The data shown is from 2022 of the MAMI collaboration [599]. The numbers in each plot denote the center of mass energy in MeV.

F. Fit results for $\gamma n \to \pi^- p$

In this section we are presenting the fit results to the data sets included in the analysis of Chapter 5 for the final state $\pi^- p$.

F.1. Differential cross section

We start by presenting the fit results to the different differential cross section $d\sigma/d\Omega$ data sets in Figs. 37-47. The references for the data sets can be found in Tab. 17.

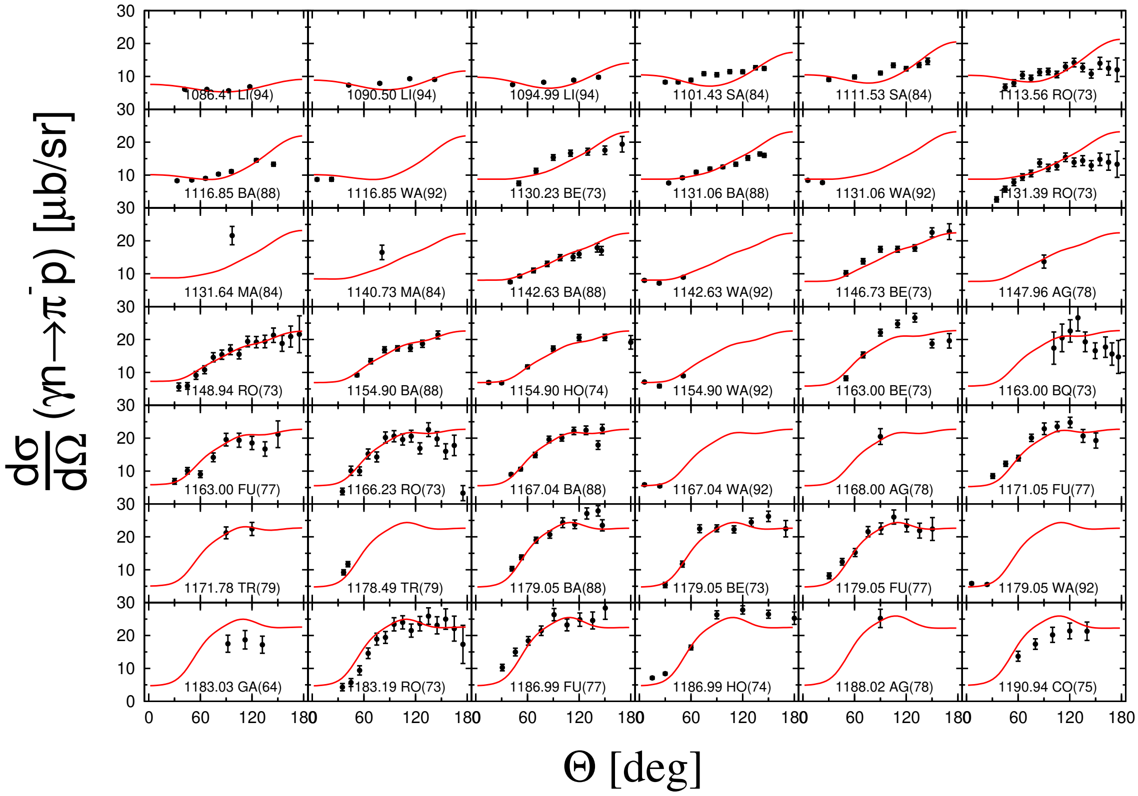

Figure 37: Fit results for the differential cross section $d\sigma/d\Omega$ for the process $\gamma n \to \pi^- p$ are shown in red. The abbreviations are taken from the first author and year of the data sets up to 1994 as listed in Tab. 17. The numbers in each plot denote the center of mass energy in MeV.

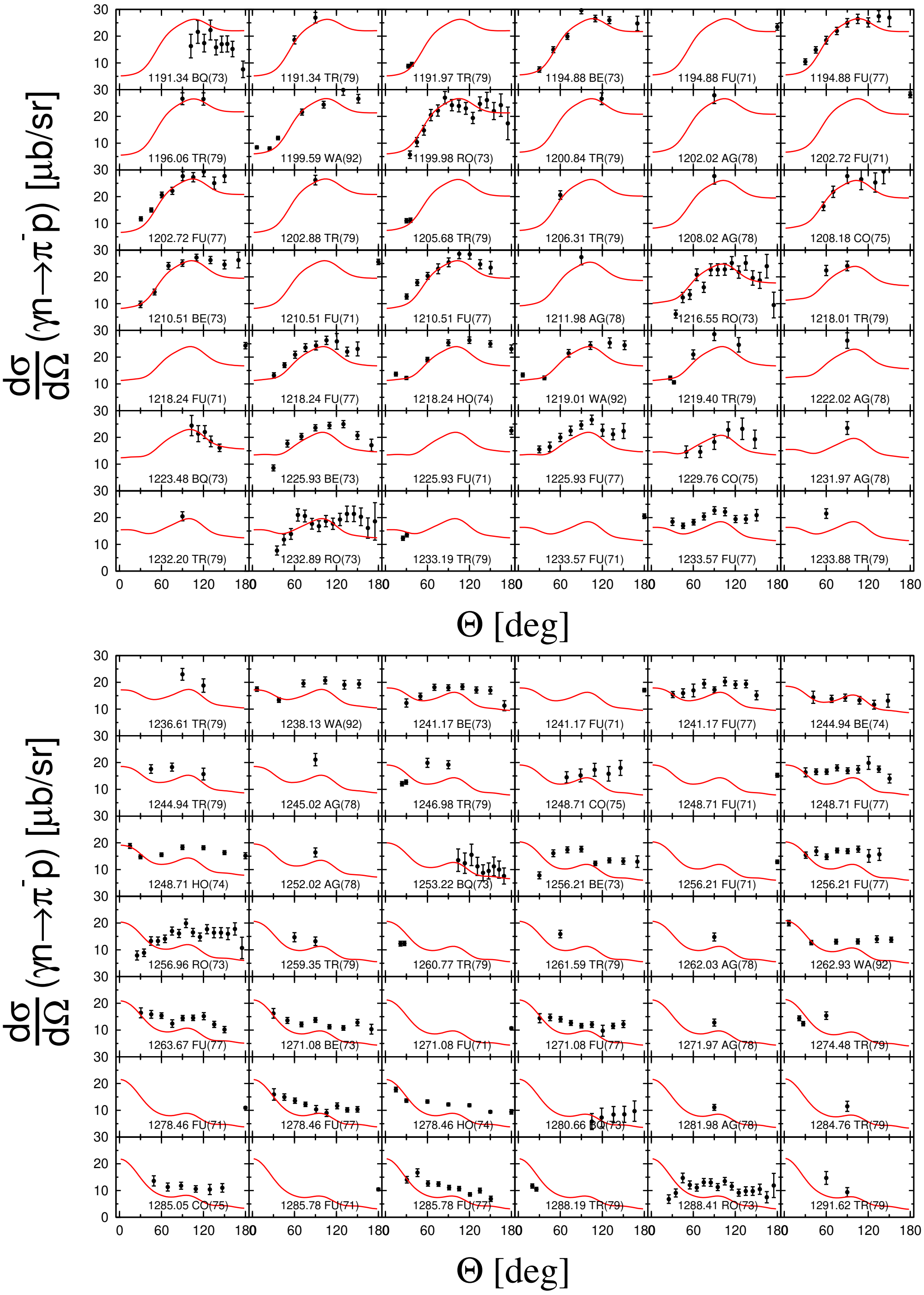

Figure 38: Fit results for the differential cross section $d\sigma/d\Omega$ for the process $\gamma n \to \pi^- p$ are shown in red. The abbreviations are taken from the first author and year of the data sets up to 1994 as listed in Tab. 17. The numbers in each plot denote the center of mass energy in MeV.

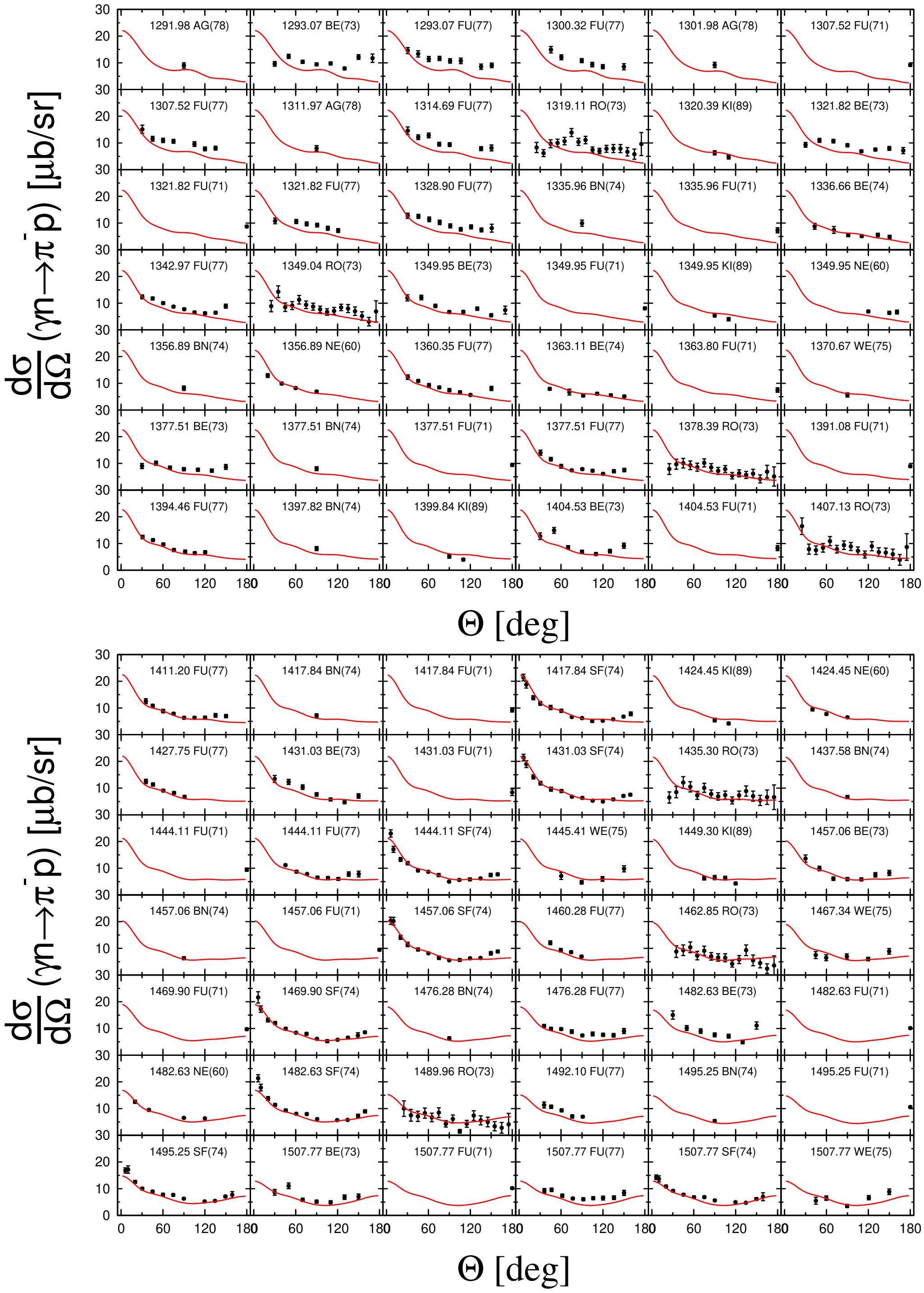

Figure 39: Fit results for the differential cross section $d\sigma/d\Omega$ for the process $\gamma n \to \pi^- p$ are shown in red. The abbreviations are taken from the first author and year of the data sets up to 1994 as listed in Tab. 17. The numbers in each plot denote the center of mass energy in MeV.

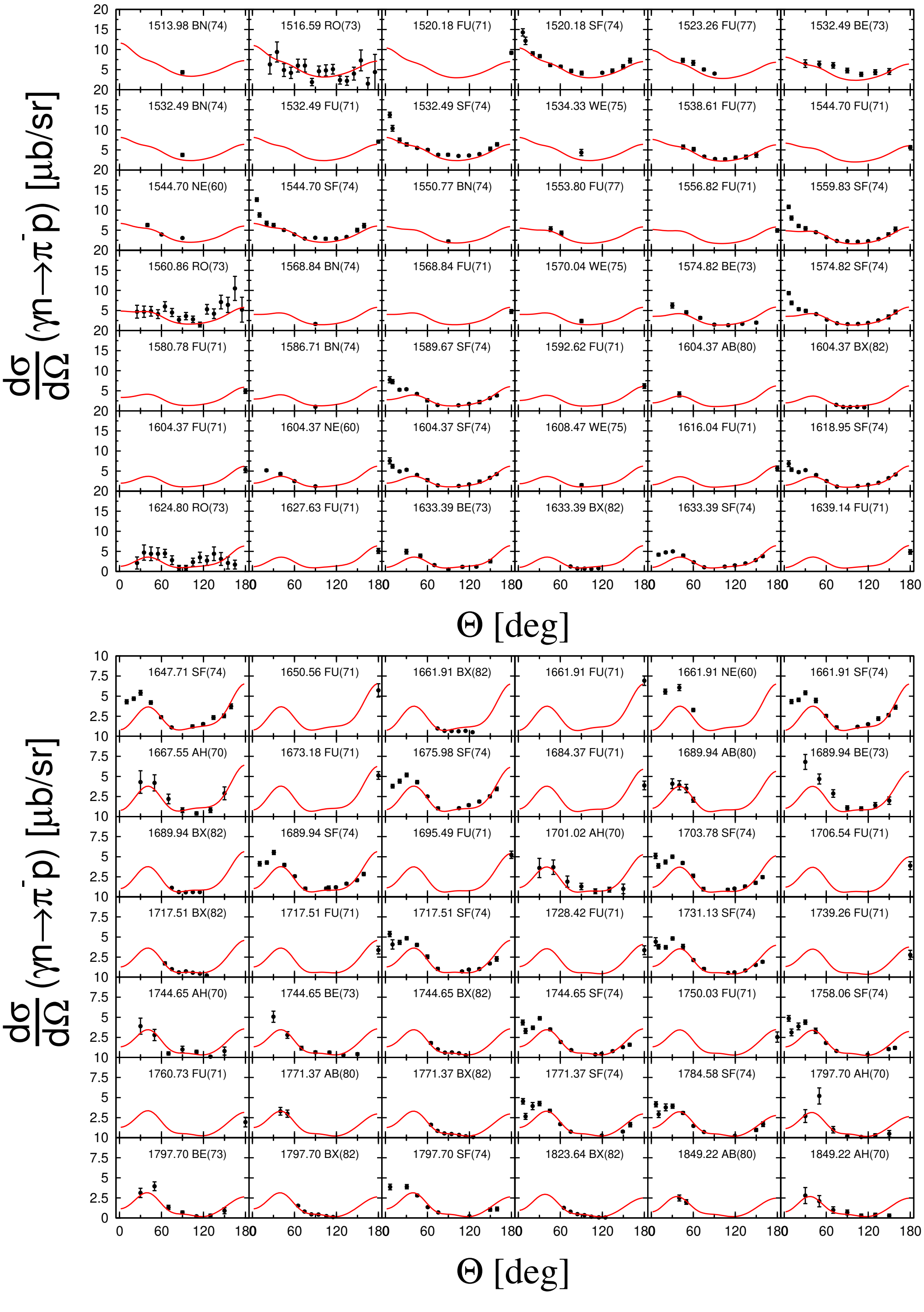

Figure 40: Fit results for the differential cross section $d\sigma/d\Omega$ for the process $\gamma n \to \pi^- p$ are shown in red. The abbreviations are taken from the first author and year of the data sets up to 1994 as listed in Tab. 17. The numbers in each plot denote the center of mass energy in MeV.

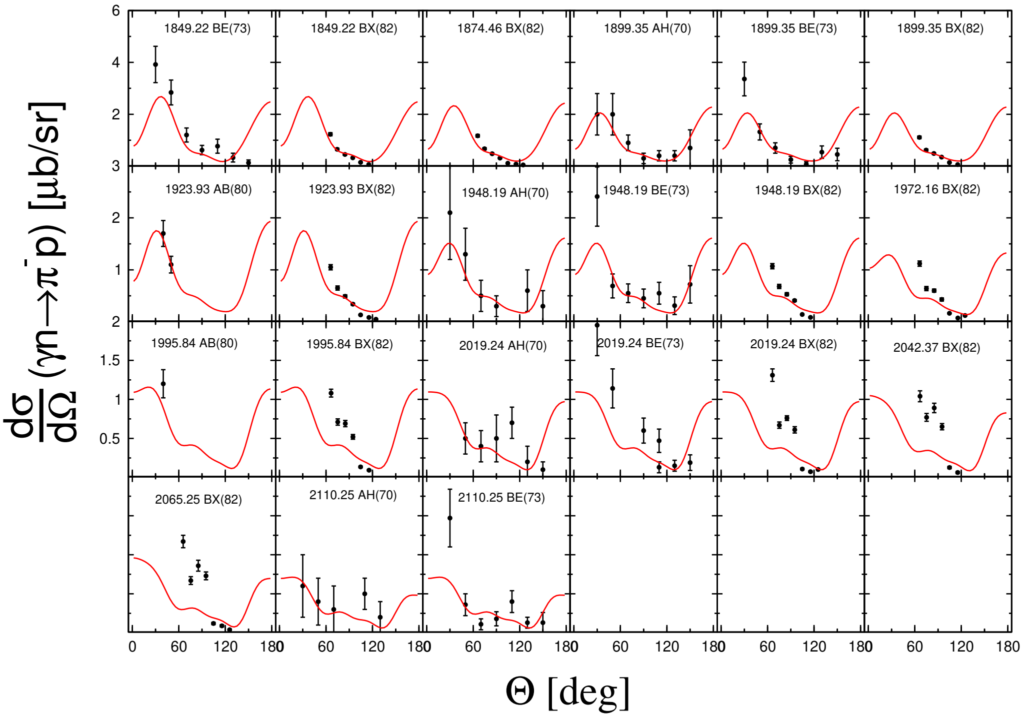

Figure 41: Fit results for the differential cross section $d\sigma/d\Omega$ for the process $\gamma n \to \pi^- p$ are shown in red. The abbreviations are taken from the first author and year of the data sets up to 1994 as listed in Tab. 17. The numbers in each plot denote the center of mass energy in MeV.

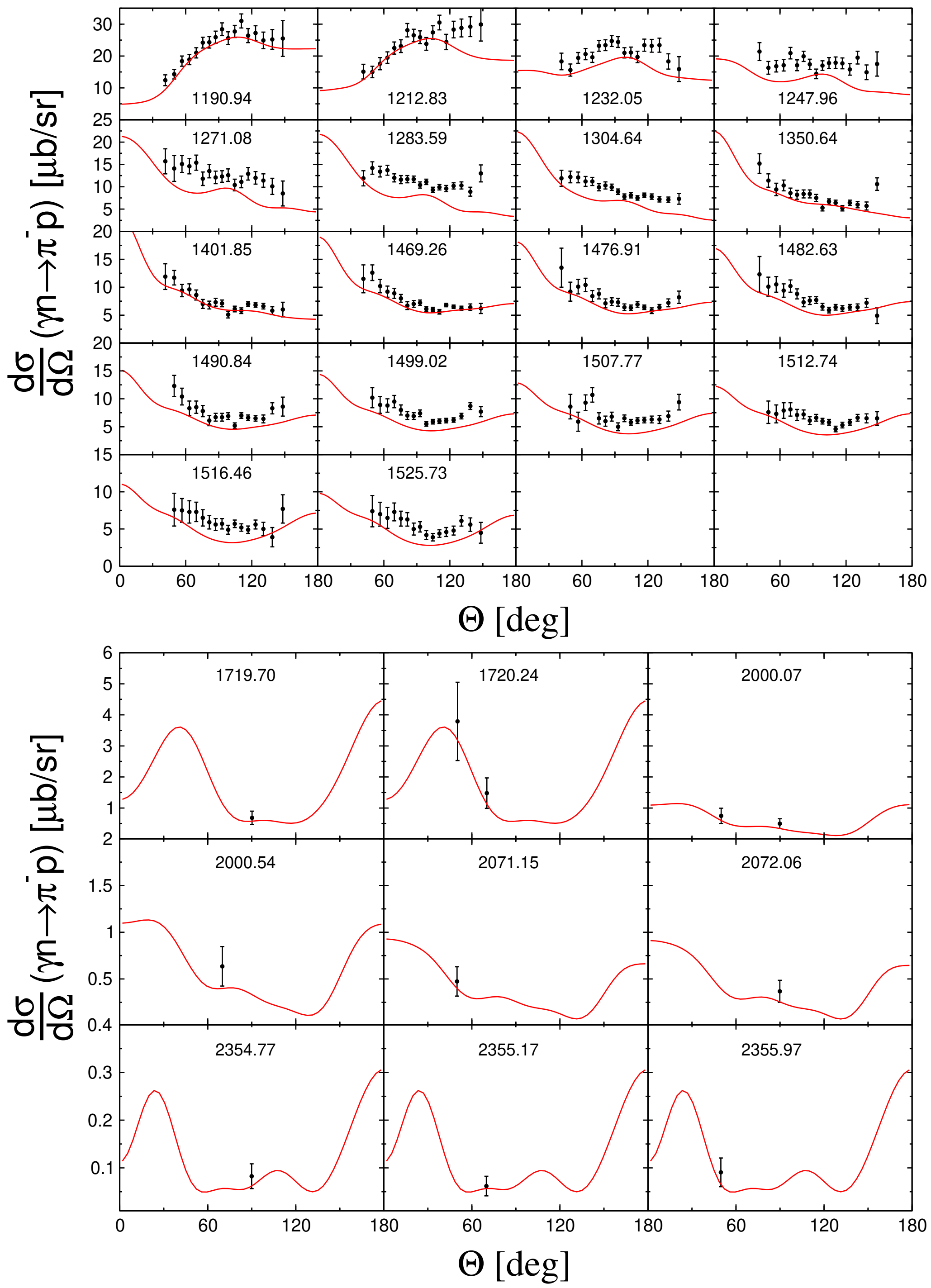

Figure 42: Fit results for the differential cross section for the process $\gamma n \to \pi^- p$ are shown in red. The data points shown in the upper plot are from Crystall Ball Collaboration published in Ref. [605] and the data in the lower plot are from JLAB. [469]. The numbers in each plot denote the center of mass energy in MeV.

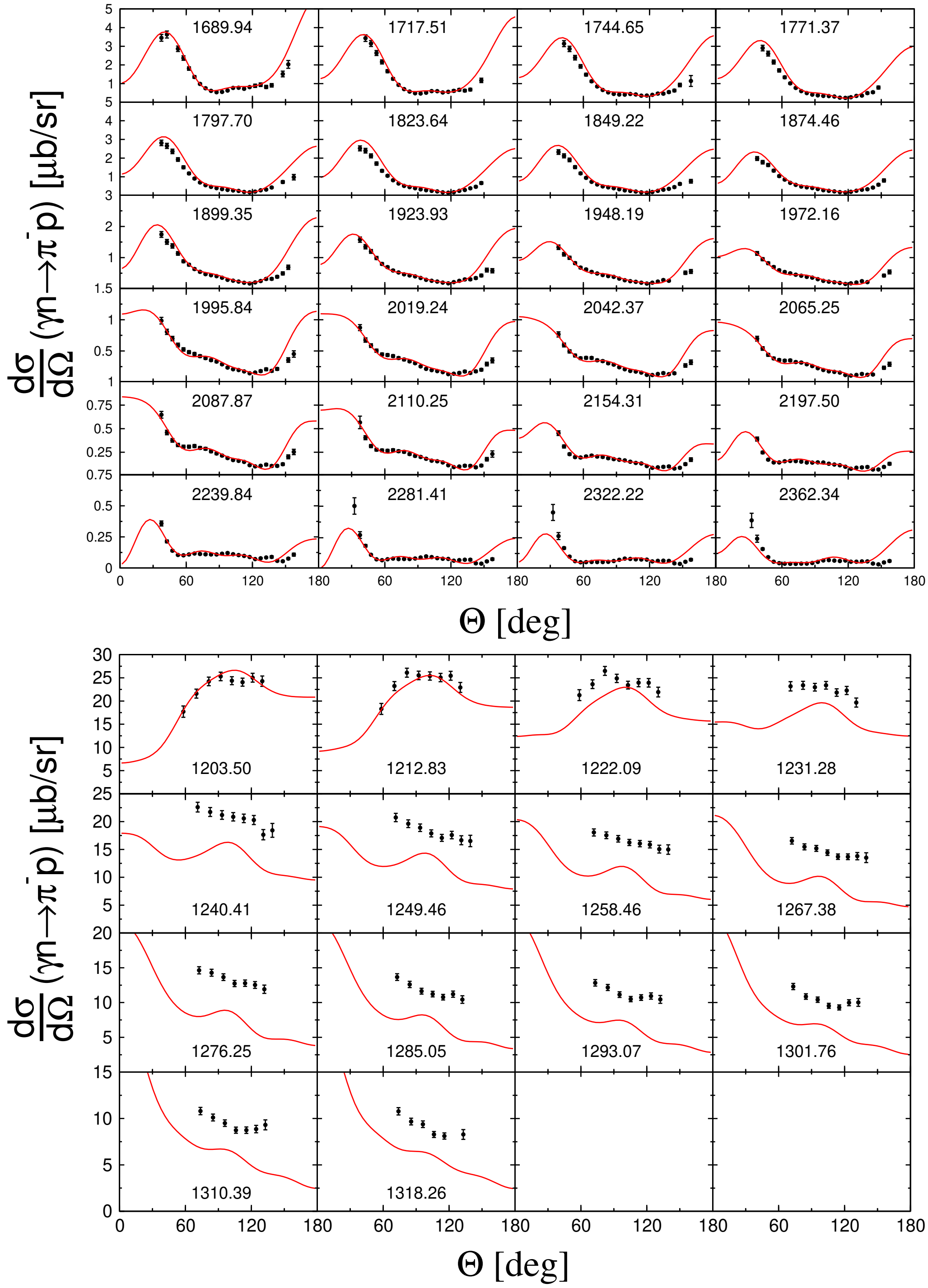

Figure 43: Fit results for the differential cross section $d\sigma/d\Omega$ for the process $\gamma n \to \pi^- p$ are shown in red. The data shown in the upper plot is from 2012 of the CLAS collaboration [603] and in the lower plot from 2012 of the MAMI collaboration [604]. The numbers in each plot denote the center of mass energy in MeV.

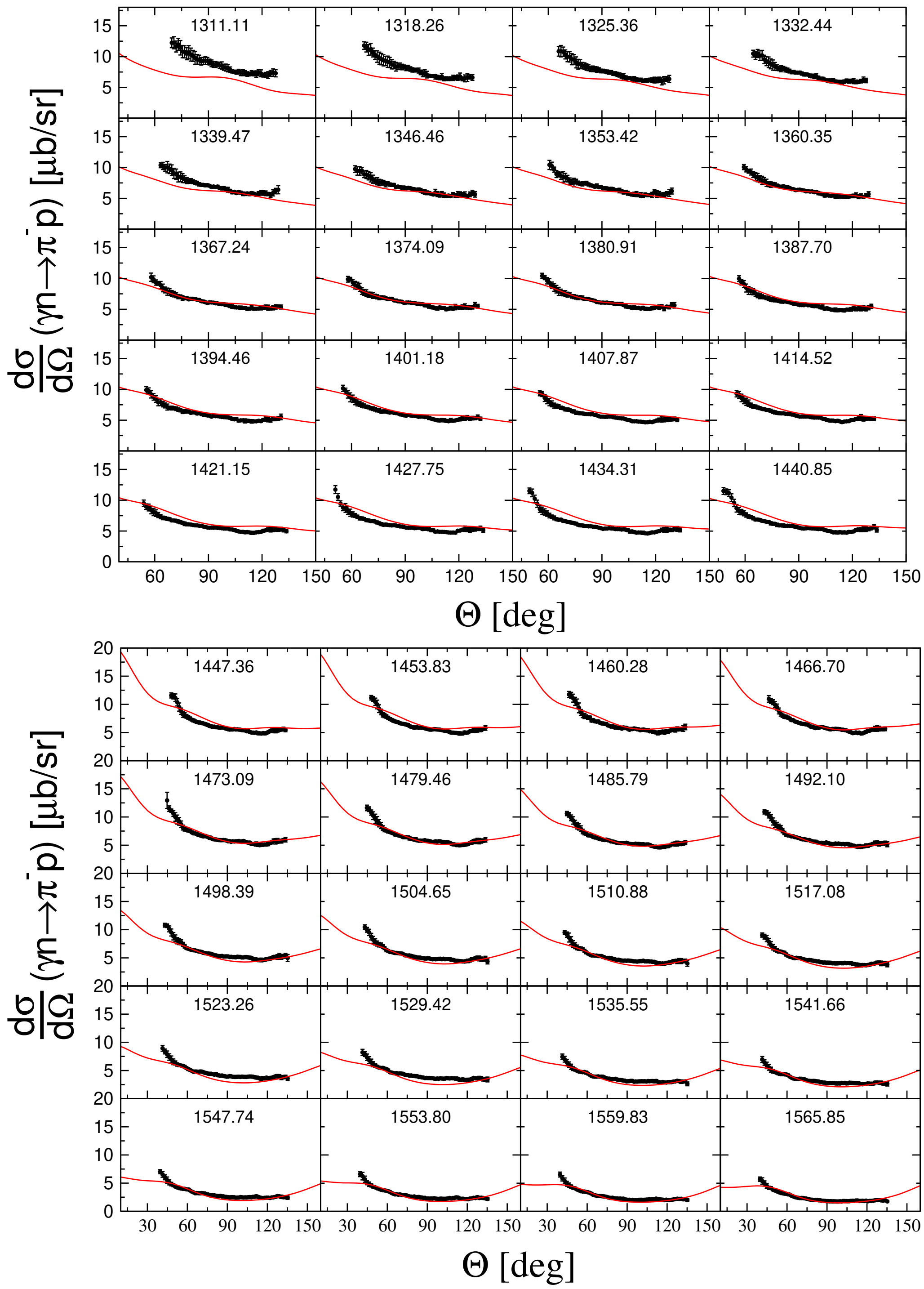

Figure 44: Fit results for the differential cross section $d\sigma/d\Omega$ for the process $\gamma n \to \pi^- p$ are shown in red. The data shown is from 2017 of the CLAS collaboration [602]. The numbers in each plot denote the center of mass energy in MeV.

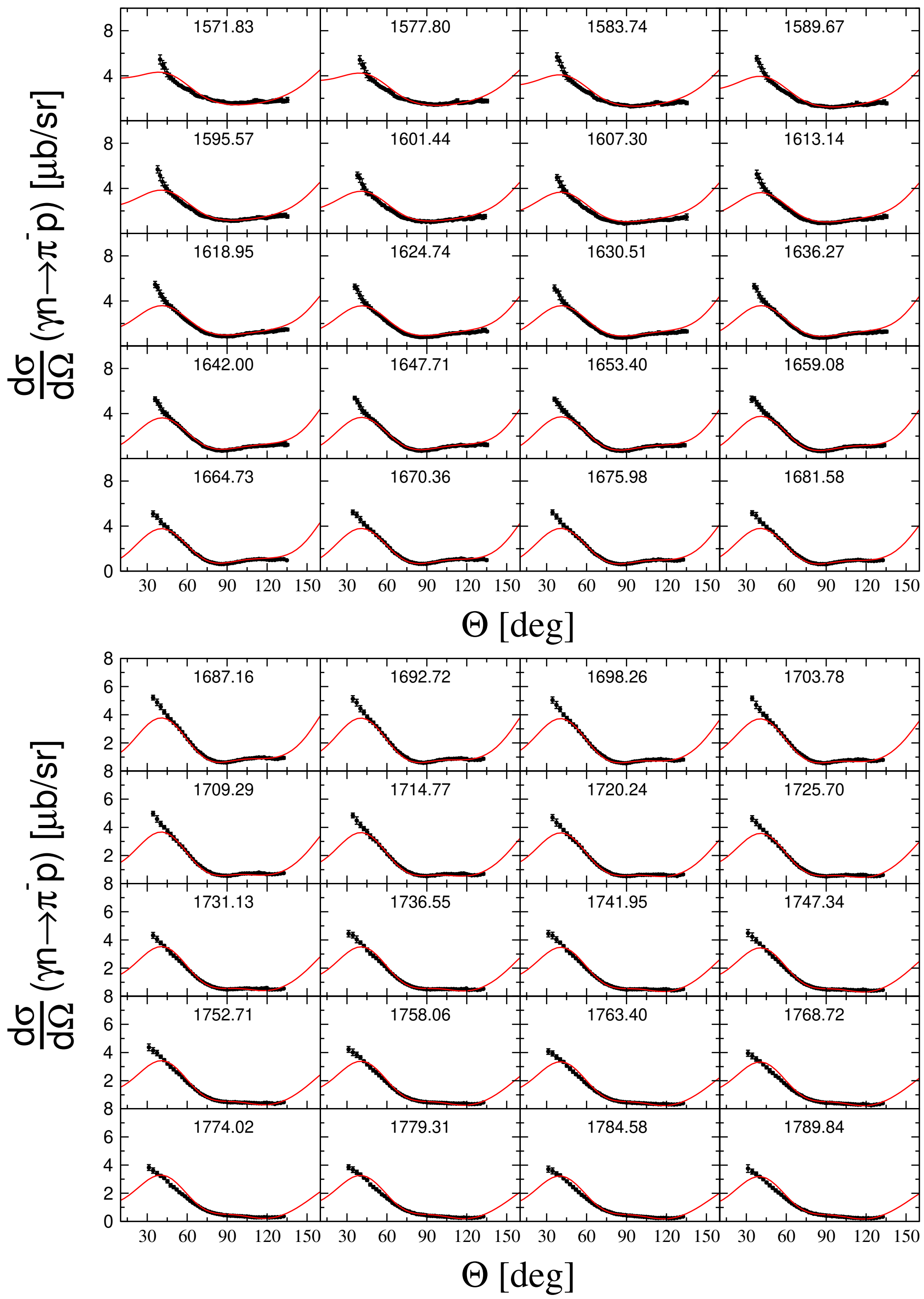

Figure 45: Fit results for the differential cross section $d\sigma/d\Omega$ for the process $\gamma n \to \pi^- p$ are shown in red. The data shown is from 2017 of the CLAS collaboration [602]. The numbers in each plot denote the center of mass energy in MeV.

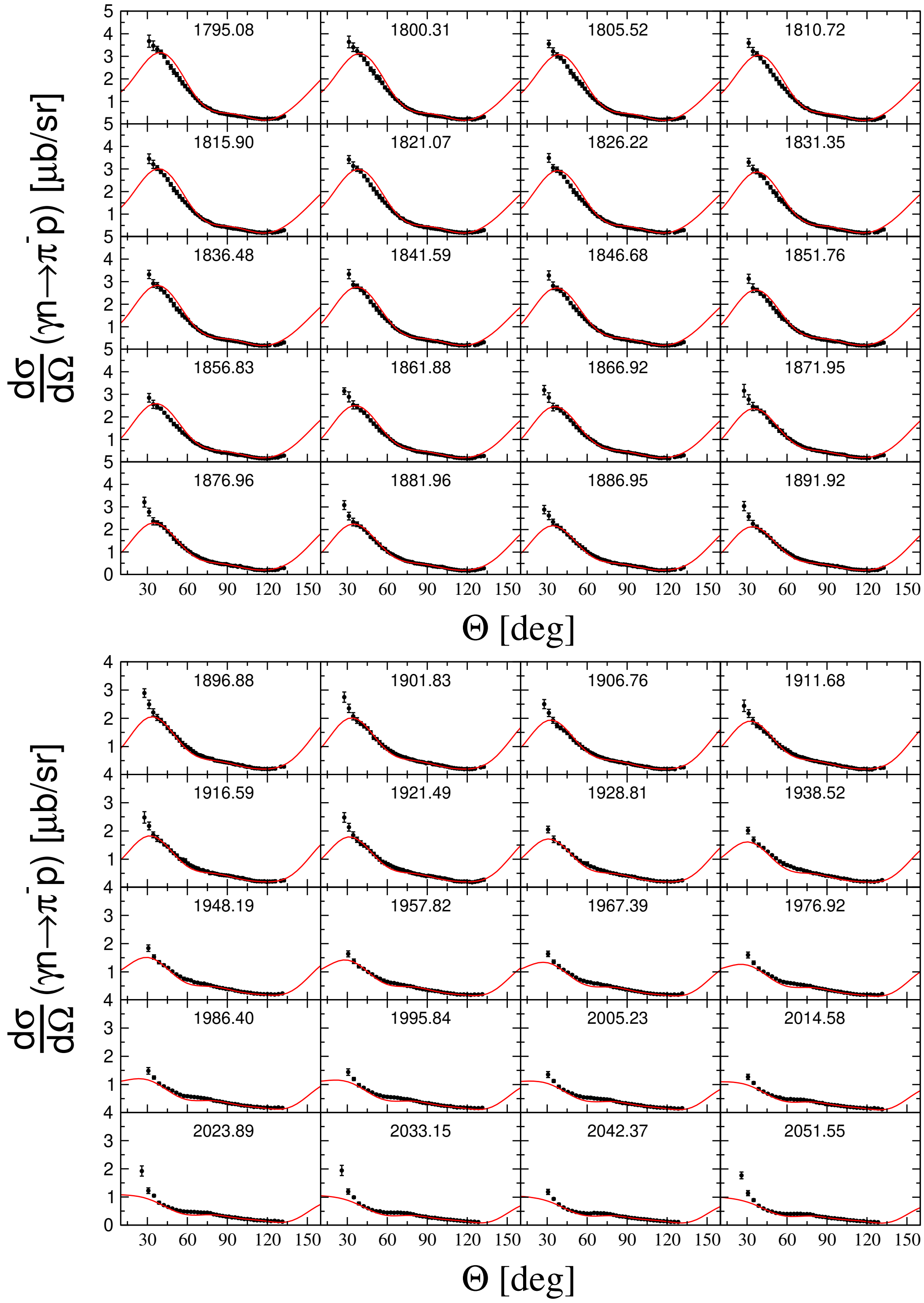

Figure 46: Fit results for the differential cross section $d\sigma/d\Omega$ for the process $\gamma n \to \pi^- p$ are shown in red. The data shown is from 2017 of the CLAS collaboration [602]. The numbers in each plot denote the center of mass energy in MeV.

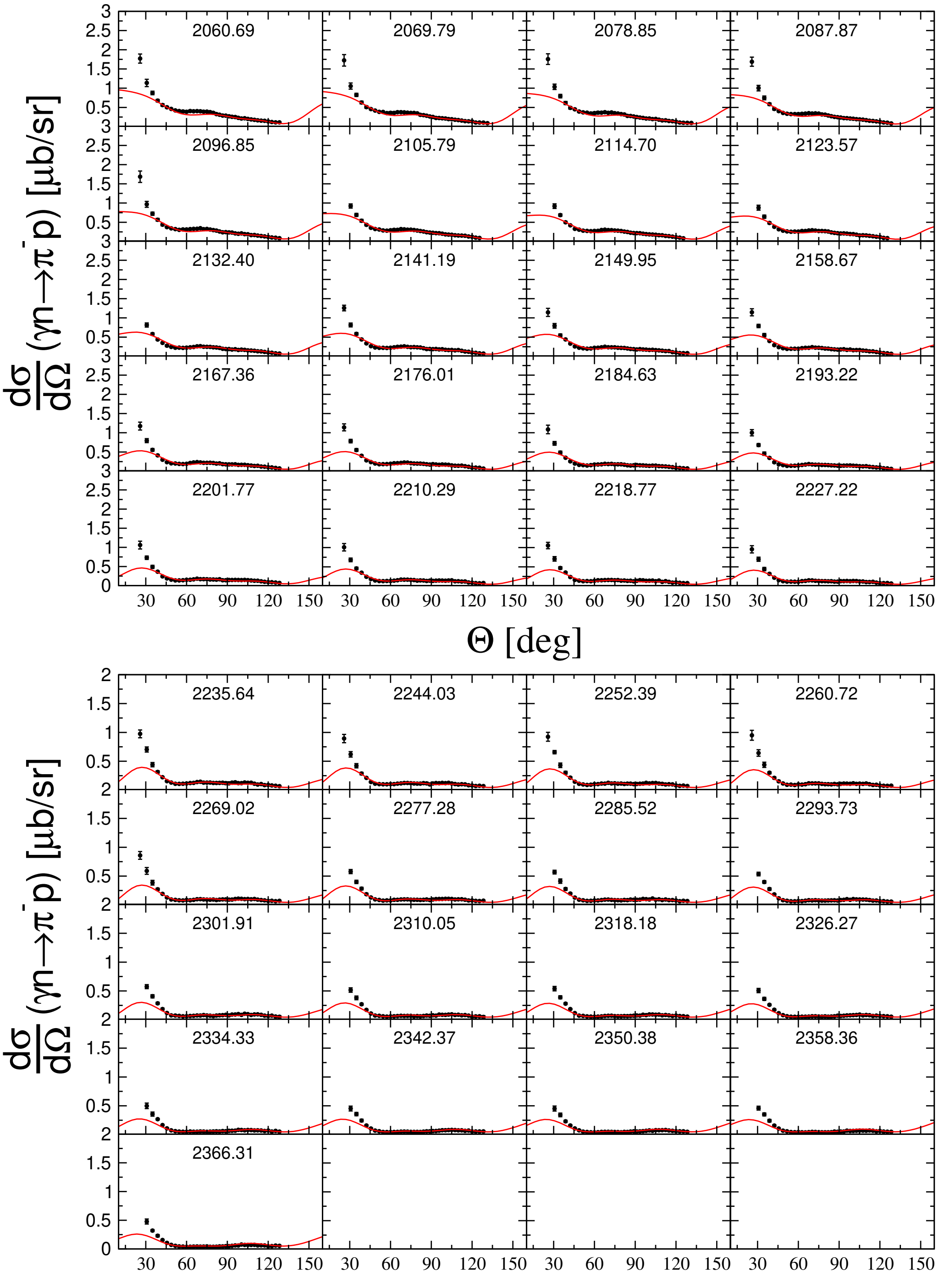

Figure 47: Fit results for the differential cross section $d\sigma/d\Omega$ for the process $\gamma n \to \pi^- p$ are shown in red. The data shown is from 2017 of the CLAS collaboration [602]. The numbers in each plot denote the center of mass energy in MeV.

F.2. Polarization observables

Here we present the fit results for the final state $\pi^- p$ to the polarization data sets. One can find the Σ data in Figs. 48-54, the data for P in Fig. 55, the T data in Figs. 56-57 and the E data in Fig. 58. The references for the data sets can be found in Tab. 18.

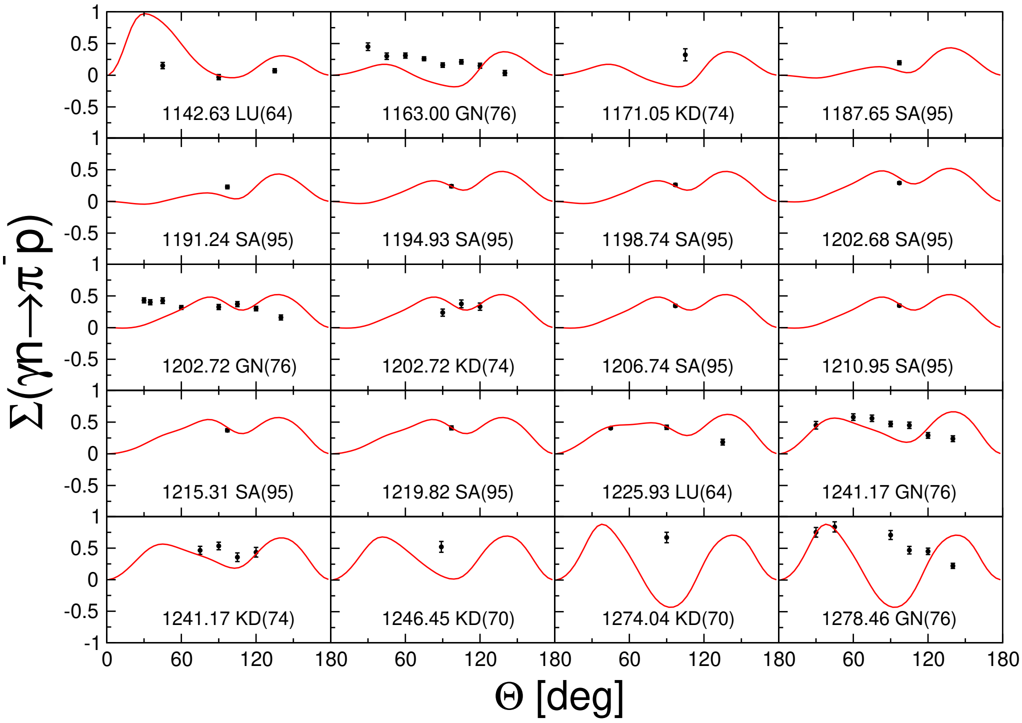

Figure 48: Fit results for the beam asymmetry Σ for the process $\gamma n \rightarrow \pi^- p$ are shown in red. The abbreviations are taken from the first author and year of the data sets up to 1995 as listed in Tab. 18. The numbers in each plot denote the center of mass energy in MeV.

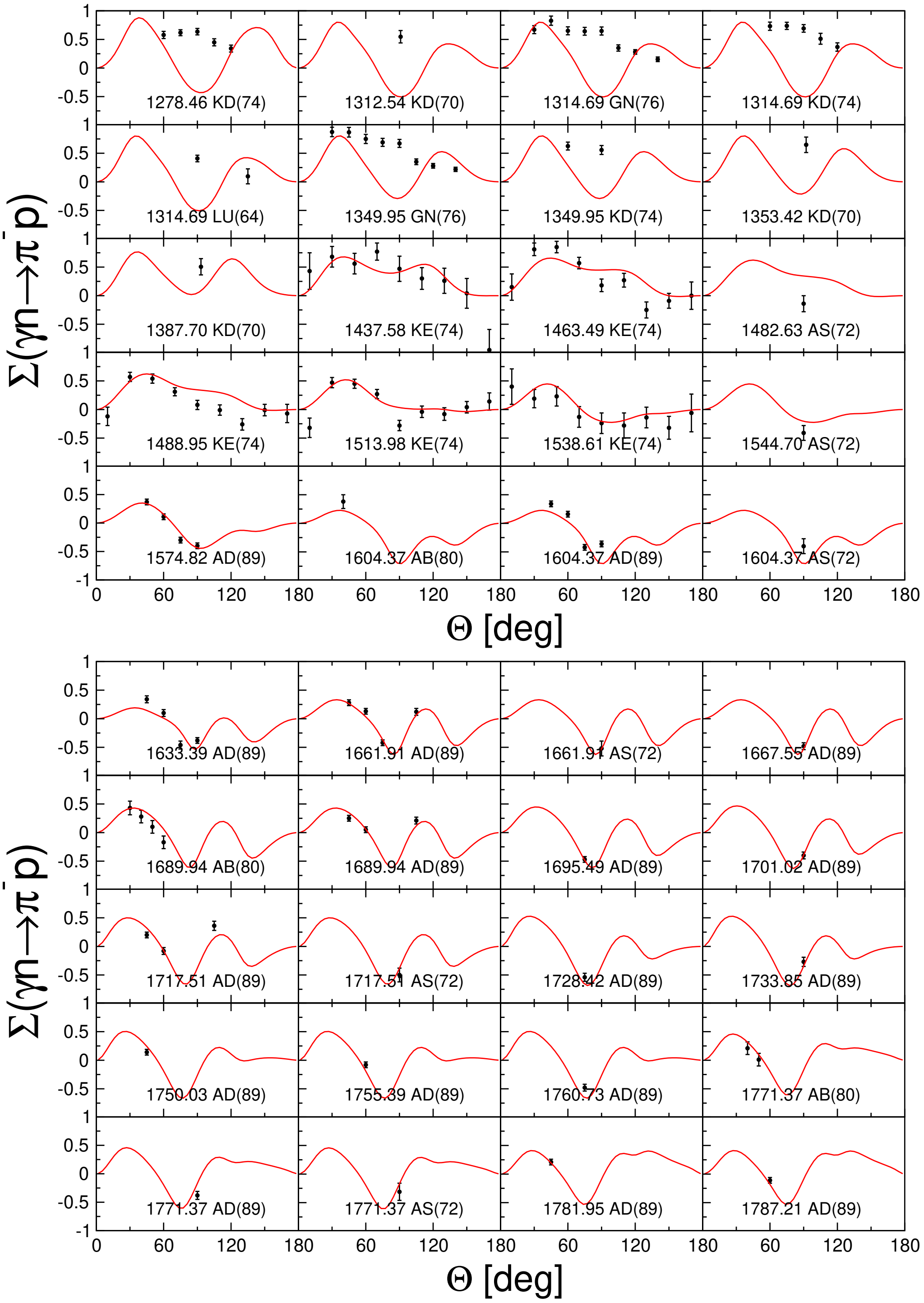

Figure 49: Fit results for the beam asymmetry Σ for the process $\gamma n \to \pi^- p$ are shown in red. The abbreviations are taken from the first author and year of the data sets up to 1995 as listed in Tab. 18. The numbers in each plot denote the center of mass energy in MeV.

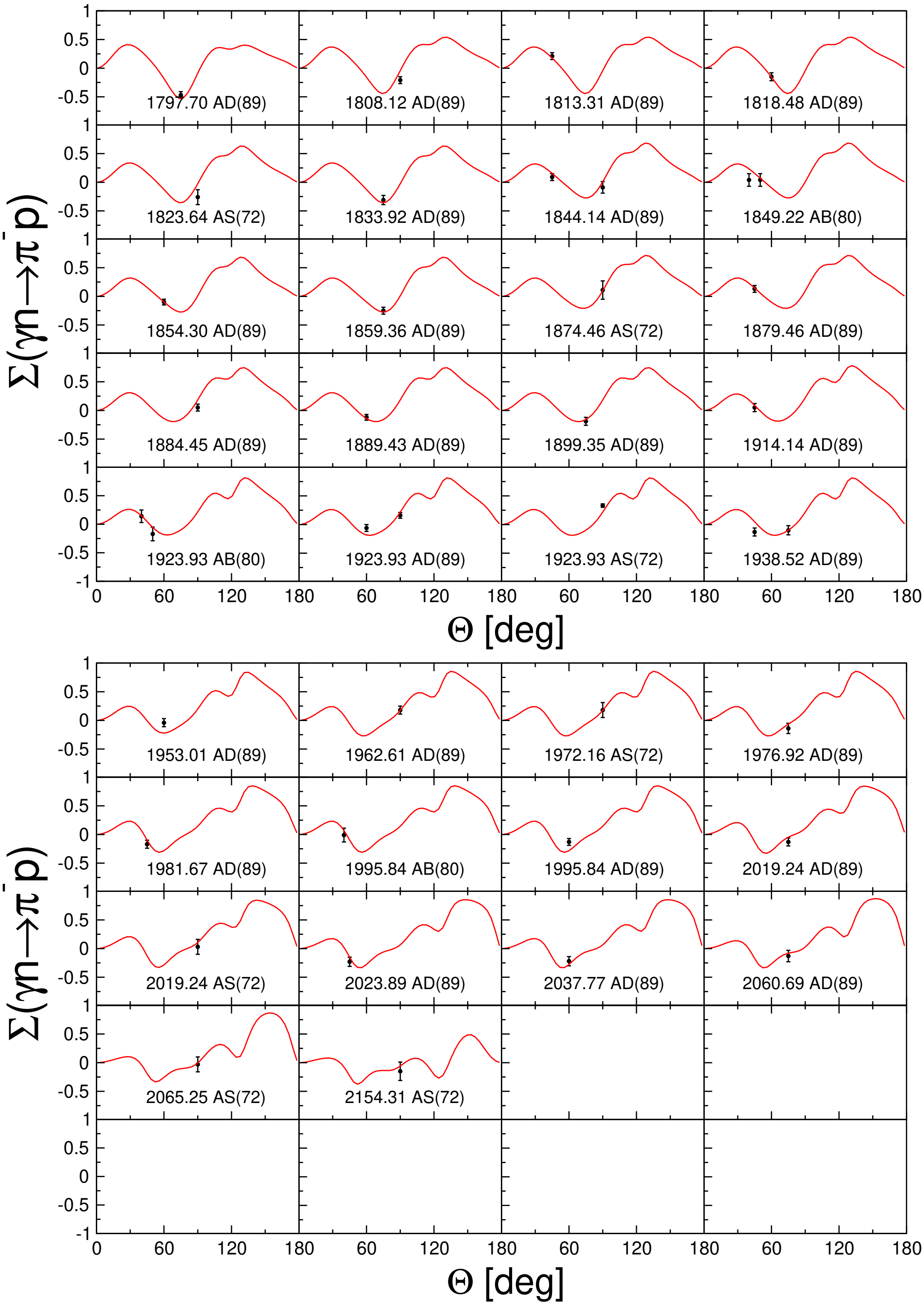

Figure 50: Fit results for the beam asymmetry Σ for the process $\gamma n \to \pi^- p$ are shown in red. The abbreviations are taken from the first author and year of the data sets up to 1995 as listed in Tab. 18. The numbers in each plot denote the center of mass energy in MeV.

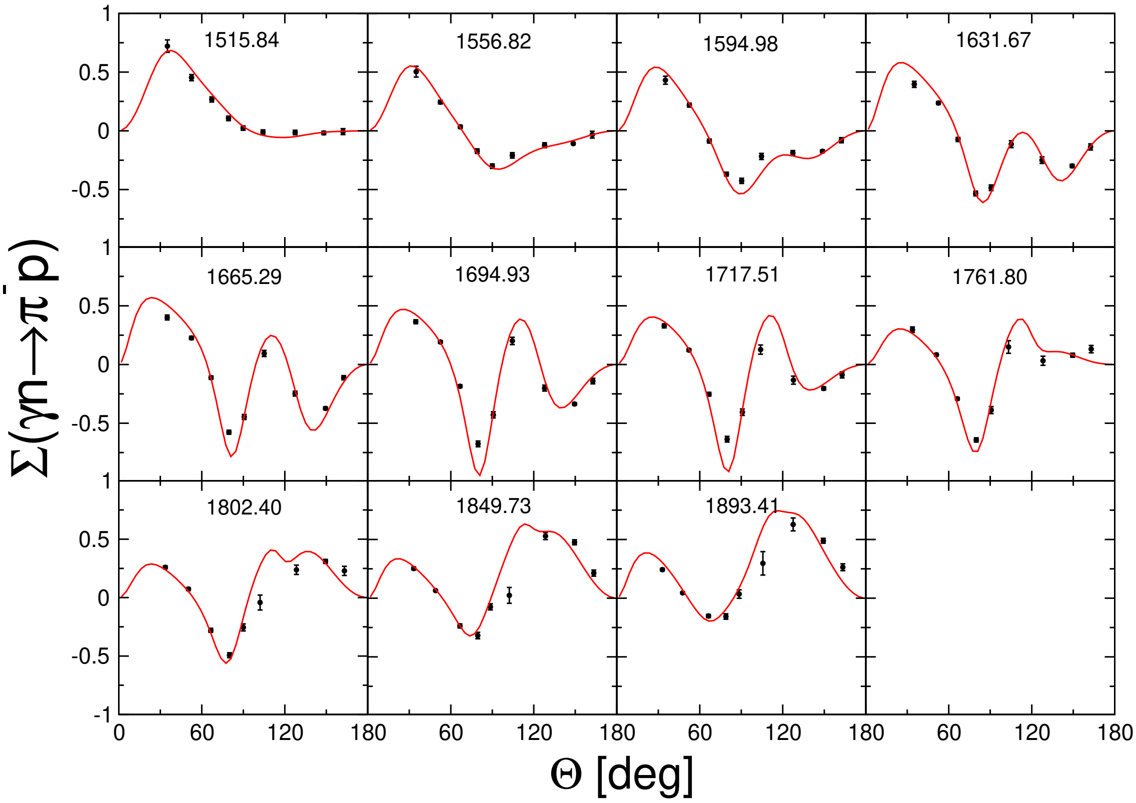

Figure 51: Fit results for the beam asymmetry Σ for the process $\gamma n \to \pi^- p$ are shown in red. The data shown is GRAAL [621]. The numbers in each plot denote the center of mass energy in MeV.

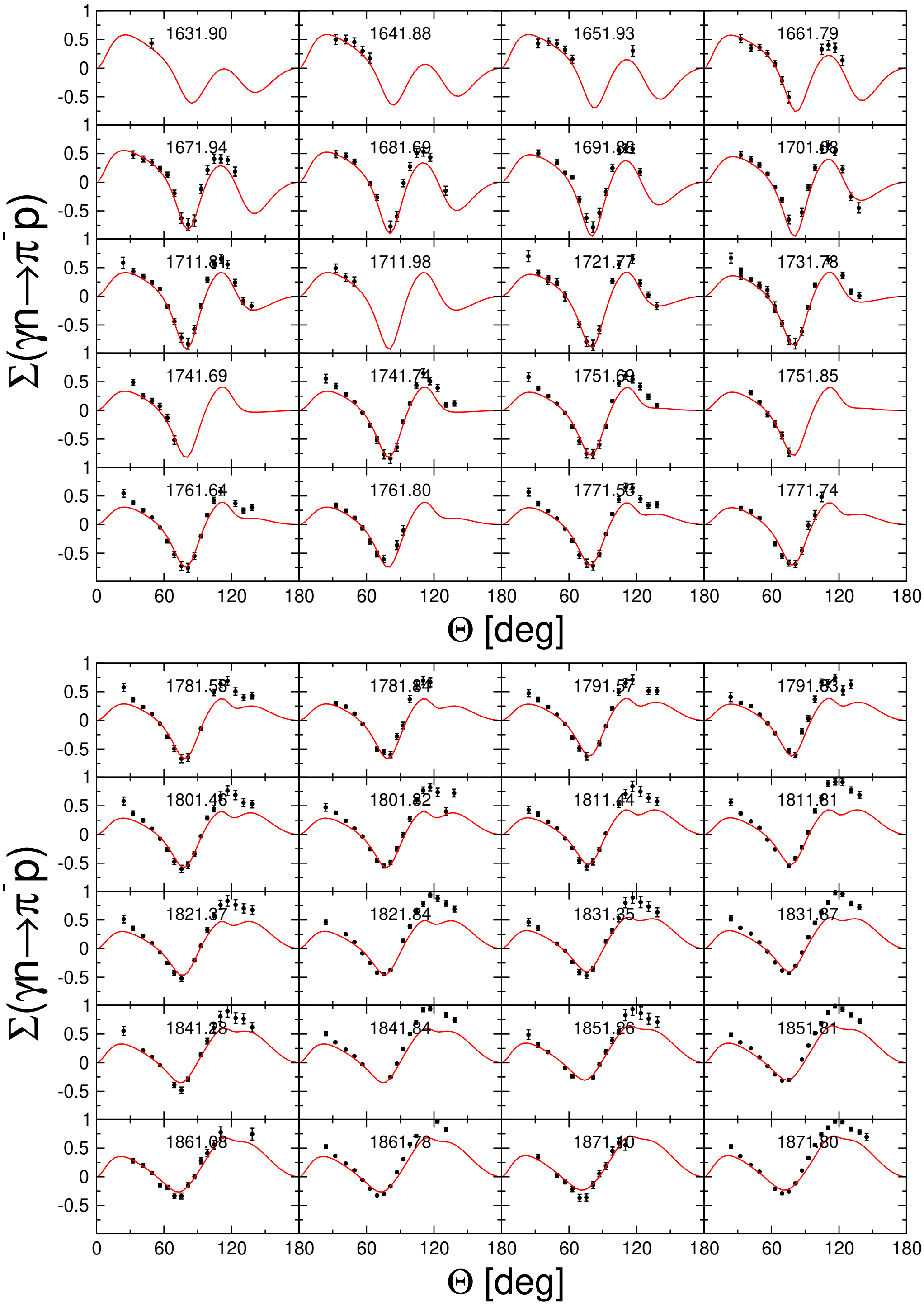

Figure 52: Fit results for the beam asymmetry Σ for the process $\gamma n \to \pi^- p$ are shown in red. The data shown is from Sokhan [126]. The numbers in each plot denote the center of mass energy in MeV.

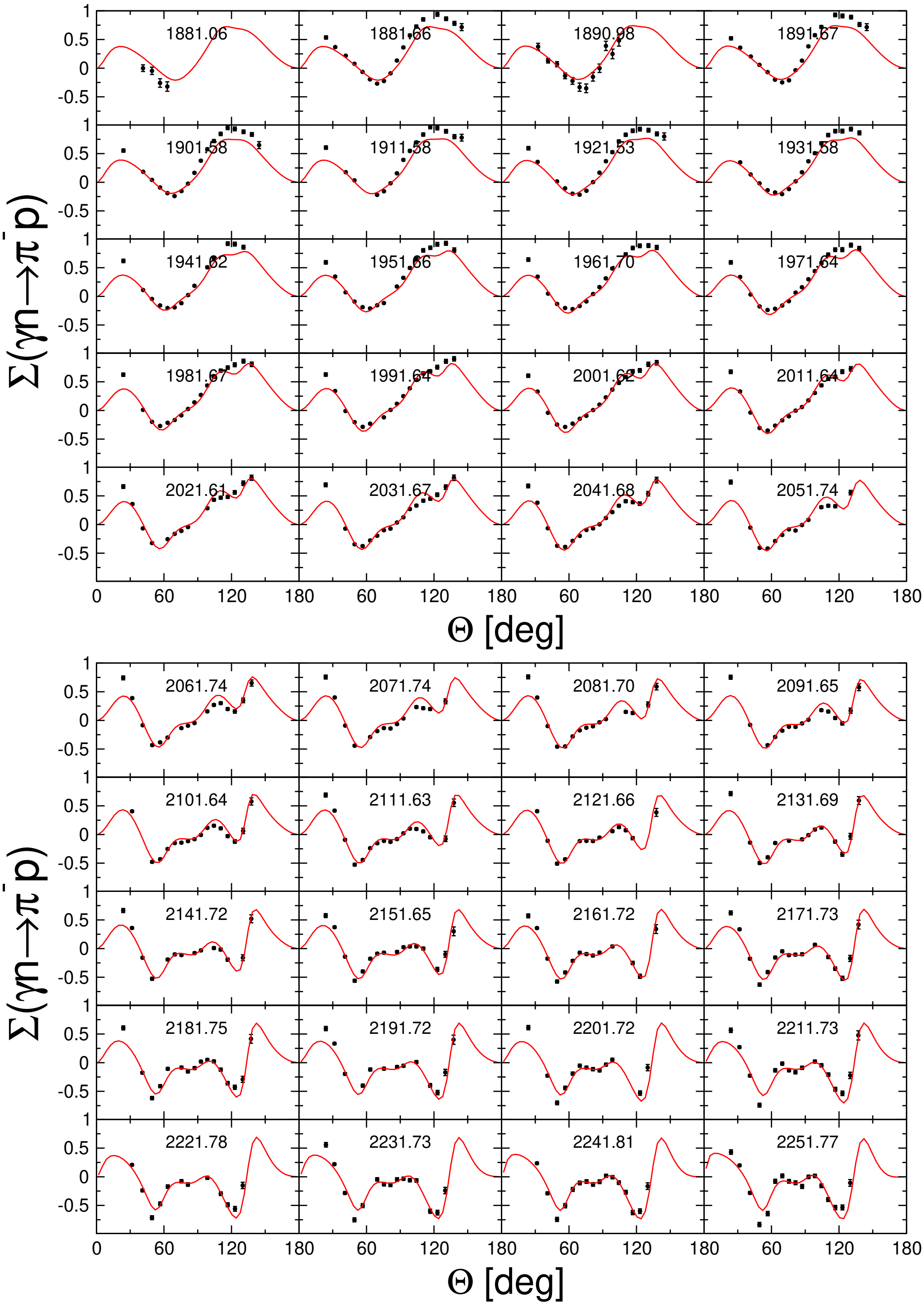

Figure 53: Fit results for the beam asymmetry Σ for the process $\gamma n \to \pi^- p$ are shown in red. The data shown is from Sokhan [126]. The numbers in each plot denote the center of mass energy in MeV.

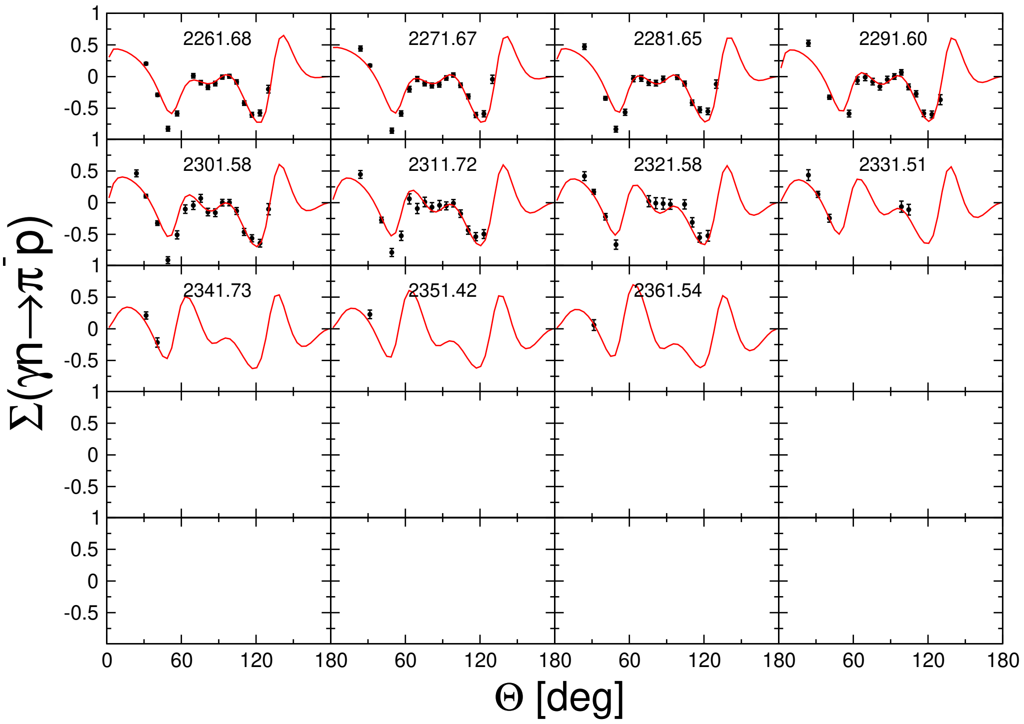

Figure 54: Fit results for the beam asymmetry Σ for the process $\gamma n \rightarrow \pi^- p$ are shown in red. The data shown is from Sokhan [126]. The numbers in each plot denote the center of mass energy in MeV.

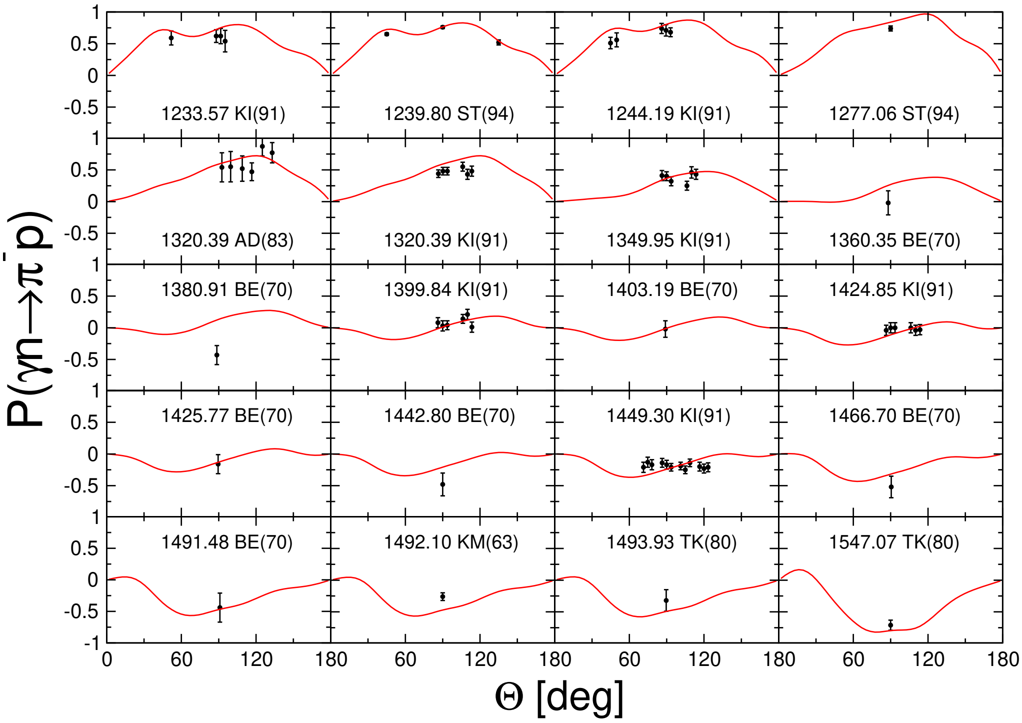

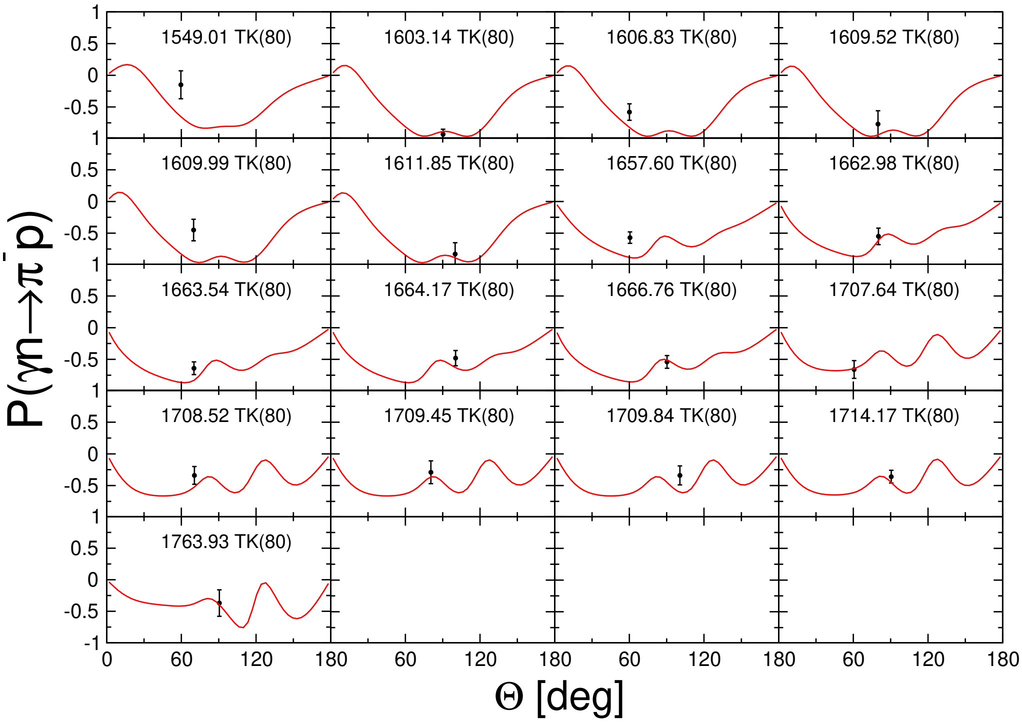

Figure 55: Fit results for the recoil polarization P for the process $\gamma n \to \pi^- p$ are shown in red. The abbreviations are taken from the first author and year of the data sets up to 1994 as listed in Tab. 18. The numbers in each plot denote the center of mass energy in MeV.

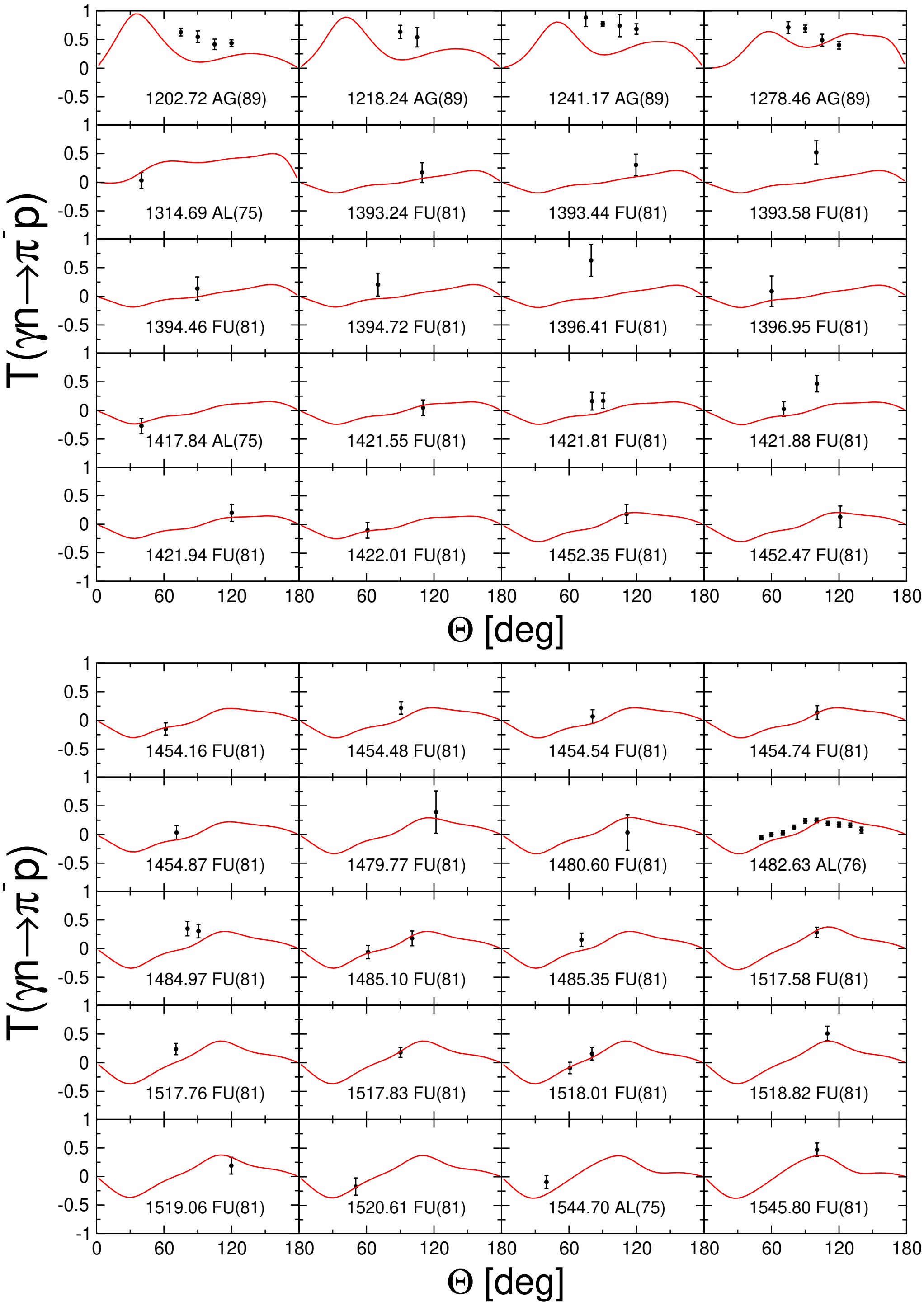

Figure 56: Fit results for the target polarization T for the process $\gamma n \to \pi^- p$ are shown in red. The abbreviations are taken from the first author and year of the data sets up to 1989 as listed in Tab. 18. The numbers in each plot denote the center of mass energy in MeV.

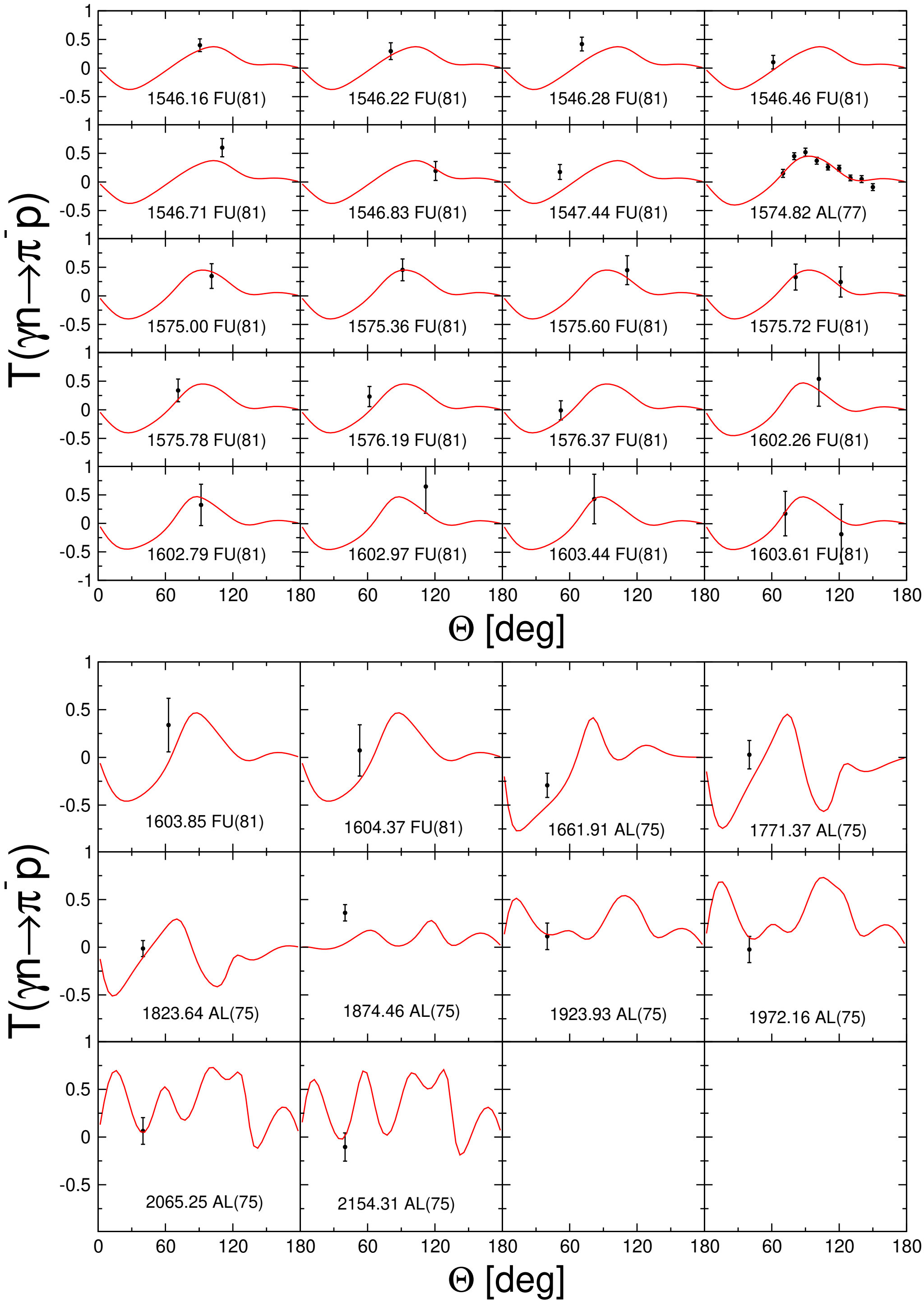

Figure 57: Fit results for the target polarization T for the process $\gamma n \to \pi^- p$ are shown in red. The abbreviations are taken from the first author and year of the data sets up to 1989 as listed in Tab. 18. The numbers in each plot denote the center of mass energy in MeV.

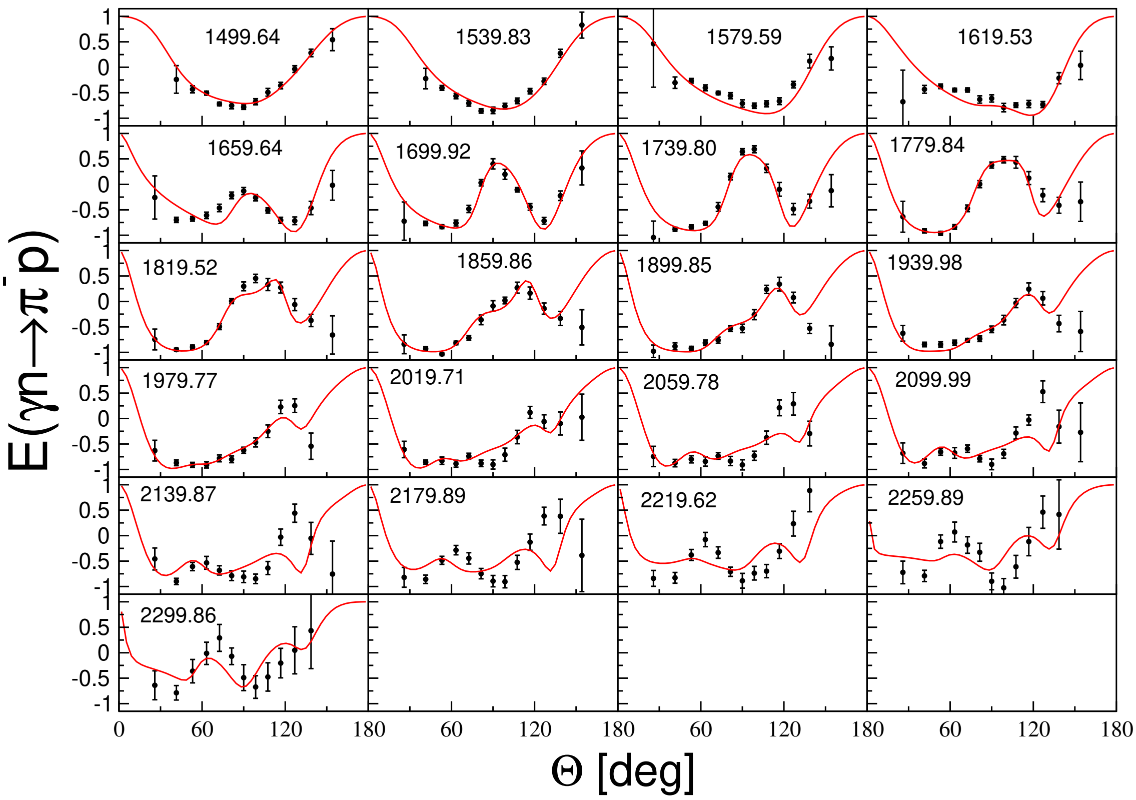

Figure 58: Fit results for the beam-target asymmetry E for the process $\gamma n \to \pi^- p$ are shown in red. The data shown is from CLAS [637]. The numbers in each plot denote the center of mass energy in MeV.

F.2.1. Selected plots with H_{19} resonance turned off

Here we present the influence of the H_{19} resonance $N(2220)$ $9/2^+$ on some $\pi^- p$ data.

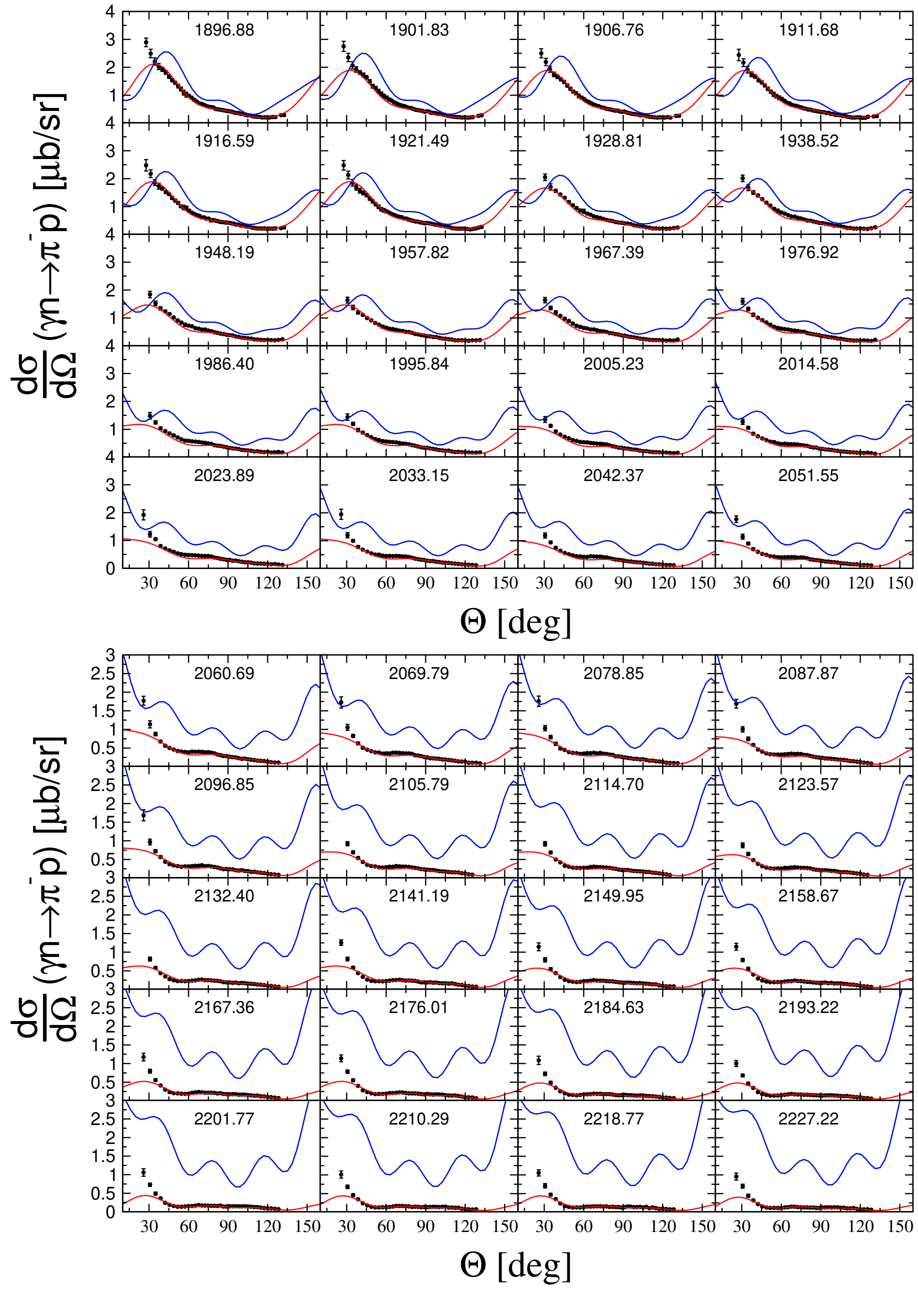

Figure 59: Current fit result (red) and the same solution without allowing H_{19} pole to couple to πN (blue) for the process $\gamma n \to \pi^- p$. The data shown is from the 2017 CLAS study [637].

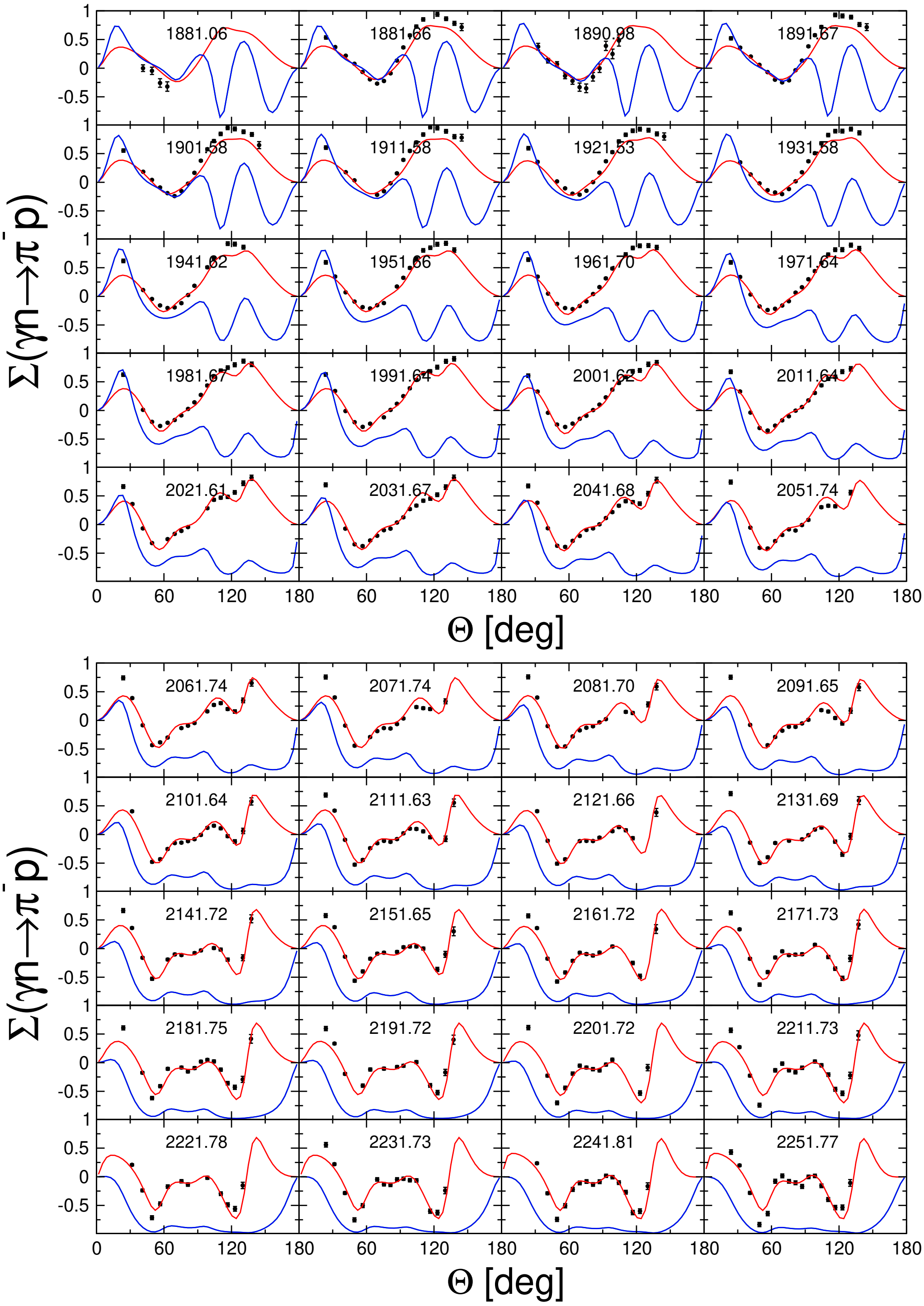

Figure 60: Current fit result (red) and the same solution without allowing H_{19} pole to couple to πN (blue) for the process $\gamma n \to \pi^- p$. The data shown is from Sokhan [126].

G. Individual channel contributions for the GDH sum rule

In the following we present the individual GDH sum rule contributions from the JüBo2025 and JüBo2026 solutions.

G.1. Results from JüBo2025 analysis

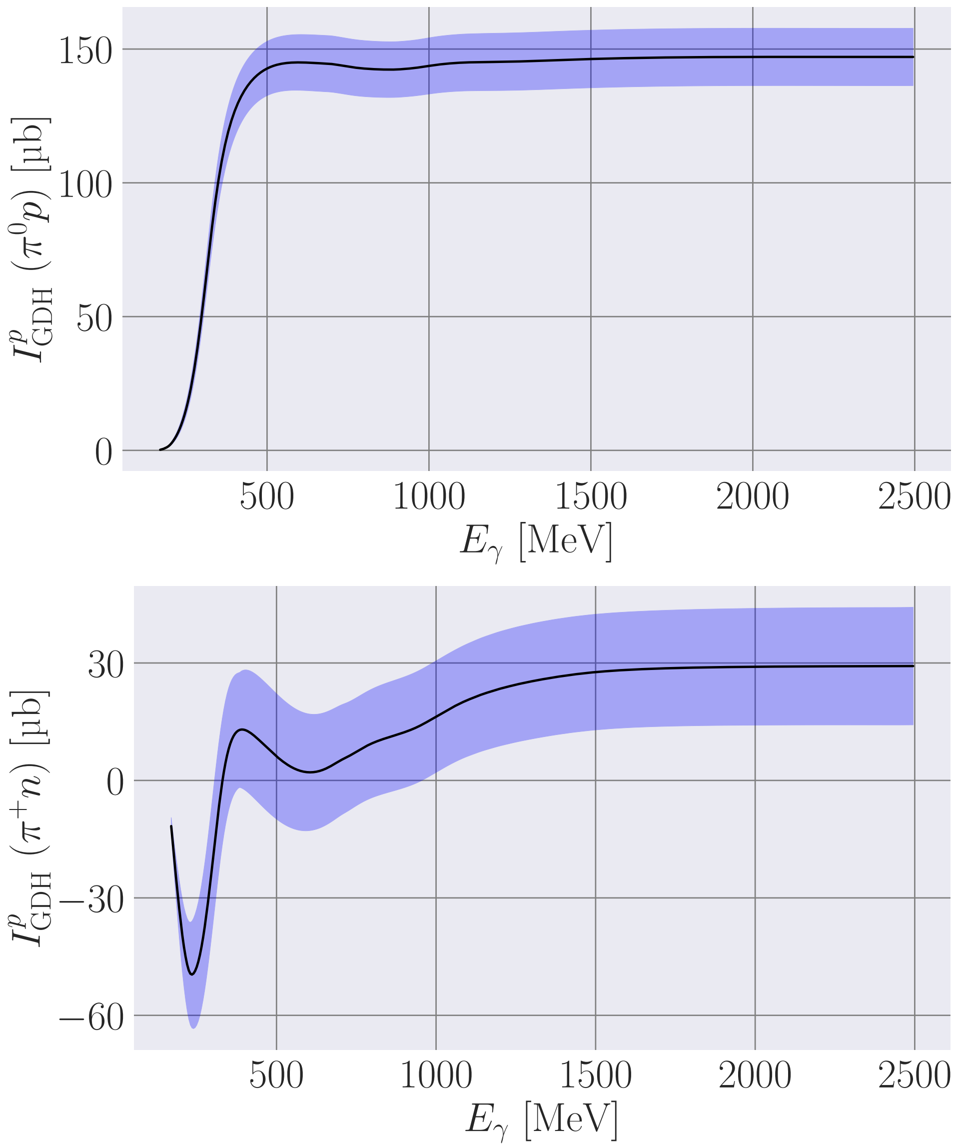

Figure 61: Running GDH integral I^p_{GDH} as in Eq. (6.1) for the $\pi^0 p$ and $\pi^+ n$ channels from the JüBo 2025 solution.

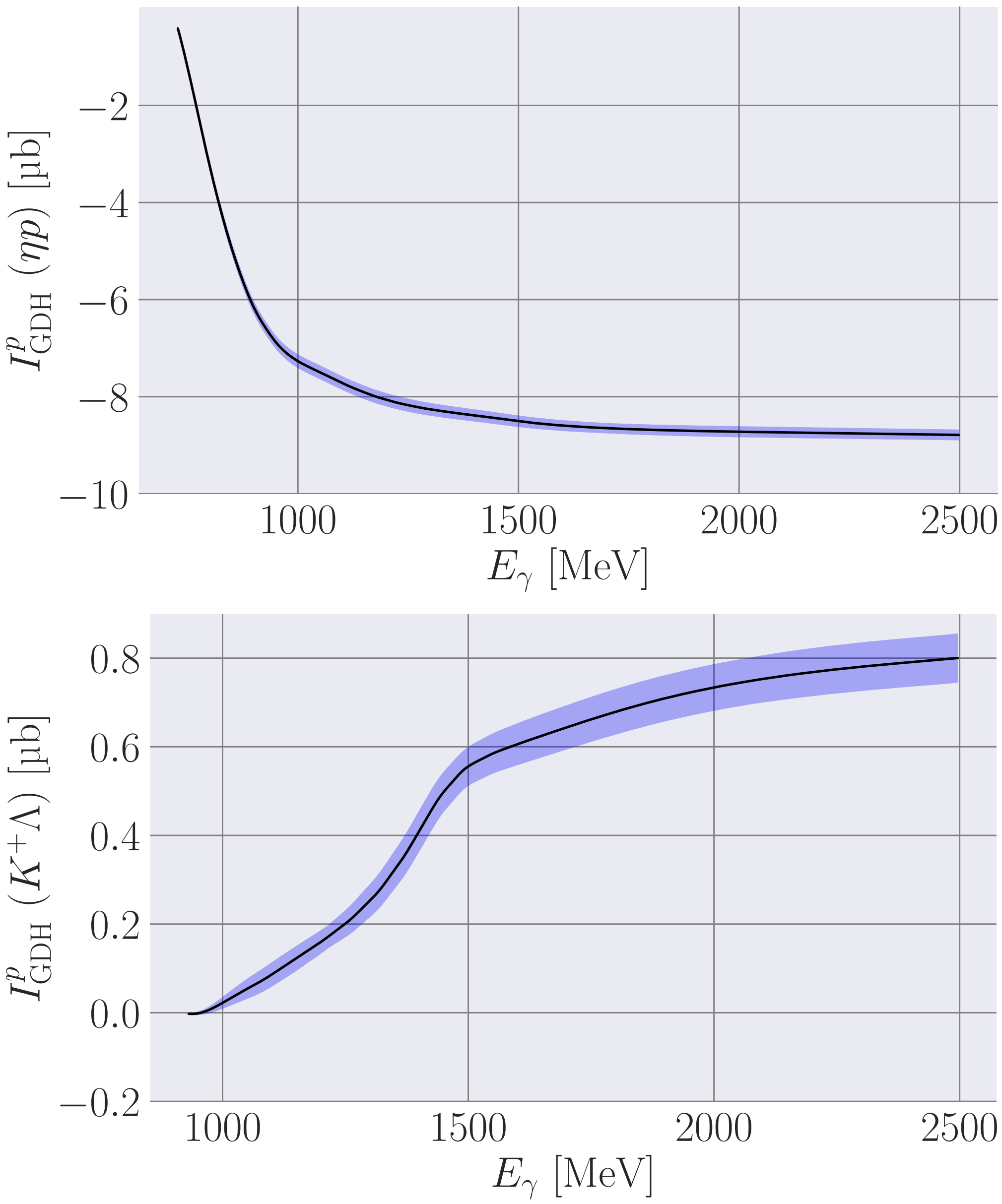

Figure 62: Running GDH integral I^p_{GDH} as in Eq. (6.1) for the ηp and $K\Lambda$ channels from the JüBo 2025 solution.

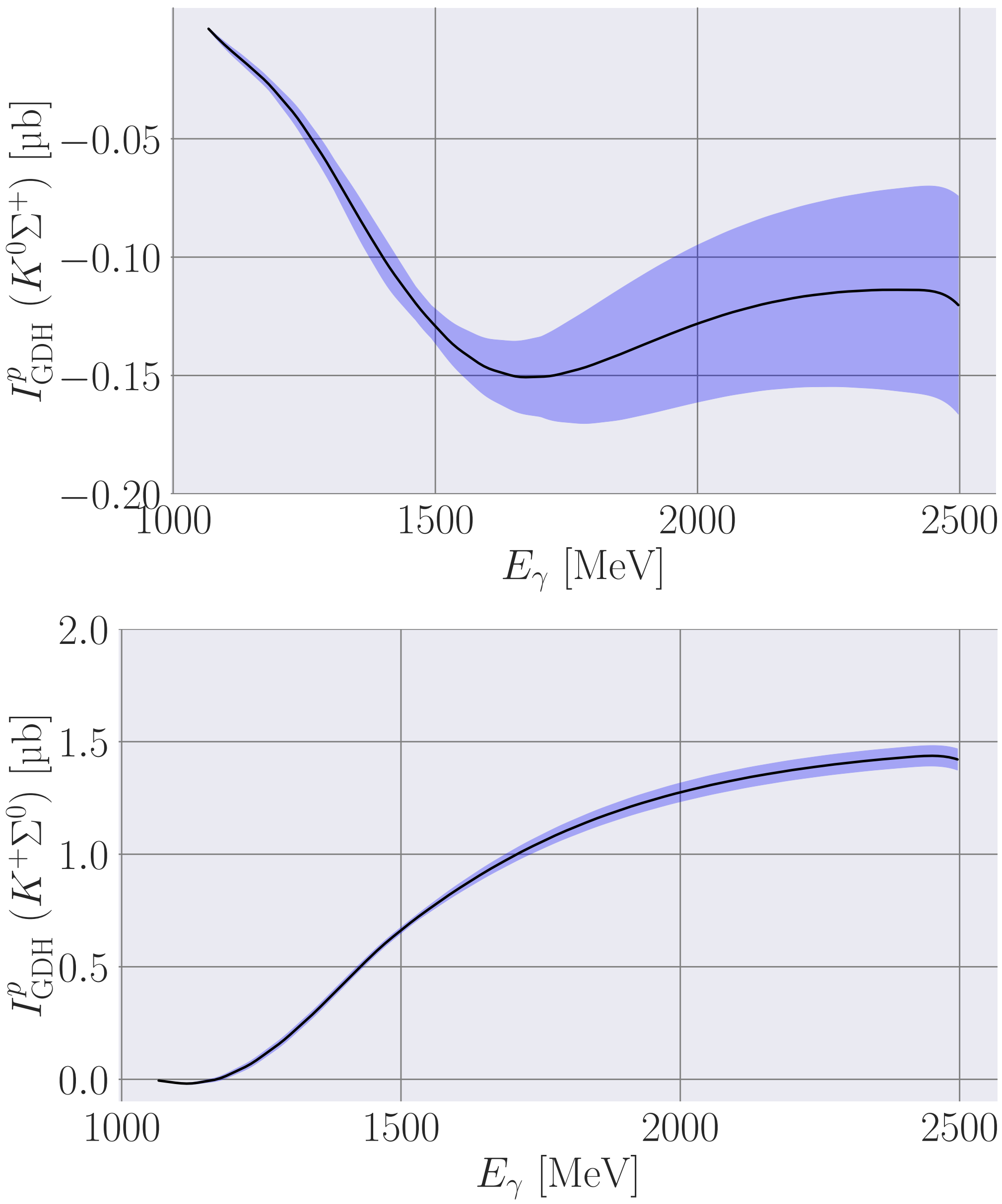

Figure 63: Running GDH integral I^p_{GDH} as in Eq. (6.1) for the $K\Sigma$ channels from the JüBo 2025 solution.

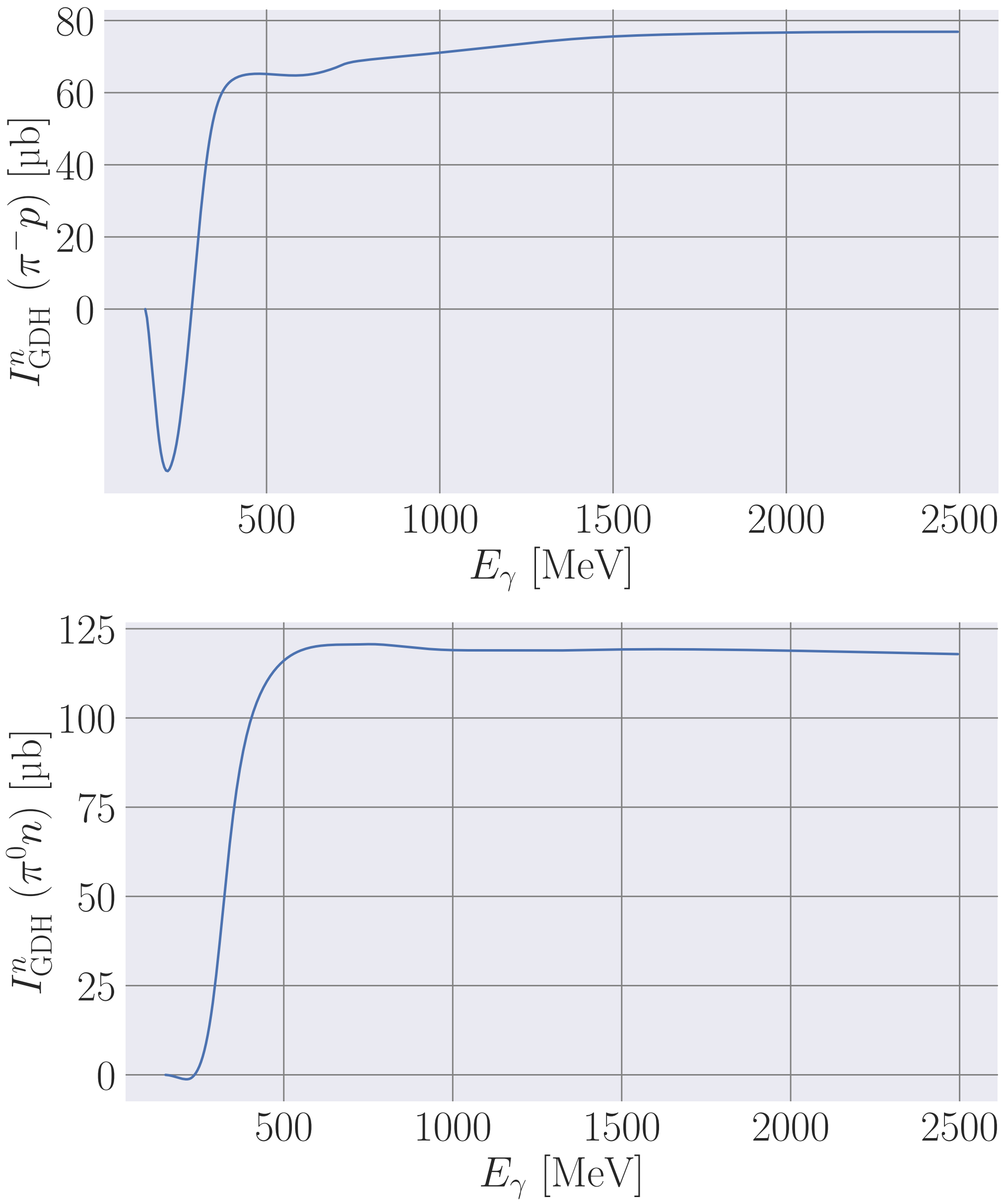

Figure 64: Running GDH integral I^n_{GDH} as in Eq. (6.1) for the $\pi^- p$ and $\pi^0 n$ channels from the JüBo 2026 solution.

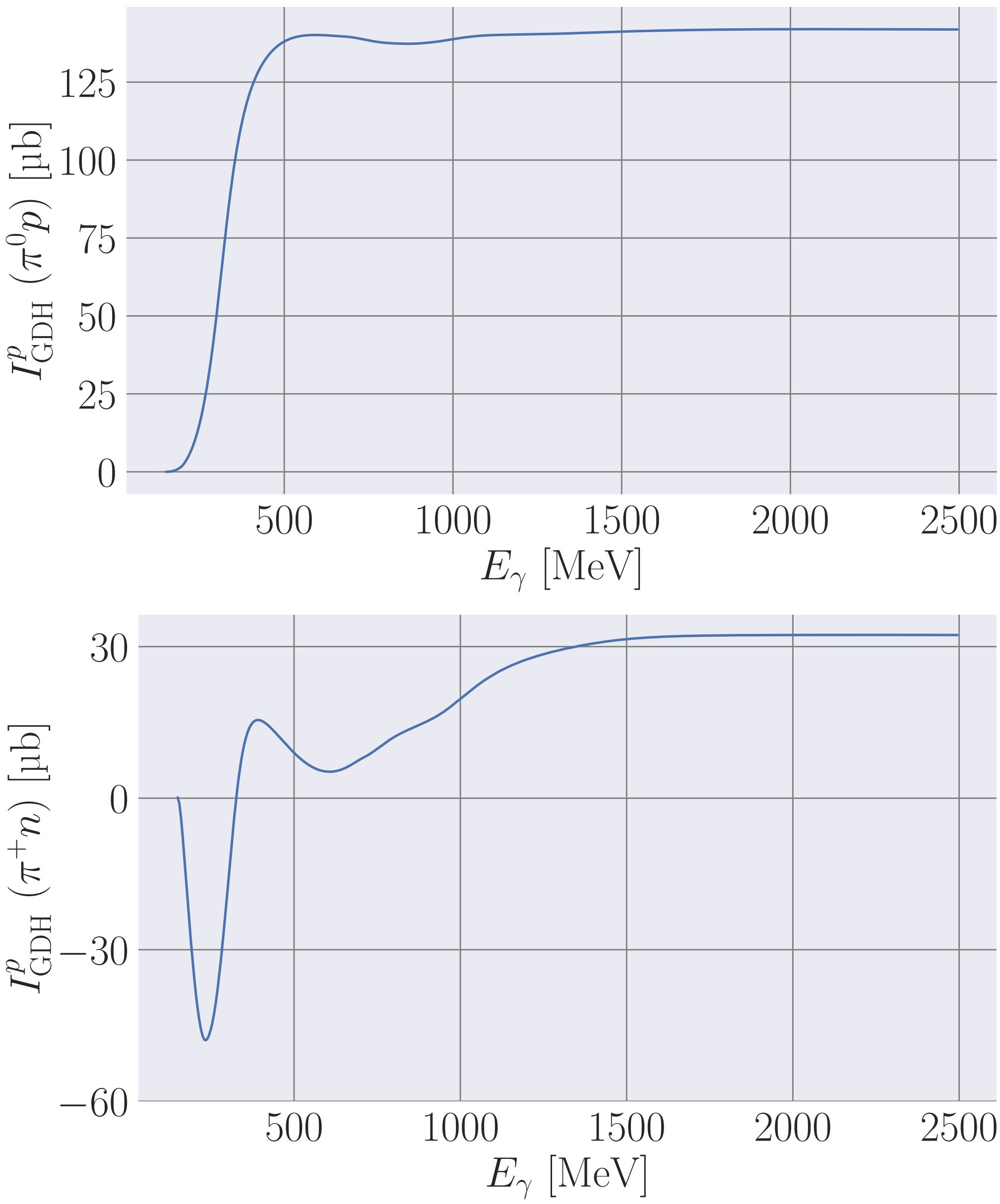

Figure 65: Running GDH integral I^p_{GDH} as in Eq. (6.1) for the $\pi^0 p$-channel.

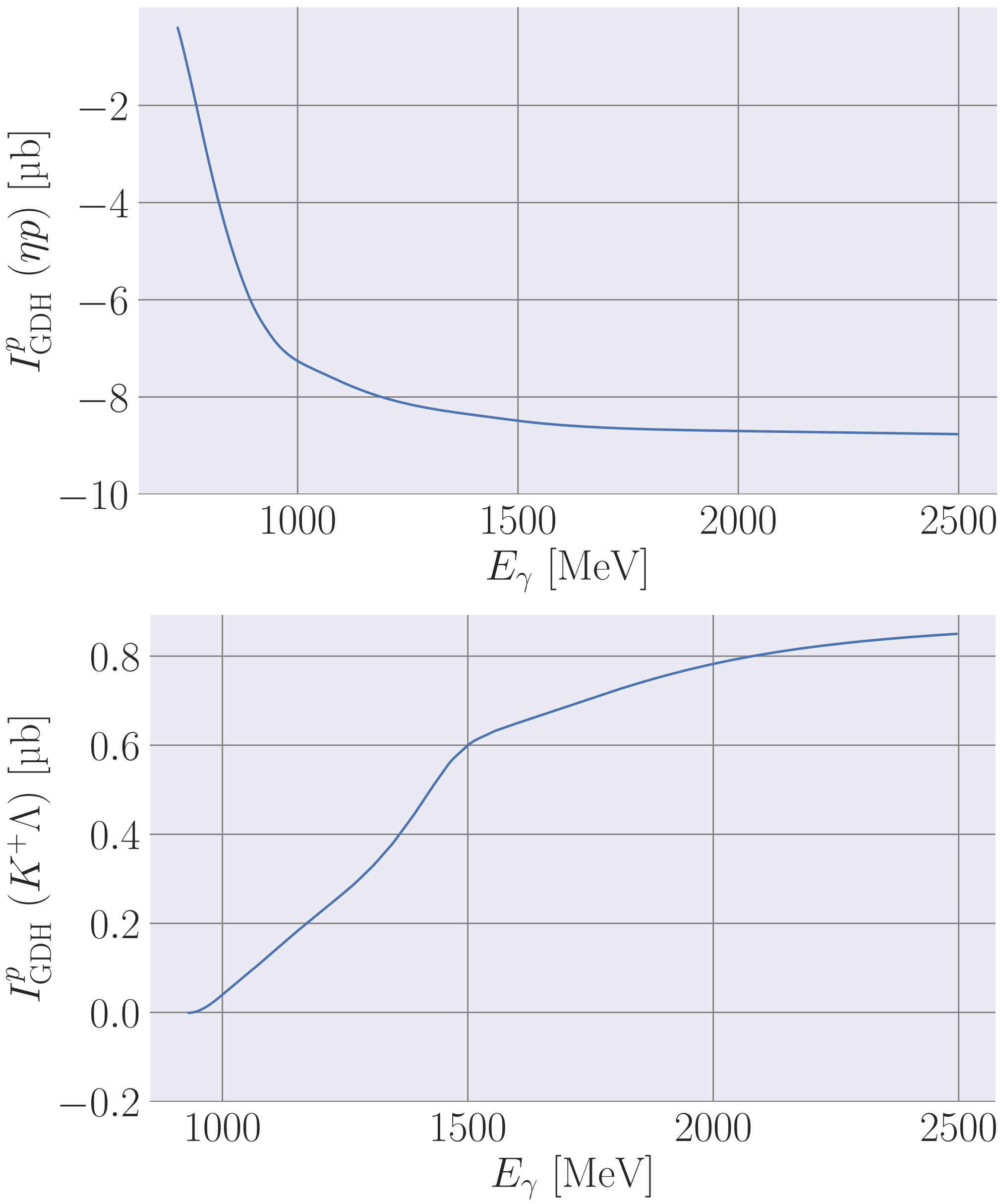

Figure 66: Running GDH integral I^p_{GDH} as in Eq. (6.1) for the ηp-channel.

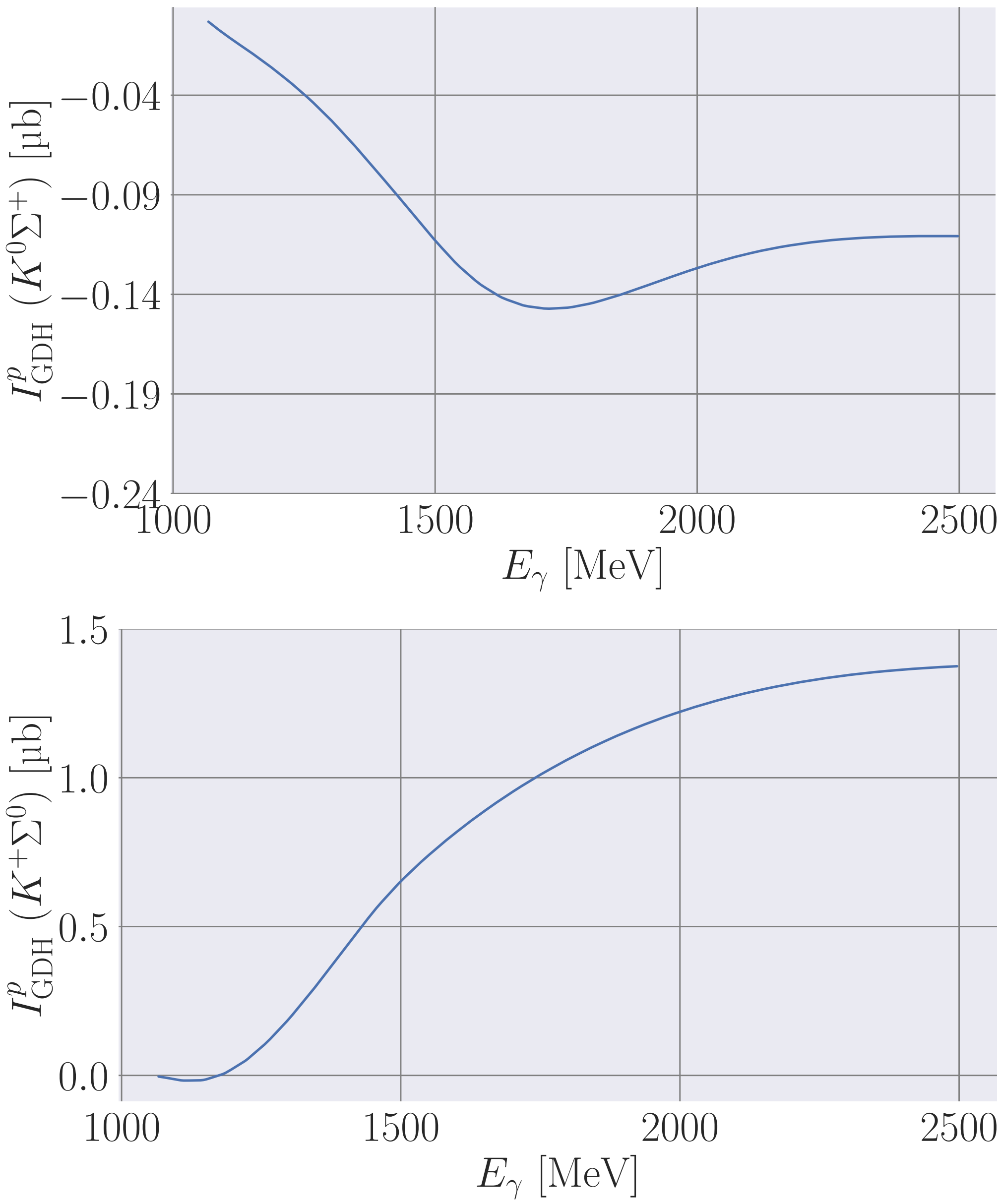

Figure 67: Running GDH integral I^p_{GDH} as in Eq. (6.1) for the $K^0\Sigma^+$-channel.

References

[1] C. Schneider et al.
"Coupled-channel contributions to the GDH sum rule from the Jülich–Bonn approach".
In: *Eur. Phys. J. A* 61.10 (2025), p. 241. DOI: 10.1140/epja/s10050-025-01719-x.
arXiv: 2508.00598 [nucl-th] (cit. on pp. 3, 12, 28, 45, 58, 91–94).

[2] Z. Maki, M. Nakagawa, and S. Sakata.
"Remarks on the Unified Model of Elementary Particles".
In: *Progress of Theoretical Physics* 28.5 (Nov. 1962), pp. 870–880. ISSN: 0033-068X.
DOI: 10.1143/PTP.28.870. eprint:
https://academic.oup.com/ptp/article-pdf/28/5/870/5258750/28-5-870.pdf.
URL: https://doi.org/10.1143/PTP.28.870 (cit. on p. 6).

[3] J. F. Donoghue, E. Golowich, and B. R. Holstein. *Dynamics of the Standard Model*.
Cambridge Monographs on Particle Physics, Nuclear Physics and Cosmology.
Cambridge University Press, 1992 (cit. on pp. 6, 18).

[4] S. M. Bilenky, J. Hosek, and S. T. Petcov.
"On Oscillations of Neutrinos with Dirac and Majorana Masses".
In: *Phys. Lett. B* 94 (1980), pp. 495–498. DOI: 10.1016/0370-2693(80)90927-2
(cit. on p. 7).

[5] F. Takahashi et al. "Review of Particle Physics".
In: *Int. J. Mod. Phys. A* 41 (2026), p. 2630011. DOI: 10.1142/S0217751X26300115
(cit. on pp. 7, 8, 14, 27, 43, 50, 54, 55, 61, 67, 68, 91, 92, 101, 117).

[6] F.-K. Guo et al. "Hadronic molecules".
In: *Rev. Mod. Phys.* 90.1 (2018). [Erratum: Rev.Mod.Phys. 94, 029901 (2022)], p. 015004.
DOI: 10.1103/RevModPhys.90.015004. arXiv: 1705.00141 [hep-ph] (cit. on p. 8).

[7] N. Brambilla et al.
"The XYZ states: experimental and theoretical status and perspectives".
In: *Phys. Rept.* 873 (2020), pp. 1–154. DOI: 10.1016/j.physrep.2020.05.001.
arXiv: 1907.07583 [hep-ex] (cit. on p. 8).

[8] L. Meng et al. "Chiral perturbation theory for heavy hadrons and chiral effective field theory for heavy hadronic molecules". In: *Phys. Rept.* 1019 (2023), pp. 1–149.
DOI: 10.1016/j.physrep.2023.04.003. arXiv: 2204.08716 [hep-ph] (cit. on p. 8).

[9] H.-X. Chen et al. "An updated review of the new hadron states".
In: *Rept. Prog. Phys.* 86.2 (2023), p. 026201. DOI: 10.1088/1361-6633/aca3b6.
arXiv: 2204.02649 [hep-ph] (cit. on p. 8).

[10] V. E. Barnes et al. "Observation of a Hyperon with Strangeness Minus Three".
In: *Phys. Rev. Lett.* 12 (1964), pp. 204–206. DOI: 10.1103/PhysRevLett.12.204
(cit. on p. 8).

[11] A. Thiel, F. Afzal, and Y. Wunderlich. "Light Baryon Spectroscopy".
In: *Prog. Part. Nucl. Phys.* 125 (2022), p. 103949. DOI: 10.1016/j.ppnp.2022.103949.
arXiv: 2202.05055 [nucl-ex] (cit. on pp. 9–11, 14, 39).

[12] M. Döring. "Phenomenology of light baryon resonances". In: (Oct. 2025).
arXiv: 2510.13133 [nucl-th] (cit. on pp. 9, 10).

[13] E. Klempt and J.-M. Richard. "Baryon spectroscopy".
In: *Rev. Mod. Phys.* 82 (2010), pp. 1095–1153. DOI: 10.1103/RevModPhys.82.1095.
arXiv: 0901.2055 [hep-ph] (cit. on pp. 9, 10).

[14] D. G. Ireland, E. Pasyuk, and I. Strakovsky.
"Photoproduction Reactions and Non-Strange Baryon Spectroscopy".

In: *Prog. Part. Nucl. Phys.* 111 (2020), p. 103752. DOI: 10.1016/j.ppnp.2019.103752. arXiv: 1906.04228 [nucl-ex] (cit. on pp. 9, 39).

[15] C. D. Roberts and A. G. Williams. "Dyson-Schwinger equations and their application to hadronic physics". In: *Prog. Part. Nucl. Phys.* 33 (1994), pp. 477–575. DOI: 10.1016/0146-6410(94)90049-3. arXiv: hep-ph/9403224 (cit. on p. 9).

[16] P. Maris and C. D. Roberts. "Dyson-Schwinger equations: A Tool for hadron physics". In: *Int. J. Mod. Phys. E* 12 (2003), pp. 297–365. DOI: 10.1142/S0218301303001326. arXiv: nucl-th/0301049 (cit. on p. 9).

[17] C. S. Fischer. "Infrared properties of QCD from Dyson-Schwinger equations". In: *J. Phys. G* 32 (2006), R253–R291. DOI: 10.1088/0954-3899/32/8/R02. arXiv: hep-ph/0605173 (cit. on p. 9).

[18] G. Eichmann, C. S. Fischer, and H. Sanchis-Alepuz. "Light baryons and their excitations". In: *Phys. Rev. D* 94.9 (2016), p. 094033. DOI: 10.1103/PhysRevD.94.094033. arXiv: 1607.05748 [hep-ph] (cit. on p. 9).

[19] J. M. Maldacena. "The Large N limit of superconformal field theories and supergravity". In: *Adv. Theor. Math. Phys.* 2 (1998), pp. 231–252. DOI: 10.4310/ATMP.1998.v2.n2.a1. arXiv: hep-th/9711200 (cit. on p. 9).

[20] O. Aharony et al. "Large N field theories, string theory and gravity". In: *Phys. Rept.* 323 (2000), pp. 183–386. DOI: 10.1016/S0370-1573(99)00083-6. arXiv: hep-th/9905111 (cit. on p. 9).

[21] M. Ammon and J. Erdmenger. *Gauge/gravity duality: Foundations and applications*. Cambridge: Cambridge University Press, Apr. 2015. ISBN: 978-1-107-01034-5, 978-1-316-23594-2. DOI: 10.1017/CBO9780511846373 (cit. on p. 9).

[22] N. Isgur and G. Karl. "Hyperfine Interactions in Negative Parity Baryons". In: *Phys. Lett. B* 72 (1977), p. 109. DOI: 10.1016/0370-2693(77)90074-0 (cit. on p. 9).

[23] N. Isgur and G. Karl. "Positive Parity Excited Baryons in a Quark Model with Hyperfine Interactions". In: *Phys. Rev. D* 19 (1979). [Erratum: Phys.Rev.D 23, 817 (1981)], p. 2653. DOI: 10.1103/PhysRevD.19.2653 (cit. on p. 9).

[24] S. Capstick and N. Isgur. "Baryons in a relativized quark model with chromodynamics". In: *Phys. Rev. D* 34.9 (1986), pp. 2809–2835. DOI: 10.1103/physrevd.34.2809 (cit. on p. 9).

[25] T. Melde, W. Plessas, and B. Sengl. "Quark-Model Identification of Baryon Ground and Resonant States". In: *Phys. Rev. D* 77 (2008), p. 114002. DOI: 10.1103/PhysRevD.77.114002. arXiv: 0806.1454 [hep-ph] (cit. on p. 9).

[26] S. Capstick and W. Roberts. "Quark models of baryon masses and decays". In: *Prog. Part. Nucl. Phys.* 45 (2000), S241–S331. DOI: 10.1016/S0146-6410(00)00109-5. arXiv: nucl-th/0008028 (cit. on p. 9).

[27] U. Loring et al. "Relativistic quark models of baryons with instantaneous forces: Theoretical background". In: *Eur. Phys. J. A* 10 (2001), pp. 309–346. DOI: 10.1007/s100500170117. arXiv: hep-ph/0103287 (cit. on p. 9).

[28] U. Loring, B. C. Metsch, and H. R. Petry. "The Light baryon spectrum in a relativistic quark model with instanton induced quark forces: The Nonstrange baryon spectrum and ground states".

In: *Eur. Phys. J. A* 10 (2001), pp. 395–446. DOI: 10.1007/s100500170105.
arXiv: hep-ph/0103289 (cit. on p. 9).

[29] U. Loring, B. C. Metsch, and H. R. Petry. "The Light baryon spectrum in a relativistic quark model with instanton induced quark forces: The Strange baryon spectrum". In: *Eur. Phys. J. A* 10 (2001), pp. 447–486. DOI: 10.1007/s100500170106. arXiv: hep-ph/0103290 (cit. on p. 9).

[30] M. Ronniger and B. C. Metsch. "Effects of a spin-flavour dependent interaction on the baryon mass spectrum". In: *Eur. Phys. J. A* 47 (2011), p. 162. DOI: 10.1140/epja/i2011-11162-8. arXiv: 1111.3835 [hep-ph] (cit. on p. 9).

[31] M. Ronniger and B. C. Metsch. "Effects of a spin-flavour dependent interaction on light-flavoured baryon helicity amplitudes". In: *Eur. Phys. J. A* 49 (2013), p. 8. DOI: 10.1140/epja/i2013-13008-9. arXiv: 1207.2640 [hep-ph] (cit. on p. 9).

[32] R. Koniuk and N. Isgur. "Where Have All the Resonances Gone? An Analysis of Baryon Couplings in a Quark Model With Chromodynamics". In: *Phys. Rev. Lett.* 44 (1980), p. 845. DOI: 10.1103/PhysRevLett.44.845 (cit. on p. 10).

[33] O. Krehl et al. "What is the structure of the Roper resonance?" In: *Phys. Rev. C* 62 (2000), p. 025207. DOI: 10.1103/PhysRevC.62.025207. arXiv: nucl-th/9911080 (cit. on pp. 10, 12, 28, 33, 34, 47, 59, 106, 117, 121, 125).

[34] A. V. Sarantsev et al. "New results on the Roper resonance and the P(11) partial wave". In: *Phys. Lett. B* 659 (2008), pp. 94–100. DOI: 10.1016/j.physletb.2007.11.055. arXiv: 0707.3591 [hep-ph] (cit. on p. 10).

[35] A. W. Thomas. "The Roper Resonance: Still Controversial 60 Years Later". In: *Acta Phys. Polon. B* 57.2 (2026), 2–A6. DOI: 10.5506/APhysPolB.57.2-A6. arXiv: 2602.15320 [hep-ph] (cit. on p. 10).

[36] K. G. Wilson. "Confinement of Quarks". In: *Phys. Rev. D* 10 (1974). Ed. by J. C. Taylor, pp. 2445–2459. DOI: 10.1103/PhysRevD.10.2445 (cit. on p. 10).

[37] M. Padmanath. "Hadron Spectroscopy and Resonances: Review". In: *PoS* LATTICE2018 (2018), p. 013. DOI: 10.22323/1.334.0013. arXiv: 1905.09651 [hep-lat] (cit. on p. 10).

[38] R. A. Briceno, J. J. Dudek, and R. D. Young. "Scattering processes and resonances from lattice QCD". In: *Rev. Mod. Phys.* 90.2 (2018), p. 025001. DOI: 10.1103/RevModPhys.90.025001. arXiv: 1706.06223 [hep-lat] (cit. on p. 10).

[39] M. Mai, U.-G. Meißner, and C. Urbach. "Towards a theory of hadron resonances". In: *Phys. Rept.* 1001 (2023), pp. 1–66. DOI: 10.1016/j.physrep.2022.11.005. arXiv: 2206.01477 [hep-ph] (cit. on p. 10).

[40] M. Luscher. "Volume Dependence of the Energy Spectrum in Massive Quantum Field Theories. 1. Stable Particle States". In: *Commun. Math. Phys.* 104 (1986), p. 177. DOI: 10.1007/BF01211589 (cit. on p. 10).

[41] M. Luscher. "Volume Dependence of the Energy Spectrum in Massive Quantum Field Theories. 2. Scattering States". In: *Commun. Math. Phys.* 105 (1986), pp. 153–188. DOI: 10.1007/BF01211097 (cit. on p. 10).

[42] M. Luscher. "Two particle states on a torus and their relation to the scattering matrix". In: *Nucl. Phys. B* 354 (1991), pp. 531–578. DOI: 10.1016/0550-3213(91)90366-6 (cit. on p. 10).

[43] W. Melnitchouk et al. “Excited baryons in lattice QCD”.
In: *Phys. Rev. D* 67 (2003), p. 114506. DOI: 10.1103/PhysRevD.67.114506.
arXiv: hep-lat/0202022 (cit. on p. 10).
[44] T. Khan, D. Richards, and F. Winter.
“Positive-parity baryon spectrum and the role of hybrid baryons”.
In: *Phys. Rev. D* 104.3 (2021), p. 034503. DOI: 10.1103/PhysRevD.104.034503.
arXiv: 2010.03052 [hep-lat] (cit. on p. 10).
[45] J. J. Dudek and R. G. Edwards. “Hybrid Baryons in QCD”.
In: *Phys. Rev. D* 85 (2012), p. 054016. DOI: 10.1103/PhysRevD.85.054016.
arXiv: 1201.2349 [hep-ph] (cit. on pp. 10, 12).
[46] C. B. Lang et al. “Pion-nucleon scattering in the Roper channel from lattice QCD”.
In: *Phys. Rev. D* 95.1 (2017), p. 014510. DOI: 10.1103/PhysRevD.95.014510.
arXiv: 1610.01422 [hep-lat] (cit. on p. 10).
[47] J. Bulava et al. “Nucleon, Δ and Ω excited states in $N_f = 2 + 1$ lattice QCD”.
In: *Phys. Rev. D* 82 (2010), p. 014507. DOI: 10.1103/PhysRevD.82.014507.
arXiv: 1004.5072 [hep-lat] (cit. on p. 10).
[48] S. Owa, D. B. Leinweber, and A. W. Thomas.
“Nucleon resonance structure up to 2 GeV and the nature of the Roper resonance”.
In: *Phys. Rev. D* 111.11 (2025), p. 116002. DOI: 10.1103/tt7s-p9gj.
arXiv: 2503.09945 [hep-ph] (cit. on p. 10).
[49] R. G. Edwards et al. “Excited state baryon spectroscopy from lattice QCD”.
In: *Phys. Rev. D* 84 (2011), p. 074508. DOI: 10.1103/PhysRevD.84.074508.
arXiv: 1104.5152 [hep-ph] (cit. on p. 10).
[50] R. G. Edwards et al. “Flavor structure of the excited baryon spectra from lattice QCD”.
In: *Phys. Rev. D* 87.5 (2013), p. 054506. DOI: 10.1103/PhysRevD.87.054506.
arXiv: 1212.5236 [hep-ph] (cit. on p. 10).
[51] M. Döring, M. Mai, and U.-G. Meißner.
“Finite volume effects and quark mass dependence of the N(1535) and N(1650)”.
In: *Phys. Lett. B* 722 (2013), pp. 185–192. DOI: 10.1016/j.physletb.2013.04.016.
arXiv: 1302.4065 [hep-lat] (cit. on p. 10).
[52] Y. Zhuge et al.
“Pion photoproduction of nucleon excited states with Hamiltonian effective field theory”.
In: *Phys. Rev. D* 110.9 (2024), p. 094015. DOI: 10.1103/PhysRevD.110.094015.
arXiv: 2407.05334 [hep-ph] (cit. on p. 10).
[53] M. Padmanath et al. “$N\pi$ scattering in the Roper channel”.
In: *EPJ Web Conf.* 175 (2018). Ed. by M. Della Morte et al., p. 05004.
DOI: 10.1051/epjconf/201817505004. arXiv: 1711.06334 [hep-lat] (cit. on p. 10).
[54] J. Bulava et al. “Elastic nucleon-pion scattering at $\mathrm{m}\pi = 200$ MeV from lattice QCD”.
In: *Nucl. Phys. B* 987 (2023), p. 116105. DOI: 10.1016/j.nuclphysb.2023.116105.
arXiv: 2208.03867 [hep-lat] (cit. on p. 10).
[55] G. Silvi et al.
“P-wave nucleon-pion scattering amplitude in the $\Delta(1232)$ channel from lattice QCD”.
In: *Phys. Rev. D* 103.9 (2021), p. 094508. DOI: 10.1103/PhysRevD.103.094508.
arXiv: 2101.00689 [hep-lat] (cit. on p. 10).
[56] C. Alexandrou et al. “Elastic nucleon-pion scattering amplitudes in the Δ channel at physical pion mass from lattice QCD”. In: *Phys. Rev. D* 109.3 (2024), p. 034509.
DOI: 10.1103/PhysRevD.109.034509. arXiv: 2307.12846 [hep-lat] (cit. on p. 10).
[57] W. Detmold et al.
“Chiral extrapolation of lattice moments of proton quark distributions”.

In: *Phys. Rev. Lett.* 87 (2001), p. 172001. DOI: 10.1103/PhysRevLett.87.172001. arXiv: hep-lat/0103006 (cit. on p. 10).
[58] S. Prakhov, B. M. K. Nefkens, C. E. Allgower, et al. "Measurement of $\pi^- p \to \eta n$ from threshold to $p(\pi^-) = 747$ MeV/c". In: *Phys. Rev. C* 72 (2005), p. 015203 (cit. on pp. 11, 45).
[59] A. Starostin et al. "Measurement of pi- p —> pi0 n in the vicinity of the eta threshold". In: *Phys. Rev. C* 72 (2005), p. 015205. DOI: 10.1103/PhysRevC.72.015205 (cit. on p. 11).
[60] J. Breitschopf et al. "Pionic charge exchange on the proton from 40-MeV to 250-MeV". In: *Phys. Lett. B* 639 (2006), pp. 424–428. DOI: 10.1016/j.physletb.2006.07.009. arXiv: nucl-ex/0605017 (cit. on p. 11).
[61] R. Meier et al. "Low-energy analyzing powers in pion proton elastic scattering". In: *Phys. Lett. B* 588 (2004), pp. 155–162. DOI: 10.1016/j.physletb.2004.02.071. arXiv: nucl-ex/0402018 (cit. on p. 11).
[62] I. G. Alekseev et al. "Backward asymmetry measurements in the elastic pion-proton scattering at resonance energies". In: *Eur. Phys. J. A* 39 (2009), pp. 163–168. DOI: 10.1140/epja/i2008-10709-0. arXiv: 0810.1143 [hep-ex] (cit. on p. 11).
[63] J. Adamczewski-Musch et al. "A facility for pion-induced nuclear reaction studies with HADES". In: *Eur. Phys. J. A* 53.9 (2017), p. 188. DOI: 10.1140/epja/i2017-12365-7 (cit. on p. 11).
[64] J. Adamczewski-Musch et al. "Two-pion production in the second resonance region in $\pi^- p$ collisions with the High-Acceptance Di-Electron Spectrometer (HADES)". In: *Phys. Rev. C* 102.2 (2020), p. 024001. DOI: 10.1103/PhysRevC.102.024001. arXiv: 2004.08265 [nucl-ex] (cit. on p. 11).
[65] W. Hillert. "The Bonn electron stretcher accelerator ELSA: Past and future". In: *Eur. Phys. J. A* 28S1 (2006). Ed. by H. Arenhoevel et al., pp. 139–148. DOI: 10.1140/epja/i2006-09-015-4 (cit. on p. 11).
[66] W. J. Schwille et al. "Design and construction of the SAPHIR detector". In: *Nucl. Instrum. Meth. A* 344 (1994), pp. 470–486. DOI: 10.1016/0168-9002(94)90868-0 (cit. on p. 11).
[67] S. Alef et al. "The BGOOD experimental setup at ELSA". In: *Eur. Phys. J. A* 56.4 (2020), p. 104. DOI: 10.1140/epja/s10050-020-00107-x. arXiv: 1910.11939 [physics.ins-det] (cit. on p. 11).
[68] K. H. Kaiser et al. "The 1.5-GeV harmonic double-sided microtron at Mainz University". In: *Nucl. Instrum. Meth. A* 593 (2008), pp. 159–170. DOI: 10.1016/j.nima.2008.05.018 (cit. on p. 11).
[69] V. O. de León et al. "Low-energy Compton scattering and the polarizabilities of the proton". In: *Eur. Phys. J. A* 10 (2001), pp. 207–215. DOI: 10.1007/s100500170132 (cit. on p. 11).
[70] J. Ahrens et al. "Helicity dependence of the $\gamma p \to N\pi$ channels and multipole analysis in the Δ region". In: *Eur. Phys. J. A* 21.2 (2004), pp. 323–333. DOI: 10.1140/epja/i2003-10216-x (cit. on pp. 11, 45, 52, 81).
[71] B. A. Mecking et al. "The CEBAF Large Acceptance Spectrometer (CLAS)". In: *Nucl. Instrum. Meth. A* 503 (2003), pp. 513–553. DOI: 10.1016/S0168-9002(03)01001-5 (cit. on p. 11).
[72] O. Bartalini et al. "Measurement of pi0 photoproduction on the proton from 550-MeV to 1500-MeV at GRAAL". In: *Eur. Phys. J. A* 26 (2005), pp. 399–419. DOI: 10.1140/epja/i2005-10191-2 (cit. on pp. 11, 52, 81).

[73] V. Vegna et al. “Measurement of the \Sigma\ beam asymmetry for the \omega\ photo-production off the proton and the neutron at GRAAL”. In: *Phys. Rev. C* 91.6 (2015), p. 065207. DOI: 10.1103/PhysRevC.91.065207. arXiv: 1306.5943 [nucl-ex] (cit. on p. 11).
[74] N. Muramatsu. “Recent Progress and Results of LEPS, LEPS2, and ELPH”. In: *Few Body Syst.* 54.7-10 (2013). Ed. by K. Sagara et al., pp. 997–1003. DOI: 10.1007/s00601-013-0614-4 (cit. on p. 11).
[75] N. Tomida et al. “Performance of TOF-RPC for the BGOegg experiment”. In: *JINST* 11.11 (2016), p. C11037. DOI: 10.1088/1748-0221/11/11/C11037. arXiv: 1606.00599 [physics.ins-det] (cit. on p. 11).
[76] S. Y. Ryu. “Current status of the LEPS2 experiment and commissioning of the solenoid spectrometer”. In: *AIP Conf. Proc.* 2249.1 (2020). Ed. by C. Meye and R. A. Schumacher, p. 030024. DOI: 10.1063/5.0008675 (cit. on p. 11).
[77] I. S. Barker, A. Donnachie, and J. K. Storrow. “Complete Experiments in Pseudoscalar Photoproduction”. In: *Nucl. Phys. B* 95 (1975), pp. 347–356. DOI: 10.1016/0550-3213(75)90049-8 (cit. on p. 11).
[78] W.-T. Chiang and F. Tabakin. “Completeness rules for spin observables in pseudoscalar meson photoproduction”. In: *Phys. Rev. C* 55 (1997), pp. 2054–2066. DOI: 10.1103/PhysRevC.55.2054. arXiv: nucl-th/9611053 (cit. on p. 11).
[79] D. G. Ireland. “Information Content of Polarization Measurements”. In: *Phys. Rev. C* 82 (2010), p. 025204. DOI: 10.1103/PhysRevC.82.025204. arXiv: 1004.5250 [hep-ph] (cit. on pp. 11, 12).
[80] J. Nys, T. Vrancx, and J. Ryckebusch. “Amplitude extraction in pseudoscalar-meson photoproduction: towards a situation of complete information”. In: *J. Phys. G* 42.3 (2015), p. 034016. DOI: 10.1088/0954-3899/42/3/034016. arXiv: 1502.01259 [nucl-th] (cit. on p. 11).
[81] R. L. Workman et al. “Amplitude reconstruction from complete photoproduction experiments and truncated partial-wave expansions”. In: *Phys. Rev. C* 95.1 (2017), p. 015206. DOI: 10.1103/PhysRevC.95.015206. arXiv: 1611.04434 [nucl-th] (cit. on pp. 11, 12).
[82] K. Nakayama. “Explicit derivation of the completeness condition in pseudoscalar meson photoproduction”. In: *Phys. Rev. C* 100.3 (2019), p. 035208. DOI: 10.1103/PhysRevC.100.035208. arXiv: 1809.00335 [nucl-th] (cit. on p. 11).
[83] K. H. Glander et al. “Measurement of gamma p —> K+ Lambda and gamma p —> K+ Sigma0 at photon energies up to 2.6-GeV”. In: *Eur. Phys. J. A* 19 (2004), pp. 251–273. DOI: 10.1140/epja/i2003-10119-x. arXiv: nucl-ex/0308025 (cit. on pp. 12, 53, 82).
[84] T. Vrancx et al. “Incompleteness of complete pseudoscalar-meson photoproduction”. In: *Phys. Rev. C* 87.5 (2013), p. 055205. DOI: 10.1103/PhysRevC.87.055205. arXiv: 1303.2936 [nucl-th] (cit. on p. 12).
[85] A. M. Sandorfi et al. “Determining pseudoscalar meson photo-production amplitudes from complete experiments”. In: *J. Phys. G* 38 (2011), p. 053001. DOI: 10.1088/0954-3899/38/5/053001. arXiv: 1010.4555 [nucl-th] (cit. on p. 12).
[86] V. Burkert, G. Eichmann, and E. Klempt. “The impact of γN and $\gamma *$N interactions on our understanding of nucleon excitations”. In: *Prog. Part. Nucl. Phys.* 146 (2026), p. 104214. DOI: 10.1016/j.ppnp.2025.104214. arXiv: 2506.16482 [hep-ph] (cit. on pp. 12, 39).

[87] P. Achenbach et al.
"Electroexcitation of Nucleon Resonances and Emergence of Hadron Mass".
In: *Symmetry* 17.7 (2025), p. 1106. DOI: 10.3390/sym17071106.
arXiv: 2505.23550 [hep-ph] (cit. on p. 12).
[88] L. Tiator et al. "Amplitude reconstruction from complete electroproduction experiments and truncated partial-wave expansions". In: *Phys. Rev. C* 96.2 (2017), p. 025210.
DOI: 10.1103/PhysRevC.96.025210. arXiv: 1702.08375 [nucl-th] (cit. on p. 12).
[89] I. G. Aznauryan and V. D. Burkert. "Electroexcitation of nucleon resonances".
In: *Prog. Part. Nucl. Phys.* 67 (2012), pp. 1–54. DOI: 10.1016/j.ppnp.2011.08.001.
arXiv: 1109.1720 [hep-ph] (cit. on p. 12).
[90] D. S. Carman.
"Nucleon Resonance Structure Studies Via Exclusive KY Electroproduction".
In: *Few Body Syst.* 57.10 (2016), pp. 941–948. DOI: 10.1007/s00601-016-1131-z.
arXiv: 1601.02488 [nucl-ex] (cit. on p. 12).
[91] V. I. Mokeev and D. S. Carman. "Photo- and Electrocouplings of Nucleon Resonances".
In: *Few Body Syst.* 63.3 (2022), p. 59. DOI: 10.1007/s00601-022-01760-2.
arXiv: 2202.04180 [nucl-ex] (cit. on p. 12).
[92] V. I. Mokeev et al. "First Results on Nucleon Resonance Electroexcitation Amplitudes from $ep \to e'\pi^+\pi^-p'$ Cross Sections at W = 1.4-1.7 GeV and Q^2 = 2.0-5.0 GeV^2".
In: *Phys. Rev. C* 108.2 (2023), p. 025204. DOI: 10.1103/PhysRevC.108.025204.
arXiv: 2306.13777 [nucl-ex] (cit. on p. 12).
[93] N. Sparveris et al. "Measurements of the γ^*p $\to \Delta$ reaction at low Q^2".
In: *Eur. Phys. J. A* 49 (2013), p. 136. DOI: 10.1140/epja/i2013-13136-2.
arXiv: 1307.0751 [nucl-ex] (cit. on p. 12).
[94] T. Mart. "Electromagnetic production of $K\Sigma$ on the nucleon near threshold".
In: *Phys. Rev. C* 90.6 (2014), p. 065202. DOI: 10.1103/PhysRevC.90.065202.
arXiv: 1412.1555 [nucl-th] (cit. on p. 12).
[95] P. Achenbach et al.
"Beam helicity asymmetries in $K^+\Lambda$ electroproduction off the proton at low Q^2".
In: *Eur. Phys. J. A* 53.10 (2017), p. 198. DOI: 10.1140/epja/i2017-12395-1
(cit. on p. 12).
[96] G. Barucca et al. "PANDA Phase One". In: *Eur. Phys. J. A* 57.6 (2021), p. 184.
DOI: 10.1140/epja/s10050-021-00475-y. arXiv: 2101.11877 [hep-ex] (cit. on p. 12).
[97] PANDA website. https://panda.gsi.de (cit. on p. 12).
[98] J. G. Messchendorp et al. "Hadron Physics Opportunities at FAIR". In: (Dec. 2025).
arXiv: 2512.15986 [hep-ex] (cit. on p. 12).
[99] W. Hillert et al. "Beam and spin dynamics in the fast ramping storage ring ELSA: Concepts and measures to increase beam energy, current and polarization".
In: *EPJ Web Conf.* 134 (2017). Ed. by F. Klein, U.-G. Meißner, and U. Thoma, p. 05002.
DOI: 10.1051/epjconf/201713405002 (cit. on p. 12).
[100] T. C. Jude. "Studies of unconventional baryon structure in the light quark sector with the BGOOD photoproduction experiment". In: *Prog. Part. Nucl. Phys.* 147 (2026), p. 104224.
DOI: 10.1016/j.ppnp.2025.104224 (cit. on p. 12).
[101] M. Amaryan et al. "Strange Hadron Spectroscopy with Secondary KL Beam in Hall D".
In: (Aug. 2020). arXiv: 2008.08215 [nucl-ex] (cit. on p. 12).
[102] M. J. Amaryan et al. "Search for Θ+ in KLp→K+n reaction in KLF at JLab".
In: *Mod. Phys. Lett. A* 39.14 (2024), p. 2450063. DOI: 10.1142/S0217732324500639.
arXiv: 2401.05887 [hep-ex] (cit. on p. 12).

[103] C. Schutz et al. "Role of correlated two pion exchange in pi N scattering". In: *Phys. Rev. C* 49 (1994), pp. 2671–2687. DOI: 10.1103/PhysRevC.49.2671 (cit. on pp. 12, 28, 36, 116).

[104] C. Schutz et al. "A Dynamical model for correlated two pion exchange in the pion - nucleon interaction". In: *Phys. Rev. C* 51 (1995), pp. 1374–1383. DOI: 10.1103/PhysRevC.51.1374. arXiv: nucl-th/9411022 (cit. on pp. 12, 28, 117).

[105] C. Schuetz. "Pion nucleon interaction and the structure of nucleon resonances. (In German)". PhD thesis. 1995 (cit. on pp. 12, 28).

[106] C. Schutz et al. "Extended coupled channels model for pi N scattering and the structure of N*(1440) and N*(1535)". In: *Phys. Rev. C* 57 (1998), pp. 1464–1477. DOI: 10.1103/PhysRevC.57.1464 (cit. on pp. 12, 28, 33, 34, 59).

[107] O. Krehl. "Investigation of the first nucleon resonances in pi N scattering." PhD thesis. Aug. 1999 (cit. on pp. 12, 28).

[108] A. Gasparyan. "Study of Pion Nucleon Scattering Up to 1.9 GeV Through a Coupled Channels Meson Nucleon Model". PhD thesis. 2002 (cit. on pp. 12, 28, 33).

[109] O. Krehl et al. "What does 'rho exchange' in pi N scattering mean?" In: *Phys. Rev. C* 60 (1999), p. 055206. DOI: 10.1103/PhysRevC.60.055206. arXiv: nucl-th/9906090 (cit. on pp. 12, 28, 36, 116).

[110] A. M. Gasparyan et al. "Pion nucleon scattering in a meson exchange model". In: *Phys. Rev. C* 68 (2003), p. 045207. DOI: 10.1103/PhysRevC.68.045207. arXiv: nucl-th/0307072 (cit. on pp. 12, 28, 47, 117, 121, 125).

[111] M. Döring et al. "Analytic properties of the scattering amplitude and resonances parameters in a meson exchange model". In: *Nucl. Phys. A* 829 (2009), pp. 170–209. DOI: 10.1016/j.nuclphysa.2009.08.010. arXiv: 0903.4337 [nucl-th] (cit. on pp. 12, 17, 28, 33, 42).

[112] M. Döring et al. "The reaction $\pi^+ p \to K^+ \Sigma^+$ in a unitary coupled-channels model". In: *Nucl. Phys. A* 851 (2011), pp. 58–98. DOI: 10.1016/j.nuclphysa.2010.12.010. arXiv: 1009.3781 [nucl-th] (cit. on pp. 12, 28, 43, 47, 117, 125).

[113] D. Rönchen et al. "Coupled-channel dynamics in the reactions $\pi N \to \pi N, \eta N, K\Lambda, K\Sigma$". In: *Eur. Phys. J. A* 49 (2013), p. 44. DOI: 10.1140/epja/i2013-13044-5. arXiv: 1211.6998 [nucl-th] (cit. on pp. 12, 17, 28, 31, 47, 57, 117, 125).

[114] D. Rönchen et al. "Photocouplings at the Pole from Pion Photoproduction". In: *Eur. Phys. J. A* 50.6 (2014). [Erratum: Eur.Phys.J.A 51, 63 (2015)], p. 101. DOI: 10.1140/epja/i2014-14101-3. arXiv: 1401.0634 [nucl-th] (cit. on pp. 12, 28, 39, 40, 57, 59, 127).

[115] D. Rönchen et al. "Eta photoproduction in a combined analysis of pion- and photon-induced reactions". In: *Eur. Phys. J. A* 51.6 (2015), p. 70. DOI: 10.1140/epja/i2015-15070-7. arXiv: 1504.01643 [nucl-th] (cit. on pp. 12, 28, 57, 59).

[116] D. Rönchen, M. Döring, and U.-G. Meißner. "The impact of $K^+\Lambda$ photoproduction on the resonance spectrum". In: *Eur. Phys. J. A* 54.6 (2018), p. 110. DOI: 10.1140/epja/i2018-12541-3. arXiv: 1801.10458 [nucl-th] (cit. on pp. 12, 28, 57, 59).

[117] D. Rönchen et al. "Light baryon resonances from a coupled-channel study including $\mathbf{K\Sigma}$ photoproduction". In: *Eur. Phys. J. A* 58.11 (2022), p. 229. DOI: 10.1140/epja/s10050-022-00852-1. arXiv: 2208.00089 [nucl-th] (cit. on pp. 12, 28, 46, 47, 50, 54–59, 67–69).

[118] Y.-F. Wang et al. “Reaction πN→ωN in a dynamical coupled-channel approach”. In: *Phys. Rev. D* 106.9 (2022), p. 094031. DOI: 10.1103/PhysRevD.106.094031. arXiv: 2208.03061 [nucl-th] (cit. on pp. 12, 28, 33).

[119] M. Mai et al. “Jülich-Bonn-Washington model for pion electroproduction multipoles”. In: *Phys. Rev. C* 103.6 (2021), p. 065204. DOI: 10.1103/PhysRevC.103.065204. arXiv: 2104.07312 [nucl-th] (cit. on pp. 12, 40).

[120] M. Mai et al. “Coupled-channel analysis of pion- and eta-electroproduction with the Jülich-Bonn-Washington model”. In: (Nov. 2021). DOI: 10.1103/PhysRevC.106.015201. arXiv: 2111.04774 [nucl-th] (cit. on pp. 12, 40).

[121] M. Mai et al. “Inclusion of $K\Lambda$ electroproduction data in a coupled channel analysis”. In: *Eur. Phys. J. A* 59.12 (2023), p. 286. DOI: 10.1140/epja/s10050-023-01188-0. arXiv: 2307.10051 [nucl-th] (cit. on pp. 12, 40).

[122] Y.-F. Wang et al. “Global Data-Driven Determination of Baryon Transition Form Factors”. In: *Phys. Rev. Lett.* 133.10 (2024), p. 101901. DOI: 10.1103/PhysRevLett.133.101901. arXiv: 2404.17444 [nucl-th] (cit. on pp. 12, 40).

[123] H. Kamano et al. “Nucleon resonances within a dynamical coupled-channels model of πN and γN reactions”. In: *Phys. Rev. C* 88.3 (2013), p. 035209. DOI: 10.1103/PhysRevC.88.035209. arXiv: 1305.4351 [nucl-th] (cit. on pp. 12, 31).

[124] H. Kamano et al. “Isospin decomposition of $\gamma N \to N^*$ transitions within a dynamical coupled-channels model”. In: *Phys. Rev. C* 94.1 (2016), p. 015201. DOI: 10.1103/PhysRevC.94.015201. arXiv: 1605.00363 [nucl-th] (cit. on pp. 12, 86, 90).

[125] M. Döring et al. “Dynamical coupled-channel models for hadron dynamics”. In: *Prog. Part. Nucl. Phys.* 146 (2026), p. 104213. DOI: 10.1016/j.ppnp.2025.104213. arXiv: 2505.02745 [nucl-th] (cit. on pp. 12, 31).

[126] SAID/GWU website. https://said.phys.gwu.edu/ (cit. on pp. 13, 45, 77, 79, 80, 86, 170–172, 178).

[127] R. A. Arndt et al. “Updated analysis of pi N elastic scattering data to 2.1-GeV: The Baryon spectrum”. In: *Phys. Rev. C* 52 (1995), pp. 2120–2130. DOI: 10.1103/PhysRevC.52.2120. arXiv: nucl-th/9505040 (cit. on p. 13).

[128] R. A. Arndt et al. “Extended partial-wave analysis of πN scattering data”. In: *Phys. Rev. C* 74 (2006), p. 045205 (cit. on pp. 13, 45).

[129] R. L. Workman et al. “Parameterization dependence of T matrix poles and eigenphases from a fit to πN elastic scattering data”. In: *Phys. Rev. C* 86 (2012), p. 035202. DOI: 10.1103/PhysRevC.86.035202. arXiv: 1204.2277 [hep-ph] (cit. on p. 13).

[130] R. L. Workman et al. “Unified Chew-Mandelstam SAID analysis of pion photoproduction data”. In: *Phys. Rev. C* 86 (2012), p. 015202. DOI: 10.1103/PhysRevC.86.015202. arXiv: 1202.0845 [hep-ph] (cit. on p. 13).

[131] A. V. Anisovich et al. “The impact of new polarization data from Bonn, Mainz and Jefferson Laboratory on $\gamma p \to \pi N$ multipoles”. In: *Eur. Phys. J. A* 52.9 (2016), p. 284. DOI: 10.1140/epja/i2016-16284-9. arXiv: 1604.05704 [nucl-th] (cit. on p. 13).

[132] W. J. Briscoe et al. “Extended SAID partial-wave analysis of pion photoproduction”. In: *Phys. Rev. C* 108.6 (2023), p. 065205. DOI: 10.1103/PhysRevC.108.065205. arXiv: 2309.06631 [hep-ph] (cit. on pp. 13, 83, 84, 86, 90).

[133] S. U. Chung et al. "Partial wave analysis in K matrix formalism". In: *Annalen Phys.* 4 (1995), pp. 404–430. DOI: 10.1002/andp.19955070504 (cit. on pp. 13, 16).

[134] A. V. Anisovich et al. "Properties of baryon resonances from a multichannel partial wave analysis". In: *Eur. Phys. J. A* 48 (2012), p. 15. DOI: 10.1140/epja/i2012-12015-8. arXiv: 1112.4937 [hep-ph] (cit. on pp. 13, 50, 62).

[135] A. Sarantsev. "Properties of Baryons from Bonn-Gatchina Partial Wave Analysis". In: *JPS Conf. Proc.* 10 (2016), p. 010005. DOI: 10.7566/JPSCP.10.010005 (cit. on p. 13).

[136] A. V. Sarantsev et al. "Decays of N* and Δ* resonances into Nρ, $\Delta\pi$, and Nf0(500)". In: *Phys. Rev. C* 112.1 (2025), p. 015202. DOI: 10.1103/qfpf-tcs3. arXiv: 2503.16636 [nucl-th] (cit. on p. 13).

[137] D. Drechsel et al. "A Unitary isobar model for pion photoproduction and electroproduction on the proton up to 1-GeV". In: *Nucl. Phys. A* 645 (1999), pp. 145–174. DOI: 10.1016/S0375-9474(98)00572-7. arXiv: nucl-th/9807001 (cit. on p. 13).

[138] D. Drechsel, S. S. Kamalov, and L. Tiator. "Unitary Isobar Model - MAID2007". In: *Eur. Phys. J. A* 34 (2007), pp. 69–97. DOI: 10.1140/epja/i2007-10490-6. arXiv: 0710.0306 [nucl-th] (cit. on pp. 13, 94).

[139] L. Tiator. "The MAID Legacy and Future". In: *Few Body Syst.* 59.3 (2018). Ed. by R. Gothe et al., p. 21. DOI: 10.1007/s00601-018-1343-5. arXiv: 1801.04777 [nucl-th] (cit. on p. 13).

[140] M. Shrestha and D. M. Manley. "Multichannel parametrization of πN scattering amplitudes and extraction of resonance parameters". In: *Phys. Rev. C* 86 (2012), p. 055203. DOI: 10.1103/PhysRevC.86.055203. arXiv: 1208.2710 [hep-ph] (cit. on p. 13).

[141] B. C. Hunt and D. M. Manley. "Partial-wave analyses of $\gamma p \to \eta p$ and $\gamma n \to \eta n$ using a multichannel framework". In: *Phys. Rev. C* 99.5 (2019), p. 055203. DOI: 10.1103/PhysRevC.99.055203. arXiv: 1804.06031 [nucl-ex] (cit. on p. 13).

[142] B. C. Hunt and D. M. Manley. "Partial-Wave Analysis of $\gamma p \to K^+\Lambda$ using a multichannel framework". In: *Phys. Rev. C* 99.5 (2019), p. 055204. DOI: 10.1103/PhysRevC.99.055204. arXiv: 1804.07422 [nucl-ex] (cit. on p. 13).

[143] B. C. Hunt and D. M. Manley. "Updated determination of N^* resonance parameters using a unitary, multichannel formalism". In: *Phys. Rev. C* 99.5 (2019), p. 055205. DOI: 10.1103/PhysRevC.99.055205. arXiv: 1810.13086 [nucl-ex] (cit. on pp. 13, 62).

[144] V. Shklyar, H. Lenske, and U. Mosel. "η-meson production in the resonance-energy region". In: *Phys. Rev. C* 87.1 (2013), p. 015201. DOI: 10.1103/PhysRevC.87.015201. arXiv: 1206.5414 [nucl-th] (cit. on p. 13).

[145] V. Shklyar, H. Lenske, and U. Mosel. "Giessen coupled-channel model for pion- and photon-induced reactions". In: *AIP Conf. Proc.* 1432.1 (2012). Ed. by V. Burkert et al., pp. 349–352. DOI: 10.1063/1.3701246 (cit. on p. 13).

[146] R. E. Cutkosky et al. "Pion - Nucleon Partial Wave Amplitudes". In: *Phys. Rev. D* 20 (1979), p. 2839. DOI: 10.1103/PhysRevD.20.2839 (cit. on p. 14).

[147] G. Hohler et al. *HANDBOOK OF PION NUCLEON SCATTERING*. Vol. 12N1. 1979 (cit. on p. 14).

[148] G. Höhler. *Tables of Data / Tabellen der Daten*. Ed. by H. Schopper. Vol. 9b1. Landolt-Boernstein - Group I Elementary Particles, Nuclei and Atoms. Springer, 1982. ISBN: 978-3-540-09694-8, 978-3-540-38527-1. DOI: 10.1007/b85780 (cit. on p. 14).
[149] R. A. Arndt et al. "Updated analysis of pi N elastic scattering data to 2.1-GeV: The Baryon spectrum". In: *Phys. Rev. C* 52 (1995), pp. 2120–2130. DOI: 10.1103/PhysRevC.52.2120. arXiv: nucl-th/9505040 (cit. on pp. 14, 50).
[150] M. E. Peskin and D. V. Schroeder. *An Introduction to quantum field theory*. Reading, USA: Addison-Wesley, 1995. ISBN: 978-0-201-50397-5, 978-0-429-50355-9, 978-0-429-49417-8. DOI: 10.1201/9780429503559 (cit. on p. 15).
[151] M. D. Schwartz. *Quantum Field Theory and the Standard Model*. Cambridge University Press, Mar. 2014. ISBN: 978-1-107-03473-0, 978-1-107-03473-0 (cit. on pp. 15, 18, 28, 30).
[152] M. Mai et al. "Three-body Unitarity with Isobars Revisited". In: *Eur. Phys. J. A* 53.9 (2017), p. 177. DOI: 10.1140/epja/i2017-12368-4. arXiv: 1706.06118 [nucl-th] (cit. on pp. 16, 31).
[153] M. Mai and M. Döring. "Three-body Unitarity in the Finite Volume". In: *Eur. Phys. J. A* 53.12 (2017), p. 240. DOI: 10.1140/epja/i2017-12440-1. arXiv: 1709.08222 [hep-lat] (cit. on p. 16).
[154] M. Mai and M. Döring. "Finite-Volume Spectrum of $\pi^+\pi^+$ and $\pi^+\pi^+\pi^+$ Systems". In: *Phys. Rev. Lett.* 122.6 (2019), p. 062503. DOI: 10.1103/PhysRevLett.122.062503. arXiv: 1807.04746 [hep-lat] (cit. on p. 16).
[155] A. Jackura et al. "Phenomenology of Relativistic $\mathbf{3} \to \mathbf{3}$ Reaction Amplitudes within the Isobar Approximation". In: *Eur. Phys. J. C* 79.1 (2019), p. 56. DOI: 10.1140/epjc/s10052-019-6566-1. arXiv: 1809.10523 [hep-ph] (cit. on p. 16).
[156] I. J. R. Aitchison. "K-MATRIX FORMALISM FOR OVERLAPPING RESONANCES". In: *Nucl. Phys. A* 189 (1972), pp. 417–423. DOI: 10.1016/0375-9474(72)90305-3 (cit. on p. 16).
[157] I. J. R. Aitchison. "Unitarity, Analyticity and Crossing Symmetry in Two- and Three-hadron Final State Interactions". In: (July 2015). arXiv: 1507.02697 [hep-ph] (cit. on p. 16).
[158] N. Hüsken, E. S. Swanson, and A. Szczepaniak. "On Dispersive and Nondispersive K-matrix Formalisms". In: (Jan. 2026). arXiv: 2601.09844 [hep-ph] (cit. on p. 17).
[159] L. D. Roper. "Evidence for a P-11 Pion-Nucleon Resonance at 556 MeV". In: *Phys. Rev. Lett.* 12 (1964), pp. 340–342. DOI: 10.1103/PhysRevLett.12.340 (cit. on p. 17).
[160] K. Ottnad et al. "New insights into the neutron electric dipole moment". In: *Phys. Lett. B* 687 (2010), pp. 42–47. DOI: 10.1016/j.physletb.2010.03.005. arXiv: 0911.3981 [hep-ph] (cit. on p. 18).
[161] S. Weinberg. "Phenomenological Lagrangians". In: *Physica A* 96.1-2 (1979). Ed. by S. Deser, pp. 327–340. DOI: 10.1016/0378-4371(79)90223-1 (cit. on pp. 19, 21).
[162] W. Heisenberg and H. Euler. "Consequences of Dirac's theory of positrons". In: *Z. Phys.* 98.11-12 (1936), pp. 714–732. DOI: 10.1007/BF01343663. arXiv: physics/0605038 (cit. on p. 19).
[163] J. Goldstone, A. Salam, and S. Weinberg. "Broken Symmetries". In: *Phys. Rev.* 127 (1962), pp. 965–970. DOI: 10.1103/PhysRev.127.965 (cit. on p. 20).

[164] J. Goldstone. “Field Theories with Superconductor Solutions”. In: *Nuovo Cim.* 19 (1961), pp. 154–164. DOI: 10.1007/BF02812722 (cit. on p. 20).
[165] C. Vafa and E. Witten. “Restrictions on Symmetry Breaking in Vector-Like Gauge Theories”. In: *Nucl. Phys. B* 234 (1984), pp. 173–188. DOI: 10.1016/0550-3213(84)90230-X (cit. on p. 20).
[166] S. Scherer. “Introduction to chiral perturbation theory”. In: *Adv. Nucl. Phys.* 27 (2003). Ed. by J. W. Negele and E. W. Vogt, p. 277. arXiv: hep-ph/0210398 (cit. on p. 20).
[167] S. R. Coleman, J. Wess, and B. Zumino. “Structure of phenomenological Lagrangians. 1.” In: *Phys. Rev.* 177 (1969), pp. 2239–2247. DOI: 10.1103/PhysRev.177.2239 (cit. on p. 21).
[168] C. G. Callan Jr. et al. “Structure of phenomenological Lagrangians. 2.” In: *Phys. Rev.* 177 (1969), pp. 2247–2250. DOI: 10.1103/PhysRev.177.2247 (cit. on p. 21).
[169] V. Bernard, N. Kaiser, and U.-G. Meißner. “Chiral dynamics in nucleons and nuclei”. In: *Int. J. Mod. Phys. E* 4 (1995), pp. 193–346. DOI: 10.1142/S0218301395000092. arXiv: hep-ph/9501384 (cit. on pp. 21, 22).
[170] S. Scherer. “Baryon chiral perturbation theory”. In: *PoS* CD09 (2009), p. 075. DOI: 10.22323/1.086.0075. arXiv: 0910.0331 [hep-ph] (cit. on p. 22).
[171] J. Gasser, M. E. Sainio, and A. Svarc. “Nucleons with chiral loops”. In: *Nucl. Phys. B* 307 (1988), pp. 779–853. DOI: 10.1016/0550-3213(88)90108-3 (cit. on p. 22).
[172] V. Bernard et al. “Chiral structure of the nucleon”. In: *Nucl. Phys. B* 388 (1992), pp. 315–345. DOI: 10.1016/0550-3213(92)90615-I (cit. on p. 22).
[173] B. Borasoy and U.-G. Meißner. “Chiral Expansion of Baryon Masses and σ-Terms”. In: *Annals Phys.* 254 (1997), pp. 192–232. DOI: 10.1006/aphy.1996.5630. arXiv: hep-ph/9607432 (cit. on pp. 22, 34).
[174] E. E. Jenkins and A. V. Manohar. “Baryon chiral perturbation theory using a heavy fermion Lagrangian”. In: *Phys. Lett. B* 255 (1991), pp. 558–562. DOI: 10.1016/0370-2693(91)90266-S (cit. on p. 22).
[175] T. Becher and H. Leutwyler. “Baryon chiral perturbation theory in manifestly Lorentz invariant form”. In: *Eur. Phys. J.* 9.4 (1999), pp. 643–671. DOI: 10.1007/PL00021673. arXiv: hep-ph/9901384 (cit. on p. 22).
[176] J. Gegelia and G. Japaridze. “Matching heavy particle approach to relativistic theory”. In: *Phys. Rev. D* 60 (1999), p. 114038. DOI: 10.1103/PhysRevD.60.114038. arXiv: hep-ph/9908377 (cit. on p. 22).
[177] T. Fuchs et al. “Renormalization of relativistic baryon chiral perturbation theory and power counting”. In: *Phys. Rev. D* 68 (2003), p. 056005. DOI: 10.1103/PhysRevD.68.056005. arXiv: hep-ph/0302117 (cit. on p. 22).
[178] U.-G. Meißner and J. A. Oller. “Chiral unitary meson baryon dynamics in the presence of resonances: Elastic pion nucleon scattering”. In: *Nucl. Phys. A* 673 (2000), pp. 311–334. DOI: 10.1016/S0375-9474(00)00150-0. arXiv: nucl-th/9912026 (cit. on p. 22).
[179] N. Kaiser, P. B. Siegel, and W. Weise. “Chiral dynamics and the S11 (1535) nucleon resonance”.

In: *Phys. Lett. B* 362 (1995), pp. 23–28. DOI: 10.1016/0370-2693(95)01203-3. arXiv: nucl-th/9507036 (cit. on p. 22).
[180] J. A. Oller and U. G. Meißner. "Chiral dynamics in the presence of bound states: Kaon nucleon interactions revisited". In: *Phys. Lett. B* 500 (2001), pp. 263–272. DOI: 10.1016/S0370-2693(01)00078-8. arXiv: hep-ph/0011146 (cit. on p. 22).
[181] M. Döring and K. Nakayama. "On the cross section ratio sigma(n)/sigma(p) in eta photoproduction". In: *Phys. Lett. B* 683 (2010), pp. 145–149. DOI: 10.1016/j.physletb.2009.12.029. arXiv: 0909.3538 [nucl-th] (cit. on p. 22).
[182] A. Gasparyan and M. F. M. Lutz. "Photon- and pion-nucleon interactions in a unitary and causal effective field theory based on the chiral Lagrangian". In: *Nucl. Phys. A* 848 (2010), pp. 126–182. DOI: 10.1016/j.nuclphysa.2010.08.006. arXiv: 1003.3426 [hep-ph] (cit. on p. 22).
[183] M. Mai, P. C. Bruns, and U.-G. Meißner. "Pion photoproduction off the proton in a gauge-invariant chiral unitary framework". In: *Phys. Rev. D* 86 (2012), p. 094033. DOI: 10.1103/PhysRevD.86.094033. arXiv: 1207.4923 [nucl-th] (cit. on p. 22).
[184] N. Fettes, U.-G. Meißner, and S. Steininger. "Pion - nucleon scattering in chiral perturbation theory. 1. Isospin symmetric case". In: *Nucl. Phys. A* 640 (1998), pp. 199–234. DOI: 10.1016/S0375-9474(98)00452-7. arXiv: hep-ph/9803266 (cit. on p. 22).
[185] N. Fettes and U.-G. Meißner. "Complete analysis of pion nucleon scattering in chiral perturbation theory to third order". In: *Nucl. Phys. A* 693 (2001), pp. 693–709. DOI: 10.1016/S0375-9474(01)00977-0. arXiv: hep-ph/0101030 (cit. on p. 22).
[186] U.-G. Meißner. "Chiral perturbation theory with nucleons". In: *Int. J. Mod. Phys. E* 1 (1992), pp. 561–602. DOI: 10.1142/S021830139200028X (cit. on p. 22).
[187] S. Scherer. "Chiral Perturbation Theory: Introduction and Recent Results in the One-Nucleon Sector". In: *Prog. Part. Nucl. Phys.* 64 (2010), pp. 1–60. DOI: 10.1016/j.ppnp.2009.08.002. arXiv: 0908.3425 [hep-ph] (cit. on p. 22).
[188] L. Geng. "Recent developments in SU(3) covariant baryon chiral perturbation theory". In: *Front. Phys. (Beijing)* 8 (2013), pp. 328–348. DOI: 10.1007/s11467-013-0327-7. arXiv: 1301.6815 [nucl-th] (cit. on p. 22).
[189] V. Bernard and U.-G. Meißner. "Chiral perturbation theory". In: *Ann. Rev. Nucl. Part. Sci.* 57 (2007), pp. 33–60. DOI: 10.1146/annurev.nucl.56.080805.140449. arXiv: hep-ph/0611231 (cit. on p. 22).
[190] V. Bernard. "Chiral Perturbation Theory and Baryon Properties". In: *Prog. Part. Nucl. Phys.* 60 (2008), pp. 82–160. DOI: 10.1016/j.ppnp.2007.07.001. arXiv: 0706.0312 [hep-ph] (cit. on p. 22).
[191] J. Wess and B. Zumino. "Lagrangian method for chiral symmetries". In: *Phys. Rev.* 163 (1967), pp. 1727–1735. DOI: 10.1103/PhysRev.163.1727 (cit. on pp. 22, 34, 35).
[192] S. B. Gerasimov. "A Sum rule for magnetic moments and the damping of the nucleon magnetic moment in nuclei". In: *Yad. Fiz.* 2 (1965), pp. 598–602 (cit. on pp. 22, 23, 27).
[193] S. D. Drell and A. C. Hearn. "Exact Sum Rule for Nucleon Magnetic Moments". In: *Phys. Rev. Lett.* 16 (1966), pp. 908–911. DOI: 10.1103/PhysRevLett.16.908 (cit. on pp. 22, 23, 27).

[194] D. Drechsel, S. S. Kamalov, and L. Tiator. “The GDH sum rule and related integrals”. In: *Phys. Rev. D* 63 (2001), p. 114010. DOI: 10.1103/PhysRevD.63.114010. arXiv: hep-ph/0008306 (cit. on p. 22).

[195] D. Drechsel and L. Tiator. “The Gerasimov-Drell-Hearn sum rule and the spin structure of the nucleon”. In: *Ann. Rev. Nucl. Part. Sci.* 54 (2004), pp. 69–114. DOI: 10.1146/annurev.nucl.54.070103.181159. arXiv: nucl-th/0406059 (cit. on pp. 22, 94, 96).

[196] M. Schumacher. “Polarizability of the nucleon and Compton scattering”. In: *Prog. Part. Nucl. Phys.* 55 (2005), pp. 567–646. DOI: 10.1016/j.ppnp.2005.01.033. arXiv: hep-ph/0501167 (cit. on p. 22).

[197] K. Helbing. “The Gerasimov-Drell-Hearn Sum Rule”. In: *Prog. Part. Nucl. Phys.* 57 (2006), pp. 405–469. DOI: 10.1016/j.ppnp.2005.09.003. arXiv: nucl-ex/0603021 (cit. on pp. 22, 23, 25, 26, 96).

[198] A. Deur, S. J. Brodsky, and G. F. De Téramond. “The Spin Structure of the Nucleon”. In: *Rept. Prog. Phys.* 82 (2019), p. 076201. DOI: 10.1088/1361-6633/ab0b8f. arXiv: 1807.05250 [hep-ph] (cit. on p. 22).

[199] M. Hosoda and K. Yamamoto. “Sum Rule for the Magnetic Moment of the Dirac Particle”. In: *Prog. Theor. Phys.* 36.2 (1966), pp. 425–426. DOI: 10.1143/ptp.36.425 (cit. on p. 23).

[200] D. A. Dicus and D. R. Palmer. “Drell-hearn sum rule from light cone current commutators”. In: *Phys. Rev. D* 6 (1972), pp. 720–722. DOI: 10.1103/PhysRevD.6.720 (cit. on p. 23).

[201] R. Pantforder. “Investigations on the foundation and possible modifications of the Gerasimov-Drell-Hearn sum rule”. PhD thesis. May 1998. arXiv: hep-ph/9805434 (cit. on p. 23).

[202] M. Jacob and G. C. Wick. “On the General Theory of Collisions for Particles with Spin”. In: *Annals Phys.* 7 (1959), pp. 404–428. DOI: 10.1006/aphy.2000.6022 (cit. on pp. 23, 106).

[203] A. C. Irving. “Springer Tracts in Modern Physics Vol 79: Elementary Particle Physics”. In: *Physics Bulletin* 28.11 (Nov. 1977), p. 522. DOI: 10.1088/0031-9112/28/11/033. URL: https://doi.org/10.1088/0031-9112/28/11/033 (cit. on p. 23).

[204] S. D. Bass. “The Drell-Hearn-Gerasimov sum rule in QCD”. In: *Mod. Phys. Lett. A* 12 (1997), pp. 1051–1068. DOI: 10.1142/S0217732397001072. arXiv: hep-ph/9703254 (cit. on p. 25).

[205] F. E. Low. “Scattering of light of very low frequency by systems of spin 1/2”. In: *Phys. Rev.* 96 (1954), pp. 1428–1432. DOI: 10.1103/PhysRev.96.1428 (cit. on p. 26).

[206] M. Gell-Mann and M. L. Goldberger. “Scattering of low-energy photons by particles of spin 1/2”. In: *Phys. Rev.* 96 (1954), pp. 1433–1438. DOI: 10.1103/PhysRev.96.1433 (cit. on p. 26).

[207] M. Gell-Mann. “The interpretation of the new particles as displaced charge multiplets”. In: *Nuovo Cim.* 4.S2 (1956), pp. 848–866. DOI: 10.1007/BF02748000 (cit. on p. 26).

[208] R. Machleidt, K. Holinde, and C. Elster. “The Bonn Meson Exchange Model for the Nucleon Nucleon Interaction”. In: *Phys. Rept.* 149 (1987), pp. 1–89. DOI: 10.1016/S0370-1573(87)80002-9 (cit. on p. 28).

[209] E. E. Salpeter and H. A. Bethe. “A Relativistic equation for bound state problems”. In: *Phys. Rev.* 84 (1951), pp. 1232–1242. DOI: 10.1103/PhysRev.84.1232 (cit. on p. 28).

[210] D. Schuette. “A brueckner theory including mesonic degrees of freedom”. In: *Nucl. Phys. A* 221 (1974), pp. 450–460. DOI: 10.1016/0375-9474(74)90475-8 (cit. on p. 28).

[211] K. Kotthoff et al. “An OBE Model for the Two Nucleon Problem Based on Noncovariant Perturbation Theory”. In: *Nucl. Phys. A* 242 (1975), pp. 429–444. DOI: 10.1016/0375-9474(75)90106-2 (cit. on p. 28).

[212] M. I. Haftel and F. Tabakin. “NUCLEAR SATURATION AND THE SMOOTHNESS OF NUCLEON-NUCLEON POTENTIALS”. In: *Nucl. Phys. A* 158 (1970), pp. 1–42. DOI: 10.1016/0375-9474(70)90047-3 (cit. on p. 28).

[213] S. Weinberg. *The Quantum Theory of Fields*. Cambridge University Press, 1995 (cit. on p. 29).

[214] E. Wigner. “Einige Folgerungen aus der Schrödingerschen Theorie für die Termstrukturen”. In: *Z. Phys.* 43 (1927), pp. 624–652. DOI: 10.1007/BF01397327 (cit. on p. 30).

[215] M. Jacob and G. C. Wick. *Quantum Collision Theory*. Amsterdam: North-Holland Publishing Company, 1975 (cit. on p. 30).

[216] D. M. Brink and G. R. Satchler. *Angular Momentum*. 2nd. Oxford Library of the Physical Sciences. Oxford, United Kingdom: Clarendon Press, 1968 (cit. on p. 30).

[217] C. Hanhart. “A New Parameterization for the Pion Vector Form Factor”. In: *Phys. Lett. B* 715 (2012), pp. 170–177. DOI: 10.1016/j.physletb.2012.07.038. arXiv: 1203.6839 [hep-ph] (cit. on p. 31).

[218] Y.-F. Wang et al. “Examination of the nature of the N* and Δ resonances via coupled-channels dynamics”. In: *Phys. Rev. C* 109.1 (2024), p. 015202. DOI: 10.1103/PhysRevC.109.015202. arXiv: 2307.06799 [nucl-th] (cit. on pp. 32, 60, 64).

[219] Y.-F. Wang et al. “Nature of the Pc states from compositeness criteria”. In: *Phys. Rev. D* 112.7 (2025), p. 074010. DOI: 10.1103/fvjn-8bl9. arXiv: 2506.21858 [hep-ph] (cit. on pp. 32, 60, 64).

[220] V. Bernard, N. Kaiser, and U.-G. Meißner. “Novel approach to pion and eta production in proton proton collisions”. In: *Eur. Phys. J. A* 4 (1999), pp. 259–275. DOI: 10.1007/s100500050229. arXiv: nucl-th/9806013 (cit. on p. 34).

[221] U.-G. Meißner. “Low-Energy Hadron Physics from Effective Chiral Lagrangians with Vector Mesons”. In: *Phys. Rept.* 161 (1988), p. 213. DOI: 10.1016/0370-1573(88)90090-7 (cit. on p. 34).

[222] C. Schütz. *Zur Dynamik des πN-Systems im Hinblick auf π-Produktionsprozesse*. Tech. rep. 3130. Jülich: Forschungszentrum Jülich, 1995 (cit. on p. 34).

[223] K. Kawarabayashi and M. Suzuki. “Partially conserved axial vector current and the decays of vector mesons”. In: *Phys. Rev. Lett.* 16 (1966), p. 255. DOI: 10.1103/PhysRevLett.16.255 (cit. on p. 35).

[224] Riazuddin and Fayyazuddin. “Algebra of current components and decay widths of rho and K* mesons”. In: *Phys. Rev.* 147 (1966), pp. 1071–1073. DOI: 10.1103/PhysRev.147.1071 (cit. on p. 35).

[225] G. Hohler and E. Pietarinen. “The rho N N Vertex in Vector Dominance Models”. In: *Nucl. Phys. B* 95 (1975), pp. 210–230. DOI: 10.1016/0550-3213(75)90042-5 (cit. on p. 36).

[226] H. Nielsen and G. C. Oades. "Consistency between the low-energy pion pion interaction and pion-nucleon scattering". In: *Nucl. Phys. B* 49 (1972), pp. 586–609. DOI: 10.1016/0550-3213(72)90621-9 (cit. on p. 36).

[227] T. P. Cheng and R. F. Dashen. "Is SU(2) x SU(2) a better symmetry than SU(3)?" In: *Phys. Rev. Lett.* 26 (1971), p. 594. DOI: 10.1103/PhysRevLett.26.594 (cit. on p. 36).

[228] G. Janssen, K. Holinde, and J. Speth. "pi rho correlations in the N N potential". In: *Phys. Rev. C* 54 (1996), pp. 2218–2234. DOI: 10.1103/PhysRevC.54.2218 (cit. on pp. 37, 121, 124, 125).

[229] R. Koch. "Improved πN Partial Waves Consistent With Analyticity and Unitarity". In: *Z. Phys. C* 29 (1985), p. 597. DOI: 10.1007/BF01560295 (cit. on p. 37).

[230] A. D. Lahiff and I. R. Afnan. "Solution of the Bethe-Salpeter equation for pion nucleon scattering". In: *Phys. Rev. C* 60 (1999), p. 024608. DOI: 10.1103/PhysRevC.60.024608. arXiv: nucl-th/9903058 (cit. on p. 37).

[231] V. Crede and W. Roberts. "Progress towards understanding baryon resonances". In: *Rept. Prog. Phys.* 76 (2013), p. 076301. DOI: 10.1088/0034-4885/76/7/076301. arXiv: 1302.7299 [nucl-ex] (cit. on p. 39).

[232] F. Huang et al. "Pion photoproduction in a dynamical coupled-channels model". In: *Phys. Rev. C* 85 (2012), p. 054003. DOI: 10.1103/PhysRevC.85.054003. arXiv: 1110.3833 [nucl-th] (cit. on pp. 39, 41).

[233] H. Haberzettl. "Gauge invariant theory of pion photoproduction with dressed hadrons". In: *Phys. Rev. C* 56 (1997), pp. 2041–2058. DOI: 10.1103/PhysRevC.56.2041. arXiv: nucl-th/9704057 (cit. on p. 39).

[234] K. Nakayama and H. Haberzettl. "On the interaction current in p p —> p p gamma". In: *Phys. Rev. C* 80 (2009), p. 051001. DOI: 10.1103/PhysRevC.80.051001. arXiv: 0910.0469 [nucl-th] (cit. on p. 39).

[235] H. Haberzettl, F. Huang, and K. Nakayama. "Dressing the electromagnetic nucleon current". In: *Phys. Rev. C* 83 (2011), p. 065502. DOI: 10.1103/PhysRevC.83.065502. arXiv: 1103.2065 [nucl-th] (cit. on p. 39).

[236] G. F. Chew et al. "Relativistic dispersion relation approach to photomeson production". In: *Phys. Rev.* 106 (1957), pp. 1345–1355. DOI: 10.1103/PhysRev.106.1345 (cit. on pp. 39, 40).

[237] K. Nakayama and W. G. Love. "Spin structure of spin-1/2 baryon and spinless meson production amplitudes in photonic and hadronic reactions". In: *Phys. Rev. C* 72 (2005), p. 034603. DOI: 10.1103/PhysRevC.72.034603 (cit. on p. 39).

[238] M. Döring et al. "The Role of the background in the extraction of resonance contributions from meson-baryon scattering". In: *Phys. Lett. B* 681 (2009), pp. 26–31. DOI: 10.1016/j.physletb.2009.09.052. arXiv: 0903.1781 [nucl-th] (cit. on p. 43).

[239] L. A. Heuser et al. "From pole parameters to line shapes and branching ratios". In: *Eur. Phys. J. C* 84.6 (2024), p. 599. DOI: 10.1140/epjc/s10052-024-12884-6. arXiv: 2403.15539 [hep-ph] (cit. on p. 44).

[240] Website of Bonn-Gatchina group with analysis results. https://pwa.hiskp.uni-bonn.de (cit. on p. 45).

[241] F. Eisler et al. In: *Nuovo Cim.* 10 (1958), p. 468 (cit. on p. 45).

[242] F. S. Crawford et al. In: *Phys. Rev. Lett.* 3 (1959), p. 394 (cit. on p. 45).

[243] L. Bertanza, P. L. Connolly, B. B. Culwick, et al. "$\Lambda^0 K^0$ production by pions on protons". In: *Phys. Rev. Lett.* 8 (1962), p. 332 (cit. on p. 45).

[244] F. S. Crawford, F. Grard, and G. A. Smith.
"Production of Σ^+K^+ by (π^+, p) interaction at 1170 MeV/c".
In: *Phys. Rev.* 128 (1962), p. 368 (cit. on p. 45).

[245] L. L. Yoder et al. "ΛK^0 and $\Sigma^0 K^0$ production in 1.5 BeV/c $\pi^- p$ interactions".
In: *Phys. Rev.* 132 (1963), p. 1778 (cit. on p. 45).

[246] J. Keren. "Associated production of ΛK at the ΣK threshold".
In: *Phys. Rev.* 133 (1964), B457 (cit. on p. 45).

[247] D. H. Miller et al. In: *Phys. Rev.* 140 (1965), B360 (cit. on p. 45).

[248] N. L. Carayannopoulos, G. W. Tautfest, and R. B. Willmann.
"Production of Σ^+K^+ by π^+p interactions at 1111, 1206, and 1265 MeV/c".
In: *Phys. Rev.* 138 (1965), B433 (cit. on p. 45).

[249] J. A. Anderson, F. S. Crawford, and J. C. Doyle. In: *Phys. Rev.* 152 (1966), p. 1139
(cit. on p. 45).

[250] O. Goussu et al. "Analysis of strange-particle production in $\pi^- p$ collisions at 1.59 GeV/c".
In: *Nuovo Cim. A* 42 (1966), p. 606 (cit. on p. 45).

[251] P. Daronian et al. In: *Nuovo Cim. A* 41 (1966), p. 503 (cit. on p. 45).

[252] S. Dagan et al. "Strange-particle production by 1.95 BeV/c π^+ in hydrogen".
In: *Phys. Rev.* 161 (1967), p. 1384 (cit. on p. 45).

[253] J. C. Doyle, F. S. Crawford, and J. A. Anderson.
"Study of $\pi^- p \to \Sigma^- K^+$ at 1170 MeV/c". In: *Phys. Rev.* 165 (1968), p. 1483
(cit. on p. 45).

[254] W. Deinet et al.
"Differential and total cross-sections for $\pi^- + p \to \eta + n$ from 718 to 1050 MeV/c".
In: *Nucl. Phys. B* 11 (1969), p. 495 (cit. on p. 45).

[255] T. O. Binford et al.
"Production of Λ^0 and Σ^0 hyperons by pions of beam momenta 1.12–1.32 BeV/c".
In: *Phys. Rev.* 183 (1969), p. 1134 (cit. on p. 45).

[256] O. I. Dahl et al. "Strange-particle production in $\pi^- p$ interactions from 1.5 to 4.2 BeV/c.
II: Two-body final states".
In: *Phys. Rev.* 163 (1967). Erratum: ibid. **183**, 1520 (1969), p. 1430 (cit. on p. 45).

[257] O. Van Dyck, R. Blumenthal, S. Frankel, et al.
"Cross section for $\pi^- + p \to \Lambda + K^0$: structure near Σ threshold".
In: *Phys. Rev. Lett.* 23 (1969), p. 50 (cit. on p. 45).

[258] M. L. Good and R. R. Kofler. "Study of $\pi^- + p \to \Sigma^- + K^+$ from 1.12 to 1.32 BeV/c".
In: *Phys. Rev.* 183 (1969), p. 1142 (cit. on p. 45).

[259] W. B. Richards, C. B. Chiu, R. D. Eandi, et al.
"Production and neutral decay of the eta meson in $\pi^- p$ collisions".
In: *Phys. Rev. D* 1 (1970), p. 10 (cit. on p. 45).

[260] G. E. Kalmus, G. Borreani, and J. Louie.
"Study of the reaction $\pi^+p \to \Sigma^+K^+$ between 1850 and 2090 MeV center-of-mass energy".
In: *Phys. Rev. D* 2 (1970), p. 1824 (cit. on p. 45).

[261] Y.-L. Pan et al. "Strange-particle production by 1.7 GeV/c π^+ on protons".
In: *Phys. Rev. D* 2 (1970), p. 449 (cit. on p. 45).

[262] J. J. Jones, T. Bowen, W. R. Dawes, et al.
"Total cross-sections for $\pi^- p \to \Lambda K^0$ from threshold to 1.13 GeV/c".
In: *Phys. Rev. Lett.* 26 (1971), p. 860 (cit. on p. 45).

[263] E. H. Bellamy et al. "Polarisation in the reaction $\pi^+p \to K^+\Sigma^+$ at 1.11 GeV/c".
In: *Phys. Lett. B* 39 (1972), p. 299 (cit. on p. 45).

[264] D. W. Thomas et al. “Strange particle production from $\pi^- p$ interactions at 1.69 GeV/c”. In: *Nucl. Phys. B* 56 (1973), p. 15 (cit. on p. 45).
[265] A. Berthon et al. “The $\pi^+ p$ interaction at 1.2 GeV/c”. In: *Nucl. Phys. B* 81 (1974), p. 431 (cit. on p. 45).
[266] J. Feltesse et al. “The reaction $\pi^- p \to \eta n$ up to $p^*(\eta) = 450$ MeV/c: Experimental results and partial wave analysis”. In: *Nucl. Phys. B* 93 (1975), p. 242 (cit. on p. 45).
[267] T. M. Knasel, J. Lindquist, B. Nelson, et al. “Experimental study of the reaction $\pi^- p \to \Lambda K^0$ at beam momenta between 930 and 1130 MeV/c”. In: *Phys. Rev. D* 11 (1975), p. 1 (cit. on p. 45).
[268] N. C. Debenham, D. M. Binnie, L. Camilleri, et al. “Backward $\pi^- p$ reactions between 0.6 GeV/c and 1 GeV/c”. In: *Phys. Rev. D* 12 (1975), p. 2545 (cit. on p. 45).
[269] M. Winik et al. “Study of the reaction $\pi^+ p \to K^+ \Sigma^+$ between 1.721 GeV and 1.954 GeV center-of-mass energy”. In: *Nucl. Phys. B* 128 (1977), p. 66 (cit. on p. 45).
[270] R. D. Baker, J. A. Blissett, I. J. Bloodworth, et al. “The reaction $\pi^- p \to K^0 \Lambda^0$ up to 1334 MeV/c”. In: *Nucl. Phys. B* 141 (1978), p. 29 (cit. on p. 45).
[271] R. D. Baker, J. A. Blissett, I. J. Bloodworth, et al. “Study of the reaction $\pi^- p \to K^0 \Sigma^0$ from threshold up to 1334 MeV/c”. In: *Nucl. Phys. B* 145 (1978), p. 402 (cit. on p. 45).
[272] R. M. Brown, A. G. Clark, P. J. Duke, et al. “Differential cross-sections for the reaction $\pi^- p \to \eta n$ between 724 MeV/c and 2723 MeV/c”. In: *Nucl. Phys. B* 153 (1979), p. 89 (cit. on p. 45).
[273] R. D. Baker, R. M. Brown, A. G. Clark, et al. “Polarized cross-section measurements for the reaction $\pi^- p \to \eta n$ from 1171 MeV/c to 2267 MeV/c and a partial wave analysis in the resonance region”. In: *Nucl. Phys. B* 156 (1979), p. 93 (cit. on p. 45).
[274] D. H. Saxon, R. D. Baker, K. W. Bell, et al. “The reaction $\pi^- p \to K^0 \Lambda^0$ up to 2375 MeV/c: New results and analysis”. In: *Nucl. Phys. B* 162 (1980), p. 522 (cit. on p. 45).
[275] J. C. Hart, R. D. Baker, K. W. Bell, et al. “The reaction $\pi^- p \to K^0 \Sigma^0$ up to 2375 MeV/c”. In: *Nucl. Phys. B* 166 (1980), p. 73 (cit. on p. 45).
[276] P. Livanos et al. “An energy dependent partial wave analysis of the reaction $\pi N \to \Sigma K$ from threshold to 2 GeV in the center-of-mass”. In: *4th Int. Conf. on Baryon Resonances.* Toronto, Canada, 1980, p. 35 (cit. on p. 45).
[277] K. W. Bell, J. A. Blissett, T. A. Broome, et al. “Spin rotation measurements in $\pi^- p \to K^0 \Lambda$”. In: *Nucl. Phys. B* 222 (1983), p. 389 (cit. on p. 45).
[278] D. J. Candlin et al. “Differential cross-section and polarization for $\pi^+ p \to K^+ \Sigma^+$ at 26 momenta between 1.282 GeV/c and 2.473 GeV/c”. In: *Nucl. Phys. B* 226 (1983), p. 1 (cit. on p. 45).
[279] D. J. Candlin et al. “An energy dependent partial wave analysis of $\pi^+ p \to K^+ \Sigma^+$ between threshold and 2.35 GeV”. In: *Nucl. Phys. B* 238 (1984), p. 477 (cit. on p. 45).
[280] J. Haba et al. “A precision measurement of polarization parameters for the $\pi^+ + p \to K^+ + \Sigma^+$ reaction at 13 laboratory momenta between 1490 MeV/c and 2069 MeV/c”. In: *Nucl. Phys. B* 299 (1988), p. 627 (cit. on p. 45).

[281] D. J. Candlin et al. “Measurement of the spin rotation parameter β in the reaction $\pi^+ p \to K^+\Sigma^+$ at 1.60 GeV/c and 1.88 GeV/c”. In: *Nucl. Phys. B* 311 (1989), p. 613 (cit. on p. 45).
[282] T. W. Morrison. “Ph.D. Thesis”. PhD thesis. The George Washington University, 2000 (cit. on p. 45).
[283] R. A. Arndt et al. “Dispersion relation constrained partial wave analysis of πN elastic and $\pi N \to \eta N$ scattering data: The Baryon spectrum”. In: *Phys. Rev. C* 69 (2004), p. 035213 (cit. on p. 45).
[284] N. G. Kozlenko, V. V. Abaev, V. S. Bekrenev, et al. “Measurement of the total and differential cross-sections for the reaction $\pi^- p \to \eta n$ with the Crystal Ball detector”. In: *Phys. Atom. Nucl.* 66 (2003). [Yad. Fiz. **66**, 112 (2003)], p. 110 (cit. on p. 45).
[285] R. L. Workman, R. A. Arndt, and M. W. Paris. “Resonance parameters from K-matrix and T-matrix poles”. In: *Phys. Rev. C* 79 (2009), p. 038201 (cit. on p. 45).
[286] D. E. Bayadilov, Y. A. Beloglazov, A. B. Gridnev, et al. “Study of eta-production reaction $\pi p \to \eta n$ in the near-threshold region”. In: *Eur. Phys. J. A* 35 (2008), p. 287 (cit. on p. 45).
[287] C. Baltay et al. In: *Rev. Mod. Phys.* 33 (1961), p. 374 (cit. on p. 45).
[288] A. Berthelot, A. Daudin, O. Goussu, et al. “Etude à 1.15 GeV/c de la création associée $\pi^+ p \to \Sigma^+ K^+$”. In: *Nuovo Cim.* 21 (1961), p. 693 (cit. on p. 45).
[289] A. Baldini et al. *Total Cross Sections of High Energy Particles: Landolt-Börnstein, Numerical Data and Functional Relationships in Science and Technology.* Ed. by H. Schopper. Vol. 12a. New York: Springer-Verlag, 1988 (cit. on p. 45).
[290] R. L. Workman et al. “Parameterization dependence of T matrix poles and eigenphases from a fit to πN elastic scattering data”. In: *Phys. Rev. C* 86 (2012), p. 035202. DOI: 10.1103/PhysRevC.86.035202. arXiv: 1204.2277 [hep-ph] (cit. on p. 45).
[291] C. W. Kim et al. “Measurement of the helicity asymmetry $\mathbb{E}$ for the $\vec{\gamma}\vec{p} \to p\pi^0$ reaction in the resonance region: The CLAS Collaboration”. In: *Eur. Phys. J. A* 59.9 (2023), p. 217. DOI: 10.1140/epja/s10050-023-01123-3. arXiv: 2305.08616 [nucl-ex] (cit. on pp. 45, 46, 50–52, 54, 81).
[292] J. Ahrens et al. “The Helicity amplitudes A(1/2) and A(3/2) for the D(13)(1520) resonance obtained from the polarized-gamma polarized-p —> p pi0 reaction”. In: *Phys. Rev. Lett.* 88 (2002), p. 232002. DOI: 10.1103/PhysRevLett.88.232002. arXiv: hep-ex/0203006 (cit. on pp. 45, 52, 81).
[293] J. Ahrens et al. “Measurement of the helicity dependence for the gamma p —> n pi+ channel in the second resonance region”. In: *Phys. Rev. C* 74 (2006), p. 045204. DOI: 10.1103/PhysRevC.74.045204 (cit. on pp. 45, 52, 81).
[294] F. Afzal et al. “First Measurement Using Elliptically Polarized Photons of the Double-Polarization Observable E for γp→pπ0 and γp→nπ+”. In: *Phys. Rev. Lett.* 132.12 (2024), p. 121902. DOI: 10.1103/PhysRevLett.132.121902. arXiv: 2402.05531 [nucl-ex] (cit. on p. 45).
[295] M. Gottschall et al. “First measurement of the helicity asymmetry for $\gamma p \to p\pi^0$ in the resonance region”. In: *Phys. Rev. Lett.* 112.1 (2014), p. 012003. DOI: 10.1103/PhysRevLett.112.012003. arXiv: 1312.2187 [nucl-ex] (cit. on pp. 45, 52, 81).
[296] M. Gottschall et al. “Measurement of the helicity asymmetry E for the reaction $\gamma p \to \pi^0 p$”.

In: *Eur. Phys. J. A* 57.1 (2021), p. 40. DOI: 10.1140/epja/s10050-020-00334-2. arXiv: 1904.12560 [nucl-ex] (cit. on pp. 45, 52, 81).

[297] J. Müller et al. "New data on $\vec{\gamma}\vec{p} \to \eta p$ with polarized photons and protons and their implications for $N^* \to N\eta$ decays". In: *Phys. Lett. B* 803 (2020), p. 135323. DOI: 10.1016/j.physletb.2020.135323. arXiv: 1909.08464 [nucl-ex] (cit. on pp. 45, 53, 82).

[298] S. Strauch et al. "First Measurement of the Polarization Observable E in the $\vec{p}(\vec{\gamma}, \pi^+)n$ Reaction up to 2.25 GeV". In: *Phys. Lett. B* 750 (2015), pp. 53–58. DOI: 10.1016/j.physletb.2015.08.053. arXiv: 1503.05163 [nucl-ex] (cit. on pp. 45, 52, 81).

[299] I. Senderovich et al. "First measurement of the helicity asymmetry E in η photoproduction on the proton". In: *Phys. Lett. B* 755 (2016), pp. 64–69. DOI: 10.1016/j.physletb.2016.01.044. arXiv: 1507.00325 [nucl-ex] (cit. on pp. 45, 53, 82).

[300] E. Mornacchi et al. "Evaluation of the E2/M1 ratio in the N→Δ(1232) transition from the γp→pπ0 reaction". In: *Phys. Rev. C* 109.5 (2024), p. 055201. DOI: 10.1103/PhysRevC.109.055201. arXiv: 2312.08211 [nucl-ex] (cit. on pp. 45, 77, 81, 141–143).

[301] N. Zachariou et al. "Double polarisation observable $\mathbb{G}$ for single pion photoproduction from the proton". In: *Phys. Lett. B* 817 (2021), p. 136304. DOI: 10.1016/j.physletb.2021.136304 (cit. on pp. 45, 46, 51, 52, 55, 56, 81).

[302] T. Hashimoto et al. "Differential cross sections and photon beam asymmetries of η photoproduction on the proton at $E_\gamma = 1.3$-2.4 GeV". In: *Phys. Rev. C* 106.3 (2022), p. 035201. DOI: 10.1103/PhysRevC.106.035201. arXiv: 2202.13688 [nucl-ex] (cit. on pp. 45, 46, 51, 53, 57, 58, 82, 144, 145).

[303] L. Clark et al. "Photoproduction of the Σ+ hyperon using linearly polarized photons with CLAS". In: *Phys. Rev. C* 111.2 (2025), p. 025204. DOI: 10.1103/PhysRevC.111.025204. arXiv: 2404.19404 [nucl-ex] (cit. on pp. 46, 53, 63, 82).

[304] F. James and M. Roos. "Minuit: A System for Function Minimization and Analysis of the Parameter Errors and Correlations". In: *Comput. Phys. Commun.* 10 (1975), pp. 343–367. DOI: 10.1016/0010-4655(75)90039-9 (cit. on p. 46).

[305] Jülich Supercomputing Centre. "JURECA: Data Centric and Booster Modules implementing the Modular Supercomputing Architecture at Jülich Supercomputing Centre". In: *Journal of large-scale research facilities* 7.A182 (2021). DOI: 10.17815/jlsrf-7-182. URL: http://dx.doi.org/10.17815/jlsrf-7-182 (cit. on p. 46).

[306] R. Tibshirani. "Regression Shrinkage and Selection Via the Lasso". In: *J. Roy. Statist. Soc. B* 58.1 (1996), pp. 267–288. DOI: 10.1111/j.2517-6161.1996.tb02080.x (cit. on pp. 47, 104).

[307] J. Landay et al. "Model Selection for Pion Photoproduction". In: *Phys. Rev. C* 95.1 (2017), p. 015203. DOI: 10.1103/PhysRevC.95.015203. arXiv: 1610.07547 [nucl-th] (cit. on pp. 47, 104).

[308] J. Landay et al. "Towards the Minimal Spectrum of Excited Baryons". In: *Phys. Rev. D* 99.1 (2019), p. 016001. DOI: 10.1103/PhysRevD.99.016001. arXiv: 1810.00075 [nucl-th] (cit. on pp. 47, 104).

[309] M. Döring et al. "Correlations of πN partial waves for multireaction analyses". In: *Phys. Rev. C* 93.6 (2016), p. 065205. DOI: 10.1103/PhysRevC.93.065205. arXiv: 1603.07265 [nucl-th] (cit. on pp. 47, 104).

[310] W. J. Briscoe et al. "Threshold π^- photoproduction on the neutron". In: *Eur. Phys. J. A* 56.8 (2020), p. 218. DOI: 10.1140/epja/s10050-020-00221-w. arXiv: 2004.01742 [nucl-th] (cit. on p. 50).

[311] R. M. Worlock. "Photoproduction of Neutral Pions at Energies 600 to 800 Mev". In: *Phys. Rev.* 117 (1960), pp. 537–543. DOI: 10.1103/PhysRev.117.537 (cit. on pp. 52, 81).

[312] R. M. Talman et al. "Evidence for Vector-Meson Effects on pi0 Photoproduction From Hydrogen". In: *Phys. Rev. Lett.* 9 (1962), pp. 177–180. DOI: 10.1103/PhysRevLett.9.177 (cit. on pp. 52, 81).

[313] H. De Staebler Jr et al. "Photoproduction of π 0 from Hydrogen near the Second Pion-Nucleon Resonance". In: *Physical Review* 140.2B (1965), B336 (cit. on pp. 52, 81).

[314] G. C. Bolon et al. "MEASUREMENTS OF PI0 PHOTOPRODUCTION CROSS-SECTIONS FOR INCIDENT GAMMA-RAY ENERGIES OF 2.0-Gev/c TO 5.0-Gev/c". In: *Phys. Rev. Lett.* 18 (1967), p. 926. DOI: 10.1103/PhysRevLett.18.926 (cit. on pp. 52, 81).

[315] C. Ward, B. Kenton, and C. York. "Photoproduction of pi0 from Hydrogen near the Second and Third Pion-Nucleon Resonances". In: *Phys. Rev.* 159 (1967), pp. 1176–1186. DOI: 10.1103/PhysRev.159.1176 (cit. on pp. 52, 81).

[316] M. Braunschweig et al. "Single photoproduction of neutral π-mesons on hydrogen at small angles between 4 and 5.8 GeV". In: *Phys. Lett. B* 26 (1968), pp. 405–409. DOI: 10.1016/0370-2693(68)90628-X (cit. on pp. 52, 81).

[317] G. Buschhorn et al. "Photoproduction of π^0 in the Backward Direction". In: *Phys. Rev. Lett.* 20 (1968), pp. 230–232. DOI: 10.1103/PhysRevLett.20.230 (cit. on pp. 52, 81).

[318] B. Govorkov, S. Denisov, and E. Minarik. "Photoproduction of Neutral Pions on Protons near Threshold". In: *Soviet Journal of Nuclear Physics* 6.3 (1968), p. 370 (cit. on pp. 52, 81).

[319] F. B. Wolverton. "Pi zero photoproduction from hydrogen between 574 and 1211 MeV". PhD thesis. Caltech, 1968 (cit. on pp. 52, 81).

[320] W. Hitzeroth. "Photoproduction of neutral pions on protons near threshold". In: *Nuovo Cim. A* 60 (1969), pp. 467–480. DOI: 10.1007/BF02757017 (cit. on pp. 52, 81).

[321] B. Delcourt et al. "$\pi°$ photoproduction on proton at backward angles between 700 MeV and 1150 MeV". In: *Physics Letters B* 29.1 (1969), pp. 70–74 (cit. on pp. 52, 81).

[322] M. Braunschweig et al. "Single photoproduction of neutral pi-mesons on hydrogen in the extreme forward direction at 4 and 5.8 gev". In: *Nucl. Phys. B* 20 (1970), pp. 191–200. DOI: 10.1016/0550-3213(70)90202-6 (cit. on pp. 52, 81).

[323] B. Lohr. Tech. rep. PI1-98. Physikalisches Institut, University of Bonn, 1970 (cit. on pp. 52, 81).

[324] P. S. L. Booth et al. Tech. rep. DNPL/P95. Daresbury Nuclear Physics Laboratory, 1971 (cit. on pp. 52, 81).

[325] S. Almehed et al. In: *Conference Proceedings, Bonn.* 1973 (cit. on pp. 52, 81).

[326] H. Becks et al. “Backward photoproduction of neutral pions off hydrogen at photon energies between 0.4 and 2.2 gev”. In: *Nucl. Phys. B* 60 (1973), pp. 267–276. DOI: 10.1016/0550-3213(73)90179-X (cit. on pp. 52, 81).
[327] Y. Hemmi et al. “Photoproduction of neutral pions off neutrons in the energy region between 500 mev and 900 mev”. In: *Nucl. Phys. B* 55 (1973), pp. 333–362. DOI: 10.1016/0550-3213(73)90384-2 (cit. on pp. 52, 81).
[328] Y. Hemmi et al. “Neutral pion photoproduction from protons at forward angles in the energy region between 350 mev and 1175 mev”. In: *Phys. Lett. B* 43 (1973), pp. 79–84. DOI: 10.1016/0370-2693(73)90549-2 (cit. on pp. 52, 81).
[329] H. Genzel et al. “PHOTOPRODUCTION OF NEUTRAL PIONS ON HYDROGEN. 4. COMBINATION OF THE CROSS-SECTION DATA OF ALL BONN EXPERIMENTS ON THE pi0 PHOTOPRODUCTION BELOW 500-MeV”. In: *Z. Phys.* 268 (1974), pp. 43–50. DOI: 10.1007/BF01670060 (cit. on pp. 52, 81).
[330] N. Tanaka et al. “Recoil-proton polarization in neutral-pion photoproduction between 1000 and 1800 mev”. In: *Phys. Rev. D* 8 (1973), pp. 1–8. DOI: 10.1103/PhysRevD.8.1 (cit. on pp. 52, 81).
[331] L. O. Abrahamian et al. “Pi0 and pi+ Production with Polarized Photons in the Energy Range 1-GeV - 2-GeV”. In: *Phys. Lett. B* 48 (1974), pp. 463–466. DOI: 10.1016/0370-2693(74)90379-7 (cit. on pp. 52, 81).
[332] A. I. Derebchinskii et al. “Polarization of secondary protons from the reaction in the region of the third resonance”. In: *Zh. Eksp. Teor. Fiz.* 66.1 (1974), pp. 68–73 (cit. on pp. 52, 81).
[333] P. Feller et al. “Photoproduction of neutral pions off hydrogen at photon energies between 0.55 and 2.2 gev at a cm-angle of 120 degrees”. In: *Phys. Lett. B* 49 (1974), pp. 197–200. DOI: 10.1016/0370-2693(74)90508-5 (cit. on pp. 52, 81).
[334] J. S. Barton et al. “The Photoproduction of Neutral Pions from Protons Between 0.7-GeV and 1.7-GeV”. In: *Nucl. Phys. B* 84 (1975), pp. 449–466. DOI: 10.1016/0550-3213(75)90317-X (cit. on pp. 52, 81).
[335] P. S. L. Booth et al. “The Photoproduction of Neutral Pions from Protons at Forward Angles in the Resonance Region”. In: *Nucl. Phys. B* 84 (1975), pp. 437–448. DOI: 10.1016/0550-3213(75)90316-8 (cit. on pp. 52, 81).
[336] P. E. Argan et al. “Two-body photodisintegration of 3 He and 4 He in the $\Delta(1236)$ region”. In: *Nucl. Phys. A* 237 (1975), pp. 447–464. DOI: 10.1016/0375-9474(75)90411-X (cit. on pp. 52, 81).
[337] W. Brefeld et al. “Forward Photoproduction of Neutral Pions from Protons in the Resonance Region”. In: *Nucl. Phys. B* 100 (1975), pp. 93–102. DOI: 10.1016/0550-3213(75)90226-6 (cit. on pp. 52, 81).
[338] P. Dougan et al. “Some cross-sections for the photo-production of neutral Pi-mesons from hydrogen at energies from 360 to 938 MeV”. In: *Z. Phys. A* 274.1 (1975), pp. 73–78. DOI: 10.1007/BF01421038 (cit. on pp. 52, 81).
[339] L. O. Abramyan et al. “Asymmetry of the cross section of the reaction $\gamma P \to P\pi^0$ in the energy interval 0.9-1.65 GeV at $\theta_\pi^{0cms} = 110°$”. In: *JETP Lett.* 23 (1976), pp. 375–378 (cit. on pp. 52, 81).
[340] M. Jung et al. Tech. rep. BONN-HE-76-15. University of Bonn, 1976 (cit. on pp. 52, 81).

[341] I. Arai et al. “Differential Cross-Sections for Single Pion Photoproduction from Protons in the Energy Range Between 500-MeV and 930-MeV”. In: *J. Phys. Soc. Jap.* 43 (1977), pp. 363–368. DOI: 10.1143/JPSJ.43.363 (cit. on pp. 52, 81).
[342] P. Dougan, V. Ramsay, and W. Stiefler. “Cross-Sections for Deuteron Photodisintegration from 74-MeV to 241-MeV”. In: *Z. Phys. A* 280 (1977), pp. 341–348. DOI: 10.1007/BF01435442 (cit. on pp. 52, 81).
[343] D. Husmann et al. “Forward Photoproduction of Neutral Pions on Protons in the Third Resonance Region”. In: *Nucl. Phys. B* 126 (1977), pp. 436–442. DOI: 10.1016/0550-3213(77)90289-9 (cit. on pp. 52, 81).
[344] Aleksandrov et al. In: *Sov. J. Nucl. Phys.* 25 (1977), p. 43 (cit. on pp. 52, 81).
[345] Aleksandrov et al. In: *Sov. J. Nucl. Phys.* 28 (1978), p. 344 (cit. on pp. 52, 81).
[346] K. H. Althoff et al. “Photoproduction of Neutral Pions in the Region of the Fourth Nucleon Resonance”. In: *Z. Phys. C* 1 (1979), p. 257. DOI: 10.1007/BF01440225 (cit. on pp. 52, 81).
[347] K. H. Althoff et al. “Photoproduction of Neutral Pions at Backward Angles in the Resonance Region and the η - Cusp”. In: *Z. Phys. C* 1 (1979), p. 327. DOI: 10.1007/BF01546970 (cit. on pp. 52, 81).
[348] P. J. Bussey et al. “Polarization Parameters in Neutral Pion Photoproduction”. In: *Nucl. Phys. B* 154 (1979), pp. 492–502. DOI: 10.1016/0550-3213(79)90044-0 (cit. on pp. 52, 81).
[349] M. A. Shupe et al. “NEUTRAL PION PHOTOPRODUCTION AND PROTON COMPTON SCATTERING AT LARGE ANGLES”. In: *Phys. Rev. D* 19 (1979), pp. 1921–1930. DOI: 10.1103/PhysRevD.19.1921 (cit. on pp. 52, 81).
[350] M. Yoshioka et al. “DIFFERENTIAL CROSS-SECTIONS OF NEUTRAL PION PHOTOPRODUCTION FROM HYDROGEN IN THE ENERGY REGION FROM 390-MEV TO 975-MEV”. In: *Nucl. Phys. B* 168 (1980), pp. 222–242. DOI: 10.1016/0550-3213(80)90108-X (cit. on pp. 52, 81).
[351] P. Zenz. “MEASUREMENT OF THE DIFFERENTIAL CROSS-SECTIONS OF THE REACTION gamma p —> pi+ n AND gamma p —> pi0 p AT A LAB ANGLE OF 45-degrees IN THE GAMMA ENERGY RANGE OF 0.8-GeV TO 2-GeV AS WELL AS PARAMETRIZATION OF THE center-of-mass ANGULAR DISTRIBUTION DURING FORMATION OF LEGENDRE POLYNOMIALS”. PhD thesis. Mar. 1988 (cit. on pp. 52, 81).
[352] R. Beck et al. “Measurement of the p (gamma, pi0) cross-section at threshold”. In: *Phys. Rev. Lett.* 65 (1990), pp. 1841–1844. DOI: 10.1103/PhysRevLett.65.1841 (cit. on pp. 52, 81).
[353] M. Fuchs et al. “Neutral pion photoproduction from the proton near threshold”. In: *Phys. Lett. B* 368 (1996), pp. 20–25. DOI: 10.1016/0370-2693(95)01488-8 (cit. on pp. 52, 81).
[354] HAERTER. “PHD THESIS”. PhD thesis. 1996 (cit. on pp. 52, 81).
[355] SCHNEIDER. “PHD THESIS”. PhD thesis. 1997 (cit. on pp. 52, 81).
[356] J. C. Bergstrom, R. Igarashi, and J. M. Vogt. “Measurement of the H-1(gamma,pi0) cross-section near threshold. II: Pion angular distributions”. In: *Phys. Rev. C* 55 (1997), pp. 2016–2023. DOI: 10.1103/PhysRevC.55.2016 (cit. on pp. 52, 81).

[357] R. M. Davidson and N. C. Mukhopadhyay.
"Mainz Measurement of the E-2/ M-1 Ratio in the N-Delta Transition".
In: *Phys. Rev. Lett.* 79 (1997), pp. 4509–4509. DOI: 10.1103/PhysRevLett.79.4509.
arXiv: nucl-th/9705035 (cit. on pp. 52, 81).
[358] B. Krusche et al. "Single and double pi0 photoproduction from the deuteron".
In: *Eur. Phys. J. A* 6 (1999), pp. 309–324. DOI: 10.1007/s100500050349
(cit. on pp. 52, 81).
[359] A. Schmidt et al.
"Test of Low-Energy Theorems for $^{1}H(\rightarrow,^{0})^{1}H$ in the Threshold Region".
In: *Phys. Rev. Lett.* 87 (2001). [Erratum: Phys.Rev.Lett. 110, 039903 (2013)], p. 232501.
DOI: 10.1103/PhysRevLett.87.232501. arXiv: nucl-ex/0105010 (cit. on pp. 52, 81).
[360] O. Bartholomy et al. "Neutral pion photoproduction off protons in the energy range
0.3-GeV < E(gamma) < 3-GeV". In: *Phys. Rev. Lett.* 94 (2005), p. 012003.
DOI: 10.1103/PhysRevLett.94.012003. arXiv: hep-ex/0407022 (cit. on pp. 52, 81).
[361] R. Beck. "Experiments with photons at MAMI".
In: *The European Physical Journal A-Hadrons and Nuclei* 28.Suppl 1 (2006), pp. 173–183
(cit. on pp. 52, 81).
[362] M. Dugger et al.
"pi0 photoproduction on the proton for photon energies from 0.675 to 2.875-GeV".
In: *Phys. Rev. C* 76 (2007), p. 025211. DOI: 10.1103/PhysRevC.76.025211.
arXiv: 0705.0816 [hep-ex] (cit. on pp. 52, 81).
[363] M. Sumihama et al. "Backward-angle photoproduction of pi0 mesons on the proton at E
gamma = 1.5-2.4-GeV". In: *Phys. Lett. B* 657 (2007), pp. 32–37.
DOI: 10.1016/j.physletb.2007.10.032. arXiv: 0708.1600 [nucl-ex]
(cit. on pp. 52, 81).
[364] S. Schumann et al.
"Radiative pi0 photoproduction on protons in the Delta+(1232) region".
In: *Eur. Phys. J. A* 43 (2010), pp. 269–282. DOI: 10.1140/epja/i2010-10925-y.
arXiv: 1001.3626 [hep-ex] (cit. on pp. 52, 81).
[365] V. Crede et al. "Photoproduction of Neutral Pions off Protons".
In: *Phys. Rev. C* 84 (2011), p. 055203. DOI: 10.1103/PhysRevC.84.055203.
arXiv: 1107.2151 [nucl-ex] (cit. on pp. 52, 81).
[366] W. Luo et al.
"Polarization components in π^0 photoproduction at photon energies up to 5.6 GeV".
In: *Phys. Rev. Lett.* 108 (2012), p. 222004. DOI: 10.1103/PhysRevLett.108.222004.
arXiv: 1109.4650 [nucl-ex] (cit. on pp. 52, 81).
[367] D. Hornidge et al. "Accurate Test of Chiral Dynamics in the γ→p→π0p Reaction".
In: *Phys. Rev. Lett.* 111.6 (2013), p. 062004. DOI: 10.1103/PhysRevLett.111.062004.
arXiv: 1211.5495 [nucl-ex] (cit. on pp. 52, 81).
[368] J. Hartmann et al. "The N(1520) 3/2- helicity amplitudes from an energy-independent
multipole analysis based on new polarization data on photoproduction of neutral pions".
In: *Phys. Rev. Lett.* 113 (2014), p. 062001. DOI: 10.1103/PhysRevLett.113.062001.
arXiv: 1407.2163 [nucl-ex] (cit. on pp. 52, 81).
[369] P. Adlarson et al. "Measurement of ^{0} photoproduction on the proton at MAMI C".
In: *Phys. Rev. C* 92.2 (2015), p. 024617. DOI: 10.1103/PhysRevC.92.024617.
arXiv: 1506.08849 [hep-ex] (cit. on pp. 52, 81).
[370] J. Hartmann et al.
"The polarization observables T , P , and H and their impact on $\gamma p \to p\pi^0$ multipoles".

In: *Phys. Lett. B* 748 (2015), pp. 212–220. DOI: 10.1016/j.physletb.2015.07.008. arXiv: 1506.06226 [nucl-ex] (cit. on pp. 52, 81).
[371] D. J. Drickey and R. F. Mozley. “Neutral Meson Production with Polarized X Rays”. In: *Physical Review* 136.2B (1964), B543 (cit. on pp. 52, 81).
[372] G. Barbiellini et al. “Photoproduction of pi0 on protons by polarized gamma rays”. In: *Phys. Rev.* 184 (1969), pp. 1402–1413. DOI: 10.1103/PhysRev.184.1402 (cit. on pp. 52, 81).
[373] G. Bologna et al. “ASYMMETRY IN SINGLE pi0 PHOTOPRODUCTION BY POLARIZED gamma RAYS ON PROTONS”. In: (July 1970) (cit. on pp. 52, 81).
[374] J. Alspector et al. “Pi+- and pi0 production by polarized photons in the resonance region”. In: *Phys. Rev. Lett.* 28 (1972), pp. 1403–1406. DOI: 10.1103/PhysRevLett.28.1403 (cit. on pp. 52, 80, 81).
[375] G. Knies et al. “Measurement of Asymmetries in Polarized gamma + n –> pi + n, with E(gamma) from 600-MeV to 900-MeV”. In: *Phys. Rev. D* 10 (1974), p. 2778. DOI: 10.1103/PhysRevD.10.2778 (cit. on pp. 52, 80, 81).
[376] Gorbenko et al. In: *JETP Lett.* 19 (1974), p. 340 (cit. on pp. 52, 81).
[377] P. J. Bussey et al. “A Measurement of the Beam Asymmetry Parameter Sigma for Neutral Pion Photoproduction in the Energy Range 1.2-GeV-2.8-GeV”. In: *Nucl. Phys. B* 104 (1976), pp. 253–276. DOI: 10.1016/0550-3213(76)90036-5 (cit. on pp. 52, 81).
[378] Avakyan et al. In: *Sov. J. Nucl. Phys.* 26.537 (1977) (cit. on pp. 52, 81).
[379] Gorbenko et al. In: *VANT* 2 (1977), p. 36 (cit. on pp. 52, 81).
[380] V. Gorbenko et al. “Double polarization experiment in investigation of the reaction. gamma. p.–>. p. pi./sup 0/with a beam of linearly polarized photons”. In: *Sov. J. Nucl. Phys.(Engl. Transl.);(United States)* 26.2 (1977) (cit. on pp. 52, 81).
[381] V. Gorbenko et al. “Measurement of recoil-proton polarization in the reaction. gamma. p.–> pi./sup 0/p with polarized photons at energies 360, 400, 450, and 500 MeV”. In: *Sov. J. Nucl. Phys.(Engl. Transl.);(United States)* 27.5 (1978) (cit. on pp. 52, 81).
[382] R. Avakyan et al. “Measurement of the asymmetry of the cross section for photoproduction of. pi./sup 0/mesons for cms pion angles 40/sup 0/and 50/sup 0/in the resonance region”. In: *Sov. J. Nucl. Phys.(Engl. Transl.);(United States)* 29.5 (1979) (cit. on pp. 52, 81).
[383] R. O. Avakyan et al. Tech. rep. EPI-674-6. Erevan Physics Institute, 1983 (cit. on pp. 52, 81).
[384] R. Avakyan, A. Avetisyan, A. Bagdasaryan, et al. “Measurements of the asymmetry in the γp$\rightarrow$ pπ0 cross section in the resonance region”. In: (1983) (cit. on pp. 52, 81).
[385] Avakyan et al. In: *Sov. J. Nucl. Phys.* 40.588 (1984) (cit. on pp. 52, 81).
[386] A. a. Belyaev et al. “EXPERIMENTAL STUDIES OF THE SIGMA, T, P POLARIZATION PARAMETERS AND THE GAMMA P —> P PI0 REACTION MULTIPOLE ANALYSIS IN THE FIRST RESONANCE REGION”. In: *Nucl. Phys. B* 213 (1983), pp. 201–222. DOI: 10.1016/0550-3213(83)90509-6 (cit. on pp. 52, 81).
[387] Asaturyan et al. In: *JETP Lett.* 44 (1986), p. 341 (cit. on pp. 52, 81).
[388] Agababyan et al. In: *Sov. J. Nucl. Phys.* 50.834 (1989) (cit. on pp. 52, 81).
[389] G. Blanpied et al. “p ($\gamma\rightarrow$, π 0) reaction and the E2 excitation of the Δ”. In: *Physical review letters* 69.13 (1992), p. 1880 (cit. on pp. 52, 81).

[390] R. Beck et al. “Measurement of the E 2/M 1 Ratio in the N→ Δ Transition using the reaction p (γ→, p) π o”. In: *Physical review letters* 78.4 (1997), p. 606 (cit. on pp. 52, 81).
[391] F. V. Adamian et al. “Measurement of the cross-section asymmetry of the reaction gamma p —> pi0 p in the resonance energy region E(gamma) = 0.5-GeV to 1.1-GeV”. In: *Phys. Rev. C* 63 (2001), p. 054606. DOI: 10.1103/PhysRevC.63.054606. arXiv: nucl-ex/0011006 (cit. on pp. 52, 81).
[392] G. Blanpied et al. “N —> delta transition and proton polarizabilities from measurements of p (gamma polarized, gamma), p (gamma polarized, pi0), and p (gamma polarized, pi+)”. In: *Phys. Rev. C* 64 (2001), p. 025203. DOI: 10.1103/PhysRevC.64.025203 (cit. on pp. 52, 81).
[393] D. Elsner et al. “Linearly polarised photon beams at ELSA and measurement of the beam asymmetry in pi0-photoproduction off the proton”. In: *Eur. Phys. J. A* 39 (2009), pp. 373–381. DOI: 10.1140/epja/i2008-10708-1. arXiv: 0810.1849 [nucl-ex] (cit. on pp. 52, 81).
[394] N. Sparks et al. “Measurement of the Beam Asymmetry Σ in the Forward Direction for $\vec{\gamma}p \to p\pi^0$ Photoproduction”. In: *Phys. Rev. C* 81 (2010), p. 065210. DOI: 10.1103/PhysRevC.81.065210. arXiv: 1003.1346 [nucl-ex] (cit. on pp. 52, 81).
[395] M. Dugger et al. “Beam asymmetry Σ for π^+ and π^0 photoproduction on the proton for photon energies from 1.102 to 1.862 GeV”. In: *Phys. Rev. C* 88.6 (2013). [Addendum: Phys.Rev.C 89, 029901 (2014)], p. 065203. DOI: 10.1103/PhysRevC.88.065203. arXiv: 1308.4028 [nucl-ex] (cit. on pp. 52, 81).
[396] R. Querzoli, G. Salvini, and A. Silverman. “The polarization of the proton from the process γ+ p→ p+ π0 in the region of the higher resonances”. In: *Il Nuovo Cimento (1955-1965)* 19.1 (1961), pp. 53–76 (cit. on pp. 52, 81).
[397] L. Bertanza et al. “Measurement of the polarization of the recoil proton in $\gamma + p \to p + \pi^0$ using a propane-ethane bubble chamber”. In: *Nuovo Cim.* 24.4 (1962), pp. 734–745. DOI: 10.1007/BF02816721 (cit. on pp. 52, 81).
[398] J. Maloy et al. “Polarization of the Recoil Proton from π 0 Photoproduction in Hydrogen”. In: *Physical Review* 139.3B (1965), B733 (cit. on pp. 52, 81).
[399] K. H. Althoff et al. “Measurement of the polarization of the recoil proton from the photoproduction of neutral pions on hydrogen in the region of the first resonance. I”. In: *Z. Phys.* 194.2 (1966), pp. 135–143. DOI: 10.1007/BF01326041 (cit. on pp. 52, 81).
[400] K. H. Althoff et al. “Measurement of the angular distribution of the polarization of the recoil proton from the photoproduction of neutral pions on hydrogen at a photon energy of 360 MeV. II”. In: *Z. Phys.* 194.2 (1966), pp. 144–155. DOI: 10.1007/BF01326042 (cit. on pp. 52, 81).
[401] E. D. Bloom et al. “RECOIL PROTON POLARIZATION IN pi0 PHOTOPRODUCTION”. In: *Phys. Rev. Lett.* 19 (1967), p. 671. DOI: 10.1103/PhysRevLett.19.671 (cit. on pp. 52, 81).
[402] K. H. Althoff et al. “Measurement of the angular dependence of the polarization of the recoil protons from the photoproduction of neutral pions on hydrogen at proton energies between 240 and 420 MeV”. In: *Phys. Lett. B* 26 (1968), pp. 677–678. DOI: 10.1016/0370-2693(68)90388-2 (cit. on pp. 52, 81).
[403] S. Hayakawa et al. “Polarization of recoil protons from neutral pion photoproduction”. In: *J. Phys. Soc. Jap.* 25 (1968), pp. 307–318 (cit. on pp. 52, 81).
[404] Bluem et al. In: *Conference Proceedings, Dares.* 1969 (cit. on pp. 52, 81).

[405] Bluem. Tech. rep. PI1-105. Physikalisches Institut, University of Bonn, 1970 (cit. on pp. 52, 81).

[406] M. N. Prentice et al. "The recoil proton polarization in the reaction gamma p —> pi0 p in the third resonance region". In: *Nucl. Phys. B* 41 (1972), pp. 353–364. DOI: 10.1016/0550-3213(72)90398-7 (cit. on pp. 52, 81).

[407] D. Trines. Tech. rep. PI1-160. Physikalisches Institut, University of Bonn, 1972 (cit. on pp. 52, 81).

[408] S. Kabe et al. "Polarization of recoil protons from proton Compton scattering in the region of the second πN resonance". In: *Nuclear Physics B* 50.1 (1972), pp. 17–28 (cit. on pp. 52, 81).

[409] N. V. Goncharov et al. "Polarization of protons from the γ + p $\rightarrow$ π0 + p reaction produced by 692-1028 MeV photons at 90 in the center-of-mass sytem". In: *Sov. Phys. JETP* 37 (1973), pp. 205–207 (cit. on pp. 52, 81).

[410] Gorbenko et al. In: *JETP Lett.* 22 (1975), p. 186 (cit. on pp. 52, 81).

[411] P. Blum et al. "Angular Dependence of the Polarization of the Recoil Proton from the Reaction gamma p –> pi0 p in the Region of the Second Resonance". In: *Z. Phys. A* 277 (1976), p. 311. DOI: 10.1007/BF01415606 (cit. on pp. 52, 81).

[412] P. Blum, R. Brockmann, and W. Mohr. "Angular Dependence of the Polarization of the Recoil Proton from the Reaction gamma p –> pi0 p in the Region of the Third Resonance". In: *Z. Phys. A* 278 (1976), p. 275. DOI: 10.1007/BF01409179 (cit. on pp. 52, 81).

[413] Derebchinski et al. In: *Sov. Phys. JETP* 43 (1976), p. 218 (cit. on pp. 52, 81).

[414] A. Zybalov et al. "Angular dependences of the polarization of secondary protons from the. gamma. p.–> pi./sup 0/p reaction at photon energies of 650 and 700 MeV". In: *Sov. J. Nucl. Phys.(Engl. Transl.);(United States)* 28.1 (1978) (cit. on pp. 52, 81).

[415] S. Kato et al. "Recoil Proton Polarization of Neutral Pion Photoproduction From Proton in the Energy Range Between 400-MeV and 1142-MeV". In: *Nucl. Phys. B* 168 (1980), pp. 1–16. DOI: 10.1016/0550-3213(80)90272-2 (cit. on pp. 52, 81).

[416] A. S. Bratashevsky et al. "POLARIZATION OF RECOIL PROTONS FROM THE REACTION GAMMA P —> PI0 P IN THE PHOTON ENERGY RANGE 450-MEV - 800-MEV". In: *Nucl. Phys. B* 166 (1980), pp. 525–533. DOI: 10.1016/0550-3213(80)90211-4 (cit. on pp. 52, 81).

[417] A. S. Bratashevsky et al. In: *Sov. J. Nucl. Phys.* 33 (1981), p. 538 (cit. on pp. 52, 81).

[418] A. S. Bratashevsky et al. In: *Sov. J. Nucl. Phys.* 35 (1982), p. 33 (cit. on pp. 52, 81).

[419] R. O. Avakian et al. "MEASUREMENT OF POLARIZATION OF RECOIL PROTONS IN PI0 PHOTOPRODUCTION FOR THETA* (PI0) = 60-degrees IN RESONANCE REGION. (IN RUSSIAN)". In: *Sov. J. Nucl. Phys.* 37 (1983), pp. 199–201 (cit. on pp. 52, 81).

[420] A. S. Bratashevsky et al. In: *Sov. J. Nucl. Phys.* 38 (1983), p. 233 (cit. on pp. 52, 81).

[421] A. S. Bratashevsky et al. In: *Sov. J. Nucl. Phys.* 42 (1985), p. 417 (cit. on pp. 52, 81).

[422] A. S. Bratashevsky et al. In: *Sov. J. Nucl. Phys.* 41 (1985), p. 960 (cit. on pp. 52, 81).

[423] M. M. Asaturian et al. "POLARIZATION PARAMETERS SIGMA, T, AND P FOR THE REACTION GAMMA P —> P PI0 IN THE ENERGY INTERVAL 0.9-GEV - 1.5-GEV AT THETA (PI0) center-of-mass = 120-DEGREES". In: *JETP Lett.* 44 (1986), pp. 341–344 (cit. on pp. 52, 81).

[424] A. S. Bratashevsky et al. "MEASUREMENTS OF POLARIZATION OF SECONDARY PROTONS IN THE

GAMMA P —> P PI0 REACTION AT THETA (PI) = 150-DEGREES CMS WITHIN THE RANGE OF E (GAMMA) = 0.45-GEV - 0.7-GEV. (IN RUSSIAN)". In: *Ukr. Fiz. Zh. (Russ. Ed.)* 31 (1986), pp. 1306–1310 (cit. on pp. 52, 81).

[425] Avakyan et al. In: *Sov. J. Nucl. Phys.* 46.853 (1987) (cit. on pp. 52, 81).

[426] A. S. Bratashevsky et al. In: *Sov. J. Nucl. Phys.* 46 (1987), p. 635 (cit. on pp. 52, 81).

[427] R. O. Avakian et al. "Measurement of proton polarization in the reaction gamma p —> p pi0 at an angle Theta*(pi0) = 80-degrees in a linearly polarized photon beam". In: *Sov. J. Nucl. Phys.* 48 (1988), pp. 1030–1031 (cit. on pp. 52, 81).

[428] K. S. Agababian et al. "Measurement of Polarization Parameters Σ, T, and P in π^0 Photoproduction at $e(\gamma) = 0.9$-GeV - 1.35-GeV. (In Russian)". In: *Sov. J. Nucl. Phys.* 50 (1989), pp. 834–837 (cit. on pp. 52, 81).

[429] R. O. Avakyan et al. "Measurement of P(x), P(y), P(z) components of the proton's polarization vector in the gamma p —> p pi0 reaction with linearly polarized photons. (In Russian)". In: *Sov. J. Nucl. Phys.* 53 (1991), pp. 448–450 (cit. on pp. 52, 81).

[430] K. Wijesooriya et al. "Polarization measurements in neutral pion photoproduction". In: *Phys. Rev. C* 66 (2002), p. 034614. DOI: 10.1103/PhysRevC.66.034614 (cit. on pp. 52, 81, 131).

[431] P. Feller et al. "The Measurement of Polarized Target Asymmetry in gamma p –> p Between 0.4-GeV-1.0-GeV Around 100-Degrees". In: *Nucl. Phys. B* 110 (1976), pp. 397–412. DOI: 10.1016/0550-3213(76)90230-3 (cit. on pp. 52, 81).

[432] M. Fukushima et al. "The Measurement of Polarized Target Asymmetry on gamma p –> pi0 p Below 1-GeV". In: *Nucl. Phys. B* 136 (1978), pp. 189–200. DOI: 10.1016/0550-3213(78)90276-6 (cit. on pp. 52, 81).

[433] H. Herr et al. "Forward photoproduction of neutral pions on polarized protons in the third resonance region". In: *Nuclear Physics B* 125.2 (1977), pp. 157–161 (cit. on pp. 52, 81).

[434] P. Booth et al. "The polarised target asymmetry for neutral pion photoproduction from protons in the photon energy range 0.7–1.45 GeV". In: *Nuclear Physics B* 121.1 (1977), pp. 45–57 (cit. on pp. 52, 81).

[435] A. Bock et al. "Measurement of the target asymmetry of eta and pi0 photoproduction on the proton". In: *Phys. Rev. Lett.* 81 (1998), pp. 534–537. DOI: 10.1103/PhysRevLett.81.534 (cit. on pp. 52, 53, 81, 82).

[436] J. R. M. Annand et al. "T and F asymmetries in ^{0} photoproduction on the proton". In: *Phys. Rev. C* 93.5 (2016), p. 055209. DOI: 10.1103/PhysRevC.93.055209 (cit. on pp. 52, 81).

[437] Booth et al. *Annual Report*. Tech. rep. 1977 (cit. on pp. 52, 81).

[438] P. J. Bussey et al. "Measurements of the Double Polarization Parameters G and H in Neutral Pion Photoproduction". In: *Nucl. Phys. B* 159 (1979), pp. 383–396. DOI: 10.1016/0550-3213(79)90341-9 (cit. on pp. 52, 81).

[439] J. Ahrens et al. "Measurement of the G asymmetry for the gamma p —> N pi channels in the Delta(1232) resonance region". In: *Eur. Phys. J. A* 26 (2005), pp. 135–140. DOI: 10.1140/epja/i2005-10158-3 (cit. on pp. 52, 81).

[440] A. Thiel et al. "Well-established nucleon resonances revisited by double-polarization measurements".

In: *Phys. Rev. Lett.* 109 (2012), p. 102001. DOI: 10.1103/PhysRevLett.109.102001. arXiv: 1207.2686 [nucl-ex] (cit. on pp. 52, 81).
[441] M. H. Sikora et al. "Measurement of the $^1H(\vec{\gamma}, \vec{p})\pi^0$ reaction using a novel nucleon spin polarimeter". In: *Phys. Rev. Lett.* 112.2 (2014), p. 022501. DOI: 10.1103/PhysRevLett.112.022501. arXiv: 1309.7897 [nucl-ex] (cit. on pp. 52, 81).
[442] J. H. Boyden. "Photoproduction of positive pions from hydrogen at small angles at energies 700 to 1025 mev". PhD thesis. Caltech, 1961 (cit. on pp. 52, 81).
[443] J. K. Walker and J. P. Burq. "Low-Energy Charged Meson Photoproduction". In: *Phys. Rev. Lett.* 8 (1962), pp. 37–40. DOI: 10.1103/PhysRevLett.8.37 (cit. on pp. 52, 81).
[444] J. R. Kilner. PhD thesis. Caltech, 1962 (cit. on pp. 52, 81).
[445] E. A. Knapp, R. W. Kenney, and V. Perez-Mendez. "Angular Distributions of Photopions from Hydrogen". In: *Phys. Rev.* 114 (1959), pp. 605–611. DOI: 10.1103/PhysRev.114.605 (cit. on pp. 52, 81).
[446] D. W. G. S. Leith, R. Little, and E. M. Lawson. "PI+ PHOTOPRODUCTION AT CONSTANT PION ENERGY, AND THE (GAMMA PI RHO) COUPLING". In: *Phys. Lett.* 8 (1964), pp. 355–357. DOI: 10.1016/S0031-9163(64)80031-7 (cit. on pp. 52, 81).
[447] G. Buschhorn et al. "Photoproduction of Single Positive Pions Between 1.2 and 3 GeV". In: *Phys. Rev. Lett.* 17 (1966), pp. 1027–1030. DOI: 10.1103/PhysRevLett.17.1027 (cit. on pp. 52, 81).
[448] G. Buschhorn et al. "π^+ Photoproduction Between 1.2 and 3 GeV at Very Small Angles". In: *Phys. Rev. Lett.* 18 (1967), pp. 571–574. DOI: 10.1103/PhysRevLett.18.571 (cit. on pp. 52, 81).
[449] S. D. Ecklund and R. L. Walker. "pi+ Photoproduction from Hydrogen at Laboratory Energies from 589 to 1269 MeV". In: *Phys. Rev.* 159 (1967), pp. 1195–1209. DOI: 10.1103/PhysRev.159.1195 (cit. on pp. 52, 81).
[450] J. P. Dowd et al. "Photoproduction of Charged Pions by 2- to 5-GeV Tagged gamma Rays". In: *Phys. Rev. Lett.* 18 (1967), pp. 414–417. DOI: 10.1103/PhysRevLett.18.414 (cit. on pp. 52, 81).
[451] C. Betourne et al. "POSITIVE PION PHOTOPRODUCTION FROM HYDROGEN FOR INCIDENT PHOTON ENERGIES 300-MEV - 750-MeV". In: *Phys. Rev.* 172 (1968), pp. 1343–1353. DOI: 10.1103/PhysRev.172.1343 (cit. on pp. 52, 81).
[452] R. A. Alvarez et al. "Photoproduction of positive pions at backward angles in the energy range 1-3 gev". In: *Phys. Rev. D* 1 (1970), pp. 1946–1960. DOI: 10.1103/PhysRevD.1.1946 (cit. on pp. 52, 81).
[453] G. Fischer et al. "Photoproduction of positive pions on hydrogen at photon energies between 220 and 425 mev". In: *Nucl. Phys. B* 16 (1970), pp. 119–124. DOI: 10.1016/0550-3213(70)90344-5 (cit. on pp. 52, 81).
[454] Aleksandrov et al. In: *Sov. J. Nucl. Phys.* 12 (1971), p. 416 (cit. on pp. 52, 81).
[455] B. Bouquet et al. "Photoproduction of positive pions at 180 degrees from 0.22 to 3.1 gev". In: *Phys. Rev. Lett.* 27 (1971), pp. 1244–1247. DOI: 10.1103/PhysRevLett.27.1244 (cit. on pp. 52, 81).

[456] T. Fujii et al. “Charged-pi photoproduction at 180 degress in the energy range between 300 and 1200 mev”. In: *Phys. Rev. Lett.* 26 (1971), pp. 1672–1675. DOI: 10.1103/PhysRevLett.26.1672 (cit. on pp. 52, 79, 81).
[457] K. Ekstrand et al. “Positive-pion photoproduction in the backward direction”. In: *Phys. Rev. D* 6 (1972), pp. 1–11. DOI: 10.1103/PhysRevD.6.1 (cit. on pp. 52, 81).
[458] G. Fischer et al. “Angular distributions of pions from gamma p —> pi+ n at photon energies between 220 and 425 mev”. In: *Z. Phys.* 253 (1972), pp. 38–52. DOI: 10.1007/BF01387168 (cit. on pp. 52, 81).
[459] T. Fujii et al. “Photoproduction of Charged pi Mesons from Hydrogen and Deuterium in the Energy Range Between 250-MeV and 790-MeV”. In: *Nucl. Phys. B* 120 (1977), pp. 395–422. DOI: 10.1016/0550-3213(77)90084-0 (cit. on pp. 52, 79, 81).
[460] E. J. Durwen. PhD thesis. 1980 (cit. on pp. 52, 81).
[461] K. H. Althoff et al. “Positive Pion Photoproduction From Hydrogen at Photon Energies Between 500-MeV and 1400-MeV in Forward Direction”. In: *Z. Phys. C* 18 (1983), p. 199. DOI: 10.1007/BF01571360 (cit. on pp. 52, 81).
[462] J. L. Faure et al. “Charged Pion Photoproduction Measurement on Deuterium in the $\Delta(1236)$ Region Using a Quasimonochromatic Photon Beam”. In: *Nucl. Phys. A* 424 (1984), pp. 383–411. DOI: 10.1016/0375-9474(84)90001-0 (cit. on pp. 52, 81).
[463] W. Heise. “MEASUREMENT OF THE DIFFERENTIAL CROSS-SECTION OF THE REACTION gamma p —> pi+ n AT AVERAGE PRODUCTION ANGLES AND PHOTON ENERGIES OF 735-MeV TO 2005-MeV AND PARAMETRIZATION OF ANGULAR DISTRIBUTIONS IN THE ENERGY RANGE 300-MeV TO 1985-MeV”. PhD thesis. Feb. 1988 (cit. on pp. 52, 81).
[464] K. Buechler et al. “Photoproduction of positive pions from hydrogen with PHOENICS at ELSA”. In: *Nucl. Phys. A* 570 (1994), pp. 580–598. DOI: 10.1016/0375-9474(94)90074-4 (cit. on pp. 52, 81).
[465] H. B. van den Brink et al. “The C-13 (gamma, pi-) N-13 reaction at E(gamma) approximately 184-MeV (T(pi) (approximately 41-MeV)”. In: *Nucl. Phys. A* 587 (1995), pp. 657–674. DOI: 10.1016/0375-9474(95)00040-8 (cit. on pp. 52, 81).
[466] K. G. Fissum et al. “Inclusive positive pion photoproduction”. In: *Phys. Rev. C* 53 (1996), pp. 1278–1289. DOI: 10.1103/PhysRevC.53.1278 (cit. on pp. 52, 81).
[467] R. Beck et al. “Determination of the E2 / M1 ratio in the gamma N —> Delta (1232) transition from a simultaneous measurement of p(polarized gamma, p) pi0 and p(polarized gamma, pi+)n”. In: *Phys. Rev. C* 61 (2000), p. 035204. DOI: 10.1103/PhysRevC.61.035204. arXiv: nucl-ex/9908017 (cit. on pp. 52, 81).
[468] H. W. Dannhausen et al. “Photoproduction of positive pions from hydrogen at large angles in the energy range 0.3-GeV - 2.0-GeV”. In: *Eur. Phys. J. A* 11 (2001), pp. 441–455. DOI: 10.1007/s100500170056 (cit. on pp. 52, 81).
[469] L. Y. Zhu et al. “Cross section measurements of charged pion photoproduction in hydrogen and deuterium from 1.1-GeV to 5.5-GeV”. In: *Phys. Rev. C* 71 (2005), p. 044603. DOI: 10.1103/PhysRevC.71.044603. arXiv: nucl-ex/0409018 (cit. on pp. 52, 79, 81, 85, 160).

[470] M. Dugger et al.
"pi+ photoproduction on the proton for photon energies from 0.725 to 2.875-GeV".
In: *Phys. Rev. C* 79 (2009), p. 065206. DOI: 10.1103/PhysRevC.79.065206.
arXiv: 0903.1110 [hep-ex] (cit. on pp. 52, 81).
[471] J. Ahrens et al. In: *Phys. Rev. C* 74 (2006), p. 054204 (cit. on pp. 52, 81).
[472] R. E. Taylor and R. F. Mozley.
"POSITIVE PION PRODUCTION BY POLARIZED BREMSSTRAHLUNG".
In: *Phys. Rev.* 117 (1960), p. 835. DOI: 10.1103/PhysRev.117.835 (cit. on pp. 52, 81).
[473] R. C. Smith and R. F. Mozley.
"Positive Pion Production by Polarized X Rays between 227 and 373 MeV".
In: *Phys. Rev.* 130 (1963), pp. 2429–2440. DOI: 10.1103/PhysRev.130.2429
(cit. on pp. 52, 81).
[474] F. F. Liu and S. Vitale. "Positive-Pion Production Asymmetry with Polarized Bremsstrahlung Near Second Resonance". In: *Phys. Rev.* 144 (1966), pp. 1093–1100. DOI: 10.1103/PhysRev.144.1093 (cit. on pp. 52, 81).
[475] C. Geweniger et al. "π^+ production with linearly polarized photons".
In: *Phys. Lett. B* 29.1 (1969), pp. 41–44. DOI: 10.1016/0370-2693(69)90130-0
(cit. on pp. 52, 81).
[476] V. A. Getman et al. "Positive Pion Production From Polarized Protons by Linearly Polarized Photons in the Energy Range 280-MeV - 420-MeV".
In: *Nucl. Phys. B* 188 (1981), pp. 397–413. DOI: 10.1016/0550-3213(81)90001-8
(cit. on pp. 52, 81).
[477] J. Ajaka et al. "Precise measurement of Sigma beam asymmetry for positive pion photoproduction on the proton from 550-MeV to 1100-MeV".
In: *Phys. Lett. B* 475 (2000), pp. 372–377. DOI: 10.1016/S0370-2693(99)01396-9
(cit. on pp. 52, 81).
[478] O. Bartalini et al. "Precise measurement of Sigma beam asymmetry for positive pion photoproduction on the proton from 800-MeV to 1500-MeV".
In: *Phys. Lett. B* 544 (2002), pp. 113–120. DOI: 10.1016/S0370-2693(02)02467-X.
arXiv: nucl-ex/0207010 (cit. on pp. 52, 81).
[479] Getman et al. In: *VANT* 8 (1989), p. 3 (cit. on pp. 52, 81).
[480] Abrahamian et al. In: *Sov. J. Nucl. Phys.* 32 (1980), p. 66 (cit. on pp. 52, 81).
[481] Ganenko et al. In: *Sov. J. Nucl. Phys.* 23 (1976), p. 52 (cit. on pp. 52, 81).
[482] Zabaev et al. In: *Sov. J. Nucl. Phys.* 21 (1975), p. 286 (cit. on pp. 52, 81).
[483] Kuznetsov et al. In: *Lett. Nuovo Cim.* 1 (1971), p. 233 (cit. on pp. 52, 81).
[484] Hampe. PhD thesis. 1980 (cit. on pp. 52, 81).
[485] K. H. Althoff et al. "Measurement of the polarization of the recoil neutron from the photoproduction of charged pions on hydrogen". In: *Phys. Lett. B* 26 (1968), pp. 640–641. DOI: 10.1016/0370-2693(68)90440-1 (cit. on pp. 52, 81).
[486] Hahn. PhD thesis. 1971 (cit. on pp. 52, 81).
[487] Wallraff. PhD thesis. 1972 (cit. on pp. 52, 81).
[488] K. Egawa et al. "POLARIZATION OF RECOIL NEUTRONS FROM SINGLE PION PHOTOPRODUCTION OFF PROTONS IN THE RESONANCE REGION".
In: *Nucl. Phys. B* 188 (1981), pp. 11–28. DOI: 10.1016/0550-3213(81)90102-4
(cit. on pp. 52, 81).
[489] P. J. Bussey et al. "Polarization Parameters in Positive Pion Photoproduction".
In: *Nucl. Phys. B* 154 (1979), pp. 205–225. DOI: 10.1016/0550-3213(79)90511-X
(cit. on pp. 52, 81).

[490] S. Arai et al. “Measurement of the asymmetry for pi+ photoproduction from polarized protons between 300 and 900 mev”. In: *Nucl. Phys. B* 48 (1972), pp. 397–414. DOI: 10.1016/0550-3213(72)90178-2 (cit. on pp. 52, 81).
[491] K. H. Althoff et al. “Photoproduction of pi+ mesons on polarized protons at photon energies between 0.5 and 2.2 gev”. In: *Nucl. Phys. B* 53 (1973), pp. 9–18. DOI: 10.1016/0550-3213(73)90303-9 (cit. on pp. 52, 81).
[492] K. H. Althoff et al. “Measurement of the Target Asymmetry for the Reaction gamma p –> pi+ n at Photon Energies Between 0.7-GeV and 2.2-GeV and a Pion CM Angle of 65-Degrees”. In: *Phys. Lett. B* 59 (1975), pp. 93–94. DOI: 10.1016/0370-2693(75)90165-3 (cit. on pp. 52, 81).
[493] H. Genzel et al. “Photoproduction of pi+ Mesons on Polarized Protons”. In: *Nucl. Phys. B* 92 (1975), pp. 196–206. DOI: 10.1016/0550-3213(75)90178-9 (cit. on pp. 52, 81).
[494] P. Feller et al. “Polarized Target Asymmetry in π^+ Photoproduction Between 0.3-GeV and 1.0-GeV at 130°”. In: *Nucl. Phys. B* 102 (1976), p. 207. DOI: 10.1016/0550-3213(76)90095-X (cit. on pp. 52, 81).
[495] K. H. Althoff et al. “Angular Distribution of the Target Asymmetry on Polarized Protons for the Reaction gamma p (Polarized) –> pi+ n at a Photon Energy of 700-MeV”. In: *Phys. Lett. B* 63 (1976), pp. 107–110. DOI: 10.1016/0370-2693(76)90479-2 (cit. on pp. 52, 81).
[496] K. H. Althoff et al. “Photoproduction of Pions on Polarized Protons and Neutrons in the Second Resonance Region”. In: *Nucl. Phys. B* 131 (1977), pp. 1–6. DOI: 10.1016/0550-3213(77)90181-X (cit. on pp. 52, 80, 81).
[497] M. Fukushima et al. “The Measurement of Polarized Target Asymmetry on gamma p –> pi+ n Below 1.02-GeV”. In: *Nucl. Phys. B* 130 (1977), pp. 486–504. DOI: 10.1016/0550-3213(77)90251-6 (cit. on pp. 52, 81).
[498] Getman et al. In: *Sov. J. Nucl. Phys.* 31 (1980), p. 480 (cit. on pp. 52, 81).
[499] K. Fujii et al. “Measurement of Polarized Target Asymmetry on $\gamma p \to \pi^+ n$ in the Third Resonance Region”. In: *Nucl. Phys. B* 197 (1982), pp. 365–377. DOI: 10.1016/0550-3213(82)90448-5 (cit. on pp. 52, 81).
[500] H. Dutz et al. “Photoproduction of positive pions from polarized protons”. In: *Nucl. Phys. A* 601 (1996), pp. 319–332. DOI: 10.1016/0375-9474(96)00008-5 (cit. on pp. 52, 81).
[501] P. J. Bussey et al. “Measurements of the Polarization Parameters in G and H in Positive Pion Photoproduction”. In: *Nucl. Phys. B* 169 (1980), pp. 403–414. DOI: 10.1016/0550-3213(80)90095-4 (cit. on pp. 52, 81).
[502] Belyaev et al. In: *Sov. J. Nucl. Phys.* 40 (1984), p. 83 (cit. on pp. 52, 81).
[503] P. J. Bussey et al. *Physik Daten*. Tech. rep. 1977 (cit. on pp. 52, 81).
[504] Belyaev et al. In: *Sov. J. Nucl. Phys.* 43 (1986), p. 947 (cit. on pp. 52, 81).
[505] C. Bacci, G. Penso, and G. Salvini. “Photoproduction and Neutral Decay Models of the eta Particle”. In: *Phys. Rev. Lett.* 11 (1963), p. 37. DOI: 10.1103/PhysRevLett.11.37 (cit. on pp. 53, 82).
[506] P. L. Kelley. “Self-Focusing of Optical Beams”. In: *Phys. Rev. Lett.* 16 (1966), pp. 384–384. DOI: 10.1103/PhysRevLett.16.384 (cit. on pp. 53, 82).
[507] C. Bacci et al. “Angular Distribution for Eta-Meson Photoproduction from Hydrogen at 775-850 MeV”.

In: *Phys. Rev. Lett.* 20 (1968), pp. 571–574. DOI: 10.1103/PhysRevLett.20.571 (cit. on pp. 53, 82).

[508] B. Delcourt et al. "Photoproduction of eta meson between threshold and 900 mev". In: *Phys. Lett. B* 29 (1969), pp. 75–78. DOI: 10.1016/0370-2693(69)90138-5 (cit. on pp. 53, 82).

[509] Holt et al. In: *Lett. Nuovo Cim.* 2 (1969), p. 69 (cit. on pp. 53, 82).

[510] M. Hongoh et al. "Differential cross-section and recoil proton polarization of eta-meson photoproduction at 890 mev". In: *Lett. Nuovo Cim.* 2S2 (1971), pp. 317–320. DOI: 10.1007/BF02803931 (cit. on pp. 53, 82).

[511] A. Christ et al. "Photoproduction of eta-mesons on hydrogen at photon energies between 1.5 and 2.2 gev". In: *Lett. Nuovo Cim.* 8S2 (1973), pp. 1039–1043. DOI: 10.1007/BF02725722 (cit. on pp. 53, 82).

[512] P. S. L. Booth et al. "Differential cross-sections for the photoproduction of eta mesons from protons near 2 gev". In: *Nucl. Phys. B* 71 (1974), pp. 211–216. DOI: 10.1016/0550-3213(74)90392-7 (cit. on pp. 53, 82).

[513] G. A. Vartapetian and S. E. Piliposian. "Measurements of Cross-section Asymmetry by Polarized Photons and Models of Eta0 Meson Photoproduction in the Energy Range E_γ = 1-GeV to 2-GeV". In: *Sov. J. Nucl. Phys.* 32 (1980), p. 804 (cit. on pp. 53, 82).

[514] S. Homma et al. "Photoproduction of η Mesons from Protons at Incident Energies below 1 GeV". In: *Journal of the Physical Society of Japan* 57.3 (1988), pp. 828–843 (cit. on pp. 53, 82).

[515] N. C. Mukhopadhyay, J. F. Zhang, and M. Benmerrouche. "Photoproduction of the Etas near threshold". In: *Phys. Rev. Lett.* 75 (1995), p. 3022. DOI: 10.1103/PhysRevLett.75.3022. arXiv: hep-ph/9508396 (cit. on pp. 53, 82).

[516] S. A. Dytman et al. "Study of baryon resonances through gamma p —> eta p differential cross-sections". In: *Phys. Rev. C* 51 (1995), pp. 2710–2715. DOI: 10.1103/PhysRevC.51.2710 (cit. on pp. 53, 82).

[517] J. Ahrens et al. "First measurement of the helicity-dependent gamma(pol.) p(pol.) –> p eta differential cross-section". In: *Eur. Phys. J. A* 17 (2003), pp. 241–244. DOI: 10.1140/epja/i2002-10153-2 (cit. on pp. 53, 82).

[518] V. Crede et al. "Photoproduction of eta mesons off protons for 0.75-GeV < E(gamma) < 3-GeV". In: *Phys. Rev. Lett.* 94 (2005), p. 012004. DOI: 10.1103/PhysRevLett.94.012004. arXiv: hep-ex/0311045 (cit. on pp. 53, 82).

[519] T. Nakabayashi et al. "Photoproduction of eta mesons off protons for Egamma <= 1.15-GeV". In: *Phys. Rev. C* 74 (2006), p. 035202. DOI: 10.1103/PhysRevC.74.035202 (cit. on pp. 53, 82).

[520] O. Bartalini et al. "Measurement of eta photoproduction on the proton from threshold to 1500-MeV". In: *Eur. Phys. J. A* 33 (2007), pp. 169–184. DOI: 10.1140/epja/i2007-10439-9. arXiv: 0707.1385 [nucl-ex] (cit. on pp. 53, 82).

[521] M. Dugger et al. "Eta photoproduction on the proton for photon energies from 0.75-GeV to 1.95-GeV". In: *Phys. Rev. Lett.* 89 (2002). [Erratum: Phys.Rev.Lett. 89, 249904 (2002)], p. 222002. DOI: 10.1103/PhysRevLett.89.222002 (cit. on pp. 53, 82).

[522] M. Williams et al. “Differential cross s ections for the reactions gamma p —> p eta and gamma p —> p eta-prime”. In: *Phys. Rev. C* 80 (2009), p. 045213. DOI: 10.1103/PhysRevC.80.045213. arXiv: 0909.0616 [nucl-ex] (cit. on pp. 53, 82).
[523] V. Crede et al. “Photoproduction of eta and eta-prime mesons off protons”. In: *Phys. Rev. C* 80 (2009), p. 055202. DOI: 10.1103/PhysRevC.80.055202. arXiv: 0909.1248 [nucl-ex] (cit. on pp. 53, 82).
[524] M. Sumihama et al. “Backward-angle eta photoproduction from protons at E(gamma) = 1.6 - 2.4 GeV”. In: *Phys. Rev. C* 80 (2009), p. 052201. DOI: 10.1103/PhysRevC.80.052201. arXiv: 0910.0900 [nucl-ex] (cit. on pp. 53, 82).
[525] E. F. McNicoll et al. “Study of the $\gamma p- > \eta p$ reaction with the Crystal Ball detector at the Mainz Microtron(MAMI-C)”. In: *Phys. Rev. C* 82 (2010). [Erratum: Phys.Rev.C 84, 029901 (2011)], p. 035208. DOI: 10.1103/PhysRevC.84.029901. arXiv: 1007.0777 [nucl-ex] (cit. on pp. 53, 82).
[526] V. L. Kashevarov et al. “Study of η and η’ Photoproduction at MAMI”. In: *Phys. Rev. Lett.* 118.21 (2017), p. 212001. DOI: 10.1103/PhysRevLett.118.212001. arXiv: 1701.04809 [nucl-ex] (cit. on pp. 53, 82).
[527] D. Elsner et al. “Measurement of the beam asymmetry in eta-photoproduction off the proton”. In: *Eur. Phys. J. A* 33 (2007), pp. 147–155. DOI: 10.1140/epja/i2007-10447-9. arXiv: nucl-ex/0702032 (cit. on pp. 53, 82).
[528] P. Collins et al. “Photon beam asymmetry Σ for η and η' photoproduction from the proton”. In: *Phys. Lett. B* 771 (2017), pp. 213–221. DOI: 10.1016/j.physletb.2017.05.045. arXiv: 1703.00433 [nucl-ex] (cit. on pp. 53, 62, 82).
[529] F. Afzal et al. “Observation of the pη’ Cusp in the New Precise Beam Asymmetry Σ Data for γp$\rightarrow$pη”. In: *Phys. Rev. Lett.* 125.15 (2020), p. 152002. DOI: 10.1103/PhysRevLett.125.152002. arXiv: 2009.06248 [nucl-ex] (cit. on pp. 53, 82).
[530] C. A. Heusch et al. “RECOIL PROTON POLARIZATION IN ETA PHOTOPRODUCTION”. In: *Phys. Rev. Lett.* 25 (1970), p. 1381. DOI: 10.1103/PhysRevLett.25.1381 (cit. on pp. 53, 82).
[531] C. S. Akondi et al. “Measurement of the Transverse Target and Beam-Target Asymmetries in η Meson Photoproduction at MAMI”. In: *Phys. Rev. Lett.* 113.10 (2014), p. 102001. DOI: 10.1103/PhysRevLett.113.102001. arXiv: 1408.3274 [nucl-ex] (cit. on pp. 53, 82).
[532] P. L. Donoho and R. L. Walker. “Photoproduction of K+ Mesons in Hydrogen”. In: *Phys. Rev.* 112 (1958), pp. 981–986. DOI: 10.1103/PhysRev.112.981 (cit. on pp. 53, 82).
[533] H. M. Brody, A. M. Wetherell, and R. L. Walker. “Photoproduction of K+ Mesons in Hydrogen”. In: *Phys. Rev.* 119 (1960), pp. 1710–1716. DOI: 10.1103/PhysRev.119.1710 (cit. on pp. 53, 82).
[534] B. McDaniel et al. “Polarization of Λ 0 from Photoproduction in Hydrogen”. In: *Physical Review Letters* 4.1 (1960), p. 33 (cit. on pp. 53, 82).
[535] R. L. Anderson et al. “Photoproduction of K+ mesons in hydrogen”. In: *Phys. Rev. Lett.* 9 (1962), pp. 131–133. DOI: 10.1103/PhysRevLett.9.131 (cit. on pp. 53, 82).

[536] H. Thom et al. "Polarization of Lambda Hyperons from Photoproduction in Hydrogen". In: *Phys. Rev. Lett.* 11 (1963), pp. 433–435. DOI: 10.1103/PhysRevLett.11.433 (cit. on pp. 53, 82).

[537] C. W. Peck. "K+ Λ Photoproduction from Hydrogen at 1200 MeV". In: *Physical Review* 135.3B (1964), B830 (cit. on pp. 53, 82).

[538] Anderson et al. In: *Conference, Hamburg*. 1965 (cit. on pp. 53, 82).

[539] Mori. PhD thesis. Cornell University, 1966 (cit. on pp. 53, 82).

[540] D. E. Groom and J. H. Marshall. "Lambda Polarization at 90-degrees in K+Lambda Photoproduction". In: *Phys. Rev.* 159 (1967), pp. 1213–1219. DOI: 10.1103/PhysRev.159.1213 (cit. on pp. 53, 82).

[541] T. Fujii et al. "Photoproduction of k+ mesons and polarization of lambda0 hyperons in the 1-gev range". In: *Phys. Rev. D* 2 (1970), pp. 439–448. DOI: 10.1103/PhysRevD.2.439 (cit. on pp. 53, 82).

[542] A. Bleckmann et al. "Photoproduction of k+ lambda and k+ sigma0 from hydrogen between 1.3 and 1.45 gev". In: *Z. Phys.* 239 (1970), pp. 1–15. DOI: 10.1007/BF01408507 (cit. on pp. 53, 82).

[543] D. Decamp et al. *Photoproduction of $K^+\Lambda^0$ and $K^+\Sigma^0$*. Tech. rep. LAL-1236. Laboratoire de l'Accélérateur Linéaire, Orsay, 1970 (cit. on pp. 53, 82).

[544] H. Goeing et al. "Photoproduction of k+ lambda and k+ sigma0 in hydrogen between 1.19 and 1.68 gev". In: *Nucl. Phys. B* 26 (1971), pp. 121–133. DOI: 10.1016/0550-3213(71)90509-8 (cit. on pp. 53, 82).

[545] P. Feller et al. "Photoproduction of k+ lambda0 and k+ sigma0 from hydrogen at constant momentum transfer t between 1.05 and 2.2 gev". In: *Nucl. Phys. B* 39 (1972), pp. 413–420. DOI: 10.1016/0550-3213(72)90379-3 (cit. on pp. 53, 82).

[546] M. Bockhorst et al. "Measurement of gamma p —> K+ Lambda and gamma p —> K+ Sigma0 at photon energies up to 1.47-GeV". In: *Z. Phys. C* 63 (1994), pp. 37–47. DOI: 10.1007/BF01577542 (cit. on pp. 53, 82).

[547] M. Q. Tran et al. "Measurement of gamma p –> K+ Lambda and gamma p –> K+ Sigma0 at photon energies up to 2-GeV". In: *Phys. Lett. B* 445 (1998), pp. 20–26. DOI: 10.1016/S0370-2693(98)01393-8 (cit. on pp. 53, 82).

[548] J. W. C. McNabb et al. "Hyperon photoproduction in the nucleon resonance region". In: *Phys. Rev. C* 69 (2004), p. 042201. DOI: 10.1103/PhysRevC.69.042201. arXiv: nucl-ex/0305028 (cit. on pp. 53, 82).

[549] R. Bradford et al. "Differential cross sections for gamma + p —> K+ + Y for Lambda and Sigma0 hyperons". In: *Phys. Rev. C* 73 (2006), p. 035202. DOI: 10.1103/PhysRevC.73.035202. arXiv: nucl-ex/0509033 (cit. on pp. 53, 82).

[550] M. Sumihama et al. "The Polarized-gamma p —> K+ Lambda and polarized-gamma p —> K+ Sigma0 reactions at forward angles with photon energies from 1.5-GeV to 2.4-GeV". In: *Phys. Rev. C* 73 (2006), p. 035214. DOI: 10.1103/PhysRevC.73.035214. arXiv: hep-ex/0512053 (cit. on pp. 53, 82).

[551] M. E. McCracken et al. "Differential cross section and recoil polarization measurements for the gamma p to K+ Lambda reaction using CLAS at Jefferson Lab". In: *Phys. Rev. C* 81 (2010), p. 025201. DOI: 10.1103/PhysRevC.81.025201. arXiv: 0912.4274 [nucl-ex] (cit. on pp. 53, 82).

[552] S. Alef et al. "$K^+\Lambda$ photoproduction at forward angles and low momentum transfer". In: *Eur. Phys. J. A* 57.2 (2021), p. 80. DOI: 10.1140/epja/s10050-021-00392-0. arXiv: 2006.12350 [nucl-ex] (cit. on pp. 53, 82).

[553] R. G. T. Zegers et al. "Beam polarization asymmetries for the p(gamma, K+) Lambda and p(gamma, K+) Sigma0 reactions at E(gamma) = 1.5 Gev - 2.4 GeV". In: *Phys. Rev. Lett.* 91 (2003), p. 092001. DOI: 10.1103/PhysRevLett.91.092001. arXiv: nucl-ex/0302005 (cit. on pp. 53, 82).

[554] K. Hicks et al. "Measurement of the $\gamma\to$ p$\to$ K+ Λ reaction at backward angles". In: *Physical Review C—Nuclear Physics* 76.4 (2007), p. 042201 (cit. on pp. 53, 82).

[555] A. Lleres et al. "Polarization observable measurements for gamma p —> K+ Lambda and gamma p —> K+ Sigma0 for energies up to 1.5-GeV". In: *Eur. Phys. J. A* 31 (2007), pp. 79–93. DOI: 10.1140/epja/i2006-10167-8 (cit. on pp. 53, 82).

[556] C. A. Paterson et al. "Photoproduction of Λ and Σ^0 hyperons using linearly polarized photons". In: *Phys. Rev. C* 93.6 (2016), p. 065201. DOI: 10.1103/PhysRevC.93.065201. arXiv: 1603.06492 [nucl-ex] (cit. on pp. 53, 82).

[557] B. Borgia et al. "Λ^0 polarization from the reaction $\gamma + p = K^+ + \Lambda^0$ in the energy range (950÷1050) MeV". In: *Nuovo Cim.* 32.1 (1964), pp. 218–223. DOI: 10.1007/BF02732605 (cit. on pp. 53, 82).

[558] M. Grilli et al. "Λ^0-polarization from the reaction $\gamma + p = \Lambda^0 + K^+$ in the energy range (950÷1050)MeV". In: *Nuovo Cim.* 38.4 (1965), pp. 1467–1488. DOI: 10.1007/BF02750071 (cit. on pp. 53, 82).

[559] R. Haas et al. "Measurement of the Polarization of the Lambda0 in the Reaction gamma p –> K+ Lambda0 in the Resonance Region". In: *Nucl. Phys. B* 137 (1978), pp. 261–268. DOI: 10.1016/0550-3213(78)90519-9 (cit. on pp. 53, 82).

[560] K. H. Althoff et al. "Photoproduction of K+ Lambda0 on Polarized Protons". In: *Nucl. Phys. B* 137 (1978), pp. 269–275. DOI: 10.1016/0550-3213(78)90520-5 (cit. on pp. 53, 82).

[561] A. Lleres et al. "Measurement of beam-recoil observables O(x), O(z) and target asymmetry for the reaction gamma p —> K+ Lambda". In: *Eur. Phys. J. A* 39 (2009), pp. 149–161. DOI: 10.1140/epja/i2008-10713-4. arXiv: 0807.3839 [nucl-ex] (cit. on pp. 53, 82).

[562] R. K. Bradford et al. "First measurement of beam-recoil observables C(x) and C(z) in hyperon photoproduction". In: *Phys. Rev. C* 75 (2007), p. 035205. DOI: 10.1103/PhysRevC.75.035205. arXiv: nucl-ex/0611034 (cit. on pp. 53, 82).

[563] H. Kohri et al. "Differential cross section and photon beam asymmetry for the polarized-gamma n —> K+ Sigma- reaction at E(gamma) = 1.5GeV-2.4GeV". In: *Phys. Rev. Lett.* 97 (2006), p. 082003. DOI: 10.1103/PhysRevLett.97.082003. arXiv: hep-ex/0602015 (cit. on pp. 53, 82).

[564] M. R. Pahlavani, J. Sadeghi, and R. Morad. "Binding energy of a holographic deuteron and tritium in anti-de-Sitter space/conformal field theory (AdS/CFT)". In: *Phys. Rev. C* 82 (2010), p. 025201. DOI: 10.1103/PhysRevC.82.025201. arXiv: 1309.0640 [hep-th] (cit. on pp. 53, 82).

[565] T. C. Jude et al. "$K^+\Lambda$ and $K^+\Sigma^0$ photoproduction with fine center-of-mass energy resolution". In: *Phys. Lett. B* 735 (2014), pp. 112–118. DOI: 10.1016/j.physletb.2014.06.015. arXiv: 1308.5659 [nucl-ex] (cit. on pp. 53, 82).

[566] T. C. Jude et al. “Observation of a cusp-like structure in the γp $\to$ K+Σ0 cross section at forward angles and low momentum transfer”. In: *Phys. Lett. B* 820 (2021), p. 136559. DOI: 10.1016/j.physletb.2021.136559. arXiv: 2006.12437 [nucl-ex] (cit. on pp. 53, 82).

[567] S. Goers et al. “Measurement of gamma p –> K0 Sigma+ at photon energies up to 1.55-GeV”. In: *Phys. Lett. B* 464 (1999), pp. 331–338. DOI: 10.1016/S0370-2693(99)01031-X (cit. on pp. 53, 82).

[568] B. Carnahan. “Strangeness photoproduction in the $\gamma p \to K^0\Sigma^+$ reaction”. PhD thesis. Catholic U. America, 2003. DOI: 10.2172/824935 (cit. on pp. 53, 82).

[569] R. Lawall et al. “Measurement of the reaction gamma p —> K0 Sigma+ at photon energies up to 2.6-GeV”. In: *Eur. Phys. J. A* 24 (2005), pp. 275–286. DOI: 10.1140/epja/i2005-10002-x. arXiv: nucl-ex/0504014 (cit. on pp. 53, 82).

[570] R. Castelijns et al. “Nucleon resonance decay by the K0 Sigma+ channel”. In: *Eur. Phys. J. A* 35 (2008), pp. 39–45. DOI: 10.1140/epja/i2007-10529-8. arXiv: nucl-ex/0702033 (cit. on pp. 53, 82).

[571] R. Ewald et al. “Anomaly in the $K^0_S\Sigma^+$ photoproduction cross section off the proton at the K^* threshold”. In: *Phys. Lett. B* 713 (2012), pp. 180–185. DOI: 10.1016/j.physletb.2012.05.066. arXiv: 1112.0811 [nucl-ex] (cit. on pp. 53, 82).

[572] P. Aguar-Bartolome et al. “Measurement of the $\gamma p \to K^0\Sigma^+$ reaction with the Crystal Ball/TAPS detectors at the Mainz Microtron”. In: *Phys. Rev. C* 88.4 (2013), p. 044601. DOI: 10.1103/PhysRevC.88.044601. arXiv: 1306.1243 [hep-ex] (cit. on pp. 53, 82).

[573] C. S. Akondi et al. “Experimental study of the $\gamma p \to K^0\Sigma^+$, $\gamma n \to K^0\Lambda$, and $\gamma n \to K^0\Sigma^0$ reactions at the Mainz Microtron”. In: *Eur. Phys. J. A* 55.11 (2019), p. 202. DOI: 10.1140/epja/i2019-12924-x. arXiv: 1811.05547 [nucl-ex] (cit. on pp. 53, 82).

[574] C. S. Nepali et al. “Transverse polarization of $^+$(1189) in photoproduction on a hydrogen target in CLAS”. In: *Phys. Rev. C* 87.4 (2013), p. 045206. DOI: 10.1103/PhysRevC.87.045206. arXiv: 1302.0322 [nucl-ex] (cit. on pp. 53, 82).

[575] L. Tiator et al. “Eta and Etaprime Photoproduction on the Nucleon with the Isobar Model EtaMAID2018”. In: *Eur. Phys. J. A* 54.12 (2018), p. 210. DOI: 10.1140/epja/i2018-12643-x. arXiv: 1807.04525 [nucl-th] (cit. on p. 55).

[576] R. E. Cutkosky et al. “PION - NUCLEON PARTIAL WAVE ANALYSIS”. In: *4th International Conference on Baryon Resonances*. July 1980, p. 19 (cit. on p. 62).

[577] W. J. Briscoe et al. “On the photoproduction reactions $\gamma d \to \pi NN$”. In: *Eur. Phys. J. A* 58.2 (2022), p. 23. DOI: 10.1140/epja/s10050-022-00671-4. arXiv: 2112.08150 [nucl-th] (cit. on p. 72).

[578] J.-J. Wu, T. Sato, and T. .-. H. Lee. “Incoherent pion production in neutrino-deuteron interactions”. In: *Phys. Rev. C* 91.3 (2015), p. 035203. DOI: 10.1103/PhysRevC.91.035203. arXiv: 1412.2415 [nucl-th] (cit. on p. 72).

[579] M. Salomon et al. “Radiative Capture and Charge Exchange of Negative Pions on Protons at 27.4-MeV and 39.3-MeV”. In: *Nucl. Phys. A* 414 (1984), pp. 493–507. DOI: 10.1016/0375-9474(84)90615-8 (cit. on pp. 72, 79).

[580] K. Liu. “Radiative negative pion proton capture and the low energy theorem”. PhD thesis. University of Kentucky, 1994 (cit. on pp. 72, 79).

[581] K. M. Watson. “The Hypothesis of Charge Independence for Nuclear Phenomena”. In: *Phys. Rev.* 85 (5 Mar. 1952), pp. 852–857. DOI: 10.1103/PhysRev.85.852. URL: https://link.aps.org/doi/10.1103/PhysRev.85.852 (cit. on p. 72).

[582] K. M. Watson. “Some General Relations between the Photoproduction and Scattering of π Mesons”. In: *Phys. Rev.* 95 (1 July 1954), pp. 228–236. DOI: 10.1103/PhysRev.95.228. URL: https://link.aps.org/doi/10.1103/PhysRev.95.228 (cit. on p. 72).

[583] R. G. Moorhouse, H. Oberlack, and A. H. Rosenfeld. “Analysis of π^+, π^-, and π^0 photoproduction from the first through the third resonance region”. In: *Phys. Rev. D* 9 (1 Jan. 1974), pp. 1–41. DOI: 10.1103/PhysRevD.9.1. URL: https://link.aps.org/doi/10.1103/PhysRevD.9.1 (cit. on p. 74).

[584] HEP-data website. https://www.hepdata.net (cit. on p. 77).

[585] V. Bernard, N. Kaiser, and U.-G. Meißner. “Neutral pion photoproduction off nucleons revisited”. In: *Z. Phys. C* 70 (1996), pp. 483–498. DOI: 10.1007/s002880050126. arXiv: hep-ph/9411287 (cit. on pp. 77, 78).

[586] M. Hoferichter, B. Kubis, and U.-G. Meißner. “Isospin breaking in the pion-nucleon scattering lengths”. In: *Phys. Lett. B* 678 (2009), pp. 65–71. DOI: 10.1016/j.physletb.2009.05.068. arXiv: 0903.3890 [hep-ph] (cit. on pp. 77, 83).

[587] M. A. Kovash. In: *PiN Newslett.* 12N.3 (1997), p. 51 (cit. on p. 77).

[588] V. Bernard, N. Kaiser, and U.-G. Meißner. “Chiral corrections to the Kroll-Ruderman theorem”. In: *Phys. Lett. B* 383 (1996), pp. 116–120. DOI: 10.1016/0370-2693(96)00699-5. arXiv: hep-ph/9603278 (cit. on p. 77).

[589] S. R. Beane et al. “Neutral pion photoproduction on deuterium in baryon chiral perturbation theory to order q**4”. In: *Nucl. Phys. A* 618 (1997), pp. 381–401. DOI: 10.1016/S0375-9474(97)00133-4. arXiv: hep-ph/9702226 (cit. on p. 77).

[590] W. J. Briscoe et al. “Cross section for $\gamma n \to \pi^0 n$ at the Mainz A2 experiment”. In: *Phys. Rev. C* 100.6 (2019), p. 065205. DOI: 10.1103/PhysRevC.100.065205. arXiv: 1908.02730 [nucl-ex] (cit. on pp. 78, 83, 149).

[591] M. Dieterle et al. “Photoproduction of π^0 mesons off protons and neutrons in the second and third nucleon resonance regions”. In: *Phys. Rev. C* 97 (6 June 2018), p. 065205. DOI: 10.1103/PhysRevC.97.065205. URL: https://link.aps.org/doi/10.1103/PhysRevC.97.065205 (cit. on pp. 78, 83, 148).

[592] K. Kossert et al. “Quasifree pi0 photoproduction from the bound nucleon”. In: *Eur. Phys. J. A* 19 (2004), pp. 391–399. DOI: 10.1140/epja/i2003-10130-3. arXiv: nucl-ex/0310028 (cit. on p. 78).

[593] A. Ando. *in Physik-Daten. Physics data. Sekt.7: Compilation of pion photoproduction data. No 1 ed. by Behrens, H. and Ebel, G. and Menze, D. and Pfeil, W. and Wilcke, R.* Tech. rep. Eggenstein-Leopoldshafen: ZAED 1977. 306 S. 1977 (cit. on p. 78).

[594] Y. Hemmi et al. “Photoproduction of neutral pions off neutrons in the energy region between 500 MeV and 900 MeV”. In: *Nuclear Physics B* 55.2 (1973), pp. 333–362. ISSN: 0550-3213. DOI: https://doi.org/10.1016/0550-3213(73)90384-2. URL: https://www.sciencedirect.com/science/article/pii/0550321373903842 (cit. on p. 78).

[595] C. Bacci et al. "Angular distributions for single neutral pion photoproduction from neutrons at 450-800 mev". In: *Phys. Lett. B* 39 (1972), pp. 559–562. DOI: 10.1016/0370-2693(72)90344-9 (cit. on p. 78).
[596] C. R. Clinesmith. "π^0 PHOTOPRODUCTION FROM THE DEUTERON AT FORWARD ANGLES IN THE ENERGY RANGE FROM 900-MeV TO 1400-MeV". PhD thesis. Caltech, 1967 (cit. on p. 78).
[597] C. Mullen et al. "Single π^0 production off neutrons bound in deuteron with linearly polarized photons". In: *Eur. Phys. J. A* 57.6 (2021), p. 205. DOI: 10.1140/epja/s10050-021-00521-9. arXiv: 2103.08400 [nucl-ex] (cit. on pp. 78, 83, 150).
[598] R. Di Salvo et al. "Measurement of Sigma beam asymmetry in pi0 photoproduction off the neutron in the second and third resonances region". In: *Eur. Phys. J. A* 42 (2009), pp. 151–157. DOI: 10.1140/epja/i2009-10870-x (cit. on pp. 78, 83, 150).
[599] F. Cividini et al. "Measurement of the helicity dependence for single π^0 photoproduction from the deuteron". In: *Eur. Phys. J. A* 58.6 (2022), p. 113. DOI: 10.1140/epja/s10050-022-00760-4. arXiv: 2203.00535 [nucl-ex] (cit. on pp. 78, 85, 100, 101, 154).
[600] M. Dieterle et al. "First measurement of the polarization observable E and helicity-dependent cross sections in single π 0 photoproduction from quasi-free nucleons". In: *Phys. Lett. B* 770 (2017), pp. 523–531. DOI: 10.1016/j.physletb.2017.04.079. arXiv: 1705.07342 [nucl-ex] (cit. on pp. 78, 85, 153).
[601] N. Jermann et al. "Measurement of polarization observables **T**, **P**, and **H** in $\boldsymbol{\pi^0}$ and η photoproduction off quasi-free nucleons". In: *Eur. Phys. J. A* 59.10 (2023), p. 232. DOI: 10.1140/epja/s10050-023-01134-0 (cit. on pp. 78, 85, 151, 152).
[602] P. T. Mattione et al. "Differential cross section measurements for $\gamma n \to \pi^- p$ above the first nucleon resonance region". In: *Phys. Rev. C* 96.3 (2017), p. 035204. DOI: 10.1103/PhysRevC.96.035204. arXiv: 1706.01963 [nucl-ex] (cit. on pp. 79, 85, 162–165).
[603] W. Chen et al. "Amplitude analysis of $\gamma n- > pi^- p$ data above 1 GeV". In: *Phys. Rev. C* 86 (2012), p. 015206. DOI: 10.1103/PhysRevC.86.015206. arXiv: 1203.4412 [hep-ph] (cit. on pp. 79, 85, 161).
[604] W. J. Briscoe et al. "Evaluation of the gn–>pi-p differential cross sections in the Delta-isobar region". In: *Phys. Rev. C* 86 (2012), p. 065207. DOI: 10.1103/PhysRevC.86.065207. arXiv: 1209.0024 [nucl-th] (cit. on pp. 79, 85, 161).
[605] A. Shafi et al. "Measurement of inverse pion photoproduction at energies spanning the N(1440) resonance". In: *Phys. Rev. C* 70 (2004), p. 035204. DOI: 10.1103/PhysRevC.70.035204. arXiv: nucl-ex/0405026 (cit. on pp. 79, 85, 160).
[606] G. J. Kim et al. "DIFFERENTIAL CROSS-SECTION FOR PI- P —> GAMMA N FROM 427-MEV/C TO 625-MEV/C". In: *Phys. Rev. D* 40 (1989), pp. 244–247. DOI: 10.1103/PhysRevD.40.244 (cit. on p. 79).
[607] A. Bagheri et al. "The Reaction $\pi^- p \to \gamma n$ Below the Δ Resonance". In: *Phys. Rev. C* 38 (1988), pp. 875–884. DOI: 10.1103/PhysRevC.38.875 (cit. on p. 79).
[608] H. j. Besch et al. "PHOTOPRODUCTION OF CHARGED PIONS FROM DEUTERIUM AT GAMMA ENERGIES FROM 900-MEV TO 1800-MEV AND PION ANGLES BETWEEN 65-DEGREES AND 125-DEGREES". In: *Z. Phys. C* 16 (1982), pp. 1–6. DOI: 10.1007/BF01573740 (cit. on pp. 79, 85).

[609] L. O. Abrahamian et al.
"PHOTOPRODUCTION OF pi- MESONS ON NEUTRONS WITH POLARIZED PHOTONS IN THE ENERGY RANGE E (gamma) = 0.9-GeV TO 1.65-GeV".
In: (Oct. 1979) (cit. on p. 79).

[610] M. T. Tran et al. "DIFFERENTIAL CROSS-SECTIONS FOR RADIATIVE CAPTURE OF PIONS ON HYDROGEN IN THE DELTA (1232) REGION: A TEST OF THE ISOSPIN STRUCTURE AND T SYMMETRY OF HADRONIC ELECTROMAGNETIC INTERACTIONS". In: *Nucl. Phys. A* 324 (1979), pp. 301–334.
DOI: 10.1016/0375-9474(79)90586-4 (cit. on p. 79).

[611] P. E. Argan et al. "STUDY OF THE GAMMA D —> P P PI- REACTION IN THE DELTA (1236) REGION FOR WELL DEFINED KINEMATICAL CONDITIONS".
In: *Nucl. Phys. A* 296 (1978), pp. 373–387. DOI: 10.1016/0375-9474(78)90080-5 (cit. on p. 79).

[612] A. J. Weiss et al. "Measurement of Differential Cross-Sections for Radiative Pion-Proton Capture in the Second Resonance Region". In: *Nucl. Phys. B* 101 (1975), pp. 1–18.
DOI: 10.1016/0550-3213(75)90289-8 (cit. on p. 79).

[613] J. C. Comiso et al. "Inverse Pion Photoproduction in the Vicinity of the p33 (1232) Resonance and a Test of Time Reversal Invariance". In: *Phys. Rev. D* 12 (1975), p. 719.
DOI: 10.1103/PhysRevD.12.719 (cit. on p. 79).

[614] P. E. Scheffler and P. L. Walden.
"Photoproduction of pi- from deuterium at laboratory energies 600 to 1250 mev".
In: *Nucl. Phys. B* 75 (1974), pp. 125–158. DOI: 10.1016/0550-3213(74)90469-6 (cit. on p. 79).

[615] G. Von Holtey et al.
"Photoproduction of charged pions on deuterium in the first resonance region".
In: *Nucl. Phys. B* 70 (1974), pp. 379–389. DOI: 10.1016/0550-3213(74)90436-2 (cit. on p. 79).

[616] P. A. Berardo et al. "Differential cross-sections of pi- p —> gamma n for 317, 452, and 491 mev/c incident pion momentum". In: *Phys. Rev. D* 9 (1974), pp. 621–643.
DOI: 10.1103/PhysRevD.9.621 (cit. on p. 79).

[617] J. Boucrot et al. "Photoproduction of pi- mesons on deuteron monochromatic photons in the first resonance region". In: *Nuovo Cim. A* 18 (1973), pp. 635–653.
DOI: 10.1007/BF02727581 (cit. on p. 79).

[618] P. Benz et al.
"Measurement of the reaction $\gamma d \to \pi^- pp$, and determination of cross-sections for the reaction $\gamma n \to \pi^- p$, at photon energies between 0.2-GeV and 2.0-GeV".
In: *Nucl. Phys. B* 65 (1973), pp. 158–209. DOI: 10.1016/0550-3213(73)90280-0 (cit. on p. 79).

[619] V. Rossi et al.
"Analysis of the reaction gamma n —> p pi- in the first and second resonance regions".
In: *Nuovo Cim. A* 13 (1973), pp. 59–89. DOI: 10.1007/BF02788907 (cit. on p. 79).

[620] G. Neugebauer, W. Wales, and R. L. Walker. "Photoproduction of Negative and Positive Pions from Deuterium for Photon Energies 500 to 1000 Mev".
In: *Phys. Rev.* 119 (1960), pp. 1726–1735. DOI: 10.1103/PhysRev.119.1726 (cit. on p. 79).

[621] G. Mandaglio et al.
"Beam asymmetry Σ measurements on the π^- photoproduction off neutrons".
In: *Phys. Rev. C* 82 (2010), p. 045209. DOI: 10.1103/PhysRevC.82.045209.
arXiv: 1010.1715 [nucl-ex] (cit. on pp. 80, 86, 169).

[622] F. V. Adamian et al. “Single π^- Meson Photoproduction on Neutrons by Linearly Polarized Photons in the Third and Fourth Resonance Region”. In: *J. Phys. G* 15 (1989), pp. 1797–1803. DOI: 10.1088/0954-3899/15/12/006 (cit. on p. 80).
[623] A. et al. In: *Soviet Journal of Nuclear Physics* 32 (1980), p. 69 (cit. on p. 80).
[624] G. et al. In: *Soviet Journal of Nuclear Physics* 23 (1976), p. 511 (cit. on p. 80).
[625] K. Kondo et al. “Negative-pion photoproduction from neutrons by linearly polarized photons in the first resonance region”. In: *Phys. Rev. D* 9 (1974), pp. 529–533. DOI: 10.1103/PhysRevD.9.529 (cit. on p. 80).
[626] K. Kondo et al. “The Production Asymmetry in $\gamma + n \to \pi^- + p$ Process with Polarized Photons ”. In: *Journal of the Physical Society of Japan* 9 (1970), pp. 13–29. DOI: 10.1143/JPSJ.29.13 (cit. on p. 80).
[627] F. F. Liu, D. J. Drickey, and R. F. Mozley. “Charged-Pion Photoproduction from Deuterium with Polarized Bremsstrahlung”. In: *Phys. Rev.* 136 (1964), B1183–B1186. DOI: 10.1103/PhysRev.136.B1183 (cit. on p. 80).
[628] J. C. Stasko et al. “Radiative decay of the Delta resonance: Analyzing powers for pi- p (polarized) —> gamma n”. In: *Phys. Rev. Lett.* 72 (1994), pp. 973–976. DOI: 10.1103/PhysRevLett.72.973 (cit. on p. 80).
[629] G. J. Kim et al. “Measurement of the left-right asymmetry in pi- p —> gamma n from 301-GeV/c to 625-MeV/c at backward angles”. In: *Phys. Rev. D* 43 (1991), pp. 687–695. DOI: 10.1103/PhysRevD.43.687 (cit. on p. 80).
[630] J. c. Alder et al. “MEASUREMENT OF THE ASYMMETRY PARAMETER A IN PI- P ELASTIC AND CHARGE EXCHANGE SCATTERING AT PION ENERGIES T (PI) = 98-MEV, 238-MEV, 292-MEV, AND 310-MEV”. In: *Phys. Rev. D* 27 (1983), pp. 1040–1055. DOI: 10.1103/PhysRevD.27.1040 (cit. on p. 80).
[631] H. Takeda et al. “Measurement of Recoil Proton Polarization in the Process of π^- Photoproduction From Neutrons in the Energy Range Between 700-MeV and 1200-MeV”. In: *Nucl. Phys. B* 168 (1980), pp. 17–31. DOI: 10.1016/0550-3213(80)90273-4 (cit. on p. 80).
[632] M. Beneventano et al. “Polarization of the recoil proton from the process gamma n —> p pi- in deuterium for (theta pi)c.m.=90 degrees in the second-resonance region”. In: *Lett. Nuovo Cim.* 3S1 (1970), pp. 840–844. DOI: 10.1007/BF02753470 (cit. on p. 80).
[633] J. R. Kenemuth and P. C. Stein. “Polarization of the Proton from the gamma+n –> p+pi- Reaction”. In: *Phys. Rev.* 129 (1963), pp. 2259–2264. DOI: 10.1103/PhysRev.129.2259 (cit. on p. 80).
[634] K. Fujii et al. “Measurement of Polarized Target Asymmetry on $\gamma n \to \pi^- p$ Around the Second Resonance Region”. In: *Nucl. Phys. B* 187 (1981), pp. 53–70. DOI: 10.1016/0550-3213(81)90116-4 (cit. on p. 80).
[635] K. H. Althoff et al. “Photoproduction of Negative Pions on Polarized Neutrons in the Region of the Second Resonance”. In: *Nucl. Phys. B* 116 (1976), pp. 253–260. DOI: 10.1016/0550-3213(76)90343-6 (cit. on p. 80).
[636] K. H. Althoff et al. “Photoproduction of Negative Pions on a Polarized Neutron Target in the Resonance Region”. In: *Nucl. Phys. B* 96 (1975), pp. 497–508. DOI: 10.1016/0550-3213(75)90345-4 (cit. on p. 80).

[637] D. Ho et al.
"Beam-Target Helicity Asymmetry for $\vec{\gamma}\vec{n} \to \pi^- p$ in the N^* Resonance Region".
In: *Phys. Rev. Lett.* 118.24 (2017), p. 242002. DOI: 10.1103/PhysRevLett.118.242002.
arXiv: 1705.04713 [nucl-ex] (cit. on pp. 80, 86, 100, 176, 177).

[638] A. V. Anisovich et al. "Neutron helicity amplitudes".
In: *Phys. Rev. C* 96.5 (2017), p. 055202. DOI: 10.1103/PhysRevC.96.055202
(cit. on pp. 86, 90).

[639] K. P. Adhikari et al. "Measurement of the Q^2 Dependence of the Deuteron Spin Structure Function g_1 and its Moments at Low Q^2 with CLAS".
In: *Phys. Rev. Lett.* 120.6 (2018), p. 062501. DOI: 10.1103/PhysRevLett.120.062501.
arXiv: 1711.01974 [nucl-ex] (cit. on p. 94).

[640] X. Zheng et al. "Measurement of the proton spin structure at long distances".
In: *Nature Phys.* 17.6 (2021), pp. 736–741. DOI: 10.1038/s41567-021-01198-z.
arXiv: 2102.02658 [nucl-ex] (cit. on p. 94).

[641] V. Bernard, N. Kaiser, and U.-G. Meißner.
"Small momentum evolution of the extended Drell-Hearn-Gerasimov sum rule".
In: *Phys. Rev. D* 48 (1993), pp. 3062–3069. DOI: 10.1103/PhysRevD.48.3062.
arXiv: hep-ph/9212257 (cit. on p. 94).

[642] X.-D. Ji, C.-W. Kao, and J. Osborne. "Generalized Drell-Hearn-Gerasimov sum rule at order O(p**4) in chiral perturbation theory". In: *Phys. Lett. B* 472 (2000), pp. 1–4.
DOI: 10.1016/S0370-2693(99)01365-9. arXiv: hep-ph/9910256 (cit. on p. 94).

[643] V. Bernard, T. R. Hemmert, and U.-G. Meißner.
"Spin structure of the nucleon at low-energies". In: *Phys. Rev. D* 67 (2003), p. 076008.
DOI: 10.1103/PhysRevD.67.076008. arXiv: hep-ph/0212033 (cit. on p. 94).

[644] V. Bernard et al. "New insights into the spin structure of the nucleon".
In: *Phys. Rev. D* 87.5 (2013), p. 054032. DOI: 10.1103/PhysRevD.87.054032.
arXiv: 1209.2523 [hep-ph] (cit. on p. 94).

[645] J. M. Alarcón et al.
"Forward doubly-virtual Compton scattering off the nucleon in chiral perturbation theory: II. Spin polarizabilities and moments of polarized structure functions".
In: *Phys. Rev. D* 102.11 (2020), p. 114026. DOI: 10.1103/PhysRevD.102.114026.
arXiv: 2006.08626 [hep-ph] (cit. on p. 94).

[646] J. Ahrens et al. "First measurement of the Gerasimov-Drell-Hearn integral for Hydrogen from 200 to 800 MeV". In: *Phys. Rev. Lett.* 87 (2001), p. 022003.
DOI: 10.1103/PhysRevLett.87.022003. arXiv: hep-ex/0105089
(cit. on pp. 94, 100, 101).

[647] H. Dutz et al. "First measurement of the Gerasimov-Drell-Hearn sum rule for H-1 from 0.7-GeV to 1.8-GeV at ELSA". In: *Phys. Rev. Lett.* 91 (2003), p. 192001.
DOI: 10.1103/PhysRevLett.91.192001 (cit. on p. 94).

[648] H. Dutz et al. "Experimental Check of the Gerasimov-Drell-Hearn Sum Rule for H-1".
In: *Phys. Rev. Lett.* 93 (2004), p. 032003. DOI: 10.1103/PhysRevLett.93.032003
(cit. on p. 94).

[649] R. A. Arndt et al. "Helicity-dependent photoabsorption cross sections on the nucleon".
In: *Phys. Rev. C* 72 (2005), p. 058203. DOI: 10.1103/PhysRevC.72.058203.
arXiv: nucl-th/0508064 (cit. on p. 94).

[650] I. Strakovsky et al.
"Single-pion contribution to the Gerasimov-Drell-Hearn sum rule and related integrals".
In: *Phys. Rev. C* 105.4 (2022), p. 045202. DOI: 10.1103/PhysRevC.105.045202.
arXiv: 2201.06495 [nucl-th] (cit. on pp. 94, 95, 100–102).

[651] T. Mart and M. J. Kholili. “Partial wave analysis for $K\Sigma$ photoproduction on the nucleon valid from threshold up to $W = 2.8$ GeV”. In: *J. Phys. G* 46.10 (2019), p. 105112. DOI: 10.1088/1361-6471/ab34c6 (cit. on pp. 94, 96).
[652] Q. Zhao, J. S. Al-Khalili, and C. Bennhold. “Contributions of vector meson photoproduction to GDH sum rule”. In: *Phys. Rev. C* 65 (2002), p. 032201. DOI: 10.1103/PhysRevC.65.032201. arXiv: nucl-th/0201002 (cit. on pp. 94, 96, 100, 101).
[653] G. Penner and U. Mosel. “Vector meson production and nucleon resonance analysis in a coupled channel approach for energies m(N) less than S**(1/2) less than 2-GeV. 2. Photon induced results”. In: *Phys. Rev. C* 66 (2002), p. 055212. DOI: 10.1103/PhysRevC.66.055212. arXiv: nucl-th/0207069 (cit. on p. 96).
[654] J. Ahrens et al. “Helicity dependence of the gamma(pol.) p(pol.) –> n pi+ pi0 reaction in the second resonance region”. In: *Phys. Lett. B* 551 (2003), pp. 49–55. DOI: 10.1016/S0370-2693(02)03008-3 (cit. on p. 96).
[655] M. Hirata, N. Katagiri, and T. Takaki. “Pi N N coupling and two pion photoproduction on the nucleon”. In: *Phys. Rev. C* 67 (2003), p. 034601. DOI: 10.1103/PhysRevC.67.034601. arXiv: nucl-th/0210063 (cit. on p. 96).
[656] N. Bianchi and E. Thomas. “Parameterization of [sigma(1/2) - sigma(3/2)] for Q**2 >= 0 and nonresonance contribution to the GDH sum rule”. In: *Phys. Lett. B* 450 (1999), pp. 439–447. DOI: 10.1016/S0370-2693(99)00176-8. arXiv: hep-ph/9902266 (cit. on p. 96).
[657] S. D. Bass and M. M. Brisudova. “The Spin and flavor dependence of high-energy photoabsorption”. In: *Eur. Phys. J. A* 4 (1999), pp. 251–258. DOI: 10.1007/s100500050228. arXiv: hep-ph/9711423 (cit. on p. 96).
[658] S. D. Bass, M. Skurzok, and P. Moskal. “Updating spin-dependent Regge intercepts”. In: *Phys. Rev. C* 98.2 (2018), p. 025209. DOI: 10.1103/PhysRevC.98.025209. arXiv: 1808.03202 [hep-ph] (cit. on p. 96).
[659] S. Duane et al. “Hybrid Monte Carlo”. In: *Phys. Lett. B* 195 (1987), pp. 216–222. DOI: 10.1016/0370-2693(87)91197-X (cit. on p. 104).
[660] M. D. Hoffman and A. Gelman. “The No-U-Turn Sampler: Adaptively Setting Path Lengths in Hamiltonian Monte Carlo”. In: (Nov. 2011). arXiv: 1111.4246 [stat.CO] (cit. on p. 104).
[661] J. J. de Swart. “The Octet model and its Clebsch-Gordan coefficients”. In: *Rev. Mod. Phys.* 35 (1963). [Erratum: Rev.Mod.Phys. 37, 326–326 (1965)], pp. 916–939. DOI: 10.1103/RevModPhys.35.916 (cit. on p. 121).
[662] K. Nakayama, Y. Oh, and H. Haberzettl. “Combined analysis of eta meson hadro- and photo-production off nucleons”. In: *J. Korean Phys. Soc.* 59 (2011), pp. 224–246. DOI: 10.3938/jkps.59.224. arXiv: 0803.3169 [hep-ph] (cit. on p. 121).
[663] M. Döring, E. Oset, and B. S. Zou. “The Role of the N*(1535) resonance and the pi- p —> KY amplitudes in the OZI forbidden pi N —> phi N reaction”. In: *Phys. Rev. C* 78 (2008), p. 025207. DOI: 10.1103/PhysRevC.78.025207. arXiv: 0805.1799 [nucl-th] (cit. on p. 124).
[664] U.-G. Meißner et al. “Strange vector currents and the OZI rule”. In: *Phys. Lett. B* 408 (1997), pp. 381–386. DOI: 10.1016/S0370-2693(97)00828-9. arXiv: hep-ph/9701296 (cit. on p. 124).

[665] A. Reuber, K. Holinde, and J. Speth.
"Meson exchange hyperon - nucleon interactions in free scattering and nuclear matter".
In: *Nucl. Phys. A* 570 (1994), pp. 543–579. DOI: 10.1016/0375-9474(94)90073-6
(cit. on p. 124).
[666] G. Janssen et al. "On the structure of the scalar mesons f0 (975) and a0 (980)".
In: *Phys. Rev. D* 52 (1995), pp. 2690–2700. DOI: 10.1103/PhysRevD.52.2690.
arXiv: nucl-th/9411021 (cit. on p. 125).
[667] A. Mueller- Groeling, K. Holinde, and J. Speth.
"K- N interaction in the meson exchange framework".
In: *Nucl. Phys. A* 513 (1990), pp. 557–583. DOI: 10.1016/0375-9474(90)90398-6
(cit. on p. 125).
[668] B. Holzenkamp, K. Holinde, and J. Speth.
"A Meson Exchange Model for the Hyperon Nucleon Interaction".
In: *Nucl. Phys. A* 500 (1989), pp. 485–528. DOI: 10.1016/0375-9474(89)90223-6
(cit. on p. 125).
[669] L. Wolfenstein. "Polarization of fast nucleons".
In: *Ann. Rev. Nucl. Part. Sci.* 6 (1956), pp. 43–76.
DOI: 10.1146/annurev.ns.06.120156.000355 (cit. on p. 126).
[670] C. G. Fasano, F. Tabakin, and B. Saghai.
"Spin observables at threshold for meson photoproduction".
In: *Phys. Rev. C* 46 (1992), pp. 2430–2455. DOI: 10.1103/PhysRevC.46.2430
(cit. on p. 129).
[671] A. M. Sandorfi et al.
"A Rosetta Stone Relating Conventions In Photo-Meson Partial Wave Analyses".
In: *AIP Conf. Proc.* 1432.1 (2012). Ed. by V. Burkert et al., pp. 219–222.
DOI: 10.1063/1.3701216. arXiv: 1108.5411 [nucl-th] (cit. on p. 130).

Acknowledgement

I would like to express my sincere gratitude to my supervisor and mentor, Dr. Deborah Rönchen, for her constant support, understanding, and encouragement throughout this journey. She created a very positive and supportive working atmosphere, taught me a great deal, and always helped me whenever I needed it. Thanks to her guidance, I was able to complete my doctorate and publish my first paper, with her as a co-author.

I would also like to thank my first examiner and mentor, Prof. Dr. Christoph Hanhart, for all that he has taught me over the years and for giving me the opportunity to work with him during both my Bachelor's and Master's theses. I have learned a great deal from him, including valuable lessons in teaching. He was always available for questions and provided helpful answers on a wide range of topics. He also supported me greatly with my first publication and was a co-author.

I am very grateful to my second examiner, Prof. Dr. Dr. h.c. Ulf-G. Meißner, for agreeing to serve as my second examiner. He also supported me with my publication and was likewise a co-author.

My thanks also go to Anuvind Asokhan for the many good conversations and helpful discussions in the office. I would also like to thank my colleagues in the Institute of Advanced Simulation 4 (IAS-4) for the pleasant working atmosphere and a special thanks to the administrative team for their helpful assistance with all administrative tasks.

I am also grateful to my friends and family for their support, encouragement, and patience throughout this process.

Finally, I want to thank my partner Robin Kaiser for his constant support throughout this time.